"It is good to have an end to journey toward; but it is the journey that matters, in the end."

Ursula K. Leguin

University of Alberta

Regulation and Functions of Cardiac Lipins

by

Bernard Pei Cheng Kok

A thesis submitted to the Faculty of Graduate Studies and Research
in partial fulfillment of the requirements for the degree of

Doctor of Philosophy

Department of Biochemistry

©Bernard Pei Cheng Kok
Fall 2012
Edmonton, Alberta

To my mother and father,

who have always offered love, patience and guidance.

To Nancy,

for the journey so far and the one yet taken.

To my siblings,

for all that we've been through in liveliness and laughter.

To friends,

and the moments always remembered.

Abstract

The heart requires an uninterrupted supply of fuels to sustain its physiological function. Fatty acids are the predominant substrates and endogenous triglyceride turnover contributes significantly to fatty acid oxidation. Lipins are cytosolic, bifunctional enzymes involved in both glycerolipid synthesis and fatty acid oxidation. All three mammalian lipins (lipin-1, -2 and -3) function as phosphatidate phosphatases (PAP) in glycerolipid synthesis. Lipin-1 also acts as a transcriptional co-activator with peroxisome proliferator-activated receptor-α (PPARα) and PPARγ co-activator-1α (PGC-1α) to upregulate genes involved in hepatic fatty acid oxidation. We demonstrated that the fatty acid, oleate, stimulates the translocation of cytosolic lipin-1 and -2 onto membranes. Less-phosphorylated forms of lipins associated with membranes preferentially compared to hyperphosphorylated lipins. We showed preliminary evidence that lipin-1B can interact with the protein phosphatase-1γ catalytic subunit, which could mediate lipin dephosphorylation and promote membrane binding. We also showed that the gene expressions of the lipins are upregulated in neonatal rat ventricular myocytes by glucocorticoid- and cAMP-dependent signalling, which is reflective of fasting, whereas insulin acts antagonistically. The predominant lipin isoform in the heart is lipin-1 and we showed that lipin-1 deficient (fatty liver dystrophy, *fld*) mice had impaired systolic function. However, lipin-1 deficiency does not impair glycerolipid synthesis in perfused working hearts. Thus, lipin-2 and -3 in the heart are sufficient to sustain physiological activity. Furthermore, we demonstrated that only a small proportion of the cytosolic PAP activity is required for glycerolipid synthesis in cardiomyocytes. However, there was an aberrant accumulation of newly synthesized phosphatidate in *fld* hearts, accompanied by

hyper-activation of the mammalian target of rapamycin complex 1 (mTORC1) pathway and increased endoplasmic reticulum stress response. We conclude that the cardiac dysfunction in *fld* mice stems from systemic effects of whole-body lipin-1 deficiency, the accumulation of phosphatidate and increased stress response. Overall, our studies have delineated the regulation of cardiac lipins and we have shown that the presence of three lipin isoforms can sustain cardiac glycerolipid synthesis. Finally, the interaction of lipin-1 with protein phosphatase 1γ provides an avenue to determining how its subcellular localization and thus, physiological actions are regulated.

Acknowledgments

To begin with, I would like to acknowledge my family and the support they have always given me throughout my endeavours in school, university and life. I am thankful for the bonds we share and all that we have experienced together. I would also like to thank Nancy for always knowing what to say and do, and for making this little corner of existence a better place.

I would like to thank Dave for all that he has done for me these past six years. Research can be difficult and challenging but it has been a stimulating and rewarding experience and I am thankful that you were always there to support and advise me. I will always remember the wonderful times in this lab because of all the characters with whom I have shared my time. Thanks to Jay, Mel, Sabina, Carlos, Nasser, Le, Vitali, Chif, Cris, Bori, Dora, Raie, Ganesh, Matthew, Daniel, Meghan, Kari, Tete, Hanna, Sachin and Betty (in order of seniority) for your diverse personalities and lunchtime sessions. Life is never boring in the Brindley lab!

I would also like to thank my friends and colleagues in the department and in this university who have made this experience one I will always remember: Sammie, Tamara, Gina, Ply, Danny, Roshani, Richard, Denise, Luis, Rory, Johnny, Mim, Emma, Kristen, Przemek, Delaine, Lorissa, Stacey, Adrienne, Dennis, Jean, Rene, Laura, Vern, Jelske, Bill, Bella, Randy, Russ, Audric, Barb, Kelly, Aruna, Asia, Allison, Helen, J.P., Sue-Ann, O.J., Andrea, Grant, Craig, Pam, Vesna, Kathy, Huajin, Magnus, Hector, Angela, Charles, Stephen, Nobu, Steve, Ian, Samuel, Sandy, Wang, Nico, Ariel, Robin, Flora, Shannon, Tina, Ala,

Petra, Thomas, Suzy, Carrie, Jamie, Amy, Miranda, Anita, Debbie, Rachel, Adrienne, Jo, Shannon, Luc, Charles, Steve and other members of the STRG.

Thanks to my committee members, Dr. Richard Lehner and Dr. Marek Michalak, for your support and kindness. I would also like to extend my gratitude and appreciation to Dr. Grant Hatch and Dr. Gary Lopaschuk for agreeing to participate in my thesis defense. I would also like to acknowledge my friends for always reminding how long I've spent in grad school and for fun times in general: Edda, Chris, Thye, Justin, Pate, BoJo, Brian, Habeeb, Henri, Joey, McHugh and others. Finally, I would like to acknowledge the collaborators who have made this work possible: Dr. Jason Dyck, Dr. Charles Holmes, Dr. Thurl Harris, Dr. Karen Reue, Dr. Zemin Yao, Tamara Arnold, Dr. Petra Kienesberger, Grant Masson, Donna Beker, Sandra Kelly, Suzanne Kovacic, Carrie-Lynn Soltys, Amy Barr and Brandi Sidlick.

Table of Contents

List of Tables

List of Figures

CHAPTER 1

INTRODUCTION

1.1 Cardiac fuel utilization and its regulation

1.1.1 Fuel demand and usage in the heart

On average, the human heart completes 60 – 80 cardiac cycles per minute. With a life expectancy of 78 years, the heart will potentially beat 2.9 billion times in an average lifetime. The continuous pumping of blood driven by the heart throughout the circulatory system is required to sustain a delivery system whereby substrates and oxygen can reach other organs in the body. Carbon dioxide is then transported through pulmonary circulation and expelled through the lungs, and other metabolites are channelled for disposal through the liver and kidneys. It is clear that the proper functioning of the heart is essential, and this is highlighted by the morbidities and mortalities linked to the development of heart failure and cardiovascular disease. This continual work performed by the heart can only be sustained by a constant, uninterrupted supply and oxidation of fuels.

The heart is an "omnivorous" organ that can utilize various substrates such as fatty acids (FAs), glucose, ketone bodies, amino acids and lactate to meet its energy demand [1, 2]. Out of these substrates, cardiac ATP production is largely dependent on FA oxidation (FAO) with 50 – 75% of ATP produced from FAs and the majority of the remaining ATP derived from glycolysis and glucose oxidation [1, 2]. The utilization of FA versus glucose is tightly regulated with preference for one substrate over the other depending on substrate supply, diurnal variations and fed/fasted states.

Studies in the 1960s up to the last decade have delineated the coordinated regulation of FA versus glucose oxidation in muscle [3-9]. When FA

supply is abundant, e.g. during fasting, glycolysis and glucose oxidation are inhibited due to the production of high energy molecules from FAO such as nicotinamide adenine dinucleotide (NADH) and adenosine triphosphate (ATP) (2, 3, 10, 11). Phosphofructokinase, which catalyzes the essentially irreversible step in glycolysis, is inhibited by high levels of ATP and citrate (12, 13). Pyruvate dehydrogenase, which acts as the bridge between glycolysis and the tricarboxylic acid (TCA) cycle, is phosphorylated and inhibited when pyruvate dehydrogenase kinase is activated by high levels of acetyl-CoA and NADH (14, 15).

Conversely, high levels of glycolysis can lead to the inhibition of carnitine palmitoyltransferase I (CPT I), which is a principal enzyme involved in controlling the rate of FAO by regulating FA entry into mitochondria. Pyruvate formed during glycolysis is converted to acetyl-CoA by pyruvate dehydrogenase in the mitochondrial matrix. Acetyl-CoA formed in this manner is more easily transported to the cytosol by carnitine acetyltransferase than acetyl-CoA formed during β-oxidation (16). Cytosolic acetyl-CoA carboxylase (ACC) then catalyzes the formation of malonyl-CoA from acetyl-CoA, and malonyl-CoA allosterically inhibits CPT I activity (6, 9, 17). Thus, increased ACC activity and malonyl-CoA levels limit the rate of mitochondrial FA entry mediated by CPT I when the heart is in the fed state and glycolysis is stimulated (8, 9, 18).

Malonyl-CoA can be converted back to acetyl-CoA by malonyl-CoA decarboxylase (MCD) (7, 19). Of note, malonyl-CoA decarboxylase expression is increased during conditions where FA supply is increased such as diabetes or fasting in a peroxisome proliferator-activated receptor-α-(PPARα) dependent manner (20-23). Furthermore, acetyl-CoA carboxylase itself can be inhibited by

3

AMP-activated protein kinase in energy-depleted conditions, thus enabling increased rates of mitochondrial FA entry through CPT I (24, 25). After taking all these factors into consideration, it is clear that the ratio of acetyl-CoA to malonyl-CoA serves as another critical regulatory juncture in determining the balance between FA and glucose utilization.

The absolute requirement for a continual supply of ATP in the heart is accomplished by the flexible usage of different substrates. Furthermore, the balance between FA and glucose catabolism is reliant upon a series of intricately linked counter-regulatory steps. In essence, the entry and utilization of the predominant fuel supply in the cardiomyocyte can dynamically shift the activation profile of its metabolic enzymes. The heart is able to perform optimally by maintaining this metabolic flexibility. Unfortunately, this level of functionality is severely perturbed in diseases such as diabetes.

1.1.2 Type 2 diabetes and cardiovascular disease

The incidence of type 2 diabetes has increased in a modern society faced with a rise in the rates of obesity and food consumption coupled to a decline in physical activity and an increasingly aging population. In conjunction with Type 2 diabetes, there is an increased risk of developing cardiovascular disease and stroke when a common set of co-morbidities including upper body obesity, insulin resistance, dyslipidemia and hypertension are present in a condition called the Metabolic Syndrome (26, 27). Increased awareness and treatment of the factors leading to the occurrence of cardiovascular disease has resulted in a decrease in rates of heart disease in both Canada and the USA (28, 29). However, cardiovascular disease still remains the number one cause of death in both

countries. Furthermore, the incidence of non insulin-dependent diabetes mellitus (NIDDM) in the North American and other populations has not slowed even with the rise in public awareness (30, 31).

Strikingly, a large proportion of diabetic patients develop cardiovascular disease (32, 33). Moreover, patients diagnosed with diabetes are 2-4 times more likely to develop coronary artery disease, heart failure or diabetic cardiomyopathy (33-35). One important parameter of healthy cardiac function is the dynamic and tightly regulated process of fuel metabolism in the heart, especially that of FA metabolism. There is an exclusive and aberrant dependence on FAs in the absence of insulin action and the relative inability to utilize glucose in the diabetic heart. The processes of FA uptake, oxidation and storage as well as the detrimental changes driven by the diabetic state will be examined in the following sections.

1.1.3 Regulation of fatty acid supply and entry

In order to fully appreciate the mechanisms underlying the metabolism of FAs in the heart and the consequences thereof, one must first comprehend the means by which the heart is supplied by FAs. Cardiac utilization of FAs is reliant on plasma FAs and the hydrolysis of triacylglycerol (TG) derived from lipoprotein particles as well as the rate of substrate entry (Figure 1.1) (36-38).
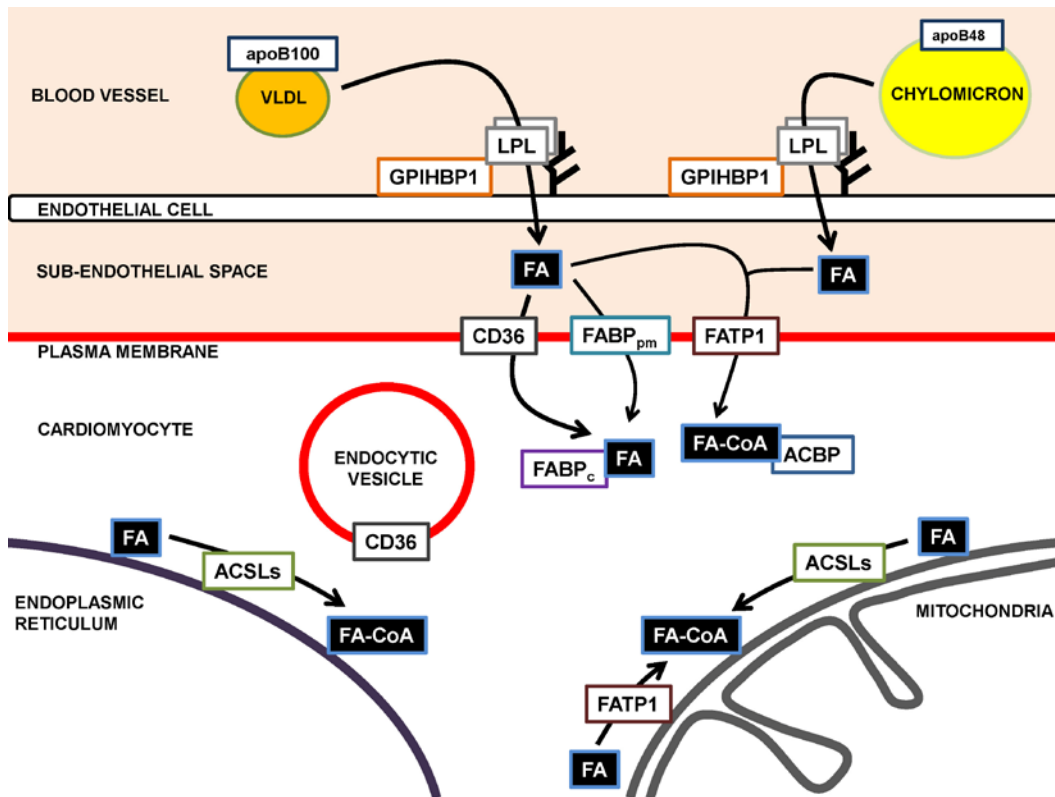
Figure 1.1 FA supply and uptake in the cardiomyocyte. Triacylglycerol contained in circulating apoB48-containing (chylomicrons) and apoB100-containing (very low density lipoprotein) particles are hydrolyzed by an active dimer of lipoprotein lipase (LPL) anchored to the lumenal side of endothelial cells lining the blood vessel by heparan sulfate proteoglycans and glycosylphosphatidylinositol anchored high density lipoprotein binding protein 1 (GPIHBP1). The fatty acids are taken up by the endothelial cells and converted to acyl-CoAs before esterification to triacylglycerol or transported by fatty acid binding proteins. Triacylglycerol is subsequently hydrolyzed and the non-esterified fatty acids are released from the endothelial cells into the sub-endothelial space. The fatty acids (FAs) cross the sub-endothelial space and enter the cardiomyocyte through facilitated transport by CD36 as well as plasma membrane-localized fatty acid binding protein (FABPpm) and fatty acid transport protein 1 (FATP1). FATP1 is also an acyl-CoA synthetase and can convert FAs to acyl-CoA esters, which are bound to acyl-CoA binding proteins (ACBP) in the cytosol. CD36 is not permanently localized to the plasma membrane and can cycle into endocytic vesicles. FAs are bound to cytosolic fatty acid binding protein (FABPc) and are activated to acyl-CoA esters by different isoforms of long chain acyl-CoA synthetases (ACSLs), including FATP, at the mitochondrial or endoplasmic reticulum membranes before entry into the oxidative or biosynthetic pathways.

6

The hydrolysis of TG stores from adipose tissue provides a large proportion of plasma FAs, which are transported bound to albumin. FA supply to the heart is also derived from the hydrolysis of TG in circulating lipoprotein particles like chylomicrons and very low density lipoprotein particles (VLDL). Chylomicron formation in enterocytes mainly in the jejunum occurs post-prandially whereby exogenously derived TG (80-90%) and a small proportion of free and esterified cholesterol (5-10%) are packaged with apolipoproteins including apolipoprotein B48 (39-42). Chylomicrons are then secreted into the mesenteric lymph and enter the vasculature through the thoracic duct (39-41). VLDLs are mainly secreted from hepatocytes and each VLDL particle contains one apolipoprotein B100 while consisting of approximately 40-60% TG and 20-30% cholesterol (free and esterified) (40, 42). TG in VLDL particles consist mainly of endogenously derived FAs, e.g. from adipose tissue lipolysis (40), with some contribution from dietary FAs post-prandially (43). The cardiac uptake and utilization of TG-derived FAs from VLDLs and chylomicrons depends on lipoprotein lipase (LPL) action (Figure 1.1) (38, 44, 45).

LPL is synthesized in the cardiomyocytes (46) and secreted as an active dimer to the lumenal side of the endothelial vessel wall through the action of glycosylphosphatidylinositol-anchored high density lipoprotein-binding protein 1 (GPIHBP1) (47-49). Glycosylphosphatidylinositol-anchored LPL (GPI-LPL) directly expressed on the surface of cardiomyocytes can also facilitate lipid uptake (50). The authors proposed that increased FA entry is mediated by GPI-LPL action on partially hydrolyzed lipoprotein particles that exited the vasculature and entered the subendothelial space. It should also be noted that the hydrolysis

of lipoprotein TG by LPL as well as the transport of LPL to the capillary lumen appears to be partly mediated by the VLDL receptor (51-53).

Besides the utilization of FA hydrolyzed from TG in lipoprotein particles, cardiac FA supply also depends on the uptake of plasma albumin-bound FA by membrane-localized FA transporters. These include CD36 (cluster of differentiation 36) (54, 55), plasma membrane FA binding protein (FABPpm) (56), and FA transport proteins, FATP1 and 6 (57) (Figure 1.1). The major transporter of FA across the cardiomyocyte plasma membrane appears to be CD36 since inhibition of CD36 decreases cardiac FA uptake by more than 50% (54, 58). Furthermore, CD36 can be dynamically cycled between the plasma membrane and intracellular compartments of cardiomyocytes depending on signals such as insulin and/or contraction, unlike the other FA transporters (59). CD36 also facilitates the uptake of FAs derived from VLDLs, but it does not appear to be involved in FA uptake from chylomicrons (38). Although CD36 is thought to be the major mode of cardiac FA uptake, forced overexpression of FATP1 in the heart leads to increased FA uptake and metabolism (60), showing that the other FA transporters could play significant roles in regulating cardiac FA supply.

The rate of FA uptake is also dictated by the intracellular flux of FA into oxidative or biosynthetic pathways. Cytoplasmic FA binding protein (FABPc), acyl-CoA binding protein (ACBP) and long-chain fatty acyl-CoA synthetases, including FATP1, can promote FA uptake by binding and directing FAs or acyl-CoA to the mitochondria for oxidation or to the endoplasmic reticulum (ER) for glycerolipid synthesis, thus reducing the intracellular FA concentration and establishing an inward FA gradient (Figure 1.1) (61).

8

1.1.4 Cardiac fatty acid uptake in the diabetic state

Fuel utilization in the heart is tightly regulated such that sustained disruption in substrate supply and/or oxidation promotes various deleterious phenotypes such as cardiac dysfunction, cardiomyopathies, reduced recovery from ischemia and heart failure (11, 62-65). In obese, type II diabetics, there is increased lipolysis from adipose tissue stores leading to increased FA delivery and accumulation in non-adipose tissues such as the liver and heart (66-72). The lack of insulin action coupled to increased glucocorticoid secretion and signalling can also stimulate apolipoprotein B production, VLDL secretion and gluconeogenesis in the liver (66, 73, 74). Furthermore, large quantities of FAs in the form of TG are secreted in chylomicrons due to excessive caloric intake and often the consumption of a high fat diet. Therefore, the heart has a considerable supply of FAs from the plasma in the diabetic state, either available in VLDL- and chylomicron-derived TG or as non-esterified FAs bound to albumin.

The rate of cardiac FA uptake is also increased since both LPL activity and CD36 expression are increased in diabetes and insulin resistance (75-80). Besides increased expression in diabetes, CD36 localization to the sarcolemmal membrane is also increased (81). Ultimately, increased FA supply and uptake promote an increased rate of FAO (37, 82). Finally, cardiac glucose oxidation is downregulated due to insulin resistance, and FAO is heavily favoured instead (1). This will be explored in more detail in Section 1.1.6.

1.1.5 Fate of fatty acids upon cardiomyocyte entry

Once taken up by the cell, FAs are esterified to acyl-CoA by acyl-CoA synthetases (ACSL) of which there are currently five known isoforms [reviewed in

(83)]. The subcellular distribution of the ACSL isoforms is varied with localization to the plasma membrane, mitochondria, endoplasmic reticulum and lipid droplets depending on cell type (83). In the heart, ACSL1 appears to be the major isoform since increases in ACSL activity during development in newborn mice is linked to increases in *Acsl1* transcript levels while *Acsl3* expression is decreased (84). Furthermore, the use of isoform-dependent inhibitors demonstrated the minor contribution of the remaining isoforms (ACSL4, 5 and 6) to cardiac ACSL activity as measured by an enzymatic assay using [^{3}H]palmitate as the substrate (84). Further evidence that ACSL1 plays a major role in the heart is emphasized by the detrimental phenotype of ACSL1 deficient mice. Cardiac FAO is impaired in these mice with compensatory increases in glucose and amino acid catabolism (85). As a consequence, the hearts of these mice are hypertrophic and dysfunctional (85). Although cardiac TG levels were unchanged in these mice, further investigation has to be performed to determine if the rates of TG synthesis and hydrolysis in these hearts are both decreased. This is important since decreased TG hydrolysis can also contribute to decreased mitochondrial β-oxidation (86-90).

Acyl-CoA esters are channeled towards oxidation or glycerolipid synthesis. Approximately 75% of FAs entering the heart are oxidized immediately in the mitochondrial matrix under normal conditions (82). The entry of FAs into the mitochondria is controlled by CPT I, which converts acyl-CoA to acylcarnitine (Figure 1.2) (1, 91). As mentioned previously in Section 1.1.1, CPT I can be allosterically inhibited by malonyl-CoA and the levels of malonyl-CoA are dependent on the activities of ACC and MCD (Figure 1.2) (6, 8, 17) (19, 92).
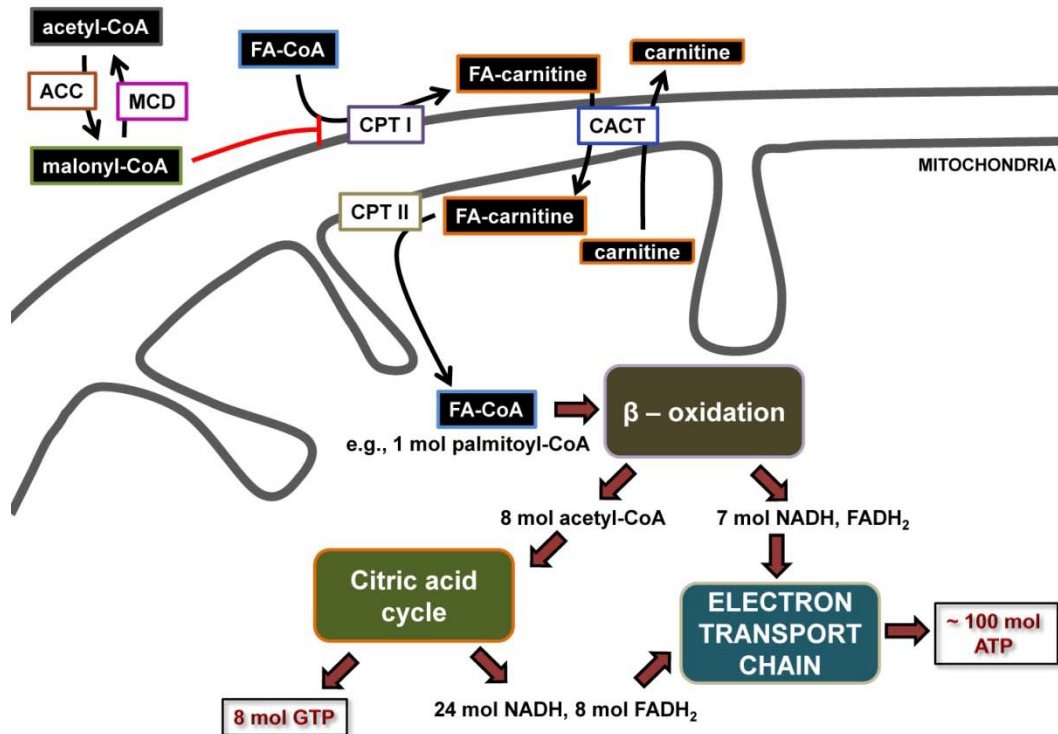
Figure 1.2 FA transport into mitochondria and energy output from β-oxidation. Acyl-CoA esters are converted to acylcarnitines by carnitine palmitoyltransferase I (CPT I) at the outer mitochondrial membrane. CPT I is inhibited by malonyl-CoA synthesized from acetyl-CoA through acetyl-CoA carboxylase (ACC) when the heart is in the fed state and glycolysis is stimulated. Malonyl-CoA decarboxylase (MCD) catalyzes the reverse reaction and can relieve CPT I inhibition. Acylcarnitines are transported across the intermembrane space by carnitine acylcarnitine translocase (CACT) where they are converted back to acyl-CoA esters by CPT II. The acyl-CoA ester can then undergo β-oxidation with the end-products of 8 mol acetyl-CoA, 7 mol NADH and 7 mol FADH$_2$ obtained from 1 mol palmitoyl-CoA. The entry of the 8 mol acetyl-CoA moieties into the citric acid cycle produces 24 mol NADH, 8 mol FADH$_2$ and 8 mol GTP. Finally, the reducing equivalents provided by NADH and FADH$_2$ can produce approximately 100 mol ATP through the electron transport chain from the initial 1 mol palmitoyl-CoA based on a calculated theoretical yield of 2.5 mol ATP from 1 mol NADH and 1.5 mol ATP from 1 mol FADH$_2$.

The acylcarnitine produced by CPT I is transported across the inner mitochondrial membrane by carnitine:acylcarnitine translocase (CACT), followed by its conversion back to acyl-CoA by CPT II (Figure 1.2) (1, 91). In the mitochondrial matrix, acyl-CoA is metabolized through β-oxidation, which consists of the sequential actions of acyl-CoA dehydrogenase, enoyl-CoA hydratase, L-3-hydroxylacyl-CoA dehydrogenase and 3-ketoacyl-CoA thiolase (1, 93). Each cycle results in the hydrolysis of 2 carbons from the acyl-CoA chain and the production of acetyl-CoA, flavin adenine dinucleotide ($FADH_2$) and NADH (Figure 1.2). The enzymes 2,4-dienoyl-CoA reductase and enoyl-CoA isomerase are also important for the conversion of cis double bonds in unsaturated FAs to $trans$ double bonds, which can then be acted upon by enoyl-CoA hydratase in the β-oxidation cycle. Acetyl-CoA is further oxidized in the TCA cycle to yield more $FADH_2$ and NADH, which are subsequently used to produce ATP through oxidative phosphorylation (Figure 1.2).

The coordinated regulation of genes involved in FAO by the peroxisome proliferator-activated receptors (PPARs) and PPAR γ co-activator-1α (PGC-1α) is also important in controlling cardiac FAO [reviewed in (65, 94-97)]. Of the three PPAR isoforms, the role of PPARα in FAO has been the most extensively studied. PPARα is a nuclear receptor that acts in conjunction with PGC-1α to induce the expression of various genes including CD36, FATP1, FABP, MCD, CPT1, medium-chain and long-chain acyl-CoA dehydrogenase with the net outcome of increasing the cellular capacity for FAO (65, 98). Cardiac PPARα activation can also promote the synthesis of cardiolipin (an essential mitochondrial-enriched phospholipid), demonstrating the role of PPARα in maintaining and/or promoting mitochondrial function (99). PGC-1α acts as a

transcriptional co-activator with PPARα as previously mentioned. Furthermore, another protein known as lipin-1 is required to act in combination with PGC-1α and PPARα to induce PPARα target genes at least in the liver (100). Lipin-1 also acts as a phosphatidate phosphatase in glycerolipid synthesis and this function will be discussed in detail later.

PGC-1α can also bind to other nuclear receptors, e.g. estrogen-related receptors and nuclear respiratory factors to induce mitochondrial biogenesis and increase oxidative phosphorylation (94, 96). The importance of PPARα and PGC-1α in cardiac metabolism and function is highlighted by studies in knockout mouse models. Fasting-induced expression of PPARα target genes and rates of FAO were blunted in PPARα knockout mice (23, 101, 102). Furthermore, abnormal changes in mitochondrial architecture and the development of myocardial fibrosis were observed in the PPARα null mice as they aged (101). Predictably, mitochondrial gene expression, oxidative metabolism, response to stimulation and exercise capacity are decreased in PGC-1α knockout mice (103-105).

1.1.6 Fatty acid oxidation in the diabetic heart

As mentioned previously, diabetic hearts rely heavily on FAO for ATP production (36, 63, 106). Increased consumption of oxygen is required to drive β-oxidation resulting in augmented levels of reactive oxygen species, which eventually cause mitochondrial damage (1, 64, 107-111). Thus, this inflexible dependence on one major substrate leads to decreases in cardiac mechanical efficiency and power as well as reduced recovery from ischemia (11, 63, 112, 113). The detrimental effects of increased rates of FAO on cardiac function are also demonstrated by studies on transgenic mice, which overexpress PPARα

13

specifically in the heart. Similar to the phenotype of diabetic hearts, these mice have an increased reliance on FAO concurrent with a decrease in glucose oxidation resulting in cardiac dysfunction (114, 115). In contrast, the major phenotype of transgenic mice with cardiac-specific overexpression of PGC-1α is indicative of the role of PGC-1α in mitochondrial biogenesis. There is excessive mitochondrial proliferation in the hearts of these mice, leading to cardiac hypertrophy, dilated left and right ventricular chambers, decreased cardiac function and premature death (116).

Interestingly, increasing the contribution of glucose oxidation to energy production in hearts after ischemia can improve cardiac function and recovery due to decreased reliance on FAO (7, 19, 112, 117, 118). Additionally, one study showed the beneficial effect of preventing fatty acid uptake by knocking out CD36 in transgenic mice with cardiac-specific overexpression of PGC-1α, thus demonstrating the possibility of targeting cardiac FAO in diabetes (119). Preventing the excessive production of reactive oxygen species could be another option in alleviating the effects of excessive FAO in diabetic hearts (109, 111). Admittedly, it should be clear that targeting cardiac FAO as an intervention in diabetes might only be possible with the use of reversible or partial inhibitors because of the need to maintain flexible substrate utilization in the heart (113, 120, 121).

1.2 The glycerolipid biosynthetic pathway

1.2.1 From the acylation of glycerol 3-phosphate to the formation of triacylglycerol

Besides the utilization of acyl-CoAs in mitochondrial β-oxidation, acyl-CoAs also serve as substrates for glycerolipid synthesis through the Kennedy pathway with the end-products being triacylglycerol (TG) or phospholipids (122, 123). All the enzymes involved in TG synthesis, except the lipins, are integral membrane proteins localized to the ER or the mitochondria (124, 125). Moreover, each step of the TG biosynthetic pathway is catalyzed by multiple enzymatic isoforms, demonstrating the importance of compensatory mechanisms to enable sufficient synthesis of phospholipids for membrane homeostasis as well as to sequester excess FAs into neutral lipid storage.
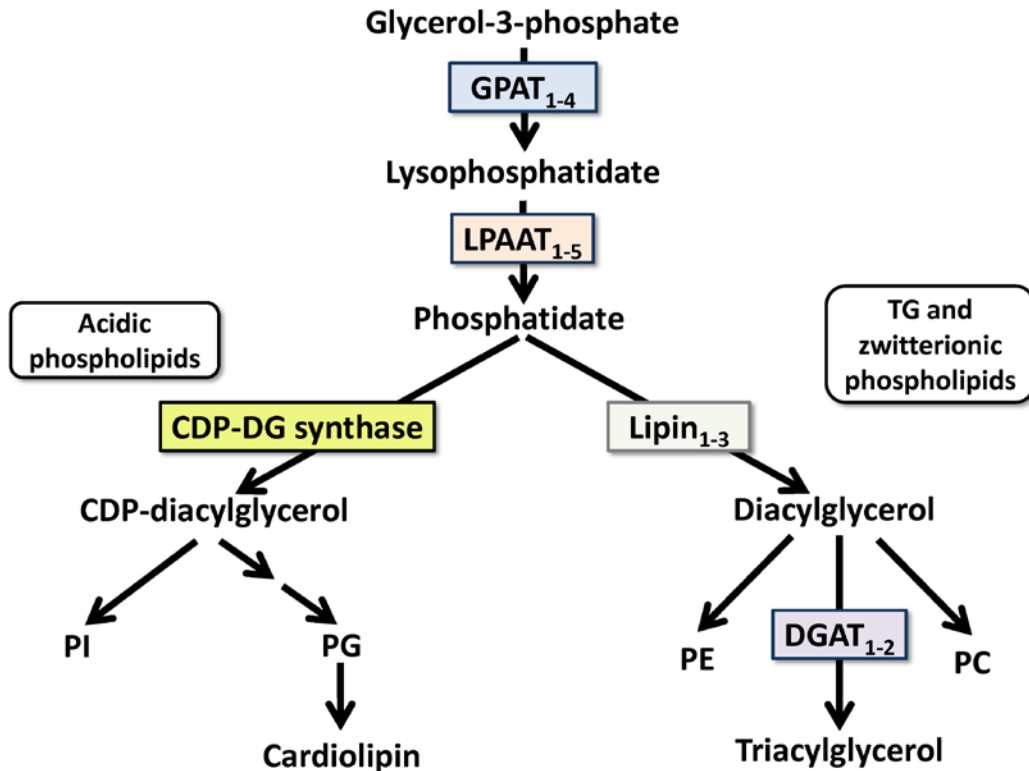
Figure 1.3 The Kennedy pathway for glycerolipid synthesis. Acyl-CoA esters are sequentially incorporated into the *sn*-1 and *sn*-2 positions of glycerol 3-phosphate (G3P) by glycerol 3-phosphate acyltransferases (GPATs) and acylglycerol 3-phosphate acyltransferases (AGPATs) to form lysophosphatidate (LPA) and phosphatidate (PA), respectively. These reactions can be catalyzed by endoplasmic reticulum- and mitochondrial-localized isoforms of GPATs and AGPATs as described in the text. PA is dephosphorylated to diacylglycerol (DG) by membrane-associated lipins after they translocate from the cytosol. Alternatively, PA can serve as the substrate for the synthesis of phosphatidylglycerol (PG), cardiolipin (CL) and phosphatidylinositol (PI). Finally, diacylglycerol acyltransferases (DGATs) can incorporate acyl-CoA into DG to form triacylglycerol (TG). DG is also an essential precursor for phosphatidylcholine (PC) and phosphatidylethanolamine (PE) synthesis.

The first step of the pathway is the acylation of glycerol 3-phosphate (G3P) at the *sn*-1 position by glycerol 3-phosphate acyltransferases (GPATs) to form lysophosphatidate (LPA) (Figure 1.3). The formation of G3P is catalyzed by glycerol 3-phosphate dehydrogenase action on dihydroxyacetone phosphate, which is a metabolite formed during glycolysis (125, 126). Relatively low levels of glycerol kinase in the heart can also phosphorylate glycerol to form G3P (127, 128).

Out of the four GPAT isoforms currently known, GPAT1 is the most extensively studied (129, 130). GPAT1 is localized to the outer mitochondrial membrane and accounts for 30% of the total cardiac GPAT enzymatic activity (131). The importance of GPAT1 to glycerolipid synthesis is highlighted by the observation that hearts from GPAT1 deficient mice were protected from diet-induced TG accumulation compared to controls. However, this phenotype could be partially attributed to lower plasma TG levels and rates of VLDL secretion in the GPAT1 deficient animals (131). Furthermore, palmitate incorporation into phospholipids was decreased in GPAT1 deficient mice with compensatory increases in the utilization of oleate, stearate and arachidonate (131). This result suggests that other GPAT isoforms are compensating for the loss of cardiac GPAT1. The microsomal GPATs (GPAT3 and -4) appear to provide the majority of GPAT enzymatic activity in most tissues except the liver (125). Although the contributions of GPAT3 and -4 to glycerolipid synthesis in adipose tissue and liver have been determined (129, 130), their roles in regulating cardiac glycerolipid metabolism and the effects of GPAT3 and/or -4 deficiencies on cardiac function and metabolism have yet to be elucidated.

Acylglycerol 3-phosphate acyltransferases (AGPATs) catalyze the next step in glycerolipid synthesis, which is the formation of phosphatidate (PA) from LPA (Figure 1.3). There are at least four AGPAT isoforms (AGPAT1, 2, 3, 5) expressed in the mouse heart (132), with the caveat that several putative AGPAT isoforms have not been fully characterized (129). PPARα appears to be an important regulator with cardiac AGPAT activity and the gene expression of AGPAT3 increases when PPARα is activated by clofibrate (132). However, more studies are required since little else is known about AGPATs in the heart.

PA can then be hydrolyzed to diacylglycerol (DG) by the phosphatidate phosphatase (PAP) activities of a family of oligomeric, bifunctional proteins called lipins (lipin-1, -2 and -3) (124, 133-137). As previously mentioned, the lipins also function as transcriptional co-activators with PGC-1α and PPARα in the liver (100, 138). Further details of the roles and regulations of the lipins will be discussed in Section 1.4 onwards.

The final step in the Kennedy pathway for TG synthesis is the conversion of DG to TG by DG acyltransferases (DGAT1 and 2) (Figure 1.3) (139, 140). Both DGATs are found predominantly in the endoplasmic reticulum (140, 141), and they catalyze the formation of TG, which accumulate in lipid droplets (142-144). DGAT1 can also function as an acyl-CoA:retinol acyltransferase to esterify retinol (145, 146), whereas DGAT2 activity is more specific for DG (140). DGAT1 also possesses monoacylglycerol acyltransferase (MGAT) activity to catalyze the formation of DG from monoacylglycerol (MG) (145). Of note, DGAT2 knockout mice are not viable due to impaired TG homeostasis and deficiencies in the permeability barrier of the skin (147). The overexpression of DGAT1 and DGAT2

in various cell types (140) and in mouse models (148-151) leads to increased TG accumulation. Significantly, the consequences of increased TG stores are not detrimental for the most part; instead, DGAT overexpression decreased the levels of potentially toxic lipid metabolites like ceramides and DG (149, 152).

Paradoxically, one study showed that TG accumulation due to overexpressing DGAT2 in glycolytic muscle was accompanied by increased ceramide and DG levels, resulting in insulin resistance (150). This discrepancy can be explained by the lower contribution of FAs as a fuel in the glycolytic muscle compared to the mitochondria-rich heart or soleus muscle. However, it is important to note that the chronic overexpression of DGAT1 in 52-week old mice induces cardiomyopathy, cardiac fibrosis and decreases mitochondrial biogenesis (153).

1.2.2 Lipid accumulation in diabetes

While the consequences of increased FAO on function and metabolism in the diabetic heart are well-characterized, it is important to note that increased cardiac lipid accumulation is an accompanying co-morbidity in many of these diabetic models (154-158). Indeed, FA uptake through CD36 could be an important factor in both increased FAO and lipid accumulation (78, 159). This is because augmented FAO can still be exceeded by increased uptake of FAs and the excess FAs are channeled into glycerolipid synthesis. Cardiac steatosis has been correlated with cardiac dysfunction in several studies, leading to the term "lipotoxic cardiomyopathy" (60, 154, 155, 160).

However, studies in the DGAT transgenic mice show that TG accumulation by itself does not cause a detrimental phenotype (149, 151, 152). Rather, the deleterious effects of lipid accumulation on the heart appear to be mediated by lipid metabolites like ceramides, long-chain acyl-CoAs, and DG, which can strongly influence cardiac signalling and viability (156-158, 161-163). Various studies in cell and mouse models have shown the detrimental effects of DG and ceramide accumulation on insulin signalling, β-adrenergic responsiveness, oxidative stress, mitochondrial function and mechanical efficiency (50, 60, 150, 160, 164-172).

The lipid intermediate PA also serves an important function in various signalling pathways. Intracellular PA accumulation activates numerous downstream targets including protein kinase C-ζ, mTORC1, Sos (Son of sevenless), Raf (Rapidly accelerated fibrosarcoma protein kinase), phospholipase C-γ, sphingosine kinase-1, ERK and nicotinamide adenine dinucleotide phosphate (NADPH) oxidase, which regulate various cellular processes such as cell proliferation, cell growth, cytoskeletal dynamics, and stress response [reviewed in (173-175)]. DG can also act as a signaling lipid to activate novel and classical protein kinase C isoforms, e.g. protein kinase C θ which can phosphorylate and inactivate insulin receptor substrate-1 and impair insulin signaling (176). In fact, increased protein kinase C activation is associated with the development of insulin resistance in diabetes (176).

1.3 Hydrolysis of cardiac triacylglycerol stores

1.3.1 Lipases in the heart

Cardiac TG stores have long been considered as inert lipid droplets; however, it is now quite evident that TG turnover in the heart is rapid and provides a significant source of FAs for ATP production (88-90, 177). Hydrolysis of TG stores is catalyzed by adipose triacylglycerol lipase (ATGL) (87, 178), hormone-sensitive lipase (HSL) (179), TG hydrolase (TGH) (180), and monoacylglycerol (MG) lipase (181). ATGL, in combination with CGI-58 (comparative gene identification-58) (182), catalyzes the first and rate-limiting step in the hydrolysis of TG to DG (Figure 1.4) (87, 178).
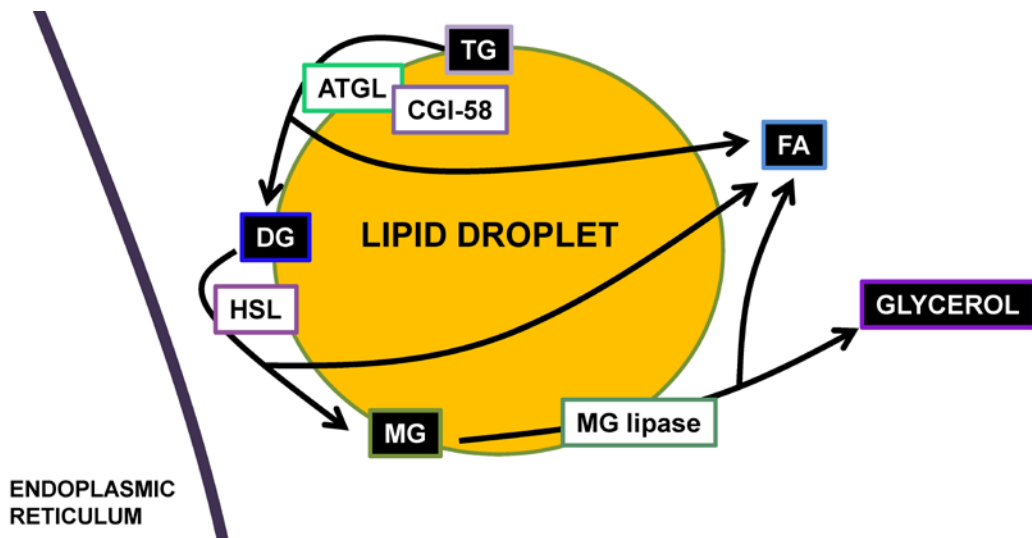
Figure 1.4 TG hydrolysis from lipid droplets. TGs stored in lipid droplets can be hydrolyzed by adipose triacylglycerol lipase (ATGL) in combination with CGI-58 (comparative gene identification-58) to form DG, which is then acted upon by hormone-sensitive lipase (HSL) to form monoacylglycerol (MG). Finally, MG is hydrolyzed by MG lipase to form glycerol. FAs are released from each step of TG hydrolysis and can be used for β-oxidation.

CGI-58 also has a second function as an AGPAT (183, 184). This secondary function as an AGPAT has been linked to the hepatic response to inflammation with CGI-58 required for the formation of PA downstream to activate stress-activated kinases like c-Jun N-terminal kinase 1/2 (JNK1/2) and mammalian target of rapamycin complex 1 (mTORC1) (185). It is possible that CGI-58 might function similarly in the heart.

Mice deficient in ATGL have decreased TG lipolysis and accumulate high levels of TG in most of the organs, especially the heart (87, 186). Additionally, ATGL-mediated lipolysis in the heart releases FAs that act as essential ligands for PPARα activation, which is needed to promote FAO and to maintain mitochondrial function and substrate utilization (86). LPL is critically important in providing the FAs that act as PPARα ligands in the heart as shown by studies using PPARα transgenic/LPL-knockout mice (187). Consequently, the absence of ATGL leads to severe metabolic derangements and cardiomyopathy (86, 87). This finding is recapitulated in human patients with mutations in the human *ATGL* gene (188, 189).

The hydrolysis of DG to MG is catalyzed by HSL (178) (Figure 1.4). The specificity of HSL for DG as a substrate was demonstrated by the elevated levels of DG in the organs of HSL-deficient mice (190). In addition, decreased plasma FA levels and reduced FA flux in the adipose tissue of HSL-knockout mice results in decreased myocardial TG accumulation and improved insulin response after a three-week high fat diet (191, 192). The importance of HSL in regulating cardiac TG stores is highlighted by studies using cardiac-specific HSL transgenic mice. Fasting-induced TG accumulation is blunted in HSL transgenic mice (193).

Similarly, TG accumulation is lower in streptozotocin-induced diabetic mice with HSL overexpression compared to diabetic controls (194). Furthermore, the stimulation of gene expression of PPARα and proteins involved in FA uptake was diminished in the streptozotocin-treated HSL transgenic mice (194). Consequently, there was less myocardial fibrosis and decreased mortality in these mice. Overall, the overexpression of HSL in the heart appears to protect against diabetic cardiomyopathy by modulating the expression of PPARα and its target genes involved in FA uptake.

Cardiac overexpression of ATGL in transgenic mice also produces a similar phenotype whereby TG accumulation is reduced and the expressions of proteins involved in FA uptake and oxidation are decreased (195). In this model, cardiac glucose oxidation is augmented, and cardiac function and exercise performance is enhanced (195). Thus, the forced overexpression of ATGL and HSL appears to induce an inhibitory feedback signal to prevent the uptake of FAs and decrease FAO in favour of glucose utilization. Alternatively, augmented rates of TG hydrolysis in these transgenic mice chronically depletes the cardiac TG pools to such an extent that the release of FAs from these stores does not reach a threshold concentration high enough to activate PPARα and its target genes as put forth by Haemmerle, et al. (86, 195). Future studies will be required to clarify these observations.

Finally, MG lipase hydrolyzes MG to FA and glycerol in the heart (Figure 1.4) (181). Although studies in MG lipase-deficient mice show that MG lipase is important in adipose and hepatic lipolysis and can influence insulin sensitivity under high-fat fed conditions (196), the contribution of MG lipase in the heart is

unknown. MG can also be cycled back to DG by the MGAT activity of DGAT1 (145). It is unlikely that the MGATs themselves would perform this function in hearts since they are predominantly expressed in the small intestine (197) as well as the stomach, kidney, adipose tissue and liver (198). The contribution of TGH to cardiac lipid homeostasis is also unclear. TG hydrolase functions to provide TG for VLDL assembly in hepatocytes (199, 200). Since cardiac lipoprotein secretion has been demonstrated (201, 202), TGH might play a similar role in the heart.

1.3.2 Cardiac lipolysis in the diabetic state

Recent studies have demonstrated the importance of cardiac TG lipolysis in providing significant quantities of FAs for energy production (86-89, 148). Importantly, PPARα appears to be intimately involved in lipolysis since increasing PPARα expression amplifies ATP production from TG-derived FAs (89). Moreover, the release of exogenous FAs from TG stores by ATGL governs the level of PPARα activation and its target genes involved in FAO in the heart (86, 187).

Thus, it could be envisaged that increased TG turnover and ATGL-mediated lipolysis in the heart could exacerbate the dependence on FAO in diabetes and obesity especially since ATGL and HSL activity are positively regulated by β-adrenergic signalling (178). Furthermore, ATGL and HSL expression are increased in streptozotocin-induced diabetes (194).

1.4 Lipins: Phosphatidate phosphatases and transcriptional regulators

1.4.1 Introduction and a historical perspective

The tight and dynamic regulation of FA and lipid metabolism in the heart is clearly required for optimal function and efficiency, as described in the previous sections. The focus will now switch to the characterization of the lipins and their roles in regulating FAO and glycerolipid synthesis.

PAP activity was first characterized and studied in the 1950s with regard to the Kennedy pathway for glycerolipid biosynthesis, which was described in Section 1.2 (123, 203, 204). PAP activity catalyzes the conversion of PA to DG (Figure 1.3) (133, 205). The balance between PA and DG levels represents an important branch-point in phospholipid synthesis. PA is used as the substrate for the synthesis of phosphatidylinositol (PI), phosphatidylglycerol (PG), and cardiolipin (CL), whereas DG is the precursor required for the formation of TG, phosphatidylcholine (PC) and phosphatidylethanolamine (PE) (Figure 1.3) (124, 133, 206, 207).

Early studies measured a PAP activity that was localized to microsomal membranes. It was natural to expect that the PAP activity would be located in these membranes since the majority of the enzymes in the Kennedy pathway of glycerolipid synthesis are localized to the endoplasmic reticulum and, to some extent, mitochondrial membranes. However, there was surprisingly low TG synthesis when microsomal fractions were subjected to *in vitro* assays using glycerol 3-phosphate and fatty acids as substrates (208-210). Instead, TG synthesis was stimulated when the cytosolic fraction was added to the assay and

it was noted that one of the stimulating factors was heat-labile (210, 211). Subsequent studies demonstrated that this cytosolic factor was a soluble PAP enzyme (208, 209), which provides the major activity responsible for catalyzing the production of DG required for glycerolipid biosynthesis (203).

This finding was unexpected because of the membrane-bound PAP activity, which could readily convert PA to DG and no one before had measured detectable levels of cytosolic PAP activity. This discrepancy can be attributed to the substrate used in the *in vitro* assays for measuring PAP activity in the late 1950s and early 1960s (212). PA was often synthesized by hydrolyzing egg PC using a plant phospholipase D with high concentrations of Ca^{2+} to stimulate this activity. Therefore, PA isolated from this reaction was chelated strongly with Ca^{2+}, and was very difficult to displace. The Ca^{2+}-salt form of PA is a poor substrate for the cytosolic PAP activity, whereas most of the membrane-bound PAP could readily act upon this substrate (213).

It was later shown that the membrane-bound PAP activity was probably catalyzed by Mg^{2+}-independent Type 2 phosphatidate phosphatases (PAP-2) (213), which are now called lipid phosphate phosphatases (LPPs) (214). The enzymes were renamed LPPs because of their promiscuous activity against various lipid phosphates, including ceramide-1-phosphate (C1P), LPA and sphingosine-1-phosphate (S1P) (215, 216). Research in the 1990s showed that the endoplasmic reticulum was not the major location of LPP activity, but rather that it is found to a large extent in the plasma membrane (213, 217). This location indicated that the LPPs are unlikely to participate in the glycerolipid biosynthesis pathway and it was suggested that they probably regulate cell signalling (213).

Conversely, the cytosolic PAP activity, which was described at the time as Mg^{2+}-dependent Type 1 phosphatidate phosphatase (PAP-1), showed the properties and regulation expected of an enzyme involved in glycerolipid synthesis (203, 209, 218).

The importance of PAP in metabolism is highlighted by the dynamic regulation of this activity in various metabolic states. PAP activity in the liver is increased in diabetes, stress, hypoxia, alcoholic liver disease and during starvation (219-223). All of these conditions result in the increased supply of excess FAs from the plasma, which may exceed the requirements of various organs for β-oxidation (133). The increased expression of PAP activity in these conditions was shown to depend on the release of glucocorticoids as a part of the animal's stress response (224). Subsequent studies with cultured hepatocytes confirmed the role of glucocorticoids and showed that glucagon through cyclic adenosine monophosphate (cAMP) amplified this effect (225, 226). Conversely, insulin antagonized the effects of both glucocorticoids and cAMP. This profile of hormonal regulation resembles that of several enzymes involved in regulating gluconeogenesis and amino acid catabolism (226), and is compatible with the increases in hepatic PAP activity seen in starvation and diabetes. The increased PAP activity in the liver probably provides an increased capacity to sequester excess FAs that are mobilized from adipose tissue in these conditions (173, 227).

Although much of the importance and regulation of glycerolipid metabolism by PAP was elucidated in these early years, further detailed mechanistic studies were not forthcoming due to the difficulty in purifying the enzyme and identifying the gene(s) responsible for encoding the PAP(s). The

identity of the PAP enzyme remained a mystery until Han et al. (135) identified the yeast orthologue of PAP in 2006. These authors showed that a mammalian family of proteins known as lipins were related structurally to the yeast enzyme and that mammalian lipin-1 exhibits PAP activity (135).

Each of the three members of this family, lipin-1B, -1A (a splice variant of the *Lpin1* gene), -2 and -3, were demonstrated to possess PA-specific and Mg^{2+}-dependent PAP activities (134). It should be noted that lipin-1A and -1B were initially described to have unique subcellular localizations (228). However, numerous studies have now shown that the lipins can translocate to their sites of action and perform similar functions (229-232). A subsequent study identified a third splice variant of lipin-1, which is called lipin-1γ. This form is enriched in the brain and its specific PAP activity is lower than lipin-1A and -1B (137, 233). Lipin-1B and -1γ have additional amino acids insertions that differentiate these splice variants from lipin-1A (137, 228). Relatively little is known about the alternative splicing of the *Lpin1* gene, however, it has been shown that downregulation of a splicing factor SFRS10 (splicing factor, arginine/serine-rich 10) leads to increased lipin-1B expression (234).

1.4.2 The fatty liver dystrophy (*fld*) mice and the subsequent discovery of the lipins

Lipins were originally identified by positional cloning of lipin-1 in the fatty liver dystrophy (*fld*) mutant mouse strain (235). The *fld* mice were derived from a spontaneously occurring mutation in a mouse colony from Jackson Laboratories in 1988 (236). These mice are characterized by having a fatty liver and

hypertriglyceridemia in the pre-weaning period when they are consuming a relatively high fat diet through the milk (236). The most obvious phenotype of these mice is the complete lack of mature adipose tissue (237), and consequently, there is decreased circulating levels of adipokines such as adiponectin and leptin (235, 238). The *fld* mouse is also insulin resistant and is prone to developing atherosclerosis when fed a high cholesterol/cholate diet (237, 238). Lastly, the *fld* mice develop peripheral neuropathy due to demyelination in Schwann cells through aberrant ERK1/2 activation (239, 240).

The identity of the gene responsible for the *fld* mutation was not discovered until 2001 when Peterfy et al. showed that the *fld* phenotype can be ascribed to homozygous recessive mutant alleles of the *Lpin1* gene, which expresses three splice variants (235). The other two members of the lipin family, lipin-2 and -3 were shown to be related to lipin-1 by sequence comparison especially in two conserved regions called the N- and C- terminal lipin domains (NLIP and CLIP) respectively (Figure 1.5) (235). Further research showed that the lipins can also act as transcriptional regulators involved in processes such as adipogenesis and fatty acid oxidation (100, 138, 228).
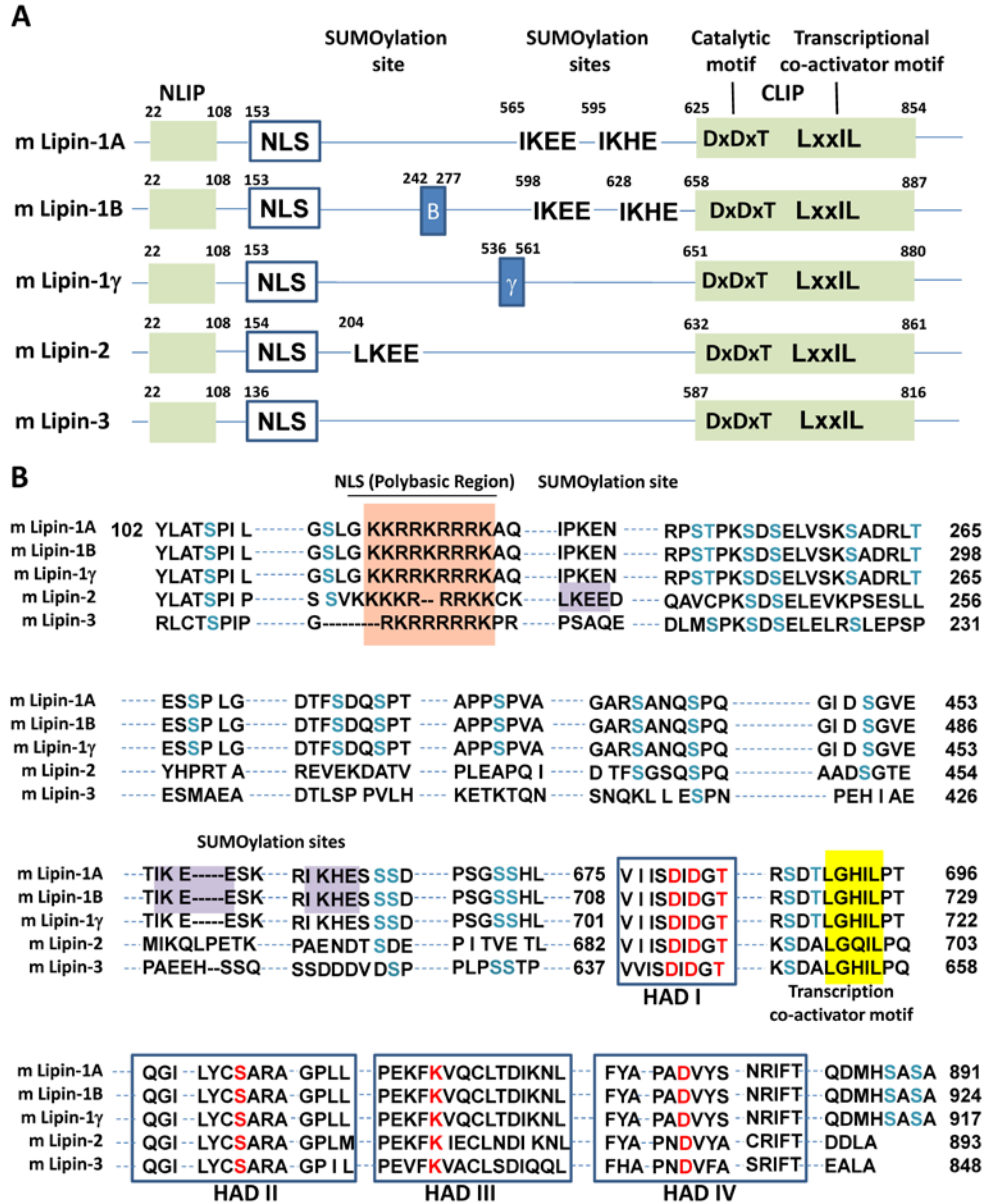
Figure 1.5 Schematic representation and sequence alignment of mouse lipin isoforms. (A) The conserved N- and C-terminal lipin (NLIP and CLIP) domains and nuclear localization sequence (NLS) in the mouse lipins are shown. Numbers indicate residue numbers. Lipin-1 is SUMOylated at the indicated amino acid residues and the putative SUMOylation site on lipin-2 is also shown. Lipin-1B and -1γ have unique amino acid insertions that differentiate these splice variants from lipin-1A as indicated by the blue regions. **(B)** Multiple sequence alignment of protein sequences from mouse lipin isoforms made using Clustal W2. Numbers indicate residue numbers. The polybasic nuclear localization sequence (NLS) is highlighted in red. The haloacid dehalogenase (HAD) domains I to IV are shown and the SUMOylation sites are highlighted in gray. The DxDxT catalytic motif and the other residues involved in the active site are indicated in red lettering, and the conservation of phosphorylation sites is indicated in blue.

1.4.3 The involvement of lipins in glycerolipid synthesis through their phosphatidate phosphatase activities

As mentioned previously, the PAP activity of the lipins is responsible for converting PA to DG in the Kennedy pathway of glycerolipid synthesis (134, 135, 241-244). Each step of the pathway is catalyzed by multiple enzymatic isoforms, which are all membrane-bound, except for the cytosolic lipins. The lipins are differentially expressed depending on the tissue type (134, 138). There appears to be some level of redundancy since the absence of one lipin isoform can, to some extent, be compensated for by the other lipins (243). The major lipin isoform in the adipose tissue, skeletal muscle and heart appears to be lipin-1 (134, 241). Lipin-2 is highly enriched in the liver, red blood cells, and specific regions of the brain (138) whereas lipin-3 appears to be highly expressed in the intestine (134).

1.4.4 The roles of PAP activity in yeast and plants

In *Saccharomyces cerevisiae,* where there is only one lipin isoform, Pah1p (lipin yeast homologue also known as Smp2) deficiency leads to aberrant changes in phospholipid species as well as decreased esterification of FA in the stationary phase and the subsequent induction of cytotoxicity caused by FA accumulation (245). Pah1p also regulates nuclear membrane growth in cell division since loss of Pah1p leads to increased nuclear membrane size, whereas expression of non-phosphorylable Pah1p inhibits cell division (246). Lipid droplet formation is also regulated by Pah1p since decreasing Pah1p expression results in decreased lipid droplet biogenesis (247). However, the neutral lipid levels themselves are unchanged; instead, there is aberrant lipid accumulation at the

endoplasmic reticulum. The authors also showed that this phenotype can be abrogated by knocking out DG kinase-1 (247). The study concluded that DG formed by Pah1p activity is required for normal lipid droplet formation (247).

The regulation of PA levels in *S. cerevisiae* by yeast lipin Pah1p also appears to control Opi1p-dependent and Opi1-independent repression of genes encoding enzymes involved in phospholipid synthesis (246, 248, 249). Opi1p binds to PA at the endoplasmic reticulum. When PA levels are low, Opi1p translocates to the nucleus where it acts as a transcriptional repressor of phospholipid biosynthesis (250). These results indicate the importance of PAP activity in controlling phospholipid synthesis and sequestering FAs into TG storage. Similar studies in *Caenorhabditis elegans* demonstrate the role of its lipin homologue in regulating endoplasmic reticulum membrane homeostasis as well as dictating the dynamic regulation of nuclear envelope assembly and disassembly (251, 252).

Furthermore, the lipin homologues of *Arabidopsis thaliana* are essential for phospholipid remodelling to galactolipids, which is a mechanism designed to cope with phosphate starvation (253). While studies in *Saccharomyces cerevisiae* and *Caenorhabditis elegans* show that their lipin homologues are critically important in nuclear membrane maintenance and regulation of phospholipid synthesis, there is no direct evidence for this occurring in mammalian cells. One recent study did show that accumulation of lipin-1 in the nucleus modifies the shape of the nuclear membrane and this is dependent on its PAP activity (229).

1.4.5 Domain structure of the phosphatidate phosphatase enzymes

The PAP activity of all mammalian lipins as well as the non-mammalian lipin homologues depends on a conserved C-terminus domain (CLIP) with sequence homology to the catalytic domain of the Haloacid Dehalogenase (HAD) superfamily (Figure 1.5B) (254, 255). The catalytic DxDxT motif (where D and T represent aspartate and threonine respectively and x represents any amino acid) (133, 135) is present in all HAD-like domains (Figure 1.5), together with a characteristic and conserved sequence of α-helices and β-sheets (138, 255).

Mutation of either of the catalytic aspartate residues to glutamate results in the complete loss of PAP activity for lipin-1 and lipin-2 (138, 256). The NLIP (N-terminal lipin) domain is also essential for PAP activity (241), although little is known about the role of this domain in the active site due to the lack of a crystal structure. A point mutation of Gly84 to Arg in the NLIP domain of lipin-1 in the fld^{2J} mouse is associated with decreased PAP activity and increased lipodystrophy in these animals (129, 256).

Based on the secondary structure comparison to related members of the HAD-superfamily, four conserved HAD motifs are predicted to be important for PAP function (Figure 1.5B) (138, 255). Motif I consists of a β-strand followed by the DxDxT motif while motif II consists of a β-sheet flanked by two α-helices. A highly conserved serine or threonine residue at the end of the β-strand of motif II appears to help in the stabilization of reaction intermediates in the catalytic site (Figure 1.5B) (255). A conserved lysine residue in the α-helix of motif III also participates in coordination and stabilization of the substrate (Figure 1.5B). Motif IV consists of an α-helix flanked by two β-strands. A conserved acidic residue at

33

the end of the first β-strand of motif IV is thought to be involved in coordinating the Mg^{2+} ion along with the acidic residues in domain I (Figure 1.5B); other HAD family members possess two acidic residues in motif IV (255).

A recessive allele in the rat, which results from a mutation in the HAD motif IV, leads to a complete loss of PAP activity, and is associated with neuropathy and lipodystrophy as in the *fld* mice (257). *Lpin1²⁰⁸⁸⁴* (²⁰⁸⁸⁴ denotes the mutant mouse line) is a partial loss-of-function allele where a tyrosine residue at position 873 on lipin-1B is mutated to an asparagine, resulting in a significant reduction in PAP activity (258). Expression of this lipin-1 allele together with a truncation mutation in the gene that encodes the neuronal cell adhesion molecule, *Nrcam²⁰⁸⁸⁴*, acts synergistically to produce severe peripheral neuropathy and hind limb paralysis in mice (258). Additionally, a rare autosomal recessive disease called Majeed syndrome (259) is caused by a mutation of the conserved serine residue of motif II in the CLIP domain of lipin-2, which leads to an absolute loss of PAP activity (138). Mutation of the equivalent serine in mouse lipin-1 (138) and in plant lipins (260) also leads to the loss of PAP activity.

1.4.6 Regulation of phosphatidate phosphatase activity

As mentioned previously, the LPPs can act against various lipid substrates whereas the lipins show a specific requirement for PA as a substrate (129, 173). PAP activity assays of the mammalian lipins show that they do not dephosphorylate LPA, S1P, or C1P, and Pah1p in yeast does not show catalytic activity towards diacylglycerol pyrophosphate (134, 135). The PAP activity of the mammalian lipins depends on Mg^{2+} and it can be inhibited by the alkylating reagent, N-ethyl maleimide (129, 137). Furthermore, Mn^{2+} ions also have a

concentration-dependent effect on the stimulation of PAP activity in the human lipin-1A, -1B, and –1γ isoforms *in vitro* (137). It should also be noted that the specific PAP activity of lipin-1A and -1B *in vitro* is higher than that of lipin-2 or lipin-3 (261). The lipin-1 isoforms show little preference with regards to the species of the acyl chains at the *sn*-1 and *sn*-2 positions of PA when assayed in mixed PA/Triton X-100 micelles with the exception of dipalmitoyl-PA and distearoyl-PA, which are poor substrates in the PAP reaction (137). The basic requirement is that at least one unsaturated fatty acyl moiety is needed for maximum activity.

Both the mammalian lipins and yeast Pah1p demonstrate surface dilution kinetics (137, 262). PAP activity is reduced in a dose-dependent manner when the surface concentration of PA is decreased in Triton-X-100/PA micelles (137, 173). The lipin proteins can assemble into homo- and hetero-oligomers (136). However, catalytic activity does not depend on the oligomerization state since oligomers of wildtype lipin-1 with catalytically inactive lipin mutants are not inhibited with each subunit possessing its own independent activity (136). It was suggested from studies in yeast Pah1p and mammalian lipins that PA binds allosterically and activates catalytic activity against PA in the active site due to positive cooperative kinetics in the surface dilution model (134, 173, 263, 264). This result is supported by the presence of a polybasic region in lipin-1 (Figure 1.5), which dictates association with PA secondary to the active site and also acts as a nuclear localization sequence (NLS) (231).

As indicated by work performed before the lipins were discovered, the sphingoid bases sphingosine and sphinganine, which are amphiphilic amines,

inhibit the PAP activity of the lipins (137, 263, 265). Moreover, Zn^{2+} or Ca^{2+}salts of PA can also inhibit PAP activity (137, 212). In general, phosphorylation of mammalian lipin-1 does not affect the PAP activity as measured *in vitro*, but it does control subcellular localization and thus physiological activity (229, 241) as will be discussed below in Section 1.5.1.

1.4.7 Lipins as transcriptional regulators

Mammalian lipins contain a polybasic nuclear localization sequence (Figure 1.5), which enables them to translocate to the nucleus where they promote the transcription of genes required for fatty acid uptake and oxidation (133, 138, 231). In hepatocytes, lipin-1 acts in concert with peroxisome proliferator activated receptor-γ coactivator-1α (PGC-1α) to increase the expression of the nuclear receptor peroxisome proliferator-activated receptor (PPARα) and its target genes (Figure 1.6) (133).
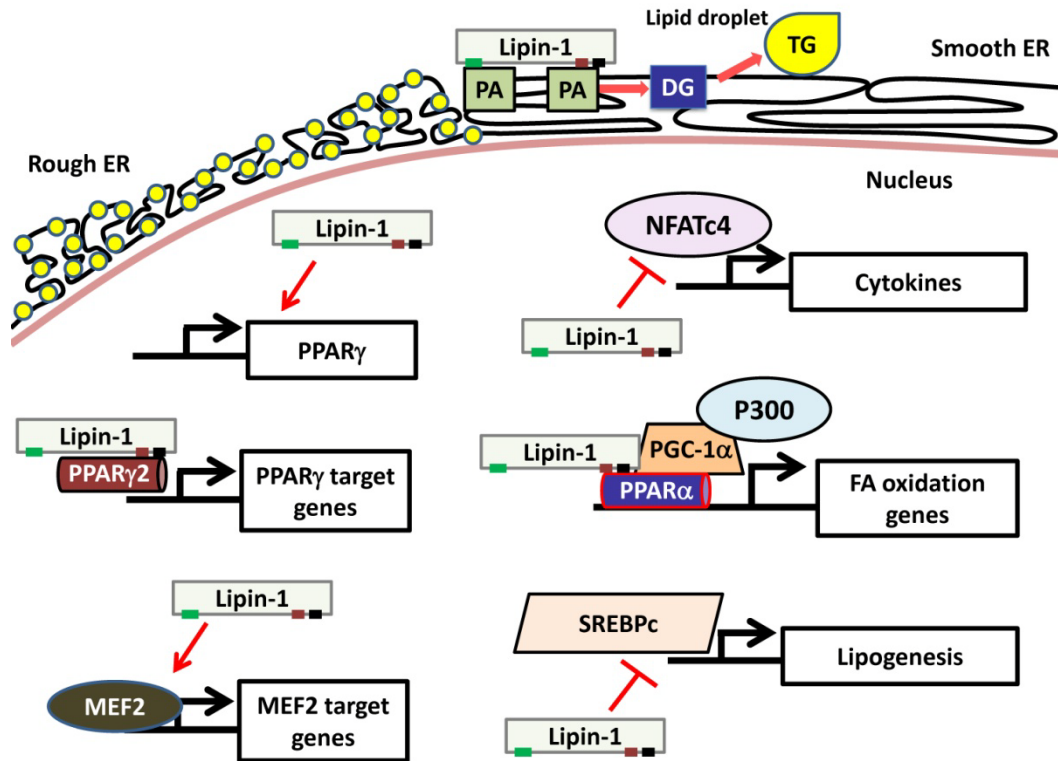
Figure 1.6 Lipin-1 as a transcriptional regulator. Lipin-1 associates with PPARα and PGC-1α in the nucleus of hepatocytes to promote genes involved in fatty acid (FA) oxidation. The green box denotes the nuclear localization sequence whereas the brown and black boxes represent the catalytic phosphatidate phosphatase motif and the transcriptional co-activator motif, respectively. Lipin-1 can also act to repress cleaved sterol regulatory element binding protein (SREBP) localization in the nucleus and prevent the induction of the genes regulated by SREBP. Lipin-1 nuclear localization can also interact with and activate myocyte enhancement factor-2A and C. In adipocytes, lipin-1 can inhibit nuclear factor of activated transcription c4 (NFATc4), thus repressing cytokine signalling. Lipin-1 is also critical in inducing PPARγ expression in adipocyte differentiation. PPARγ2 can also interact with lipin-1 to induce its target genes, e.g. phosphoenol pyruvate carboxykinase, which is involved in glyceroneogenesis. Abbreviations: DG, diacylglycerol; ER, endoplasmic reticulum; PA, phosphatidate; PPAR, peroxisome proliferator-activated receptor; PGC-1α, peroxisome proliferator-activated receptor gamma coactivator-1α; TG, triacylglycerol.

In fasting, lipin-1 gene expression in mouse liver is activated by PGC-1α (100). It has also been shown that estrogen-related receptor α (ERRα) and ERRγ are required for the action of PGC-1α on lipin-1 gene induction in the heart (266). Lipin-1 appears to form a complex with PGC-1α and PPARα (100), which bind to PPARα response elements (PPRE) at the promoters of PPARα target genes such as carnitine palmitoyl transferase 1 (*Cpt1*) and acyl-CoA oxidase 1 (*Aox1*) (100, 261). Since lipin-1 contains no DNA-binding motifs, the association between lipin and the PPARα promoter is probably through the association of lipin-1 with the transcriptional activating complex (261). Lipin-1, -2 and -3 each contain a hydrophobic α-helical LxxIL motif that resembles a nuclear receptor interaction motif in the conserved CLIP domain (Figure 1.5) (100, 267). Experiments using site-directed mutagenesis demonstrated that the LxxIL motif is required for lipin-1 to interact with PGC-1α and PPARα (100). Lipin-2 can also act as a transcriptional co-activator with PGC-1α and PPARα as demonstrated *in vitro* (138).

Lipin-1 is also required to induce the expression of PPARγ during adipogenesis (Figure 1.6) (268). Furthermore, lipin-1 directly binds to and activates PPARγ$_2$ in mature adipocytes (Figure 1.6) (269). Lipin-1A and -1B expression are differentially regulated during adipocyte differentiation. Lipin-1A is most prominently expressed in the early stages when PPARγ is activated, which subsequently drives adipocyte differentiation. Following this, lipin-1B expression is induced in the latter phases of adipocyte differentiation (228). Rosiglitazone, which is a PPARγ agonist, also increases lipin-1 expression in subcutaneous fat depots and to a lesser extent in visceral fat (270). This preferential increase in

lipin-1 expression could divert FA esterification and deposition to peripheral rather than visceral fat. This effect on body fat distribution could contribute to the action of Rosiglitazone in promoting insulin sensitivity.

The requirement of lipin-1 for pre-adipocyte differentiation is demonstrated by the lack of mature adipose tissue in lipin-1 deficient (*fld*) mice (235, 237). Interestingly, lipin-1 deficient children do not develop lipodystrophy, as will be discussed below (271). The high expression of lipin-2 mRNA levels in human adipose tissue could possibly substitute for the transcriptional functions of lipin-1 as opposed to the minimal lipin-2 expression in mouse adipose tissue.

Lipin-1 and lipin-2 can also inhibit the transcriptional activity of the nuclear factor of activated T cells 4 (NFATc4) (Figure 1.6) (272). This repression appears to be required for inhibition of the expression of cytokines and other inflammatory factors (272-274). Conversely, TNFα signalling inhibits lipin-1 gene expression in 3T3-L1 adipocytes (275). Lipin-1 localization to the nucleus is also required to promote the transcriptional activity of myocyte-enhancer factor 2 (MEF2), a transcription factor that regulates neuronal survival and differentiation (Figure 1.6) (276). Of the four isoforms of MEF2, lipin-1 can interact with and activate MEF2A and MEF2C, although interaction with the other MEF2 isoforms cannot be ruled out (276).

1.4.8 Lipin-deficient and transgenic overexpressing mouse models

Besides determining the functions of lipins in cell systems, the influence of lipins on metabolism has also been investigated using animal models that are either deficient in lipin expression or which overexpress different lipin isoforms.

Aberrant changes in the expressions of the lipins have been shown to be detrimental to glucose and fatty acid metabolism. For example, diurnal variations in fuel utilization are blunted in the *fld* mice with decreased FA oxidation in the fasted state and decreased glucose oxidation in the fed state compared to wildtype mice as measured by respiratory quotient (277). However, it is probable that these aberrant changes are a result of the systemic effects of whole body lipin-1 deficiency such as lipodystrophy and insulin resistance (237, 238, 277, 278). The lack of adipose tissue in *fld* mice also impairs liver regeneration since lipolysis from adipose tissue stores provides a major energy source during the regenerative process (238). Moreover, large increases in PAP activity (presumably through the effect of glucocorticoids in increasing lipin-1 expression, which will be discussed in Section 1.5.2) normally accompany liver regeneration (279).

On the other hand, the specific overexpression of lipin-1 in mouse skeletal muscle leads to TG accumulation and insulin resistance (278). Adipose TG accumulation is also increased when lipin-1 is overexpressed specifically in the adipose tissue; however, these transgenic mice had improved insulin sensitivity (278). This is probably caused by increased sequestration of FA in adipose tissue TG, which decreases FA-induced insulin resistance in other organs. Increased lipin-2 expression in the liver regulates hepatic insulin responses, e.g. induction of lipin-2 expression by feeding mice a high-fat diet or by the use of agents that promote endoplasmic reticulum stress leads to decreased insulin-stimulated signalling (280).

1.4.9 Lipins: Redundancy, compensation and Selective Functions

The lipin isoforms show redundancy and overlapping functions in some tissues. Depletion of lipin-1 by siRNA (small interfering ribonucleic acid) in human monocyte-derived macrophages did not decrease the formation of TG although the composition of TG in lipid droplets was altered (281). In liver, depletion of lipin-1 does not affect TG synthesis because of the abundant levels of lipin-2 (243, 282). Similarly, lipin-3 expression has been demonstrated to compensate for the loss of lipin-1 in the livers of *fld* mice (134). PAP activity in hepatoma cells was not reduced when lipin-1 was knocked down and this effect was likely due to the expression of lipin-2 and lipin-3 in these cells (242).

Studies of lipin-2 deficient Majeed Syndrome patients, who present a severe disease phenotype including congenital dyserythropoietic anemia, extensive osteomyelitis and recurrent high fever, demonstrate that lipin-1 and lipin-3 do not compensate completely for the loss of lipin-2 activity in some tissues (259, 283, 284). Additionally, rare cases of lipin-1 deficiency have been reported in children and this condition is associated with rhabdomyolysis and myoglobinuria leading to premature mortality, suggesting a unique role in skeletal muscle maintenance (271). These children do not show defects in adipose tissue formation unlike the lipodystrophic *fld* mice (271). Lipin-2 is expressed at significant levels in human adipose tissue and it is possible that lipin-2 may be able to compensate for the functions of lipin-1 in human adipose tissue (134, 173).

Conversely, lipin-2 mRNA levels are virtually undetectable in mouse adipose tissue (134). Therefore, the lipodystrophy in the lipin-1 deficient *fld* mice

demonstrates the lack of compensation by lipin-2 or -3. However, overexpressing wildtype lipin-1, -2 or -3 in *fld* mouse embryonic fibroblasts enables the differentiation of these cells into adipocytes (230). This result demonstrates that the lack of compensation by the other lipin isoforms could be occurring because the levels of expression of these lipins are not high enough.

Further studies will determine whether each lipin isoform has unique functions or characteristics. Alternatively, it is likely that the main difference between lipin isoforms is the regulation of their subcellular localization and expression since the lipins share similar functional capabilities from the studies performed so far (134, 138, 230).

1.4.10 Known and putative roles of lipins in lipid signalling

Lipin-1 is demonstrated to play a role in lipid signalling during the process of myelination in Schwann cells (240). As mentioned previously, *fld* mice exhibit progressive peripheral neuropathy in addition to lipodystrophy and insulin resistance (235). PA accumulates in the endoneurium of Schwann cells from these mice as a result of the loss of lipin-1 (240). This accumulation of PA leads to the aberrant activation of mitogen-activated protein kinase/ extracellular signal-regulated kinase kinase (MEK) and extracellular signal-regulated kinase 1/2 (ERK1/2), which was shown to be associated with demyelination of the Schwann cells (240). Treatment of myelinated ganglia cultured from rat embryos with PA caused demyelination, whereas treatment with MEK-ERK1/2 inhibitors PD98059 or U0126 restored myelination of ganglia (240). Thus, lipin-1 appears to dephosphorylate the specific pool of PA that acts as a bioactive signal to activate

the MEK-ERK1/2 pathway. Loss of lipin-1 thereby leads to the inhibition of myelination signalling pathways in Schwann cells (173, 240).

The aberrant activation of ERK1/2 by PA accumulation is also responsible for inhibiting PPARγ activation in the absence of lipin-1 during adipogenesis (230). The authors showed that relieving the inhibition of PPARγ activation by ERK1/2 was dependent on PAP activity and overexpressing any lipin isoform was able to rescue this phenotype. In human tissues, lipin-1 may also play a role in regulating the cellular levels of the bioactive lipids PA and DG since an accumulation of PA was reported as a result of lipin-1 deficiency in skeletal muscle, but this was from only one patient (271).

Other evidence that the lipins could be involved in receptor-mediated signal transduction emerged from early studies on signalling through the epidermal growth factor receptor (EGFR) (285). PAP activity was proposed to be regulated by association with EGF signalling in A431 cells since PAP activity was co-immunoprecipitated with the EGFR (286). Treatment with EGF decreased the association of PAP activity with the EGFR and simultaneously increased association with protein kinase C-ε (PKCε) (286).

DG is a bioactive lipid and plays a role in stimulating inflammatory responses in immune cells (287). PAP has been proposed to play a role in immune signalling through DG production (287). Stimulation of the inflammatory response in RAW 264.7 and U937 macrophages with lipopolysaccharide leads to a transient increase in cellular DG levels with a concomitant decrease in cytosolic

PAP activity (287). This result suggested that PAP activity translocated onto membranes and catalyzed the hydrolysis of PA to form DG , which can then activate PKC and downstream inflammatory signalling such as group IVA phospholipase A_2 and increased COX-2 (cyclooxygenase-2) gene expression (288, 289). Corroborating evidence is provided by a recent study showing that decreasing lipin-1 expression with siRNA in human macrophages decreases group IVA phospholipase A_2 activation (281).

The PA substrate acted upon by PAP in this signalling pathway appears to be generated from phospholipase D (PLD)-dependent hydrolysis of phosphatidylcholine (290, 291). Moreover, treatment of adipocytes with the dual PLD1/PLD2 inhibitor FIPI promotes lipin-1 localization to the nucleus, which suggests that PA produced through PLD activation could regulate the subcellular localization of lipin-1 (231). Collectively, these studies provide evidence that the lipins are involved in signal transduction pathways.

1.5 Regulation of lipin compartmentalization and expression

The importance of lipins in regulating cellular metabolism and signalling is highlighted by the dynamic regulation of their subcellular localization as well as gene expression. The control of the subcellular localization of lipins is important for dictating their participation in glycerolipid synthesis and transcriptional regulation. Lipin-1 and -2 are present in the cytosol and they translocate to the endoplasmic reticulum and the nucleus (133, 138, 241, 292).

1.5.1 Lipins and their subcellular localization

Studies in the 1980s first characterized the translocation of the cytosolic PAP onto the endoplasmic reticulum where it could act in the glycerolipid biosynthesis pathway (293). This translocation was stimulated by unsaturated FAs, acyl-CoA esters and phosphatidate (294, 295). Saturated FAs, such as palmitate, had relatively less effect than unsaturated FAs in cell-free systems and intact hepatocytes (294-296). These are all anionic amphiphiles and the results suggest that increased negative charge on membranes is a component in the binding of the soluble PAP (224). It was proposed from this combined work on the translocation of PAP to membranes that the cytosolic pool of PAP acts as a reservoir of enzyme activity. This reservoir provides the capacity to respond to an increased FA load by recruiting PAP to the site where PA is produced and therefore stimulating the sequestration of FAs in TG.

Conversely, treating the microsomal membranes with a variety of cationic amphiphilic drugs blocked PAP activity and also the binding of PAP to emulsions of PA (297). The potency of these cationic amphiphiles was proportional to their oil/water partition coefficients (265). This indicates that the displacement of PAP from the membranes depends on the partitioning of the cations into the membranes and the acquisition of a positive charge on the membrane surface. The importance of this displacement of PAP from membranes was demonstrated in rat hepatocytes incubated with different concentrations of the cationic amphiphile, chlorpromazine (298). The displacement of membrane-bound PAP by chlorpromazine is paralleled by a decrease in the conversion of PA to DG and decreases in the synthesis of TG and PC. The effects of cationic drugs in blocking PAP activity and in stimulating the activity of CDP-DG (cytidine

diphosphate-diacylglycerol) synthase cause the diversion of glycerolipid synthesis towards the production of acidic phospholipids (Figure 1.3) (299). It was proposed that these combined actions explain why amphiphilic cationic drugs have the side-effect of producing a phospholipidosis that is characterized by the accumulation of acidic phospholipids in lysosomes (300).

As predicted from early studies, the association of PAP with membranes is also regulated by phosphorylation of the PAP enzyme (301). Lipin-1 has at least 17 serine/threonine residues, which are phosphorylated (Figure 1.5) (241, 302). From sequence homology analysis of these 17 residues, 8 homologous residues in lipin-2 and 10 residues in lipin-3 are similarly predicted to be phosphorylation sites (241). Insulin stimulates the hyperphosphorylation of lipin-1, which increases its cytosolic localization (Figure 1.7) (241). Conversely, unsaturated fatty acids and phosphatidate promote the binding of lipins to membranes (Figure 1.7) (138, 231, 241), as expected from the experiments performed in the 1980s (296, 303).
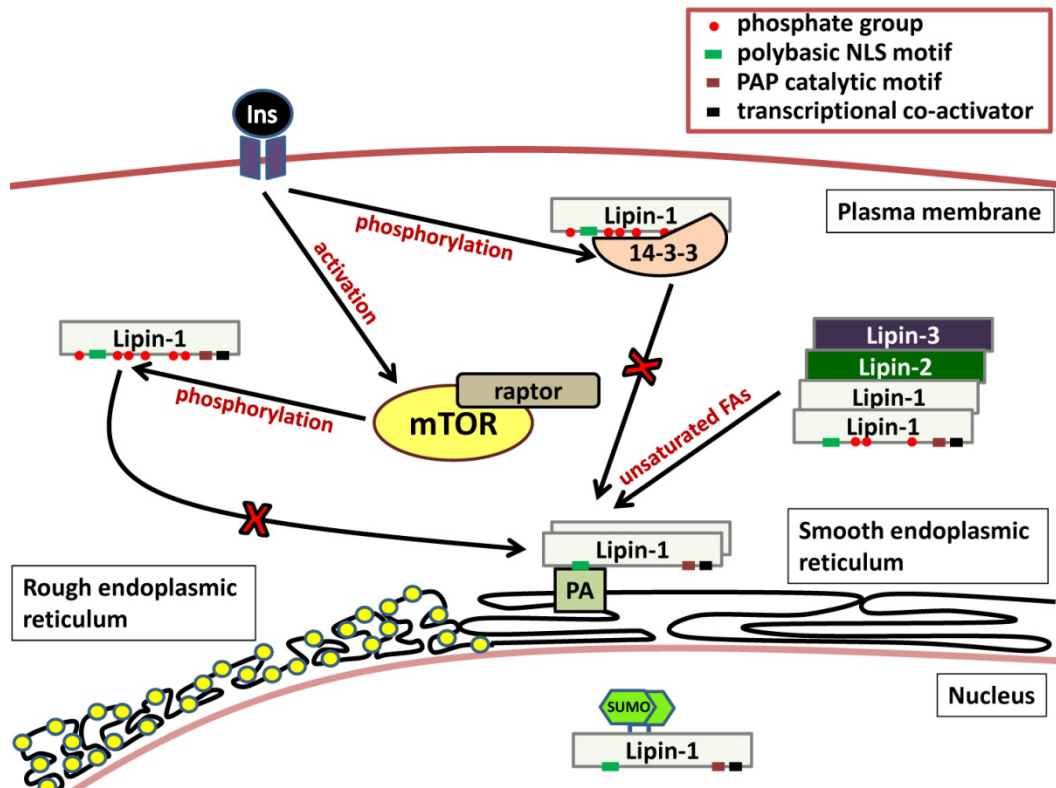
Figure 1.7 Regulation of the subcellular localization of lipins. The phosphorylation of lipins is stimulated by insulin signalling. One of the downstream kinases responsible for lipin-1 phosphorylation is mTORC1 (mTOR-raptor complex). Insulin-stimulated phosphorylation of lipin-1 promotes 14-3-3 association to a serine-rich region downstream of the lipin-1 polybasic motif. Lipin-1 phosphorylation promotes its cytosolic localization. Lipins can exist in dimeric or tetrameric states in a head-to-head, tail-to-tail conformation with each subunit able to catalyze its own independent phosphatidate phosphatase (PAP) activity. Association of lipin-1 with membranes is promoted by unsaturated fatty acids, and also requires the presence of the polybasic nuclear localization motif (NLS). SUMOylation of lipin-1 stimulates its localization to the nucleus. Abbreviations: Ins, insulin; mTOR, mammalian target of rapamycin; PA, phosphatidate.

From the culmination of all these studies, it was hypothesized that membrane association is dictated by electrostatic interactions between a negatively charged membrane surface interacting with positively charged regions of the lipins. The evolutionarily conserved polybasic motifs of the lipins now provide such a binding domain, especially since PA was shown to interact with this motif (Figure 1.5) (231). The introduction of negative charges by phosphorylating the lipins would also disrupt these electrostatic interactions. The dephosphorylation of lipin-1 or its yeast orthologue is regulated in part by the Dullard phosphatase and its regulatory subunit nuclear envelope phosphatase 1-regulatory subunit 1 (NEP1-R1) (246, 304, 305).

Phosphorylation of lipin-1 at a serine-rich region downstream of the polybasic motif also promotes interaction of 14-3-3 proteins at this site (Figure 1.7) (232). This interaction with 14-3-3 favors lipin-1 localization in the cytosol. The mammalian target of rapamycin complex 1 (mTORC1) is responsible for phosphorylating several serine residues on lipin-1 (Figure 1.7) (229, 241, 306). As mentioned previously, phosphorylation of lipin-1 at most of the sites identified does not affect PAP activity as measured *in vitro*, but rather it changes its subcellular localization in intact cells and thus, its physiological activity (229, 241). Phosphorylation of mammalian lipin-1 and -2 on CDK1 recognition motifs does appear to affect PAP activity (292); however, the specific serine/threonine residues have only been identified in yeast (249, 302). A recent study showed that the inhibition of mTORC1 phosphorylation of lipin-1 promotes the nuclear localization of lipin-1, where it inhibits sterol regulatory element-binding protein (SREBP) signalling (229).

Lipin-1 localization to the nucleus is also dependent on SUMOylation (Small Ubiquitin-like Modifier) (Figure 1.7) (276). SUMOylation motifs consisting of a φKxE sequence (where φ represents any hydrophobic amino acid and x represents any amino acid) have been identified in lipin-1A, lipin-1B, and lipin-2 (Figure 1.5) (276). Only lipin-1A and -1B have been positively demonstrated to be SUMOylated (276).

In summary, the subcellular localization of lipins is dynamically regulated by post-translational modifications as well as changes in electrostatic interactions with membranes, which enables an active response to rapid changes in cellular signalling and nutrient status.

1.5.2 Transcriptional regulation of the lipins

The gene expressions of lipin-1 and -2 have also been shown to be tightly regulated by the differential actions of various hormones in the feed/fast cycle. Glucocorticoids, which are elevated in the plasma during stress, starvation, diabetes, and after feeding ethanol or fructose (293), stimulate the transcriptional upregulation of *Lpin1* gene expression through interaction of the activated glucocorticoid receptor with the glucocorticoid receptor response element upstream of the *Lpin1* promoter (Figure 1.8) (307, 308). This induction by glucocorticoids is synergized by the action of glucagon through cyclic adenosine monophosphate (cAMP) and it is antagonized by insulin (307). These effects mirror the changes in lipin-1 gene expression in the liver during fasting, diabetes and ethanol feeding (307). Lipin-2 expression is also induced by fasting (243, 307), and is increased by acute endoplasmic reticulum stress as well as high fat feeding (280).
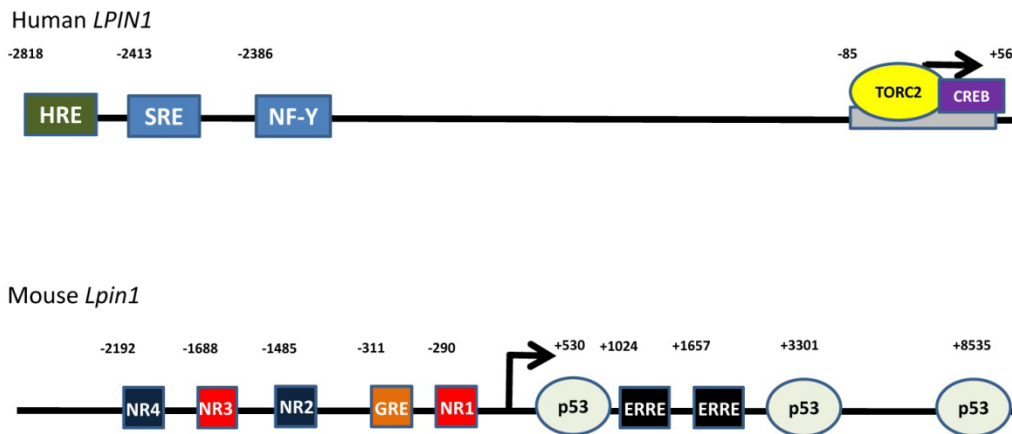
Figure 1.8 Transcriptional regulatory sites on the *LPIN1* (human)/*Lpin1* (mouse) gene. Sterol regulatory element binding protein-1 (SREBP1) and nuclear factor-Y bind to the sterol response element (SRE) and nuclear factor-Y (NF-Y) binding site on the *LPIN1* promoter respectively. Hypoxia inducible factor-1 binds to the hypoxia response element (HRE). Transducer of regulated CREB activity 2 (TORC2) and cAMP response element binding protein (CREB) bind to the -85 to +56 region of the promoter. Nuclear orphan receptor-1 binds to nuclear orphan receptor half-sites 1 and 3 (NR1 and 3) on the *Lpin1* promoter as well as NR2 and 4 on the reverse strand. Glucocorticoid receptors bind to the glucocorticoid response element (GRE) upstream of the *Lpin1* promoter and estrogen-related receptors α and γ bind to the estrogen-related receptor response elements (ERRE) in the first intron downstream of the promoter. The tumour suppressor, p53, has also been shown to bind in the first intron of the *Lpin1* gene.

Although cAMP does not increase *Lpin1* transcription in hepatocytes by itself, β_2-adrenergic receptor signalling in mouse skeletal muscle and C2C12 myotubes can induce the upregulation of lipin-1 gene expression by activating nuclear orphan receptor-1, which binds to its response elements in the promoter region (Figure 1.8) (309). TORC2 (transducer of regulated CREB activity) in conjunction with cAMP response element binding protein (CREB) can also increase *Lpin1* expression in hepatocytes (Figure 1.8) (310). TORC2 activation

and localization to the nucleus is induced by its dephosphorylation on serine 171 (311). Glucagon and fasting promote the dephosphorylation of serine 171, whereas insulin and feeding cause its phosphorylation (311, 312). Therefore, TORC2 appears to be a major player in the cAMP- and insulin-dependent regulation of *Lpin1* transcription, at least in the liver.

Transcription of the *Lpin1* gene also depends on PGC-1α and estrogen-related receptors-α and -γ (ERRα and γ), which bind to their response elements in the first intron (Figure 1.8) (100, 266). Gene expression of PGC-1α is increased in hepatocytes by cAMP and this action is synergized by glucocorticoids (307). These changes in PGC-1α mRNA levels coincide with the increase in *Lpin1* mRNA that is stimulated by glucocorticoids and cAMP. Moreover, glucocorticoids induce PPARα gene expression 1-2 h after the induction of *Lpin1* expression (307). These observations support the findings by Finck et al. who demonstrated the role of lipin-1 as a transcriptional co-activator with PGC-1α in regulating PPARα levels in the liver (100). It should also be noted that insulin does not antagonize the transcriptional upregulation of the genes encoding PGC-1α or PPARα (307).

SREBP-1, in combination with its binding partner nuclear factor Y, is also involved in the induction of *LPIN1* gene expression in Huh7 hepatocarcinoma cells (Figure 1.8) (313). Ethanol can also increase hepatic PAP activity through the action of glucocorticoids (219, 222), and this was related to the development of the ethanol-induced fatty liver (314, 315). A recent study showed that SREBP also regulates the ethanol-induced upregulation of *Lpin1* expression (244). On the other hand, activation of AMP-activated protein kinase (AMPK) appears to

inhibit the effects of ethanol on *Lpin1* expression. Moreover, the nuclear localization of lipin-1 induced by inhibition of mTORC1 leads to a decrease in SREBP signalling by decreasing the amount of nuclear SREBP (229). The combination of these findings suggests that the induction of lipin-1 by SREBP-1 followed by lipin-1 nuclear localization could act as a negative feedback mechanism to fine-tune SREBP signalling.

As mentioned previously, hypoxia increases PAP activity in rat livers after 1 day (223), and a recent study showed that this increase is mediated by hypoxia inducible factor 1 (HIF1) binding to the hypoxia response element on the *LPIN1* promoter and inducing transcriptional upregulation of the *LPIN1* gene (Figure 1.8) (316). Other cellular stresses that induce reactive oxygen species production and p53 activation such as glucose deprivation and DNA damage also induce lipin-1 gene expression in C2C12 myotubes and human fibroblasts (317). The authors showed that p53 binds to the first intron of the *Lpin1* gene in the mouse DP16.1 p53/ts cell line with a temperature-sensitive activation of p53 at 32°C (Figure 1.8) (317). Lastly, the authors postulated that lipin-1 is important for p53-induced upregulation of FAO in C2C12 myotubes. This was based on their demonstration that the increase in FAO in glucose-deprived conditions was decreased by 20% and 10% when knocking down lipin-1 or p53 expression, respectively. Further studies will clarify the role of lipin-1 in p53 signalling.

The regulation of lipin gene expression can be viewed as a compensatory mechanism to increase the reservoir of lipins during periods of high FA entry and lipid turnover. During fasting or starvation, the action of glucagon and glucocorticoids in the presence of low insulin signalling leads to an increase in

lipin-1 expression. Lipin-1 localization in the nucleus and increased transcription of genes involved in FAO occurs simultaneously with increased lipin-1 expression and association with the endoplasmic reticulum due to increased plasma FA supply from the blood following lipolysis in adipose tissue. These combined actions allow concurrent increases in glycerolipid synthesis and FA oxidation. Classically, these two pathways were considered to be mutually antagonistic since they compete for acyl-CoA esters; however, recent evidence shows that TG turnover and FA oxidation are complementary processes, as described in Section 1.3.

1.6 Thesis objectives

Lipins play important roles in fatty acid oxidation, glycerolipid synthesis, and lipid signalling. Lipin-1 can act as a transcriptional co-activator with PPARα and PGC-1α to induce genes involved in hepatic fatty acid oxidation. The lipins serve as essential PAP enzymes in the Kennedy pathway for synthesizing TG. Lipins also control the balance between PA and DG, which are two essential precursors in phospholipid synthesis. PA is a substrate for the synthesis of phosphatidylinositol, phosphatidylglycerol and cardiolipin whereas DG is the critical precursor required for PC and PE synthesis. PA and DG are also lipid signalling molecules that affect various processes such as cell proliferation, growth, survival, insulin signalling and stress response [reviewed in (173-175)].

An important determinant in the function of the lipins is the regulation of their subcellular localization, activity and expression. The first aim of this thesis was to investigate factors that regulate the translocation of PAP activity from the cytosol to membranes. The ability of PAP activity to translocate onto membranes

when stimulated with unsaturated fatty acids was first demonstrated in the 1980s before the genes encoding the PAP enzyme(s) were identified (295, 296, 303). We wanted to definitively determine whether the translocation of PAP activity could be attributed to the different lipins. The stimulation of lipin translocation is a critical event in enabling cytosolic lipins to be located at their sites of action at the endoplasmic reticulum and the nucleus.

Two autosomal recessive mutations in lipin-1 and -2 cause rhabdomyolysis and the Majeed syndrome in human patients, respectively. We collaborated with Dr. Karen Reue at the University of California-Los Angeles, to determine whether the point mutation in lipin-2, which is found in a subset of Majeed syndrome patients, affected the ability of lipin-2 to translocate. Furthermore, the effect of the mutation on PAP activity was investigated since the mutated residue was present in the same domain as the conserved catalytic motif.

Much of the work determining the roles and regulation of the lipins has been performed in hepatocytes or adipocytes, while little is known about the regulation of lipins in the heart. The expression of lipin-1 is increased by glucocorticoids and the second messenger, cAMP, in hepatocytes, whereas insulin antagonizes this induction. These dynamic changes in lipin-1 regulation are thought to act as compensatory adaptations in conditions with high FA flux and lipid turnover, e.g. during fasting and diabetes. The second aim of the thesis was to determine whether the expression of the lipins in neonatal rat ventricular myocytes was similarly regulated by insulin, glucocorticoids and cAMP.

Furthermore, we compared the effect of fasting on lipin expression in the mouse heart and liver.

We also wanted to determine the effects of lipin-1 deficiency in the hearts of *fld* mice on the ability to synthesize glycerolipids and perform FAO since cardiac PAP activities in *fld* mice have been reported to be nearly undetectable (241). We hypothesized that the complete absence of lipin-1 in the heart would compromise FAO since lipin-1 was shown to be an essential transcriptional co-activator of PPARα target genes involved in FAO. Furthermore, glycerolipid synthesis should be impaired because of the relative lack of PAP activity in the *fld* heart. We expected that aberrant cardiac FA esterification and oxidation in the *fld* mouse would consequently lead to decreased mechanical efficiency of the heart.

CHAPTER 2

MATERIALS AND METHODS

2.1 Reagents

Common chemicals and reagents were obtained from Sigma-Aldrich (St. Louis, MO), Thermo Fisher Scientific (Waltham, MA) or EMD Chemicals (Darmstadt, Germany) and were of the highest grade available. Dulbecco's minimum essential medium (DMEM), penicillin/streptomycin and trypsin-ethylenediaminetetraacetic acid (EDTA) were purchased from Life Technologies (Carlsbad, CA). Fetal bovine serum, Dulbecco's Modified Eagle's/Nutrient Mixture Ham's F-12 (DME/F12) medium, 8-(4-chlorophenylthio)-2′-O-methyladenosine 3′,5′-cyclic monophosphate monosodium hydrate (CPT-cAMP), dexamethasone, insulin, oleic acid, palmitic acid (free acid) and protease inhibitor cocktail were from Sigma-Aldrich. All primers were obtained from Integrated DNA Technologies, Inc. (Coralville, IA).

$[9,10-^3H]$oleate, $[9,10-^3H]$palmitate and $[1-^{14}C]$oleate were obtained from Perkin-Elmer (Waltham, MA), and $[1,3-^3H]$glycerol and $[U-^{14}C]$glucose were purchased from Amersham (now part of GE Healthcare, Buckinghamshire, United Kingdom). 1,2-dioleoyl-*sn*-glycerol was purchased from Avanti Polar Lipids, Inc. (Alabaster, AL). 1,2,3-trioleoyl-*sn*-glycerol, 1,2-dioleoyl-*sn*-glycero-3-phosphoethanolamine, *L*-α-phosphatidylcholine and sphingomyelin from egg yolk, *L*-α-phosphatidate and *L*-α-phosphatidylglycerol prepared from egg yolk phosphatidylcholine, *L*-α-phosphatidylinositol from bovine liver, and *L*-α-phosphatidylserine, ceramides and cardiolipin from bovine brain were all obtained from Sigma-Aldrich. Tetrahydrolipstatin was a gift from Dr. M.K. Meier (Hoffman-La Troche Ltd, Basel, Switzerland) (318). Other reagents and their sources are mentioned within the text.

2.2 Phosphatidate phosphatase enzymatic assay

2.2.1 Introduction

The optimum conditions used to assay the phosphatidate phosphatase (PAP) activity were delineated by our group in the 1980s and 1990s (212, 319-321). However, the absence of detectable PAP activity in lipin-1 deficient *fld* (fatty liver dystrophy) hearts led us to re-optimize the PAP assay and these series of experiments are described in Appendix I. In summary, we found that the addition of 0.045% Tween-20 in the PAP assay prevented the detection of activity in *fld* hearts. Furthermore, the optimum concentration of Mg^{2+} using a phosphatidate/phosphatidylcholine substrate is dependent on the pH of the assay: PAP activity in *fld* cardiac tissue samples at pH 7.4 and 6.5 was optimum at 1.5 mM Mg^{2+} and 5 mM Mg^{2+}, respectively. Cardiac PAP activity in the *fld* mice was nearly undetectable when phosphatidate in Triton X-100 micelles was used as the substrate. The preparation of the phosphatidate substrate and the optimized PAP activity are described below.

2.2.2 Preparation of the [^{3}H]phosphatidate substrate

[^{3}H]Phosphatidate was formed in a reaction containing 16.6 mM KH_2PO_4, 8 mM ATP (Sigma-Aldrich), 5 mM *rac*-glycerol 3-phosphate (Sigma-Aldrich), 3 mg/ml FA-poor bovine serum album (BSA obtained from MP Biomedicals, Solon, OH), 0.3 mM [^{3}H]palmitate-K^+ (20 mCi/µmol), 1 mM dithiothreitol (DTT), 25 mM NaF, 13.4 mM $MgCl_2$, 25 µM coenzyme A (Sigma-Aldrich) and 3 mg/ml rat liver microsomal protein in a final volume of 167 ml (212). The reaction was carried out at 37°C for 90 min while stirring.

The microsomal fraction was prepared as follows: an adult male Sprague-Dawley rat was euthanized and the liver was perfused through the hepatic portal vein with 60 ml phosphate-buffered saline (PBS: 8.1 mM Na_2HPO_4, 1.1 mM KH_2PO_4, 138 mM NaCl and 2.7 mM KCl pH 7.4). The liver was cut into smaller pieces and resuspended in bicarbonate buffered solution containing 250 mM sucrose and 1 mM DTT pH 7.4 at 4 x volume. The tissue pieces were homogenized and the liver homogenate was centrifuged for 20 min at 27,000 x g. The supernatant was centrifuged again for 90 min for 302,000 x g to obtain a pellet of liver microsomal membranes, which was resuspended in the bicarbonate buffer containing 250 mM sucrose and 1 mM DTT pH 7.4. The stock solution of 80 mM K^+-palmitate was made by solubilizing the palmitic acid in 20% molar excess of KOH at 65°C, followed by sonication.

Once the reaction was complete, the mixture was added to a separating funnel and lipids were extracted by sequential additions of 600 ml chloroform-methanol (1:2, by vol.), 200 ml chloroform and 193 ml 2 M KCl containing 0.2 M H_3PO_4, such that the final ratio of chloroform-methanol-aqueous solution was 1:1:0.9. The separating funnel was incubated at 4°C overnight to allow for phase separation and the bottom phase was collected the next morning. The chloroform was evaporated in a round-bottomed flask using a rotary evaporator (Büchi Rotavapor®, Flawil, Switzerland), and the dried lipids were resuspended in 9 ml chloroform-methanol (9:1, by vol.). The lipids were loaded onto glass-backed, silica-coated thin layer chromatography (TLC) plates (EMD Chemicals), along with phosphatidate (PA) and lysophosphatidate (LPA) standards. A full-length development in chloroform-methanol-ammonium hydroxide (65:35:7.5, by vol.) was carried out, followed by a second full-length development in chloroform-

acetone-acetic acid-methanol-water (50:20:15:10:5, by vol.). The PA and LPA standards were identified using a 0.05% w/v primuline stain in acetone-water (8:2, by vol.) and visualized under an ultraviolet light. The extracted lipids co-migrating with the LPA and PA standards were scraped separately into glass tubes and the silica was extracted over 2 days with chloroform-methanol-acetic acid (8:10:0.1, by vol.). The [^{3}H]PA and [^{3}H]LPA were dried under a nitrogen stream and resuspended in chloroform-methanol (9:1, by vol.).

The substrate used in the phosphatidate phosphatase assay consisted of 3 mM PA (prepared from egg yolk PC), 2 mM egg yolk PC, [^{3}H]PA (1.36 µCi/ml), 10 mg/ml FA-poor bovine serum albumin (BSA obtained from MP Biomedicals, Solon, OH) and 5 mM EDTA/5 mM ethylene glycol tetraacetic acid (EGTA) pH 7.4 or 6.5 depending on the pH at which the assay was conducted. First, 60 µmol PA, 40 µmol PC and 27.2 µCi [^{3}H]PA were dried down in a glass tube under a nitrogen stream. A solution of 5.5 mM EDTA/5.5 mM EGTA pH 7.4 or 6.5 was pre-warmed at 37°C and 18 ml was added to the lipids while vortexing. The mixture was incubated at 37°C for 10 min and it was then sonicated for 10 s at setting 40 using the Sonic Dismembrator Model 300. One freeze-thaw cycle at -80°C was carried out and the solution was warmed to 37°C. While vortexing, 2 ml FA-poor BSA at a concentration of 100 mg/ml was added to the tube. Following a second freeze-thaw cycle, the solution was warmed to 37°C and sonicated as before. The substrate was then stored at -20°C before use in phosphatidate phosphatase assays. The substrate preparation was performed by Mr. Jay Dewald.

2.2.3 Measurement of activity using radiolabelled phosphatidate

Phosphatidate phosphatase (PAP) assays were performed at pH 6.5 and 7.4 using two methods for preparing the PA substrate (134). All assays were conducted at 37°C. The first method used a dispersion of PA with PC, which was designed to maximize the activity of PAP versus that of lipid phosphate phosphatase (LPP). Each sample was assayed in a total volume of 100 µl consisting of 100 mM Tris/maleate buffer pH 6.5, or 100 mM Tris/HCl buffer pH 7.4 in addition to 0.6 mM DTT, 1.5 mM $MgCl_2$ (for pH 7.4) and 5 mM $MgCl_2$ (for pH 6.5), protease inhibitor cocktail, 30 nM microcystin-LR (Enzo Life Sciences, Farmingdale, NY) (to inhibit phosphoprotein phosphatases), 0.6 mM phosphatidate (PA) labelled with [^{3}H]palmitate (approximately 6 x 10^4 dpm per assay) (Section 2.2.2), 0.4 mM PC, 1 mM EDTA/1 mM EGTA, 2 mg/ml BSA, and 200 µM tetrahydrolipstatin to inhibit the degradation of the DG product by lipase activity (321).

In the second assay, 45 mM Triton X-100 was used to disperse 5 mM PA in micelles and PC was omitted. Each sample was assayed in a total volume of 100 µl consisting of 100 mM Tris/maleate pH 6.5 or Tris/HCl pH 7.4 in addition to 0.6 mM dithiothreitol, 1 or 6 mM $MgCl_2$ (pH 7.4 and 6.5, respectively), protease inhibitor cocktail, 30 nM microcystin-LR, 1 mM PA labelled with [^{3}H]palmitate (approximately 6 x 10^4 dpm per assay), 9 mM Triton X-100 (from the substrate preparation) and 200 µM tetrahydrolipstatin.

Parallel measurements were performed in the absence of Mg^{2+}, or in the presence of 8 mM N-ethylmaleimide (NEM) to determine the contribution from lipid phosphate phosphatase (LPP) activity (134). For the assays where Mg^{2+} was

omitted, or for the assays to determine the requirement for Mg^{2+} and other monovalent and divalent cations, all buffers were depleted of bivalent cations with AG 50W-X8 resin Na^+-form (212).

LPP activity was determined directly by using the Triton X-100-based procedure at pH 6.5 and 7.4 in the presence of 6 mM NEM with the exception that $[^3H]PA$ was used instead of $[^{32}P]PA$ (215). Briefly, each sample was assayed in a total volume of 100 μl consisting of 100 mM Tris/maleate pH 6.5 or Tris/HCl pH 7.4, 2 mg/ml FA-poor BSA, 6 mM NEM, 1 mM EDTA/EGTA, protease inhibitor cocktail, 30 nM microcystin-LR, 0.6 mM PA labelled with $[^3H]$palmitate (approximately 6 x 10^4 dpm per assay), 8 mM Triton X-100 (from the substrate preparation) and 200 μM tetrahydrolipstatin.

DG formed in these assays was extracted in 2 ml chloroform-methanol (19:5, by vol.) containing 0.08% olive oil as an acylglycerol carrier (212). Activated alumina was added to remove the unreacted PA and any liberated $[^3H]$palmitate from the chloroform phase. The chloroform phase was dried down, and radioactivity was determined. PAP activity was calculated by subtracting the NEM-insensitive, or Mg^{2+}-independent LPP activity from the total activity. Each sample was assayed at three different protein concentrations (30 – 200 μg) to ensure a proportional response and the conversion of PA to DG was restricted to <20%.

2.3 The non-radioactive detection of phosphatidate phosphatase activity

2.3.1 Introduction

The radioactive PAP assay described in Section 2.2.3 is an ideal assay for determining PAP activity in cell lysates and tissue homogenates. However, we realized that there might have been a potential problem in the preparation of [^{3}H]PA as a substrate. [9,10-^{3}H]palmitate was incorporated into the glycerol 3-phosphate backbone in an excess of palmitate. The major [^{3}H]PA product could potentially have been dipalmitoyl-PA. Han et al. demonstrated that dipalmitoyl-PA was a poor substrate for lipin-1 (137). To determine if the [^{3}H]PA used in our assay was a suitable substrate for detecting PAP activity, we assayed samples in parallel using a non-radioactive method of detecting phosphate release and the formation of [^{3}H]DG under our standard PAP assay conditions. These experiments are described in Appendix I.

Briefly, the substrate used in the PAP assay consists of [^{3}H]PA (prepared as described in Section 2.2.2) and PA prepared from egg yolk PC. We measured the formation of [^{3}H]DG and the release of phosphate from PA using a method of detecting phosphate with malachite green in parallel (described in Section 2.3.2 below). The rationale was that [^{3}H]DG formation would be much lower than phosphate release from PA if PAP activity against [^{3}H]PA was decreased compared to its action against PA prepared from egg yolk PC. We found that detection of PAP activity by measuring [^{3}H]DG was only 15% lower on average than measuring phosphate release from PA. Furthermore, measuring [^{3}H]DG formation was more sensitive than using malachite green to detect phosphate

release. We concluded that the radioactive PAP assay is the more sensitive and preferred method of detecting PAP activity in our samples.

2.3.2 Measurement of PAP activity by inorganic phosphate release from phosphatidate

Cell lysates were assayed at pH 7.4 using the PA/PC liposomes as described above in Section 2.2.3. Na_2HPO_4 was assayed under the same conditions to establish a standard curve. The reaction was stopped by adding 100 µl $HClO_4$ at a final concentration of 0.5 M and the final volume was 200 µl. The tubes were centrifuged at 750 x g for 4 min to pellet the precipitated protein and bound lipids. A sample of the supernatant (150 µL) was isolated and 10 µL of 125 mM ammonium molybdate $((NH_4)_6Mo_7O_{24}\cdot4H_2O)$ was added. The mixture was extracted with 180 µL isobutanol-benzene (1:1, by vol.) and centrifuged again for 4 min at 750 x g. 140 µL of the organic phase was taken and dried down under an air stream. Two hundred and fifty µL 12 mM ammonium molybdate in 0.9 M H_2SO_4 and 250 µL 0.244 mM malachite green oxalate in 0.112% polyvinyl alcohol was added and the absorbancy of the phosphate-molybdate-malachite green complex was measured at 600 nm after 10 min incubation at room temperature. A parallel assay with the same set of samples was carried out to measure [³H]DG formation as outlined in Section 2.2.3.

2.4 Cell culture

2.4.1 Primary neonatal rat ventricular myocytes

Isolation of neonatal rat ventricular myocytes (NRVMs) was performed as previously described (322). Hearts from 2-day old rat pups were isolated and placed in ice-cold PBS. The atria were removed from the hearts, rinsed three times with ice-cold PBS and the ventricles were minced with fine-tipped scissors. The minced tissue was then digested for 20 min at 37°C on a rotary shaker with 25,000 U deoxyribonuclease I (Worthington Biochemical Corporation, Lakewood, NJ), 2,250 U trypsin (Worthington Biochemical Corporation) and 5,000 U collagenase (Worthington Biochemical Corporation) in a total volume of 19.5 ml PBS. As described by the manufacturer, 1 U deoxyribonuclease I (DNAse I) causes an increase in absorbance at 260 nm of 0.001 per minute per ml at 25°C, pH 5.0 when acting against lambda phage DNA. 1 U trypsin hydrolyzes 1 µmole of p-toluene-sulfonyl-L-arginine methyl ester per minute at 25°C, pH 8.2, in the presence of 10 mM Ca^{2+}. 1 U collagenase releases 1 µmole L-leucine equivalents from collagen in 5 h at 37°C, pH 7.5.

After digestion of the heart tissue, 20 ml Dulbecco's Modified Eagle's/Nutrient Mixture Ham's F-12 (DME/F12) medium containing 20% fetal bovine serum (FBS), 1% penicillin/streptomycin and 50 µg/ml gentamicin (denoted as DF20 medium) was added in a 50 ml Corning tube (Corning Incorporated, Lowell, MA) and the solution was centrifuged at 130 x g for 2 min using a Beckman TJ-6 low-speed centrifuge. The supernatant was discarded and the pellet was resuspended in PBS containing DNAse I, trypsin and collagenase for further digestion at 37°C for 20 min. DF20 medium was again added and the mixture was centrifuged as before. The supernatant was kept in a separate 50 ml

Corning tube and the pellet was digested one last time using the previous conditions. The supernatant was centrifuged at 650 x g for 7 min, and the resulting pellet was combined with the final digestion mixture in addition to 20 ml DF20 media. Following a final centrifugation at 650 x g for 7 min, the pellet was resuspended in plating media (DME/F12 medium containing 5% FBS, 10% horse serum, 1% penicillin/streptomycin and 50 µg/ml gentamicin).

The cells were strained through a 100 µm cell strainer (BD Biosciences, Franklin Lakes, NJ) and incubated in a T-75 cm^2 culture flask for 90 min at 37°C in a CO_2 incubator. Cardiac fibroblasts and endothelial cells readily attached to the flask surface during this time period and the supernatant containing the myocytes was isolated and centrifuged at 300 x g for 2 min. The cells were resuspended in plating media and cells were counted after diluting with trypan blue. Cell viability was usually greater than 90% and cells were plated on 35 mm primaria-coated dishes (BD Biosciences) at a density of 1.8 million cells per dish. The cardiomyocytes were cultured in DME/F2 medium containing 10% FBS and 100 µM cytosine β-*D*-arabinofuranoside (ara-C). Ara-C is a deoxy-cytosine analog, which becomes incorporated into DNA and inhibits replication without affecting transcription (323). Treatment with ara-C would selectively prevent cardiac fibroblast and endothelial cell proliferation without affecting the quiescent cardiomyocytes.

2.4.2 Preparation of primary adult rat hepatocytes

Primary hepatocytes were isolated as previously described (324). Hepatocyte preparations were performed by Boripont Manmontri and Dr. Sabina Isgandarova. Adult rats were anesthetized with ©Euthanyl (Bimeda-MTC Animal Health Inc., Cambridge, ON), or more specifically 150 mg/kg sodium pentobarbital. Once the animal reached surgical plane, the abdominal cavity was dissected and blood was drawn from the inferior vena cava before tying off. The hepatic portal vein was then cut and a blunt-end needle attached to a peristaltic pump was inserted into the vein. The liver was perfused with Hank's Balanced Salt Solution (HBSS, Life Technologies) containing 0.5 mM EGTA, 25 mM glucose, 5.33 mM KCl, 0.44 mM KH_2PO_4, 138 mM NaCl, 0.34 mM Na_2HPO_4, 4.2 mM $NaHCO_3$, 1.72 µM insulin and 25 mM HEPES (4-(2-hydroxyethyl)-1-piperazineethanesulfonic acid) pH 7.4 at 4 ml/min for 5 min. The liver was then perfused for 2 – 3 min with 1 mg/ml collagenase type IV (Sigma-Aldrich) in HBSS (Life Technologies) containing 25 mM glucose, 5.33 mM KCl, 0.44 mM KH_2PO_4, 138 mM NaCl, 0.34 mM Na_2HPO_4, 4.2 mM $NaHCO_3$, 1.72 µM insulin, 25 mM HEPES pH 7.4, 1.26 mM $CaCl_2$, 0.5 mM $MgCl_2$ and 0.4 mM $MgSO_4$. The liver was then sliced into a creamy emulsion and Dulbecco's Minimal Essential Medium (DMEM) containing 15% FBS and 1% penicillin/streptomycin was added. The mixture was strained and centrifuged at 15 x g for 5 min. The supernatant was decanted and the pellet was resuspended in 15% FBS-DMEM before centrifugation at 15 x g for 5 min again. This step was repeated twice and the final pellet was resuspended in 15% FBS-DMEM. 1.5 million cells were plated on 6 cm dishes (Corning Incorporated) coated with collagen type III (Sigma). After 1 – 2 h attachment, non-viable and unattached cells were removed and fresh media was added. Hepatocytes were used in experiments the next day.

2.4.3 Mammalian cell lines

Rat2 fibroblasts and human embryonic kidney 293 (HEK 293) cells were cultured in DMEM containing 10% FBS and 1% penicillin/streptomycin. Trypsin (0.05%) containing 0.5 mM EDTA was used to isolate and passage adherent cells.

2.4.4 Adenoviral inoculation of cultured cells

Recombinant adenovirus overexpressing N-terminal HA-tagged (hemagglutinin epitope) *Mus musculus* lipin-1B wildtype (AdLipin1b) and lipin-2 (AdLipin2) as well as adenovirus expressing shRNA against the genes encoding β-galactosidase (which was used as the vector control) (AdshRNA LacZ) or lipin-1 (AdshRNA Lipin1) were gifts from Dr. Thurl Harris (University of Virginia, Charlottesville, VA) (100, 241). The cytomegalovirus (CMV) promoter was used to drive gene expression and these constructs also possess a separate CMV promoter expressing green fluorescent protein (GFP). The Ad-Easy system was used to prepare the adenovirus expressing full-length lipin-1B wildtype. The shRNA targeting nucleotides 896-915 of the lipin-1 transcript was cloned into the pENTR vector (Life Technologies), which was then used as the entry vector in the BLOCK-iT™ adenoviral RNAi expression system. Adenovirus propagation was carried out by Amy Barr (Cardiovascular Research Centre, University of Alberta). NRVMs were inoculated with adenovirus in 10% FBS-DME/F12 medium for 38 h to obtain optimum expression. HEK 293 cells were inoculated with adenoviral vectors in 10% FBS-DMEM for 6 h, after which the media was replaced with fresh 10% FBS-DMEM. Adenoviral expression in HEK 293 cells was optimum at 24 h post-inoculation.

2.4.5 Plasmid propagation and site-directed mutagenesis

This work was performed in collaboration with Tamara Arnold from the lab of Dr. Charles Holmes. The pRK5 plasmids expressing N-terminal FLAG-tagged full-length *Mus musculus* lipin-1B wildtype and FLAG-tagged catalytically inactive lipin-1B mutant (D712, 714E) were provided as gifts from Dr. Thurl Harris (University of Virginia) (229, 241). Plasmids were transformed into subcloning efficiency DH5α™ competent *Escherichia coli* (Life Technologies) and were plated on Lysogeny Broth (LB: 10 g/l tryptone, 5 g/l yeast extract and 10g/l NaCl) agar plates containing 100 µg/ml ampicillin at 37°C. Selected *E. coli* colonies were propagated overnight on a bacterial shaker set at 230 rpm in LB media containing 100 µg/ml ampicillin. Plasmids were isolated from the *E. coli* using the QIAprep Spin Miniprep kit (Qiagen, Venlo, Netherlands). Briefly, bacteria were lysed under alkaline conditions (325) in the presence of ribonuclease A to remove any contaminating RNA and then neutralized in a high-salt buffer. The plasmid DNA can bind to a spin column containing a silica membrane under these high salt conditions and will elute using a low salt buffer. The column was washed once to remove any salt and the plasmids were eluted using nuclease-free distilled water. Plasmids were then quantified using the Nanodrop spectrophotometer ND-1000 (Thermo Scientific, Rockford, IL).

The QuikChange™ Site-Directed Mutagenesis kit from Agilent Technologies (Santa Clara, CA) was used to introduce point mutations in the putative protein phosphatase-1 binding motif from H_{49}-VRF$_{52}$ to HARA in the pRK5 plasmid encoding FLAG-tagged wildtype lipin-1B. The numbers denote the

residue numbers. The following primers were used to introduce the mutations, which are highlighted in bold:

Forward primer:

5' - TCC CCT TTC CAC **GCC** CGC **GCC** GGC AAG ATG GGT GTC CTC C - 3'

Reverse primer:

5' - G GAG GAC ACC CAT CTT GCC **GGC** GCG **GGC** GTG GAA AGG GGA - 3'

Furthermore, a NaeI restriction enzyme cut site shown in the underlined region was created when the mutations were introduced. In order to produce the plasmid containing the mutations, approximately 50 ng of the parent plasmid DNA was added to a reaction mix containing 10 mM KCl, 10 mM $(NH_4)_2SO_4$, 20 mM Tris-HCl pH 8.8, 2 mM $MgSO_4$, 0.1% Triton X-100, 0.1 mg/ml nuclease-free BSA, a proprietary formulation of deoxyribonucleotide triphosphates (dNTPs), 125 ng forward and reverse primer, and 2.5 U PfuTurbo® DNA polymerase. 1 U PfuTurbo® DNA polymerase was defined as the amount of enzyme that can incorporate 10 nmol of $[^3H]$TTP into an acid-insoluble template in 30 min at 72^0C. The reaction mix was then subjected to a thermal cycling protocol consisting of 1 cycle at 95°C for 30 s, followed by 18 sequential cycles at 95°C for 30 s, 55°C for 1 min and 68°C for 8 min. The restriction enzyme DpnI can recognize and cut its corresponding restriction site only when methylated, and since the parent plasmid was propagated in an *E. coli* strain positive for Dam methylase, 10 U DpnI was used to digest the parental, non-mutant plasmid and not the mutant strands. 1 U DpnI is defined as the quantity of enzyme used to digest 1 µg dam-methylated plasmid DNA at 37°C in 1 h.

2.4.6 Transfection of cultured cells with plasmids

Plasmids were transfected into cultured HEK 293 cells using the transfection reagent Lipofectamine™ 2000 (Life Technologies). Cells were cultured at 50-80% confluence in 35 mm dishes for 1 day in 10% FBS-DMEM in the absence of penicillin/streptomycin. On the day of transfection, media was replaced with 1.5 ml fresh 10% FBS-DMEM without penicillin/streptomycin. 3 µg plasmid DNA was incubated for 20 min with 7.5 µg Lipofectamine™ 2000 in 500 µl Opti-minimal essential media® I (Opti-MEM® I) containing reduced serum as recommended in the protocol provided by Life Technologies. The DNA-Lipofectamine complexes were then added to the dishes and left to incubate for 6 h. At this time, the media was again replaced and the cell lysates were collected 24-48 h after transfection.

2.5 Detection of protein-protein interactions by immunofluorescent antibodies

2.5.1 Detection of protein phosphatase 1γ catalytic subunit bound to the 96 well µClear® plate

Purified, recombinant protein phosphatase 1γ catalytic subunit (PP1γ) was obtained from Tamara Arnold from the laboratory of Dr. Charles Holmes. PP1γ (3 µg) was incubated in 150 µl PBS using the 96 well µClear® black-coated, tissue culture-treated plate (catalogue no. 655090, Greiner Bio-One, Kremsmuenster, Austria). The plate was gently agitated overnight at 4°C on the Lab-Line Lab Rotator (Lab-Line Instruments Inc., Melrose Park, IN) at 40 revolutions per minute (rpm). After washing in PBS containing 0.1% w/v Tween-20 (PBST), the wells were blocked with Odyssey blocking buffer (LI-COR

Biosciences) for 1 h at room temperature. The wells were washed with PBST once more and incubated overnight at 4°C while gently agitating with mouse anti-protein phosphatase 1 immunoglobulin G (IgG) (Santa Cruz Biotechnology) diluted 1:500 in Odyssey blocking buffer-PBS (1:1, by vol.) containing 0.1% w/v Tween-20.

The wells were washed with PBST before incubation with the secondary antibody. The Alexa Fluor® 680-conjugated goat anti-mouse IgG (Life Technologies, Carlsbad, CA) was diluted 1:10,000 in Odyssey blocking buffer-PBS (1:1, by vol.) containing 0.1% w/v Tween-20 and 0.01% sodium dodecyl sulfate and added to each well. The plate was then incubated for 90 min at room temperature while gently agitating at 40 rpm as before. After washing with PBST, the wells were washed once with PBS and scanned at 700 nm using the LI-COR Odyssey® Imaging System. The Odyssey® Imaging software version 1.2, in combination with the In-Cell Western plugin, was used to quantify the fluorescence in each well.

2.5.2 Interaction of recombinant lipin-1B overexpressed in human embryonic kidney 293 cells with protein phosphatase 1γ

PP1γ (3 μg/81 pmol) was bound to the 96 well plate, as outlined in Section 2.5.1. As controls, equivalent amounts (3 μg) of bovine serum albumin (BSA) or potato acid phosphatase (Sigma-Aldrich) were bound to the wells, instead. This incubation was either performed in the absence or presence of 750 pmol of microcystin-LR. HEK 293 cells overexpressing recombinant lipin-1B proteins were sonicated in 25 mM HEPES pH 7.4 containing 250 mM sucrose, 2

mM DTT, protease inhibitor cocktail (Sigma-Aldrich) and 30 nM microcystin-LR. The lysates were centrifuged for 30 s at 7,700 x g and the supernatant was used for the PP1γ interaction experiments. After washing the wells with PBS followed by blocking with Odyssey blocking buffer (LI-COR Biosciences) for 1 h at room temperature, cell lysates overexpressing recombinant lipin-1B were incubated in the wells coated with PP1γ, BSA or potato acid phosphatase overnight at 4°C on the Lab-Line Lab Rotator at 40 rpm.

The wells were treated once more with Odyssey blocking buffer for 1 h at room temperature and washed with PBST. This was followed by an overnight incubation at 4°C while gently agitating at 40 rpm with mouse IgG detecting the FLAG epitope (Clontech Laboratories Inc., Mountain View, CA) and rabbit polyclonal IgG detecting the lipin-1 C-terminus diluted 1:2,500 and 1:500, respectively in Odyssey blocking buffer-PBS (1:1, by vol.) containing 0.1% w/v Tween-20. After washing with PBST, wells were incubated for 90 min at room temperature while gently agitating at 40 rpm with Alexa Fluor® 680-conjugated goat anti-mouse IgG (Life Technologies, Carlsbad, CA) and IRDye® 800-conjugated goat anti-rabbit IgG (LI-COR Biosciences) diluted 1:10,000, respectively in Odyssey blocking buffer-PBS (1:1, by vol.) containing 0.1% w/v Tween-20 and 0.01% sodium dodecyl sulfate. After washing with PBST, the wells were washed once with PBS and scanned at 700 and 800 nm using the LI-COR Odyssey® Imaging System. The Odyssey® Imaging software version 1.2 in combination, with the In-Cell Western plugin, was used to quantify the fluorescence in each well.

2.5.3 Protein dot blot for the normalization of recombinant protein expression

Different amounts of the HEK 293 cell lysates overexpressing recombinant lipin-1B (0.1 – 1 µg) were spotted onto a nitrocellulose membrane and dried under an air stream. The blot was blocked for 1 h at room temperature, washed with PBST and incubated for 1 h at room temperature with mouse IgG detecting the FLAG epitope (Clontech Laboratories Inc., Mountain View, CA) and rabbit polyclonal IgG detecting the lipin-1 C-terminus diluted 1:2,500 and 1:500, respectively in Odyssey blocking buffer-PBS (1:1, by vol.) containing 0.1% w/v Tween-20. After washing with PBST, the blot was incubated for 1 h at room temperature with Alexa Fluor® 680-conjugated goat anti-mouse IgG (Life Technologies, Carlsbad, CA) and IRDye® 800-conjugated goat anti-rabbit IgG (LI-COR Biosciences) diluted 1:10,000, respectively in Odyssey blocking buffer-PBS (1:1, by vol.) containing 0.1% w/v Tween-20 and 0.01% sodium dodecyl sulfate. After washing with PBST, the blot was washed once with PBS and scanned at 700 and 800 nm using the LI-COR Odyssey® Imaging System. The Odyssey® Imaging software version 1.2 was used to quantify the fluorescence signal.

2.6 Measurement of mRNA levels

2.6.1 mRNA isolation and reverse transcription

The RNAqueous® kit from Life Technologies was used for the collection and isolation of mRNA from cell lysates or tissue samples. Cells plated onto dishes were collected in the Lysis/Binding buffer, which is a concentrated chaotropic guanidinium salt solution provided in the kit. The lysate was sonicated for 5 s twice with 1 min intervals at setting 20 using the Sonic Dismembrator

Model 300. Samples were centrifuged for 2 min at 16,000 x g using the DeSaga Microfuge MC-2 (Sarstedt AG & Co., Nümbrecht, Germany) to remove any insoluble material or debris. For tissue samples, approximately 10 mg of cardiac tissue per mouse was taken up in 150 µl RNAqueous lysis buffer (Life Technologies) and treated similarly. The supernatant was then combined with an equal volume of 64% ethanol and mixed by inverting several times. Each sample was then added to a filter cartridge placed in a collection tube. The filter cartridge contains a silica fibre pad which binds and retains the nucleic acids. It should be noted that the silica can only bind to mRNA as well as DNA in the presence of the chaotropic Lysis/Binding buffer (326). The bound nucleic acids were washed and eluted with a low ionic strength elution buffer that was pre-heated to 80^0C to facilitate elution.

Genomic DNA was removed using the DNA-free™ kit (Life Technologies). Samples were incubated with 2 U recombinant, purified DNAse I for 30 min at 37°C in 10 mM Tris-HCl pH 7.5, 2.5 mM $MgCl_2$ and 0.5 mM $CaCl_2$, followed by a second incubation with an additional 2 U recombinant DNAse I for another 30 min at 37°C. One U of DNAse I activity is defined by Life Technologies as an increase in the absorbance of a high molecular weight DNA substrate at a rate of 0.001 absorbance units (A_{260})/min per ml at 25°C. After 1h, DNAse Inactivation Reagent was added to inactivate the DNAse I as well as to chelate the Mg^{2+} and Ca^{2+} cations.

The isolated mRNA was then reverse-transcribed to complementary DNA (cDNA) using either SuperScript® II reverse-transcriptase from Life Technologies or qScript™ cDNA supermix from Quanta Biosciences (Gaithersburg, MD). Both

methods provided similar amounts of cDNA when a set amount of mRNA was reverse-transcribed as tested by quantitative real-time PCR for several genes including TATA-binding protein (*Tbp*), peroxisome proliferator-activated receptor β/ δ (*Pparb/d*) and heat shock protein 5 (*Hspa5*; also known as GRP78, 78 kDa glucose-regulated protein). Using the first method, 6 μg random primers (Life Technologies) was added to approximately 5-500 ng mRNA in a total volume of 23 μl. The mixture was heated at 65°C for 5 min and then cooled to 40°C using the Mastercycler® gradient thermocycler (Eppendorf AG, Hamburg, Germany). Two hundred U of SuperScript® II reverse-transcriptase and 40 U of RNaseOUT™ were added, and the cDNA synthesis reaction was carried out in a final volume of 40 μl in the presence of 50 mM Tris-HCl pH 8.3, 75 mM KCl, 3 mM $MgCl_2$, 10 mM DTT and 0.5 mM dNTP mix. One U Superscript® II reverse-transcriptase activity is defined by Life Technologies as 1 nmol dTTP incorporated into acid-precipitable material in 10 min at 37°C using poly(A) oligo(deoxythymidine)$_{25}$ as the template primer (327) and 1 U RNAseOUT™ is defined as the inhibition of 5 ng RNAse A by 50% when cytidine 2', 3' cyclic monophosphate (cCMP) is used as the substrate (328). The final mixture was incubated at 25°C for 10 min, followed by sequential incubations at 42°C for 60 min and 95°C for 5 min. The reaction mixture was then cooled to 4°C and kept at -20°C for long-term storage or at 4°C for immediate processing. With the second method, the 5 x qScript™ cDNA supermix cocktail from Quanta Biosciences was diluted to a 1 x solution when added to 5-500 ng mRNA in a total volume of 20 μl. The supermix contained optimized concentrations of $MgCl_2$, RNAse inhibitor protein, dNTPs, qScript reverse transcriptase, random primers and oligo deoxythymidine primers. The mixture was incubated at 25°C for 10 min, followed

by sequential incubations at 42°C for 60 min and 95°C for 5 min. The reaction mixture was then cooled to 4°C and kept at -20°C for long-term storage or at 4°C for immediate processing.

2.6.2 Quantitative Real Time PCR

mRNA reverse-transcribed to cDNA was measured by quantitative real time PCR using TATA-binding protein (*Tbp*) (307), hypoxanthine-guanine phosphoribosyltransferase (*Hprt*) or cyclophilin A (*Ppih*, peptidyl prolyl isomerase H) as reference genes. Results were similar when expressed relative to any of these three genes. cDNA samples were assayed with RT^2 SYBR® Green qPCR Mastermix, Low ROX™ (SABiosciences, Frederick, MD), and 10 µM forward and reverse primers. SYBR® Green PCR Master Mix (Life Technologies) and PerfeCTa® SYBR® Green FastMix, Low ROX™ (Quanta BioSciences, Gaithersburg, MD) were also used and gave similar results. The reaction mix was assayed using the Applied Biosystems 7500 real-time PCR system (Life Technologies). The thermocycling protocol started with 1 cycle at 50°C for 2 min followed by 1 cycle at 95°C for 10 min. The transcripts were then amplified during 40 cycles at 95°C for 15 s and 60°C for 1 min. Quantification of fluorescent SYBR Green bound to double-stranded DNA was performed at the end of each cycle at 60°C. The specificity of the amplicon was confirmed by melting curve analysis of amplicon dissociation performed by the Applied Biosystems 7500 software immediately after the 40 cycles of amplification. The protocol consisted of 1 cycle at 95°C for 15 s followed by 1 cycle at 60°C for 1 min and 1 final cycle at 95°C for 15 s. As the thermocycler ramped up to the final temperature of 95°C, the instrument measured the decrease in SYBR Green fluorescence when the

double-stranded amplicons dissociated. The data was displayed as a plot showing the first derivative of the rate of change in fluorescence as a function of temperature. Any non-specific products or primer dimers would be detectable as separate peaks in the dissociation curve.

Table 2.1 Primer sequences of mouse genes probed in RT-PCR assays.

Gene	Forward primer (5' to 3')	Reverse primer (5' to 3')	Ref
Ppia	CAC CGT GTT CTT CGA CAT CAC	CCA GTG CTC AGA GCT CGA AAG	(329)
Tbp	ACC CTT CAC CAA TGA CTC CTA TG	ATG ATG ACT GCA GCA AAT CGC	(278)
Hprt	GCT GGT GAA AAG GAC CTC T	CAC AGG ACT AGA ACA CCT GC	(330)
Lpin1a	GGT CCC CCA GCC CCA GTC CTT	GCA GCC TGT GGC AAT TCA	(228)
Lpin1b	CAG CCT GGT AGA TTG CCA GA	GCA GCC TGT GGC AAT TCA	(228)
Lpin2	TAG ATG CAG ACC CTG TTC CC	CTG GTG CTG GCT TCT TTG T	(307)
Lpin3	AAA GAC TGG ACA CAC CAG GG	TGC TGG ATA TCA CTC AGG CA	(307)
Ppargc1a	GGC ACG CAG CCC TAT TCA	CGA CAC GGA GAG TTA AAG GAA GA	(307)
Ppara	ACT ACG GAG TTC ACG CAT GTG	TTG TCG TAC ACC AGC TTC AGC	(119)
Pparb/d	CGG CAG CCT CAA CAT GG	AGA TCC GAT CGC ACT TCT CAT AC	(331)
Lpl	CCA ATG GAG GCA CTT TCC A	CCA CGT CTC CGA GTC CTC TCT	
Gpam	TCC TTC CTT CAA GAC CGA ATG A	CGC AGG ACT TGC TGG CGG TG	
Dgat1	TGC TAC GAC GAG TTC TTG	CTC TGC CAC AGC ATT GAG	(278)

	AG	AC	
Dgat2	AGT GGC AAT GCT ATC ATC ATC GT	AAG GAA TAA GTG GGA ACC AGA TCA	(147)
Tfam	CTT CGA TTT TCC ACA GAA CAG	TGG TAG CTC CCT CCA CAG	
Cd36	ATT GGT CAA GCC AGC T	TGT AGG CTC ATC CAC TAC	(332)
Pnpla2	TGT GGC CTC ATT CCT CCT AC	TCG TGG ATG TTG GTG GAG CT	(333)
Lipe	GGA GCA CTA CAA ACG CAA CGA	TCG GCC ACC GGT AAA GAG	
Pdk4	GAG GAT TAC TGA CCG CCT CTT TAG	TTC CGG GAA TTG TCC ATC AC	
Slc2a4	TCA TTG TCG GCA TGG GTT T	GGC AAA TAG AAG GAA GAC GTA AGG	
Cpt1b	GTC GCT TCT TCA AGG TCT GG	AAG AAA GCA GCA CGT TCG AT	(278)
Mlycd	CCT CAT GGT CAA CTA CCG CTA CT	CTT GGA GCC CAG GTA GGA GAT	
Acaca	CTG GCT GCA TCC ATT ATG TCA	TGG TAG ACT GCC CGT GTG AA	
Acox1	CAG GAA GAG CAA GGA AGT GG	CCT TTC TGG CTG ATC CCA TA	(278)
Acsl1	TCC TAC AAA GAG GTG GCA GAA CT	GGC TTG AAC CCC TTC TGG AT	
Acsl4	TTA AGA TAC TTG CAC CCC ACC C	TTA GCA GCA CCC AAC CTT GTG	
Acsl5	ACC TCC GTT TCT CTG GCA ATG	ATC AAC ACA GTC CAC CTG CTC C	

Agpat2	TTC ATC AAC CGC CAG CAA G	CAT TGT CGT TGC GTG TAC CCT	
Acadm	TGG CAT ATG GGT GTA CAG GG	CCA AAT ACT TCT TCT TCT GTT GAT CA	(332)
Hspa5	GAG GAT GTG GGC ACG GTG GT	CCC TGA TCG TTG GCT ATG AT	
Ddit3	CAT ACA CCA CCA CAC CTG AAA G	CCG TTT CCT AGT TCT TCC TTG C	
Xbp1	TCC GCA GCA CTC AGA CTA TGT	ATG CCC AAA AGG ATA TCA GAC TC	(334)
Xbp1s	GAG TCC GCA GCA GGT G	GTG TCA GAG TCC ATG GGA	(334)
Atp2a2	CTG TGG AGA CCC TTG GTT GT	CAG AGC ACA GAT GGT GGC TA	(335)
Slc27a1	TGC TTT GGT TTC TGG GAC TT	GCT CTA GCC GAA CAC GAA TC	(336)
Pdha1	GGG ACG TCT GTT GAG AGA GC	TGT GTC CAT GGT AGC GGT AA	(108)

Abbreviations used: *Ppia*, cyclophilin A; *Tbp*, TATA-binding protein; *Ppargc1a*, peroxisome proliferator-activated receptor γ co-activator-1α; *Ppara*, peroxisome proliferator-activated receptor α; *Lpl*, lipoprotein lipase; *Gpam*, glycerol 3-phosphate acyltransferase, mitochondrial; *Dgat1*, diacylglycerol acyltransferase-1; *Dgat2*, diacylglycerol acyltransferase-2; *Tfam*, transcription factor A, mitochondrial; *Pnpla2*, adipose triacylglycerol lipase; *Lipe*, hormone sensitive lipase; *Pdk4*, pyruvate dehydrogenase kinase 4; *Slc2a4*, glucose transporter 4; *Cpt1b*, carnitine palmitoyl transferase-1b; *Mlycd*, malonyl-CoA decarboxylase; *Acaca*, acetyl-CoA carboxylase α; *Acox1*, acyl-CoA oxidase 1; *Acsl1*, acyl-CoA synthetase long-chain family member 1; Agpat2, 1-acylglycerol 3-phosphate O-acyltransferase; *Acadm*, acyl-CoA dehydrogenase, medium-chain; *Hspa5,*heat shock protein 5 (also known as GRP78, 78 kDa glucose-regulated protein); *Ddit3,* DNA damage-inducible transcript 3 (also known as CHOP, CCAAT/enhancer-binding protein homologous protein); *Xbp1*, X-box binding protein 1; *Xbp1s*, X-box binding protein 1, spliced form; *Atp2a2*, sarcoplasmic reticulum Ca^{2+}-ATPase; *Slc27a1*, solute carrier family 27 (fatty acid transporter), member 1; *Pdha1*, pyruvate dehydrogenase E1 alpha 1.

Where not referenced, primers were designed using Primer Express version 2.0 software or with Primer-BLAST web software (National Centre for Biotechnology Information, Bethesda, MD) with default parameters. Primer specificity was also confirmed using Primer-BLAST.

Table 2.2 Primer sequences of rat genes probed in RT-PCR assays.

Gene	Forward primer (5' to 3')	Reverse primer (5' to 3')	Ref
Ppia	CAC CGT GTT CTT CGA CAT CAC	CCA GTG CTC AGA GCA CGA AAG	(329)
Lpin1	TAA GGG GCT GGA GTC TTT CAT	AGC AGC CTG GTA GAT TGT CA	(307)
Lpin2	TAG ATG CAG ACC CTG TTC CC	CTG GTG CTG GCT TCT TTG T	(307)
Lpin3	AAA GAC TGG ACA CAC CAG GG	TGC TGG ATA TCA CTC AGG CA	(307)
Ppargc1a	CAC AAC GCG GAC AGA ACT GA	CCG CAG ATT TAC GGT GCA TT	(307)
Ppara	TGG AGT CCA CGC ATG TGA AG	CGC CAG CTT TAG CCG AAT AG	(307)
Cpt1b	GTC GCT TCT TCA GGT TTG G	AAG AAA GCA GCA CGT CGA T	

Abbreviations used: *Ppia*, cyclophilin A; *Ppargc1a*, peroxisome proliferator-activated receptor γ co-activator-1α; *Ppara*, peroxisome proliferator-activated receptor α; *Cpt1b*, carnitine palmitoyl transferase-1b.

Where not referenced, primers were designed using Primer Express version 2.0 software or with Primer-BLAST web software (National Centre for Biotechnology Information, Bethesda, MD) with default parameters. Primer specificity was also confirmed using Primer-BLAST.

2.7 Sodium dodecyl sulfate-polyacrylamide gel electrophoresis and Western blot analysis

Sodium dodecyl sulfate-polyacrylamide gel electrophoresis (SDS-PAGE) and Western blots were performed using antibodies as described in Table 2.3 (337, 338). Protein concentration was determined using a bicinchoninic acid (BCA) (Thermo Scientific) or Bradford (Bio-Rad, Hercules, CA) assay performed according to manufacturers' instructions. BSA was used as the protein standard. 50-75 µg of protein from cell lysates were diluted in 4 x sample loading buffer (250mM Tris-HCl pH 6.8, 4% SDS, 30% glycerol, 0.003% bromophenol blue and 10% 2-mercaptoethanol added fresh) and then boiled for 5 minutes. For preparation of cardiac tissue, approximately 10 mg of each sample was sonicated in 200 µl lysis buffer containing 20 mM Tris-HCl pH 7.4, 50 mM NaCl, 50 mM NaF, 5 mM $Na_4P_2O_7$, 250 mM sucrose, 1% Triton X-100, 1 mM DTT, 30 nM microcystin-LR, 1 mM Na_3VO_4, and a protease inhibitor cocktail (Sigma-Aldrich). Samples were sonicated twice for 5 s (1 min interval between sonications) at setting 20 using the Sonic Dismembrator Model 300. Samples (35 µg of protein) were diluted in 3 x sample loading buffer (62.5 mM Tris-HCl pH 6.8, 6 M urea, 10% glycerol, 2% SDS, 0.003% bromophenol blue, and 5% 2-mercaptoethanol added fresh) and then boiled for 5 min before loading.

The treated cell lysates or tissue homogenates were loaded in a 15-well SDS-PAGE gel along with 10 µl of Precision Plus All-Blue Protein Standards (Bio-Rad) consisting of 250, 150, 100, 75, 50, 37, 25, 20, 15, and 10 kiloDalton (kDa) protein standards. The stacking gels were comprised of 0.125 M Tris-HCl pH 6.8, 0.1% SDS, 3.9% acrylamide and 0.1% bisacrylamide, and the separating

gels contained 0.375 M Tris-HCl pH 8.8, 0.1% SDS with 10% acrylamide and 0.28% bisacrylamide. Eight percent acrylamide/0.22% bisacrylamide and 6% acrylamide/0.17% bisacrylamide separating gels were used to separate lipin-1 and -2, respectively for better detection in Western blots. Proteins were separated at 120 V for 2.5 h in Laemmli electrophoresis buffer (25 mM Tris base, 192 mM glycine, 0.1% SDS pH 8.3) using a Mini-Protean II protein electrophoresis apparatus (Bio-Rad).

The proteins were transferred onto 0.45 µm Transblot nitrocellulose membranes (Bio-Rad) by overnight transfer at 115 mAmps in Tris-glycine buffer (25 mM Tris base, 192 mM glycine) containing 20% methanol and 0.05% SDS at 4°C. Two methods of protein detection were used: the enzymatic chemiluminescence (ECL) and the infrared methods of detecting horseradish peroxidase- and fluorophore-conjugated secondary antibodies, respectively. In the first method, the membranes were blocked in Tris-buffered saline (TBS: 20 mM Tris-HCl pH 7.6, 137 mM NaCl) containing 0.1% Tween-20 and 5% skimmed milk (TBS-MT) for 1 h at room temperature, followed by 4 washes with TBS containing 0.1% Tween-20 (TBS-T) for 5 min per wash on a orbital shaker. The membranes were then incubated overnight with primary antibodies diluted in TBS-T containing 1% milk. The membranes were placed in Corning tubes containing the primary antibody solutions and left to rotate on a tube rotator (VWR International, Radnor, PA) in the cold room. The primary antibodies used are shown in Table 2.3. The membranes were then washed 4 times with TBS-T for 5 min each wash at room temperature. Goat anti-rabbit immunoglobulin G (IgG), donkey anti-goat IgG, and goat anti-mouse IgG secondary antibodies that were conjugated with horseradish peroxidase (Santa Cruz Biotechnology Inc.,

Santa Cruz, CA) were diluted 1:2000, 1:2000 and 1:3000, respectively in TBS-MT and were then incubated with their respective membranes for 90 min at room temperature. Membranes were again washed with TBS-T five times in 5 min intervals. Finally, the membranes were probed using the Immunstar WesternC ECL kit (Bio-Rad) and chemiluminescence was detected by exposure to autoradiography film (Kodak, Rochester, NY). Developed films were scanned and quantitative densitometric analysis was performed using ImageJ software (NIH, Bethesda, MD).

The second method of detecting fluorophore-conjugated secondary antibodies essentially uses the same steps as the ECL method except that proprietary blocking buffers from LI-COR Biosciences (Lincoln, NE) or Rockland Immunochemicals (Gilbertsville, PA) were used instead. Furthermore, PBS containing 0.1% Tween-20 was used as the wash buffer and Alexa Fluor® 680-conjugated goat anti-mouse IgG (Life Technologies, Carlsbad, CA) and IRDye® 800CW-conjugated goat anti-rabbit IgG (LI-COR Biosciences, Lincoln, NE) diluted 1:10,000 in blocking buffer-PBS (1:1, by vol.) were used as the secondary antibodies. Fluorescent signals were detected at 700 and 800 nm using the LI-COR Odyssey® Imaging System and the Odyssey® Imaging software version 1.2 was used for quantification.

The antibody against the C-terminus of lipin-1 was a gift from Dr. Thurl Harris (University of Virginia, Charlottesville, VA). Antibodies against lipin-2 were raised in rabbits using the peptide sequence N' – PKGELIQERTKGNK – C' followed by affinity-purification against this peptide (Genscript, Piscataway, NJ). The lipin-2 antibody was verified by comparing endogenous lipin-2 in the heart to

recombinant lipin-2 protein overexpressed in MCF-7 breast cancer cells as shown later (Figure 5.1B, *top panel*).

Table 2.3 Primary antibodies used in Western blot analysis.

Primary antibody	Company	Catalogue no.
p-acetyl CoA carboxylase (serine 79)	Upstate	07-303
Acetyl CoA carboxylase	Cell Signaling Technology	3662
p-Akt/protein kinase B (serine 473)	Cell Signaling Technology	9271
Akt/protein kinase B	Cell Signaling Technology	9272
p-pyruvate dehydrogenase (serine 293)	Calbiochem	AP1062
Pyruvate dehydrogenase	Cell Signaling Technology	2784
p-AMP-activated protein kinase (threonine 172)	Cell Signaling Technology	2531
AMP-activated protein kinase	Santa Cruz Biotechnology	sc19131
Ran GTPase	BD Biosciences	610341
Fatty acid transport protein 1	Santa Cruz Biotechnology	sc14497
Sarco/endoplasmic reticulum calcium-ATPase	Cell Signaling Technology	4388
Glucose transporter 4	Chemicon	AB1346
p-hormone sensitive lipase (serine 660)	Cell Signaling Technology	4126

Hormone sensitive lipase	Cell Signaling Technology	4170
p-S6 ribosomal protein (serine 240/244)	Cell Signaling Technology	2215
S6 ribosomal protein	Cell Signaling Technology	2217
Adipose triacylglycerol lipase	Cell Signaling Technology	2138
Acyl-CoA synthetase long-chain 1	Cell Signaling Technology	4047
p-extracellular signal-regulated kinase 1/2 (ERK1/2) (threonine 202/tyrosine 204)	Cell Signaling Technology	9101
Extracellular signal-regulated kinase 1/2	Cell Signaling Technology	9102
p-mammalian target of rapamycin (mTOR) (serine 2448)	Cell Signaling Technology	2971
Mammalian target of rapamycin (mTOR)	Cell Signaling Technology	2972
p-p70S6 kinase (threonine 424)	Cell Signaling Technology	9204
p70S6 kinase	Cell Signaling Technology	9202
Glyceraldehyde-3-phosphate dehydrogenase	Sigma-Aldrich	G8795
Calnexin	Stressgen	SPA-860
protein phosphatase-1c	Santa Cruz	sc7482
Human influenza hemagglutinin (HA)-tag	Covance	MMS-101R
FLAG-tag	Clontech	635691
Simian virus 5 (V5)-tag	Life Technologies	R960-25

2.8 Measurement of lipin translocation onto membranes

2.8.1 *In vitro* translocation of lipins

Measurement of the capacity of wild-type and mutant lipin-2 proteins to translocate to endoplasmic reticulum membranes was based upon previous work using microsomal membranes obtained from rat liver (138, 295). Livers of male Sprague-Dawley rats were perfused with 60 ml of sterile ice-cold phosphate-buffered saline, pH 7.4, and homogenized in 0.25 M sucrose containing 2 mM dithiothreitol and 20 mM HEPES buffer, adjusted to pH 7.4 with KOH. The homogenates were centrifuged at 4°C for 15,300 x g for 20 min to obtain a nuclear and mitochondria-free supernatant, which we have termed cell-free rat liver homogenates. For experiments involving overexpressed lipins in HEK 293 cell lysates, the supernatant was centrifuged for a further 400,000 x g for 40 min to pellet the microsomal fraction. This pellet was resuspended at 37°C in homogenization buffer containing 0.1 mM fatty acid-free BSA and incubated for 20 min to remove fatty acids and dissociate bound lipin from the membranes. The microsomal membranes were then collected after re-centrifuging at 4°C as above and resuspended in the same buffer.

Recombinant V5-tagged lipins expressed in HEK 293 cells were obtained from Dr. Karen Reue (University of California-Los Angeles, CA) (134, 138). These cells were homogenized in 0.25 M sucrose containing 2 mM dithiothreitol and 20 mM HEPES buffer, and adjusted to pH 7.4 with KOH and phosphatase inhibitor cocktails 1 and 2 from Sigma-Aldrich. The mitochondria-free supernatant from these cell lysates was then isolated after centrifugation for 16,000 x g for 20 min to collect lipins bound to endoplasmic reticulum membranes and in the cytosol.

For the translocation experiments with overexpressed lipins, 350 µg of liver microsomal protein was incubated for 5 min at 37°C in a final volume of 20 µl of homogenizing buffer containing 0.1 mM BSA and 0 – 750 µM K^+-oleate. The 75 mM K^+-oleate stock solution was made by solubilizing the oleic acid in 20% molar excess of KOH at 65°C, followed by sonication. The extract from the HEK 293 cells containing recombinant lipin (about 250 µg of total protein) was added, and the tubes were then incubated for 10 min at 37°C to equilibrate the lipins between cytosol and membrane fractions (24). Endogenous PAP activity from rat livers was also tested in translocation experiments using the cell-free rat liver homogenates (nuclear- and mitochondria-free fractions) obtained as detailed above. In these experiments, 500 µg mitochondria-free supernatant was treated in homogenizing buffer containing 0 – 750 µM K^+ oleate at 37°C for 10 min.

Following this, all samples were cooled on ice for 5 min. The soluble proteins were then collected after centrifugation at 400,000 x g for 40 min at 4°C. The pellets (membranes) were resuspended in 45 µl of homogenization buffer. The samples were then stored at −80 °C and PAP activities were measured later. Alternatively, the cytosolic fractions were treated with 4 volumes of acetone at −20°C. The precipitated protein was collected by centrifugation and resolubilized in 45 µl of homogenization buffer. Samples for Western blotting were prepared with 4 x NuPAGE LDS SB from Life Technologies and stored at −80°C for further processing.

2.8.2 Separation of cytosol from cell ghosts using hypotonic digitonin lysis

Cells were treated with a hypotonic solution containing 10 mM HEPES pH 7.4, 0.5 mM DTT, protease inhibitors, 30 nM microcystin-LR and 80 μM digitonin for 4 min on a chilled glass plate levelled on top of an ice-filled plastic container. Digitonin binds to and extracts cholesterol from the plasma membrane and causes perforations in the plasma membrane while leaving intracellular organelles intact (339-341). The cytosolic solution was isolated and the cell ghosts were washed twice with ice-cold HBS before collection in 10 mM HEPES pH 7.4, 0.5 mM DTT, protease inhibitors, 30 nM microcystin-LR and 250 mM sucrose. Cytosolic and cell ghost samples were stored at −80°C before processing. Cell ghosts were sonicated twice for 4 s with 1 min intervals at setting 20 using the Sonic Dismembrator Model 300. Both cytosolic and cell ghost fractions were centrifuged for 2 min at 750 x g.

2.8.3 Determination of the extent of cytosolic leakage using the lactate dehydrogenase (LDH) assay

LDH activities in the cytosolic and cell ghost fractions were measured to determine the extent of cell lysis and release of cytosolic content after treatment with the hypotonic, digitonin-containing solution. LDH activity was measured in 167 mM Tris pH 7.4, 1.33 mM sodium pyruvate and 0.33 mM NADH (342). The rate of decrease in the absorbance at 340 nm due to the conversion of NADH to NAD^+ was measured using the SpectraMax 250 (Molecular Devices Corporation, Sunnyvale, CA). The initial rate of reaction was calculated using the extinction coefficient of NADH (6.22×10^{-3} M^{-1} cm^{-1}) and an approximate pathlength of 0.7 cm (derived from a total well volume of 0.22 ml and an approximate surface area of 0.32 cm^2). An average of 85±1% and 91.0±0.6% total LDH activity were

released by digitonin from rat hepatocytes and cardiomyocytes, respectively, indicating a high degree of cell permeabilization (225, 296, 340). LDH release could be complete if digitonin was used at a higher concentration (339, 343); however, the use of a hypotonic solution made the cells more susceptible to permeabilization with very low concentrations of digitonin (294). Furthermore, a minor proportion (2-5%) of LDH is localized in other compartments (344-346).

PAP activities in the cytosol and cell ghost fractions were adjusted if the minimum LDH activity in the cytosol did not reach the average cytosolic LDH value. For example, 10% of the total PAP activity was subtracted from the PAP activity in the cell ghosts if the cytosolic LDH value in rat hepatocytes was 75% of total LDH activity. The proportion of cytosolic to membrane-associated PAP activity was then re-calculated and expressed relative to the corrected total PAP activity. Only two experiments using NRVMs and one experiment with rat hepatocytes had cytosolic LDH values of 67 – 75% on average.

2.9 Analysis of radiolabelled fatty acid and glycerol incorporation into glycerolipids

2.9.1 Treatment of cells with radiolabelled substrates

NRVMs cultured in 10% FBS-DME/F12 medium were treated with DME/F12 medium containing 0.1% BSA for 4 h to decrease hormonal levels and signalling. Diethyl *p*-nitrophenyl phosphate (E600) was then added at a final concentration of 100 µM to inhibit intracellular lipases and lipid turnover. After 30 min, the cells were then treated with DME/F12 medium containing 0.3 mM fatty acid-poor BSA, 1 mM [^{3}H]glycerol (1.7 µCi/µmol), 1 mM [^{14}C]oleate (0.25

µCi/µmol) and 100 µM E600, similar to conditions used in a previous study in rat hepatocytes (347). Furthermore, choline chloride was supplemented such that its final concentration was 100 µM to ensure adequate choline levels for PC synthesis (347, 348). The stock solution of 75 mM oleate was made by solubilizing the oleic acid in 20% molar excess of KOH at 65°C, followed by sonication; the palmitate stock solution was treated similarly. In some experiments, 0.3 mM [^{3}H]glycerol (5.3 µCi/µmol), 0.5 mM [^{14}C]oleate (0.5 µCi/µmol) and 0.1 mM BSA were used instead. These conditions are similar to those used in a previous study looking at TG synthesis in NRVMs so that we could make comparisons between studies (266). When treatments were complete, cells were washed twice with ice-cold HEPES-buffered saline (HBS: 25 mM HEPES, 138 mM NaCl and 2.7 mM KCl pH 7.4) containing 1 mg/ml BSA, followed by one more wash with ice-cold HBS. Cell extracts were collected in 2 consecutive volumes of 500 µl methanol. The combined volume of methanol was sequentially extracted in 12 x 75 mm borosilicate tubes with 1 ml chloroform followed by 0.9 ml 2 M KCl containing 0.2 mM HCl (349). The tubes were centrifuged at 1,600 x g for 10 min and the top phase was aspirated.

2.9.2 Thin layer chromatography of lipid extracts

Samples of the chloroform phase (800 µl) containing the extracted lipids (out of a theoretical 1.1 ml) was isolated using a 500 µl Hamilton Syringe. The lipids were dried down under a nitrogen stream and resuspended in 100 µl chloroform. 10 µl of each sample was aliquoted into scintillation vials for measurements of total radiolabel incorporation. The majority of the lipids (80 µl) were pipetted onto glass-backed, silica-coated TLC plates (EMD Chemicals). The plates were developed halfway up using chloroform-methanol-acetic acid-

acetone-water (50:10:10:20:5, by vol.) followed by a second full-length development with hexane-diethyl ether-acetic acid (60:40:1, by vol.) (350). TLC plates were stained with iodine vapor and individual lipids were scraped from the plates and collected in scintillation vials containing 10% water and EcoLite™ scintillation fluor (MP Biomedicals). Radioactive counts were measured using the Beckman LS3801 scintillation counter (Beckman Coulter Inc., Indianapolis, IN).

2.9.3 Quantification of organic phosphates

Organic phosphate was assayed to measure phospholipid content using *rac*-glycerol 3-phosphate as a standard (351). Extracted lipids in 100 µl chloroform phase from each sample were transferred to borosilicate tubes using a 100 µl Hamilton syringe. Phospholipids were dried down and digested with 50 µl of perchloric acid at 180°C for 30 min. The reaction mixture was cooled and 278 µl water, 55 µl 2.5% ammonium molybdate and 55 µl 10% ascorbic acid were added before boiling for 15 min. Absorbance readings were quantified with a multi-well plate reader at 700 nm.

2.10 Analysis of functional and metabolic parameters in the hearts of *fld* and control mice

2.10.1 Animal care and breeding strategy

We established a breeding colony of Balb/cByJ-Lpin1fld/J mice obtained from The Jackson Laboratory, Bar Harbor, ME. Two types of breeding triads were used to produce experimental animals. The first type of triads consisted of two female *fld* mice bred with one male heterozygous mouse, which produces only *fld* and heterozygous offspring. The other triad contained two female

heterozygous mice and one male heterozygous mouse, resulting in *fld,* heterozygous and wild-type offspring. The wildtype and heterozygous mice were both designated as the control mice. Mice were fed Lab Diet 5058 containing 9% fat by weight (PMI Nutrition International, St. Louis, MO). The research was conducted in accordance with the policies of the Canadian Council on Animal Care, as approved by the University of Alberta Animal Policy and Welfare Committee.

2.10.2 Non-invasive assessment of cardiac function and tissue collection

Transthoracic echocardiography was performed by Donna Beker and Sandra Kelly from the Echocardiography Core of the Cardiovascular Research Centre (University of Alberta). The male mice were mildly anesthetized (1.5% isoflurane and 95% O_2) and readings were made using a 30 MHz transducer (RMV-707B) on the Vevo 770 Imaging System (VisualSonics, Toronto, ON) (352, 353). Mice were either 10 or 19-23 weeks of age. Two-dimensional M-mode imaging on the parasternal short axis of the left ventricle was used to determine end-diastolic and end-systolic wall thickness and left ventricular internal diameter. From these measurements, the two most common indicators of cardiac function, i.e. ejection fraction and fractional shortening, can be calculated as follows:

Fractional shortening (%):

$$\frac{(\text{LV internal diameter in diastole } - \text{ LV internal diameter in systole})}{\text{LV internal diameter in diastole}} \times 100$$

94

Ejection fraction (%):

$$\frac{(LV\ end\text{-}diastolic\ dimension\ -\ LV\ end\text{-}systolic\ dimension)}{LV\ end\text{-}diastolic\ dimension} \times 100$$

where LV stands for left ventricular

The left ventricular end-diastolic dimension is calculated using Teichholz's formula(354):

$$\frac{7 \times (LV\ internal\ diameter\ in\ diastole)^3}{2.4 + LV\ internal\ diameter\ in\ diastole}$$

The left ventricular end-systolic dimension is calculated similarly.

Pulse-wave Doppler and tissue Doppler imaging were used to determine mitral valve E and A wave velocities, and mitral valve annular velocities, respectively. Pulmonary vein wave velocities were also obtained from pulse-wave Doppler analysis. Isovolumic relaxation and contraction time as well as aortic ejection time were calculated from the analysis of mitral and aortic valve waveforms through at least 3 to 6 cardiac cycles. The Tei index, which is another measurement of cardiac function was calculated as follows (355):

Tei index:

$$\frac{Isovolumic\ relaxation\ time + isovolumic\ contraction\ time}{ejection\ time}$$

One week after echocardiographies, the 11-week old male mice were fasted from 0900 h to 1300 h (0600 h - 1800 h light/dark cycle) before euthanization by decapitation. Mouse hearts were isolated and then washed in PBS. Hearts were wiped clean of excess PBS on KimWipe (Kimberly-Clark

Corporation, Irving, TX) before being weighed. Hearts were then clamped, flash-frozen in liquid nitrogen and stored at -80°C. The hearts were ground into smaller pieces using a mortar and pestle, and portions of cardiac tissue were processed for real time PCR (RT-PCR) and Western blot analysis as described above.

2.10.3 Serum glucose, fatty acids and triacylglycerol

Serum glucose samples were also collected from the 11-week old mice by exsanguination and assayed with the glucose-c kit (Wako Chemicals USA Inc., Richmond, VA). This kit was developed using principles explained and developed by P. Trinder in 1969 (356, 357). β-*D*-glucose was oxidized by glucose oxidase at 37°C to form gluconic acid and hydrogen peroxide. The kit also contained mutarotase to convert any α-*D*-glucose molecules to the β-*D*-glucose form since glucose oxidase activity is stereo-specific. Peroxidase catalyzed the condensation of 4-amino-antipyrine and phenol to a red quinone dye using the hydrogen peroxide formed from the glucose oxidase reaction. The formation of the red quinone dye was measured at 492 nm using a multiwell plate reader, the Easy Reader EAR340AT (SLT-Lab Instruments, Austria). For serum lipid measurements, food was withheld from 19- to 23-week old male mice from 0900 to 1100 h. The mice were then euthanized by an intraperitoneal injection with 480 mg/kg ©Euthanyl (Bimeda-MTC Animal Health Inc.) and blood was collected from the inferior vena cava. Serum TG and unesterified FAs were measured using the TG GPO kit (Pointe Scientific, Canton, MI) and NEFA kit (Wako Chemicals USA Inc.) respectively.

The reactions underlying the TG GPO kit were described by Megraw et al. (358) and the kit also relies on the Trinder formation of a red quinone-like dye.

Triacylglycerol was hydrolyzed to glycerol and FAs by lipase. Glycerol kinase catalyzed the formation of *L*-glycerol 3-phosphate. Glycerophosphate oxidase (GPO) then reacted with *L*-glycerol 3-phosphate to form dihydroxyacetone phosphate and hydrogen peroxide. Finally, peroxidase, in the presence of hydrogen peroxide, catalyzed the formation of a red quinoneimine dye from 4-aminoantipyrine and 3-hydroxy-2,4,6-tribromobenzoic acid. Absorbance at 492 nm was read using the multiwell plate reader. The first step of the Wako non-esterified fatty acid (NEFA) kit involved the conversion of unesterified FAs to acyl-CoA by acyl-CoA synthetase. The acyl-CoA moieties were then oxidized by acyl-CoA oxidase to produce trans-2,3-dehydroacyl-CoA and hydrogen peroxide. Lastly, peroxidase allowed for the conversion of 4-amino-antipyrine and 3-methyl-*N*-ethyl-*N*-(β-hydroxyethyl)-aniline to a purple dye, and the absorbance was measured at 550 nm.

2.10.4 Non-invasive blood pressure measurements

This work was performed by Brandi Sidlick from the Cardiovascular Research Centre at the University of Alberta. Conscious 19- to 23-week old male mice were restrained using a rodent restrainer (IITC Life Science Inc., Los Angeles, CA) and real-time blood pressure measurements were obtained with a tail cuff system (IITC Life Science Inc.).

2.10.5 *Ex vivo* perfused working heart studies and measurements of fatty acid and glucose metabolism

These studies were performed by Grant Masson from the laboratory of Dr. Jason Dyck. Male mice (19- to 23-weeks old) were euthanized using an intraperitoneal injection of 12 mg sodium pentobarbital (Bimeda-MTC Animal

Health Inc., Cambridge, ON) and hearts were quickly excised. The aorta was cannulated and the heart was first perfused by the Langendorff retrograde perfusion method with standard Krebs-Henseleit buffer (118.5 mM NaCl, 25 mM NaHCO$_3$, 4.7 mM KCl, 1.2 mM MgSO$_4$, 1.2 mM KH$_2$PO$_4$, 2.5 mM CaCl$_2$, 0.5 mM EDTA and 5 mM glucose) (359, 360). This method was developed and described by Dr. Oskar Langendorff in 1895, following on the work by Elias Cyon at the Carl Ludwig Institute of Physiology in Leipzig, Germany; the history and background of this work have been previously described in reviews written by Heinz-Gerd Zimmer (361) and Monika Skrzypiec-Spring et al. (362). Once the Langendorff mode was set up, the pulmonary vein was cannulated and this established a connection between the preload reservoir and the left atrium (Figure 2.1 obtained from Belke et al. and Larsen et al.) (360, 363, 364).
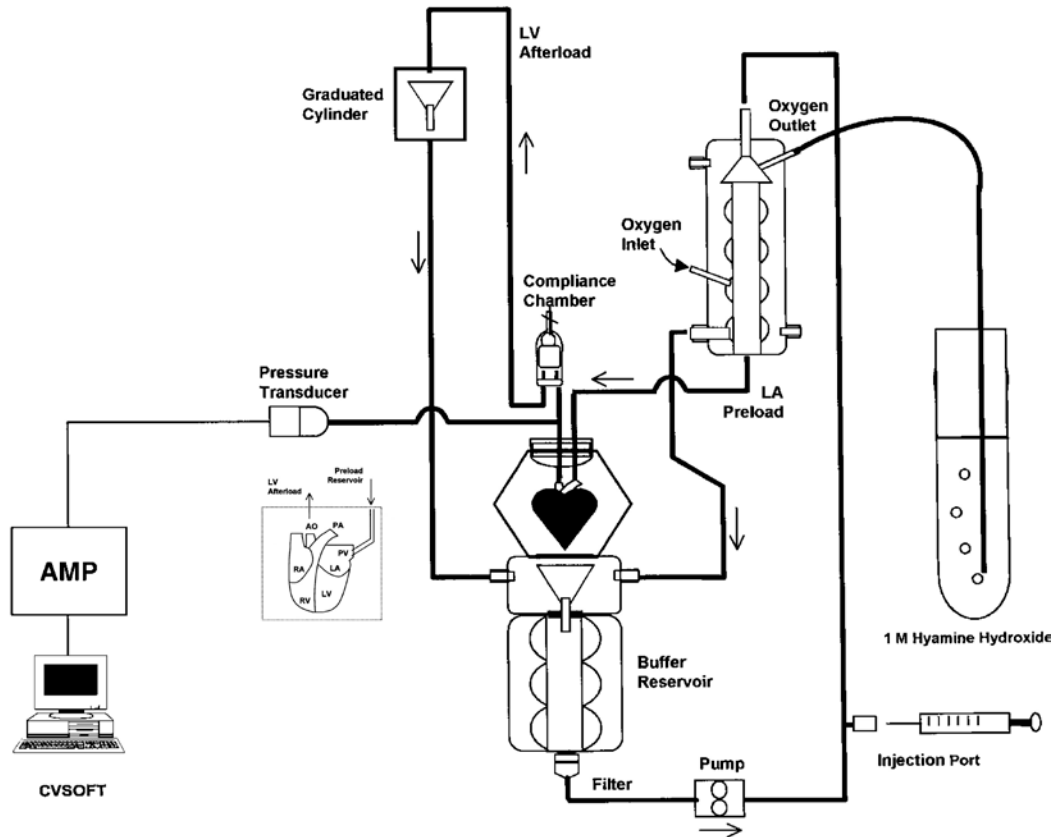
Figure 2.1 Schematic representation of a setup used for the working mouse heart perfusion method. This figure was obtained from Belke et al. and Larsen et al. (360, 363).

To switch the perfusion from Langendorff to working mode, the line from the Langendorff buffer reservoir was shunted off and the line from the preload reservoir was turned on. Buffer from the preload reservoir entered the left atrium and was pumped out through the aorta into the afterload line (Figure 2.1). Left atrial preload and aortic afterload were set to 11.5 and 50 mm Hg, respectively (364). The heart was allowed to beat spontaneously and the pressure transducer measured left ventricular pressure. The compliance chamber imitated the elastic capacity of arteries to accommodate pressure changes during the cardiac cycle.

The heart was perfused through the left atrium for the first 30 min with a modified Krebs-Henseleit buffer (KHB) containing 50 µU/ml insulin to deplete TGs as much as possible (88). Subsequently, the glucose in the modified KHB was replaced with 5 mM [U-^{14}C]glucose (16 µCi/mmol) and the hearts were perfused with this modified KHB supplemented with 1.2 mM [9,10-^{3}H]oleate (50 µCi/mmol) conjugated to 0.45 mM fatty acid-free BSA at a constant volume of 100 ml for an additional 30 min. This concentration of oleate was used because previous studies demonstrated that endogenous TG stores are depleted if lower FA concentrations are used and we wanted to avoid this in order to determine steady state TG turnover (88). Coronary and aortic effluent were measured throughout the perfusion at 10 min intervals (364, 365). Calculations used to determine cardiac function of the hearts in the working perfused heart system are described below:

Developed pressure (mm Hg):

   Peak systolic pressure – left ventricular end-diastolic pressure

Cardiac output (ml/min):

   Aortic outflow **+** coronary flow

Cardiac minute work (l/min**.**mmHg):

   $$\frac{\text{Cardiac output x peak systolic pressure}}{1000}$$

100

Cardiac Power (kg.m^2/s^3 or J/s or watts):

Cardiac output x 10^{-6} /60 (to convert to m^3/s) x (peak systolic pressure – preload) x 133.322 (to convert mmHg to Pascals or kg/m.s^2)

Rates of glucose and oleate oxidation were measured by determining the rate of ^3H_2O and $^{14}CO_2$ formation. The ^3H_2O accumulated in the perfusate and an aliquot was collected every 10 minutes. Gaseous $^{14}CO_2$ was trapped in a 1 M hyamine hydroxide solution in the air outlet line (Figure 2.1); there was also $^{14}CO_2$ in the perfusate. Perfusate and hyamine hydroxide samples were collected at 10 min intervals. The perfusate was immediately injected under mineral oil to prevent CO_2 escape. The $^{14}CO_2$ was then extracted by injecting 1 ml of perfusate into 1 ml of 9 N H_2SO_4 in sealed metabolic vials, which also contained 400 μl of 1 M hyamine hydroxide in suspended center wells. Vials were gently shaken for 1 h and the $^{14}CO_2$-containing solution from the center wells was removed and added to scintillation fluor. Once perfusions were completed, hearts were flash-frozen in liquid nitrogen and stored at -80°C until they were ready for processing.

2.10.6 Incorporation of [^{3}H]oleate and [^{14}C]glucose into glycerolipids and glycogen in perfused mouse hearts

Rates of [^{3}H]oleate incorporation into glycerolipids in 19- to 23-week old perfused hearts were also determined by TLC. Frozen perfused hearts were first ground into smaller pieces using a mortar and pestle. Cardiac tissue (10-15 mg) was extracted using chloroform-methanol-2 M KCl containing 0.2 mM HCl (1:1:0.9, by vol.) (349). A sample of the chloroform phase (800 μl out of a

theoretical total of 1.1 ml) was dried down under a stream of nitrogen. The extracted lipids were resolubilized in 100 µl of chloroform and 10 µl aliquots were added to scintillation vials for total radioactive counts. Eighty µl of each sample was loaded onto a glass-backed, silica-coated TLC plate (EMD Chemicals), which was developed halfway up the plate using chloroform-methanol-acetic acid-acetone-water (50:10:10:20:5, by vol.). This was followed by a second full-length development with hexane-diethyl ether-acetic acid (60:40:1, by vol.) to separate the neutral lipids at the top of the plate (350). TLC plates were stained with iodine vapor and individual lipids were collected in scintillation vials containing 10% water and EcoLite™ scintillation fluor (MP Biomedicals). Radioactive counts were measured using the Beckman LS3801 scintillation counter (Beckman Coulter Inc.).

A two-dimensional TLC system was used to determine the levels of radiolabelled PC, PS, phosphatidylinositol (PI), sphingomyelin and cardiolipin. Each sample was loaded onto an individual TLC plate at one corner and developed with chloroform-methanol-water-NH$_4$OH (60:40:4:0.25, by vol.) in the first direction. The plate was then turned 90° and developed with chloroform-methanol-acetic acid-acetone-water (45:15:10:20:5, by vol.) in the second direction. The phospholipids were identified by determining the retention factor (R$_f$) of the different standards on a separate plate. Furthermore, PC, PS and PI standards were loaded onto each plate at opposite corners from where the sample is loaded (Figure 2.2) to ensure good identification of these phospholipids since PC, PS and PI migrate in close proximity to one another. Ninhydrin staining for amine-containing phospholipids and Dragendorff (potassium bismuth iodide) staining for choline-containing phospholipids were also used to further validate

the identification of PS, PE and PC (366). When oleate incorporation into lipids was measured, the results were essentially identical whether we used the one- or two-dimensional TLC system.
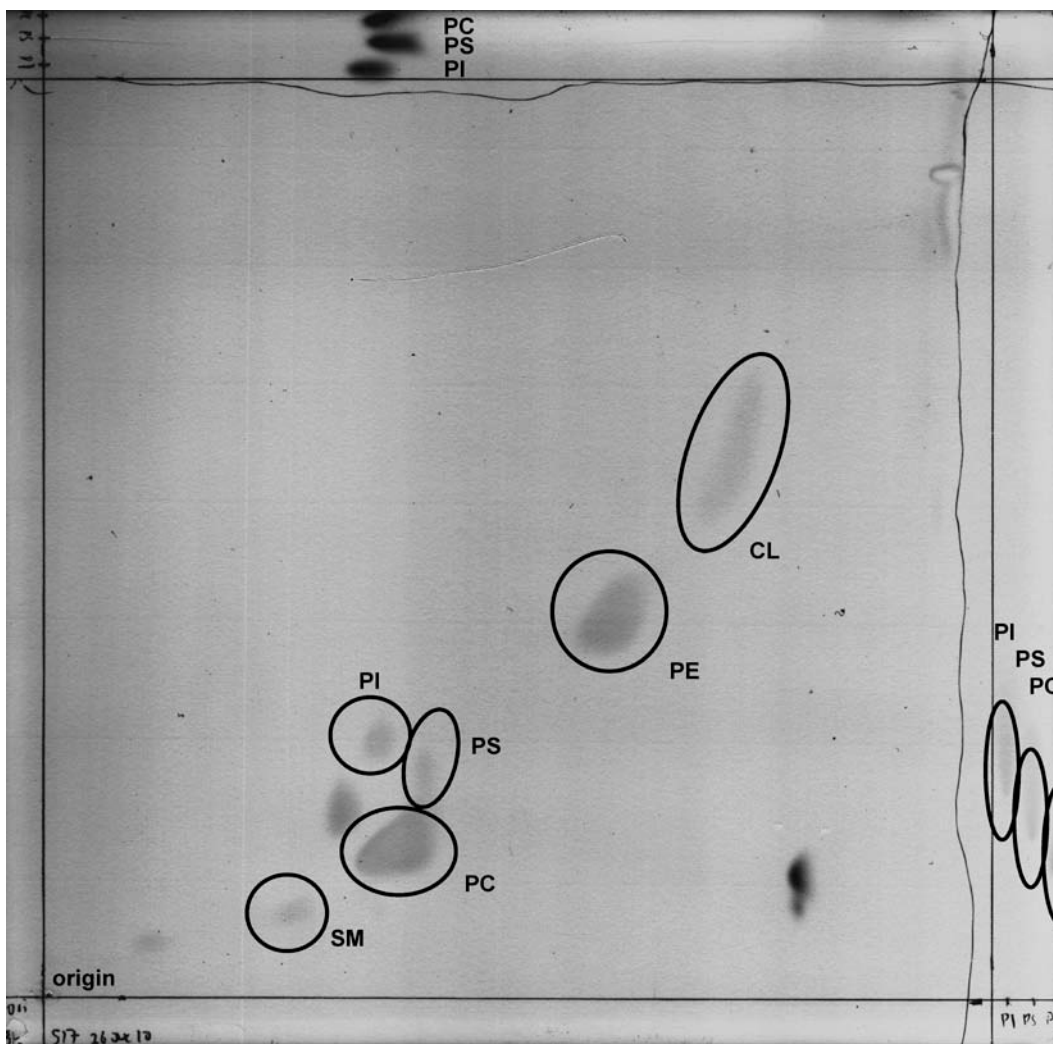
Figure 2.2 Two-dimensional TLC of lipids from a cardiac sample. The TLC plate was developed with chloroform-methanol-water-NH$_4$OH (60:40:4:0.25, by vol.) in the upward direction. The plate was then turned 90° counter-clockwise and developed with chloroform-methanol-acetic acid-acetone-water (45:15:10:20:5, by vol.) in the second direction. PC, PS and PI lipid standards were loaded onto the plate to aid phospholipid identification. Lipids were stained using iodine and the image of the plate was obtained by scanning with the ImageScanner (Amersham Pharmacia Biotech, Uppsala, Sweden).

2.10.7 Measurements of phospholipid and glycogen content in *fld* and control hearts

The two-dimensional TLC system was also used to quantify the phosphate content of individual phospholipids from the ventricles of 19- to 23-week old *fld* and control mice. Different phospholipids were scraped off the TLC plate and quantified with an organic phosphate assay using *rac*-glycerol 3-phosphate as a standard (351). Briefly, the lipid extracts were digested with 100 µl of perchloric acid at 180°C for 30 min. After cooling, 556 µl water, 110 µl 2.5% ammonium molybdate and 110 µl 10% ascorbic acid were added and the mixture was vortexed vigorously before heating at 90°C for 15 min. Absorbance readings were quantified with the Easy Reader EAR340AT (SLT-Lab Instruments, Austria) at 700 nm.

Glycogen content and glucose incorporation into glycogen were also measured (367, 368). To do this, 10mg of powdered cardiac tissue was hydrolyzed at 100°C for 30 min in 40% KOH followed by precipitation with 100% ethanol. The precipitated glycogen was washed three times with 95% ethanol and then hydrolyzed at 100°C for 3 h in 3 M HCl to hydrolyze the glycogen to glucose. After neutralization with 2 M NaOH, glucose equivalents were measured using a Glucose-c kit from Wako Chemicals. A portion of the glucose equivalents from each *fld* and control mouse heart perfused with [³H]oleate and [¹⁴C]glucose as substrates was added to EcoLite™ scintillation fluor (MP Biomedicals) and the incorporation of [¹⁴C]glucose in glycogen was also measured by scintillation counting.

2.10.8 Quantification of phosphatidate and triacylglycerol in *fld* and control hearts

Phosphatidate (PA) was measured in lipid extracts as described previously (351). Briefly, a PA standard curve (0 – 4 nmol) and lipids extracted from 19- to 23-week old cardiac samples were loaded onto plastic-backed silica TLC plates (EMD Chemicals) along with PC and PA standards on the outermost lanes. The plates were developed twice in chloroform-methanol-ammonium hydroxide (65:35:7.5, by vol.). PA does not migrate very well in this solvent system due to its negative charge. The migration of PA bands was determined by cutting the outermost lanes and identifying the PA and PC standards. The TLC plates were then cut 1 cm above the migrated PA, thus removing most other phospholipids. The plates were then developed in the reverse direction in chloroform-methanol-acetic acid-acetone-water (50:20:12:10:5, by vol.) followed by staining for 1 h with 0.3% Coomassie Brilliant Blue R250 in 20% methanol containing 100 mM NaCl. The TLC plates were destained in 20% methanol and scanned at 700 nm using the Odyssey® Infrared Imaging scanner (LI-COR Biosciences, Lincoln, NB). This chromatographic system separates PA from other phospholipids so that its levels can be determined by comparison to the PA standard curve. TG concentrations were measured in extracts of heart using the TG GPO kit (Pointe Scientific).

2.10.9 Quantification of diacylglycerol and ceramides in *fld* and control hearts

Diacylglycerol (DG) and ceramide levels in 11-week old *fld* and control hearts were measured as described previously (351). Cardiac samples were extracted in chloroform-methanol-water (1:1:0.5, by vol.) and extracted lipids (25 – 50 nmol of phospholipids as measured by phosphate assay) were dried down under a nitrogen stream. The samples were then assayed in reaction cocktails containing 50 mM imidazole/HCl pH 6.6, 1 mM diethylenetriaminepentaacetic acid (DETAPEC), 50 mM NaCl, 12.5 mM $MgCl_2$, 1 mM EGTA, 10 mM DTT, 1 mM $[\gamma\text{-}^{32}P]ATP$ (1 µCi), 10 mU DG kinase, 2.5% octyl-β-glucoside and 1 mM cardiolipin in a total volume of 100 µl for 5 min at 37°C. Different concentrations of DG (Avanti Polar Lipids) and ceramide (Sigma-Aldrich) standards were also assayed to establish standard curves. The reaction tubes were subsequently incubated for 10 min in a sonicating water bath (FS-14 sonicator, Thermo Fisher Scientific), followed by a second incubation at 37°C for 5 min. The samples were incubated for 5 min in the sonicating water bath again, followed by a final incubation at 37°C for 20 min. The samples were then extracted in chloroform-methanol-2 M KCl containing 10 mM HCl (1:1:0.8, by vol.), which contained 10 µg PA as a carrier. After centrifuging for 10 min at 400 x g, the aqueous phase was aspirated and the chloroform phase was washed twice with 1.8 ml methanol-2M KCl containing 10 mM HCl (1:0.8, by vol.) pre-treated with 1 ml chloroform. 500 µl of the chloroform phase was dried down under a nitrogen stream, resuspended in 100 µl chloroform and spotted on a plastic-backed TLC plate. PA and ceramide-1-phosphate standards were also loaded on the plate, which was then developed up the full-length of the plate in chloroform-methanol-NH_4OH

(65:35:7.5, by vol.). This was followed by a second full-length development in chloroform-acetone-acetic acid-methanol-water (50:20:15:10:5, by vol.). ^{32}P-labelled PA and ceramide 1-phosphate were identified by autoradiography as well as co-migration of lipid standards. Individual bands containing [^{32}P]PA and [^{32}P]ceramide 1-phosphate were isolated and radioactivity was measured. DG and ceramide content were then calculated from the standard curves of DG and ceramide.

2.11 Statistics

Results are expressed as means ± S.E.M. The two-tailed student's t-test and the one-way or two-way ANOVA were used to test for significance ($p < 0.05$). The two-way ANOVA was applied whenever there were two or more groups with two or more treatments in each group, and statistical significance was determined for each treatment between groups.

CHAPTER 3

INVESTIGATION OF THE TRANSLOCATION, PROTEIN PHOSPHATASE-1

INTERACTION AND CATALYTIC ACTIVITY OF THE LIPINS

3.1 Introduction

Studies in the 1980s demonstrated the translocation of the predominantly cytosolic PAP enzymes onto endoplasmic reticulum membranes (225, 293, 294, 296, 303, 350). This translocation enables the PAP enzymes to participate in glycerolipid biosynthesis (298, 369). As mentioned previously, unsaturated FAs can stimulate the association of PAP activity with membranes (294-296) whereas amphiphilic cations like chlorpromazine can reverse this translocation (295, 298). With the discovery that lipins are PAP enzymes by the laboratory of George Carman in 2006 (135) as well as by Donkor et al. in collaboration with our group (134), we wanted to demonstrate that the translocation of PAP could be attributed to the lipins. Furthermore, the phosphorylation state of the lipins is another important determinant of the extent of membrane association (229, 232, 241). Insulin-stimulated phosphorylation of lipins promotes its cytosolic localization (232, 241) whereas dephosphorylated lipins are better able to translocate to their sites of action (229, 241). We will also present preliminary evidence that lipin-1B can interact with the γ isoform of the protein phosphatase-1 catalytic subunit (PP1γ) and this interaction is dependent on a well-characterized motif. As such, the subcellular localization of lipin-1 could depend on its interaction with PP1 and possibly its subsequent dephosphorylation.

3.2 Regulation of the translocation of lipins from the cytosol onto membranes

Using the translocation protocols established by our group in the 1980s (294-296), we found that PAP activity in the cell ghosts increased while cytosolic PAP activity decreased in rat hepatocytes after 1 h treatment with increasing

concentrations of oleate, as found previously (Figure 3.1A). We also demonstrated an increase in microsomal-associated PAP activity and a decrease in cytosolic PAP activity stimulated by increasing oleate concentrations in a cell-free liver homogenate assay system (Figure 3.1B). Overall, total PAP activity between treatments did not vary significantly except in rat hepatocytes treated with 1.25 mM oleate compared to cells treated with 2 mM oleate (Figure 3.1C). This demonstrates that oleate promoted the translocation of PAP activity and did not act as a stimulatory factor.

Importantly, we showed that lipin-1 translocates from the cytosol to cell ghosts in rat hepatocytes (Figure 3.1D, *upper panel*) as well as in the cell-free rat liver homogenates by Western blot analysis (Figure 3.1D, *lower panel*). However, we had to increase the expression of lipin-1 in rat hepatocytes by treatment with 100 nM dexamethasone, as previously shown by our laboratory (307), in order to detect the translocation of lipin-1 by Western blot analysis. In contrast, lipin-1 could be detected without stimulation in the cell-free system. Therefore, the cell-free liver microsomal system was preferable for determining lipin translocation in further experiments.
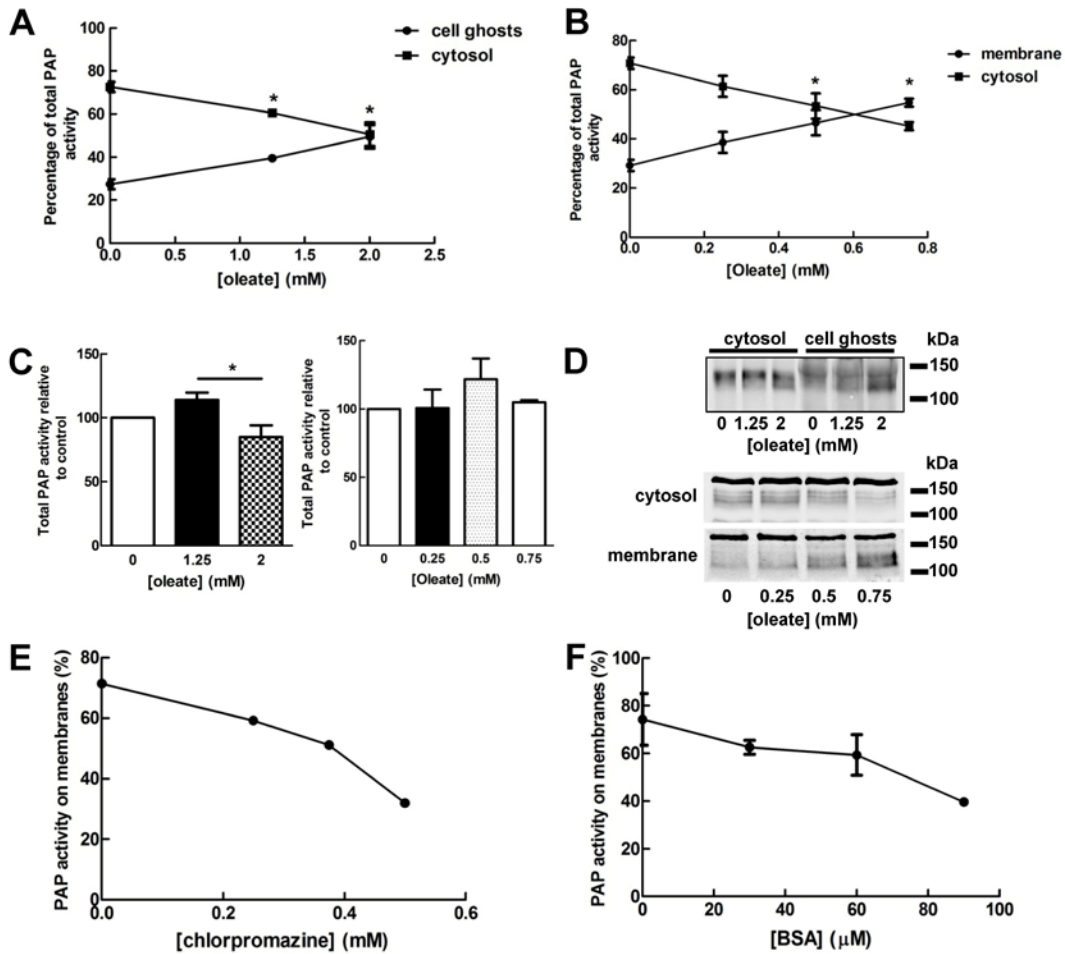
Figure 3.1 Translocation of PAP activity from the cytosol to membranes in rat hepatocytes and cell-free rat liver homogenates. (A) Rat hepatocytes (n = 3) were treated with different concentrations of oleate in DMEM containing 0.1 mM bovine serum albumin (BSA) for 1 h, and lysed with a hypotonic solution containing 0.1 mg/ml digitonin. The cytosolic fractions and cell ghosts were collected separately, and the PAP activity in each fraction was measured. Results were then expressed as percentages of total PAP activity. **(B)** Cell-free rat liver homogenates (n = 3) were treated at 37°C for 10 min with different concentrations of oleate and cytosolic fractions were separated from microsomal membranes by centrifugation. PAP activities in the cytosol and microsomal membranes were measured, and results were then expressed as percentages of total PAP activity. **(C)** Total PAP activities in rat hepatocytes (*left panel*) and in rat liver homogenates (*right panel*) treated with different concentrations of oleate as previously described (Figure 3.1A, B) were calculated as the sum of the cytosolic and membrane-associated PAP activities. **(D)** Western blot showing the distribution of lipin-1 in the cytosol and cell ghosts of rat hepatocytes treated with 100 nM dexamethasone for 12 h, followed by 1 h incubation with different concentrations of oleate (*upper panel*). Western blot showing lipin-1 in the cytosol and microsomal membranes of cell-free rat liver homogenates treated at 37°C with different concentrations of oleate for 10 min (*lower panel*). **(E)** The effects of chlorpromazine and **(F)** bovine serum albumin on the association of PAP activity

with microsomal membranes were also determined. Cell-free rat liver homogenates treated for 10 min at 37°C with 0.75 mM oleate were subsequently incubated for another 10 min period with different concentrations of chlorpromazine (n = 1) or bovine serum albumin (BSA) (n = 2). Cytosolic fractions were separated from microsomal membranes by centrifugation. PAP activities in the cytosol and microsomal membranes were measured, and results were expressed as percentages of total PAP activity. Isolated rat hepatocytes were prepared by Boripont Manmontri and Dr. Sabina Isgandarova. All experiments were performed by Bernard Kok.

Our laboratory had also previously demonstrated the dissociation of PAP activity from membranes when cell-free rat liver homogenates were treated with chlorpromazine, an amphiphilic cationic drug, or BSA (295). BSA can extract the FAs from the microsomal membranes and reduce the interaction of the PAP enzymes with membranes (295). We confirmed this study and showed that membrane-bound PAP activity stimulated by 750 μM oleate could be dissociated with increasing concentrations of chlorpromazine (Figure 3.1E) or BSA (Figure 3.1F). This latter strategy was used to minimize the association of PAP activity on rat liver microsomal membranes in our next set of experiments.

Dr. Karen Reue was interested in determining why mutations in lipin-2 lead to the hereditary Majeed syndrome in human patients as described in the introduction. One such Majeed mutation is a point mutation of serine 734 to leucine. Our hypothesis was that this mutation leads to a change in PAP activity or membrane association since the mutation is not in the active site of PAP. As part of our collaboration with Dr. Reue, we investigated the ability of several lipin-2 mutants to translocate onto membranes (138). These proteins were expressed

in HEK 293 cells, therefore, we used an excess of rat liver microsomal membranes in order to maximize the membrane binding surface. We pre-treated the rat liver microsomal membranes with 0.1 mM BSA to reduce the membrane-association of endogenous PAP activity. As proof of principle that this microsomal system could be used to assess lipin translocation onto microsomal membranes, we demonstrated the translocation of PAP activity (mainly lipin-1) isolated from the cytosol of rat adipose tissue onto rat liver microsomal membranes (Figure 3.2A). We also demonstrated that recombinant lipin-1B expressed in HEK 293 mitochondria-free lysates could translocate onto membranes when stimulated with oleate (Figure 3.2B).

As mentioned previously, one of the mutations in lipin-2 that causes the Majeed syndrome in patients is a point mutation of serine at position 734 to leucine. The laboratory of Dr. Reue mutated the analogous residue in *Mus musculus* lipin-2, serine-731, to leucine as well as to aspartate. Like lipin-1, recombinant lipin-2 wildtype protein could translocate onto rat liver microsomal membranes when stimulated with oleate (Figure 3.2C-F). The abilities of the lipin-2 Majeed (S731L) (Figure 3.2C, D) and lipin-2 S-D (S731D) (Figure 3.2E, F) mutants to translocate onto membranes were not significantly different compared to lipin-2 wildtype.
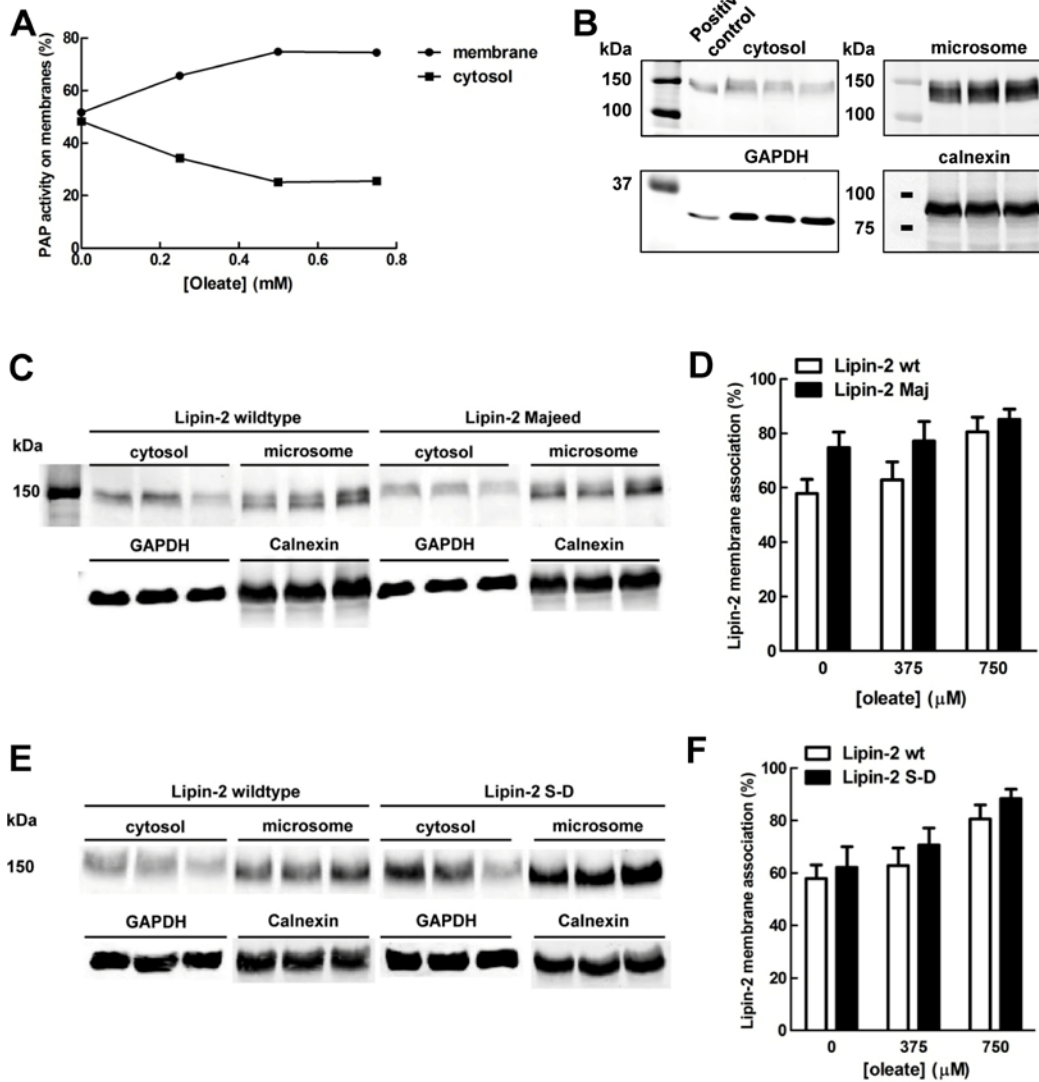
Figure 3.2 Translocation of endogenous PAP activity from rat adipose cytosol or recombinant lipin constructs from HEK 293 cell extracts to rat liver microsomal membranes. (A) Isolated rat adipose cytosol was incubated with rat liver microsomal membranes (pre-treated with bovine serum albumin to remove microsomal-associated phosphatidate phosphatase activity) for 10 min with different concentrations of oleate at 37°C. Cytosolic fractions were separated from microsomal membranes by centrifugation. PAP activities in the cytosol and microsomal membranes were measured, and results were expressed as percentages of total PAP activity. **(B)** Mitochondria-free HEK 293 cell lysates overexpressing recombinant *Mus musculus* lipin-1b were incubated with rat liver microsomal membranes (pre-treated as before) for 10 min with 0, 375 and 750 μM oleate at 37°C. Cytosolic fractions were separated from microsomal membranes and results are shown in the Western blot. Glyceraldehyde-3-phosphate dehydrogenase (GAPDH) and calnexin served as the cytosolic and microsomal protein controls, respectively. **(C)** The same protocol was used in experiments performed with mitochondria-free HEK2 93 cell lysates overexpressing recombinant *Mus musculus* lipin-2 wildtype, lipin-2 containing the

analogous Majeed mutation (S731L) and **(E)** lipin-2 with the S731D mutation, and the representative Western blots are shown. **(D)** The percentage of lipin-2 wildtype (n = 3), lipin-2 Majeed (n = 3) and **(F)** lipin-2 S731D (n = 3) associated with the microsomal membranes were quantified. The data shown in Figure 3.2B – F has been published in collaboration with Dr. Karen Reue (University of California-Los Angeles) and all the work was performed by Bernard Kok (138).

3.3 The effect of lipin mutations on its intrinsic PAP activity and protein interaction

3.3.1 The Majeed mutation in lipin-1A and -2 and its effect on PAP activity

Since mutation of this serine residue 731 in *Mus musculus* lipin-2 does not overtly affect its ability to translocate, we also tested the intrinsic PAP activity of these lipin-2 mutants. Jay Dewald in our laboratory showed that mutation of serine-731 in lipin-2 to leucine or aspartate completely abolished its PAP activity (Figure 3.3A), while not affecting the transcriptional co-activator function of lipin-2 (138). We hypothesized that this serine residue is essential in the catalytic mechanism. Cross-species analysis and sequence alignment demonstrated the conservation of this serine residue (Figure 3.3B). In single-celled eukaryotes, this residue is a threonine, which has a hydroxyl equivalent to that in serine. We determined the secondary structure of the lipins in that region using the Jpred secondary structure prediction server (370) and aligned the secondary structure of the lipins with the consensus regions surrounding the catalytic site of the haloacid dehalogenase (HAD)-like superfamily of proteins to which the lipins belong (255). The predicted secondary structures surrounding the active sites of lipin-1 and lipin-2 possess the same structural organization as previously

115

characterized HAD protein family members (Figure 3.3C). More importantly, the serine mutated in some Majeed patients is equivalent to the conserved serine residue in the predicted HAD motif II that is responsible for coordinating the phosphate group of the substrate (Figure 3.3C).

C

Lipin-1A   674 KVIIS**DIDGT**ITRSDTLGHILPTLGKDWTHQGIAKLYHKVSQNGYKFLYC**S**ARAIGMAD

Lipin-2   681 KVIIS**DIDGT**ITKSDALGQILPQLGKDWTHQGIARLYHSINENGYKFLYC**S**ARAIGMAD

Predicted
HAD motif I
         Predicted HAD motif II

Lipin-1A   733 MTRGYLHWVNERGTVLPQGPLLLSPSSLFSALHREVIEKKPEKF**K**VQCLTDIKNL----

Lipin-2   740 MTRGYLHWVNDKGTILPRGPLMLSPSSLFSAFHREVIEKKPEKF**K**IECLNDIKNL----

Predicted HAD motif II
         Predicted
HAD motif III

Lipin-1A   795 FYAAFGNRP-**D**VYSYKQVGVSLNRIFTVNPKGE

Lipin-2   802 FYAAFGNRP-**D**VYAYTQVGVPDCRIFTVNPKGE

Predicted HAD motif IV

Figure 3.3 The Majeed mutation affects the phosphatidate phosphatase (PAP) activity of lipins. (A) The lipins contain several evolutionarily conserved regions, which include the N-LIP and C-LIP domains (N- and C-terminus of lipins) as well as a polybasic motif (also described as the nuclear localization sequence or NLS), the PAP catalytic motif and the transcriptional co-activator motif (*top panel*). The serine point mutation in Majeed syndrome patients is also shown schematically. The PAP activities of lipin-1A and lipin-2 wildtype were measured along with various recombinant lipin mutant constructs (*bottom panel*). The Majeed syndrome serine to leucine mutation was generated in analogous residues of *Mus musculus* lipin-1A (S724L) and lipin-2 (S731L). These serine residues were also mutated to aspartate residues (S724D and S731D in lipin-1A and lipin-2, respectively). The lipin-1A constructs with mutations in the PAP catalytic motif (D679E) and transcriptional co-activator motif (IL693FF) were previously established as controls with no intrinsic PAP activity. The lipin constructs were expressed in HEK 293 cells, and PAP activity in cell lysates was determined. The results were then normalized to the level of recombinant protein expression as assessed by Western blot analysis and expressed relative to the PAP activity of the lipin-1A or lipin-2 wildtype proteins. The PAP assay was performed by Mr. Jay Dewald. **(B)** Sequence alignments of multiple lipins from different organisms demonstrate the evolutionarily conserved residues surrounding the serine residue mutated in the Majeed syndrome. Residues that are conserved in vertebrate species are highlighted in yellow and the serine residue mutated in the Majeed syndrome is boxed. This serine is highly conserved, although the corresponding residue is a threonine in single-celled eukaryotes. h, human; m, mouse. **(C)** The secondary structure surrounding the catalytic motif of *Mus musculus* lipin-1A and lipin-2 was predicted by jnet algorithms using the Jpred server. Similar structures were predicted by using the jhmm and jpssm algorithms. Green arrows indicate predicted β-strands, and blue cylinders indicate predicted α-helices. Conserved amino acids from the catalytic motifs of the HAD family of proteins are shown in red letters. The secondary

117

structure of the predicted HAD motifs around the active site of the lipins are conserved in all of the HAD-like proteins that have been studied by X-ray crystallography. This work has been published in collaboration with Dr. Karen Reue (University of California-Los Angeles) (138).The PAP activities were assayed with the help of Mr. Jay Dewald in our laboratory and the primary sequence alignment was performed by a member of Dr. Reue's laboratory with help from Bernard Kok. The analysis of the secondary structure prediction was performed by Bernard Kok.

3.3.2 Interaction of lipin-1B with protein phosphatase-1γ and the effects of mutating the putative interaction motif

As mentioned previously, the regulation of lipin-1 and lipin-2 subcellular localization depends on electrostatic interactions with the membranes. Another important determinant of membrane binding is the phosphorylation state of the lipins whereby hyper-phosphorylated forms of lipin-1 and -2 do not associate with membranes as readily as less-phosphorylated lipin-1 and -2. In collaboration with Dr. Charles Holmes and Tamara Arnold, we hypothesized that lipin-1B can interact with PP1γ because of a well-conserved HVRF (histidine-valine-arginine-phenylalanine) motif that is comparable to the canonical "RVXF" (arginine-valine-X-phenylalanine where X represents any amino acid except proline) motif known to facilitate the binding of regulatory subunits to PP1 (Figure 3.4) (371). This HVRF motif is present on all three lipin isoforms as well as the *Saccharomyces cerevisiae* lipin homologue (Figure 3.4).
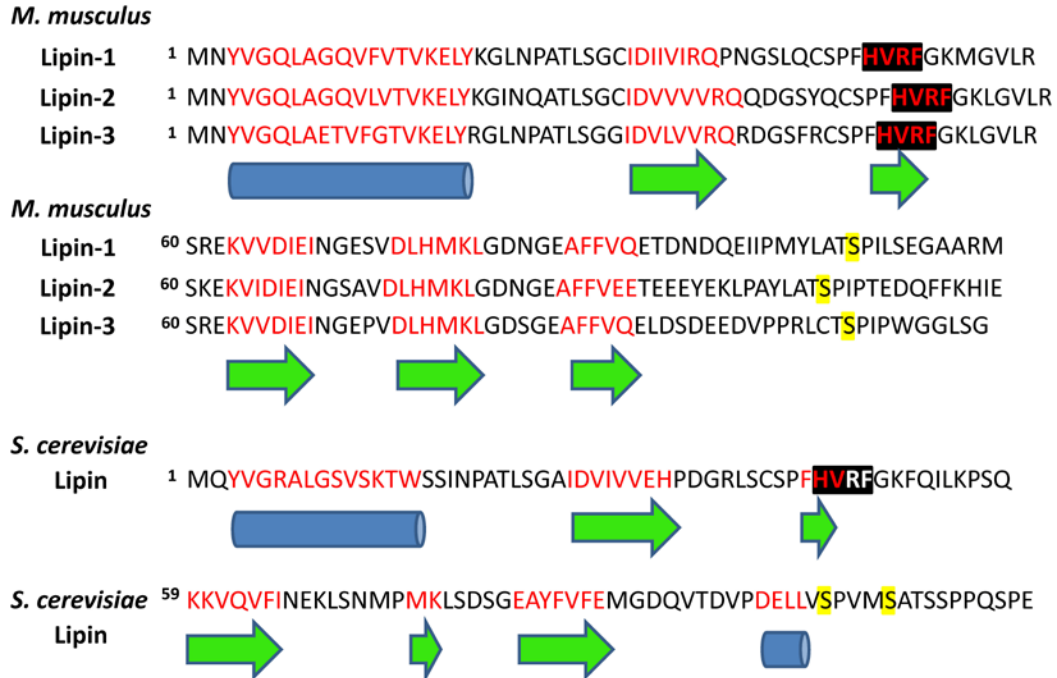
Figure 3.4 Sequence alignment and secondary structure prediction of the N-termini of *Mus musculus* lipins and the *Saccharomyces cerevisiae* lipin. The regions highlighted in red are the portions predicted to possess α-helical or β-strand secondary structure by jnet algorithms using the Jpred server (370). The blue cylinders and green arrows represent α-helices and β-strands, respectively. The HVRF motif predicted to mediate protein phosphatase-1 interaction is highlighted in black. The serine residues highlighted in yellow have been positively identified to be phosphorylated by mass spectrometry (241). Analysis of the secondary structure prediction was performed by Bernard Kok.

We used the Jpred secondary structure prediction server (370) to analyze the conserved N-terminal domain (NLIP) of the lipins. As found previously (372), there is an amphipathic α-helix present at the start of the N-terminus of the yeast lipin homologue as well as the *Mus musculus* lipin isoforms (Figure 3.4). This α-helix helps facilitate the binding of yeast lipin to phosphatidate on nuclear/endoplasmic reticulum membranes (372). Moreover, there is a

119

characteristic array of β-strands right after the α-helix in both yeast and mouse lipins (Figure 3.4). The second β-strand in the mouse lipin isoforms is predicted to encompass the HVRF motif postulated to bind to PP1 (Figure 3.4). Only the histidine and valine residues in the HVRF motif on the yeast lipin are predicted to be present in the second β-strand (Figure 3.4). The high degree of secondary structure conservation and the presence of the HVRF motif in *Saccharomyces cerevisiae* were promising since it suggests an evolutionary conserved function of lipin-1 as a PP1 interacting protein.

First, we demonstrated that recombinant, purified PP1γ could bind to the 96 well µClear® plate and that the binding was relatively consistent (average integrated intensity = 14.0±0.4) (Greiner Bio-One) (Figure 3.5A). We then showed that lipin-1B can interact with PP1γ bound to the wells (Figure 3.5B, C). Importantly, lipin-1B could be detected using antibodies detecting the FLAG epitope or the C-terminus of lipin-1 when the two antibodies were used simultaneously (Figure 3.5B, C). Low amounts of cell lysates overexpressing lipin-1B wildtype (3 µg) were enough to bind maximally to the PP1γ present in the wells (Figure 3.5D, E). Moreover, incubating the cell lysates overexpressing lipin-1B in the presence of 1.5 mM Mg^{2+} increased the amount of lipin-1B interacting with bound PP1γ (Figure 3.5D, E). This result is not surprising given that the lipins are Mg^{2+}-dependent enzymes. Mg^{2+} supplementation would ensure that the recombinant lipin-1B remains catalytically active and properly folded.
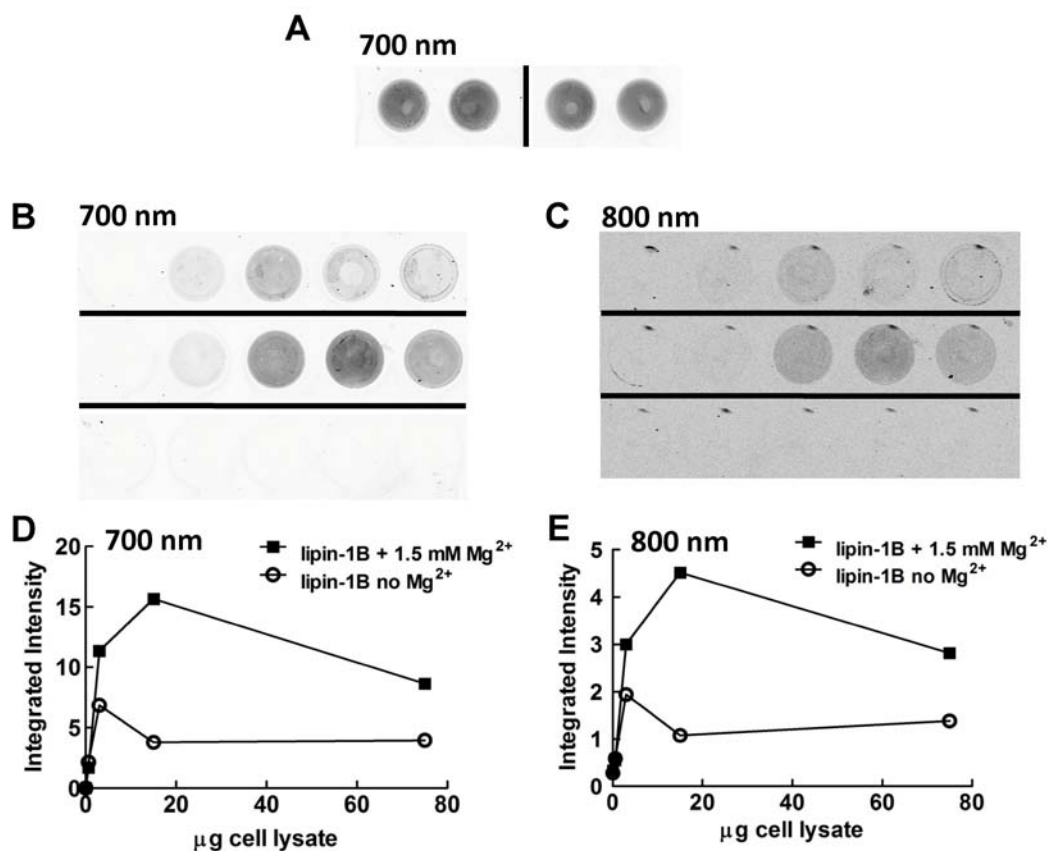
Figure 3.5 Interaction of lipin-1 with protein phosphatase 1γ bound to the 96 well μClear® plate. (A) Recombinant protein phosphatase 1γ catalytic subunit (3 μg PP1γ) was incubated in PBS overnight at 4°C while gently agitating. PP1γ bound to the 96 well plate was detected using mouse immunoglobulin G (IgG) against protein phosphatase 1 and fluorescence was measured at 700 nm using the LI-COR Odyssey® Imaging System. The average integrated intensity from the four wells was calculated to be 14.0±0.4. **(B)** Different concentrations of human embryonic kidney 293 (HEK 293) cell lysates overexpressing N-terminal FLAG-tagged recombinant lipin-1B (0.6 – 75 μg) in the presence of 4.5 pmol microcystin-LR were incubated overnight at 4°C in wells containing a constant amount of bound PP1γ in the absence (*upper panel*) or presence (*middle panel*) of 1.5 mM MgCl$_2$. The concentration curve of non-transfected HEK 293 cell lysates (*lower panel*) was used as a negative control. Recombinant lipin-1B that interacted with the bound PP1γ was detected using mouse antibodies against the FLAG epitope. **(C)** In these same wells (Figure 1B), recombinant lipin-1B was detected using rabbit antibodies against the C-terminus of lipin-1. The fluorescent-labelled secondary antibodies were detected and quantified at **(D)** 700 nm (goat anti-mouse secondary antibody) and **(E)** 800 nm (goat anti-rabbit secondary antibody) using the LI-COR Odyssey® Imaging System. Recombinant PP1γ was kindly provided by Tamara Arnold from the laboratory of Dr. Charles Holmes (University of Alberta) and the plasmid encoding recombinant lipin-1 was a gift from Dr. Thurl Harris (University of Virginia). All experiments were performed by Bernard Kok.

To determine whether the putative PP1 interacting motif (HVRF) on lipin-1B was responsible for protein interaction, we used site-directed mutagenesis to mutate HVRF to HARA. Before incubation with bound PP1γ in the 96 well plate, protein dot blots were used to normalize the expression of lipin-1B wildtype compared to the lipin-1B HARA mutant (Figure 3.6A, B). Cell lysates overexpressing lipin-1B wildtype had 2- to 2.5-fold more overexpressed protein compared to cell lysates overexpressing lipin-1B HARA mutant (Figure 3.6C, D).

However, the dot blots measure the total amount of protein by detecting the FLAG epitope or the C-terminus of lipin-1 without accounting for the presence of degradative products or non-specific interactions of the antibodies with other proteins. Therefore, we determined whether there were any other bands detected by Western blot other than the full-length recombinant lipin-1B proteins. We could not detect any other proteins or degradative products apart from full-length lipin-1B wildtype, lipin-1B HARA mutant and lipin-1B catalytically inactive mutant (Figure 3.7A). Therefore, the dot blot assay provides an easy and rapid method to quantify the expression of recombinant lipin-1.
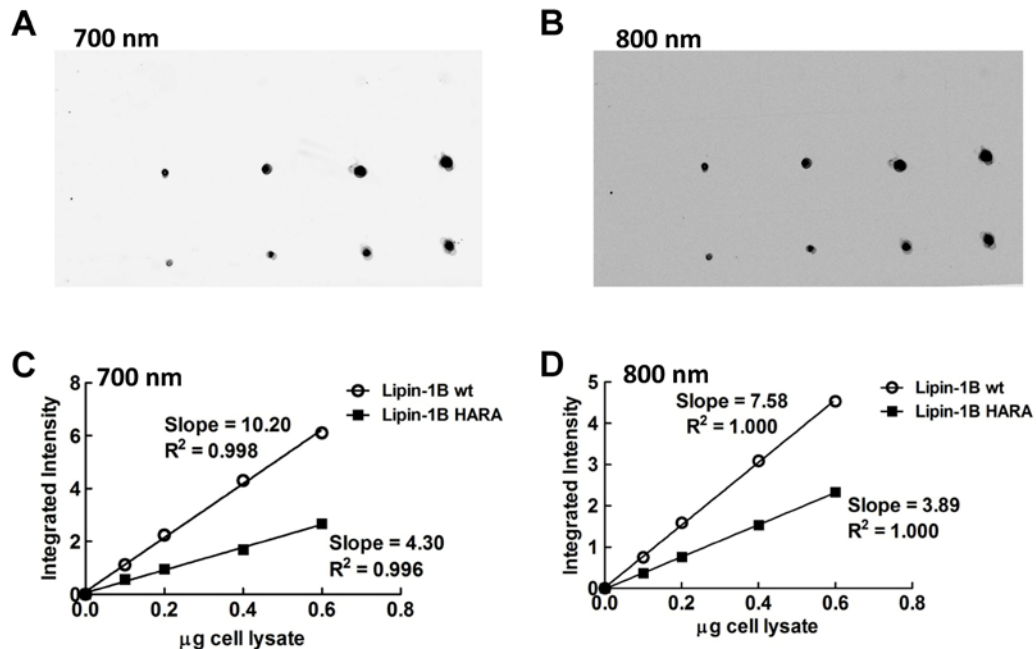
Figure 3.6 Quantification of recombinant lipin-1B proteins using a protein dot blot. Increasing amounts of human embryonic kidney 293 (HEK 293) cell lysates either treated with vehicle or overexpressing recombinant N-terminal FLAG-tagged lipin-1B wildtype or HARA mutant were spotted on a nitrocellulose membrane and probed with **(A)** mouse immunoglobulin (IgG) against the FLAG epitope or **(B)** rabbit IgG against the C-terminus of lipin-1. The fluorescent-labelled secondary antibodies were detected and quantified at **(C)** 700 nm (goat anti-mouse secondary antibody) and **(D)** 800 nm (goat anti-rabbit secondary antibody) using the LI-COR Odyssey® Imaging System. The linearity of detection was determined using linear regression analysis. The plasmid encoding recombinant lipin-1 wildtype was kindly provided by Dr. Thurl Harris (University of Virginia). Site-directed mutagenesis of the plasmid encoding lipin-1 wildtype to lipin-1 HARA mutant was performed by Tamara Arnold from the laboratory of Dr. Charles Holmes (University of Alberta). Protein dot blots were performed by Bernard Kok.
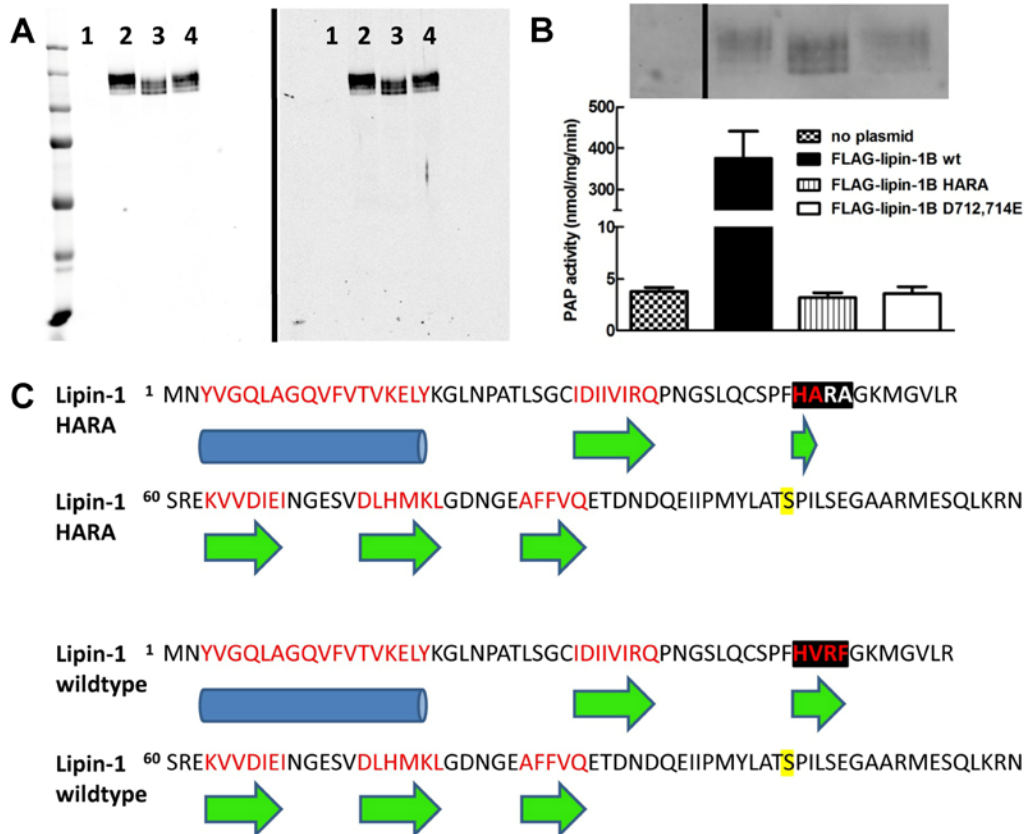
Figure 3.7 Western blot and PAP activity of recombinant lipin-1B proteins.
(A) Non-transfected human embryonic kidney 293 (HEK 293) cell lysates (lane 1) or HEK 293 cell lysates overexpressing lipin-1B wildtype (lane 2), lipin-1B HARA mutant (lane 3) and lipin-1B D712, 714E catalytically inactive mutant (lane 4) were incubated with mouse immunoglobulin (IgG) detecting the FLAG epitope (*left panel*) or rabbit IgG against the C-terminus of lipin-1 (*right panel*). **(B)** Phosphatidate phosphatase (PAP) activities of the recombinant lipin-1B proteins were measured. The expressions of non-transfected cell lysates (4 µg), and cell lysates overexpressing recombinant lipin-1B wildtype (0.1 µg), lipin-1B HARA mutant (0.3 µg) and lipin-1B D712, 714E catalytically inactive mutant (0.1 µg) were detected in the Western blot using mouse monoclonal IgG against the FLAG epitope (*upper panel*). **(C)** The amino acid sequences of the N-terminus lipin-1B HARA mutant and wildtype protein are shown along with secondary structure prediction by the Jpred server (370). The regions highlighted in red are the portions predicted to possess α-helical or β-strand secondary structure, and the blue cylinders and green arrows represent α-helices and β-strands, respectively. The HVRF and mutated HARA motifs are highlighted in black. The serine residue highlighted in yellow has been positively identified to be phosphorylated by mass spectrometry (241). The plasmids encoding recombinant lipin-1 wildtype and catalytically inactive mutant were kindly provided by Dr. Thurl Harris (University of Virginia). Site-directed mutagenesis of the plasmid encoding lipin-1 wildtype to lipin-1 HARA mutant was performed by Tamara Arnold from the laboratory of Dr. Charles Holmes (University of Alberta). Western blots, PAP assays and the analysis of secondary structure prediction were performed by Bernard Kok.

When the HVRF motif was mutated to HARA, this mutation completely abolished the catalytic activity of lipin-1B (Figure 3.7B). This result could indicate that this area is vital for catalytic activity or that the lipin-1B HARA mutant is simply misfolded. However, we still decided to test the lipin-1B HARA mutant in binding experiments since there were no degradative products and the protein appeared to be phosphorylated (Figure 3.7A), suggesting that the protein was not grossly misfolded and could still be recognized by kinases. Furthermore, mutating the HVRF motif to HARA does not completely disrupt the predicted β-strand secondary structure of the recombinant lipin-1B mutant (Figure 3.7C).

After normalizing for the different levels of lipin-1B wildtype expression compared to lipin-1B HARA mutant, we tested to see if the lipin-1B HARA mutant could bind to PP1γ. In the previous experiment, we had not included enough microcystin-LR to inhibit PP1γ. As such, the interaction of lipin-1B with PP1γ could have been due to binding of phosphorylated residues on lipin-1B to the active site of PP1γ. Therefore, we used 750 pmol microcystin-LR to inhibit PP1γ (81 pmol) during the binding step before incubating with the recombinant lipin-1B proteins. As demonstrated previously, lipin-1B wildtype interacted with PP1γ bound to the wells (Figure 3.8B). Furthermore, this interaction was linear over the lower range of proteins from cell lysates used in the binding experiment (Figure 3.8D). Lipin-1B wildtype was not detected if bovine serum albumin or potato acid phosphatase were bound to the wells instead, demonstrating the specificity of the PP1γ interaction with lipin-1B (Figure 3.8B, D). Significantly, the lipin-1B HARA mutant was unable to bind to PP1γ (Figure 3.8C, E). The results are similar if the recombinant lipin-1B proteins were detected using rabbit IgG against the C-

terminus of lipin-1 instead of mouse IgG against the FLAG epitope when the

antibodies were used simultaneously in the same wells (Figure 3.9).
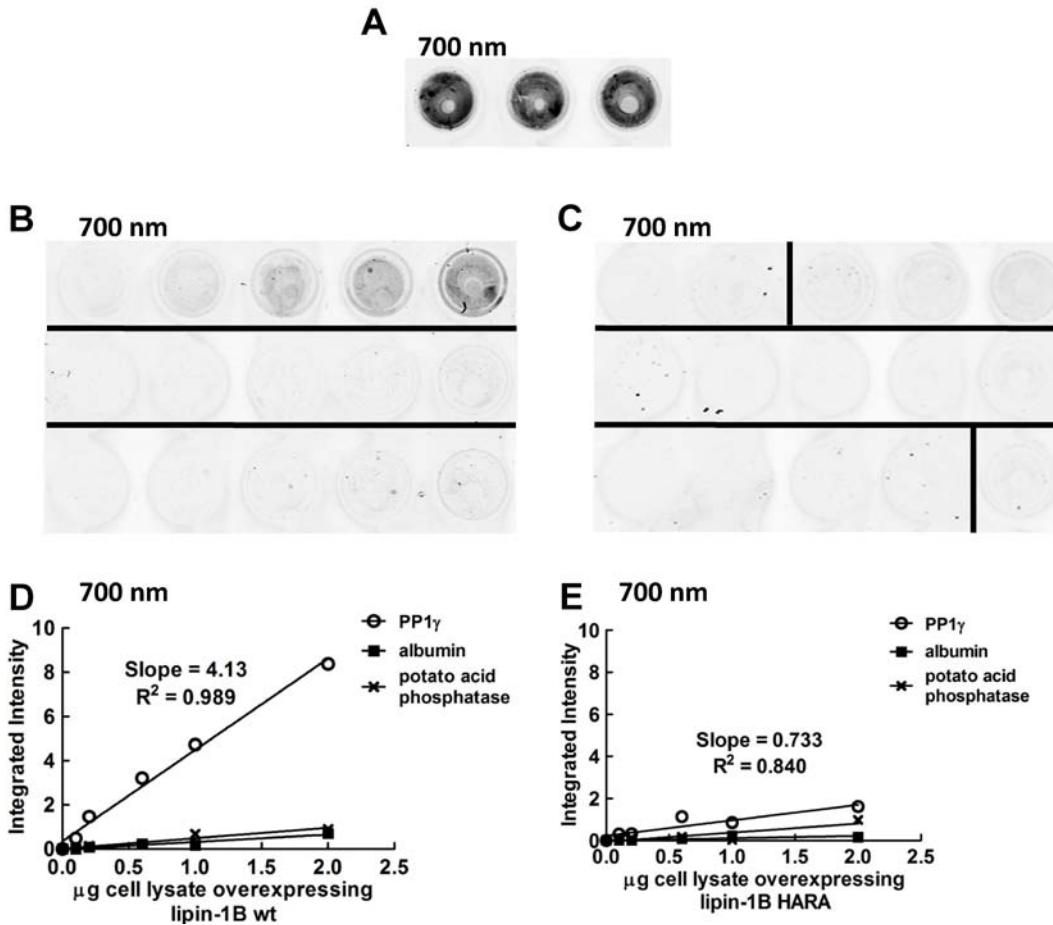
Figure 3.8 Interaction of lipin-1 wildtype and HARA mutant with protein phosphatase 1γ bound to the 96 well µClear® plate detected using anti-FLAG antibodies. (A) Recombinant protein phosphatase 1γ catalytic subunit (3 µg PP1γ) was incubated with 750 pmol microcystin-LR in PBS overnight at 4°C while gently agitating. PP1γ bound to the 96 well plate was detected using mouse immunoglobulin G (IgG) against protein phosphatase 1. Fluorescence was measured at 700 nm using the LI-COR Odyssey® Imaging System. The average integrated intensity from the four wells was calculated to be 14.7±0.4. Different concentrations of human embryonic kidney 293 (HEK 293) cell lysates overexpressing **(B)** N-terminal FLAG-tagged recombinant lipin-1B (0.1 – 2 µg) or **(C)** N-terminal FLAG-tagged recombinant lipin-1B HARA mutant (0.25 – 5 µg)

were incubated overnight at 4°C in wells containing constant and equivalent amounts (3 µg) of bound PP1γ (*upper panel*), bovine serum albumin (*middle panel*) or potato acid phosphatase (*lower panel*). PP1γ, albumin and potato acid phosphatase were all pre-treated with 750 pmol microcystin-LR while incubating overnight and adsorbing onto the well surface. **(D)** Recombinant lipin-1B wildtype and **(E)** HARA mutant were detected using mouse antibodies against FLAG tag. The fluorescent-labelled goat anti-mouse secondary antibodies were detected and quantified at 700 nm using the LI-COR Odyssey® Imaging System. The plasmid encoding recombinant lipin-1 wildtype was kindly provided by Dr. Thurl Harris (University of Virginia). Site-directed mutagenesis of the plasmid encoding lipin-1 wildtype to lipin-1 HARA mutant was performed by Tamara Arnold from the laboratory of Dr. Charles Holmes (University of Alberta). All other experiments were performed by Bernard Kok.
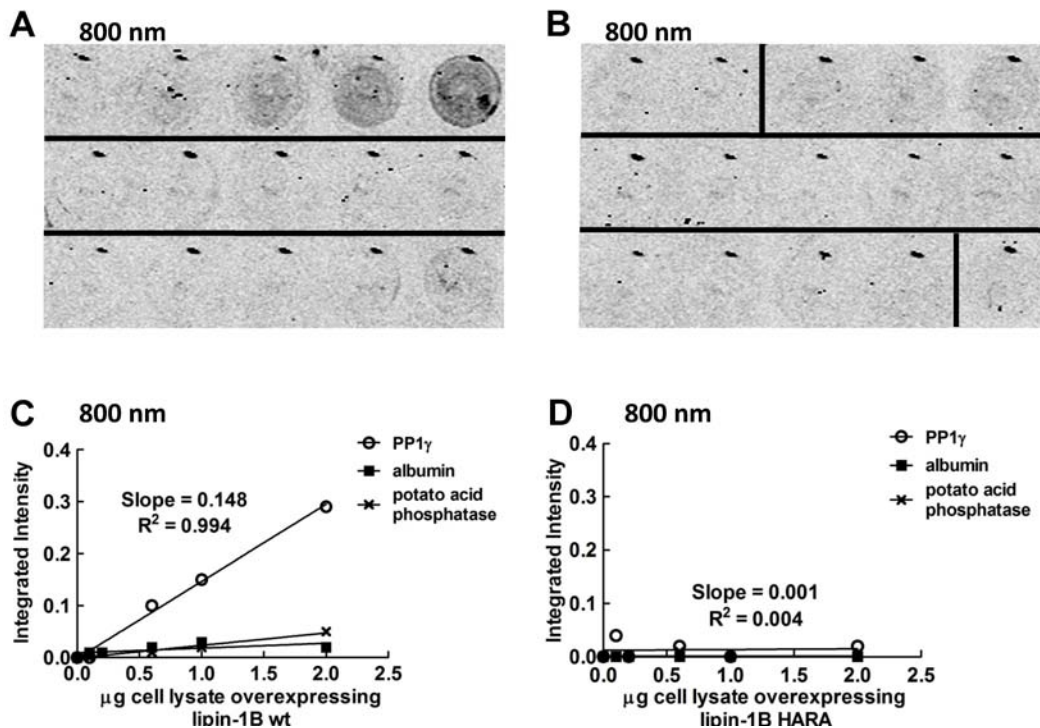
Figure 3.9 Interaction of lipin-1 wildtype and HARA mutant with protein phosphatase 1γ bound to the 96 well µClear® plate detected using anti-lipin-1 C-terminus antibodies. In the same wells as described in Figure 3.8, recombinant N-terminal FLAG-tagged recombinant lipin-1B wildtype and HARA mutant were simultaneously detected using rabbit antibodies against the C-terminus of lipin-1 and quantified. The different concentrations of human embryonic kidney 293 (HEK 293) cell lysates overexpressing **(A)** N-terminal FLAG-tagged recombinant lipin-1B (0.1 – 2 µg) or **(B)** N-terminal FLAG-tagged recombinant lipin-1B HARA mutant (0.25 – 5 µg) were incubated overnight at 4°C

in wells containing constant and equivalent amounts (3 μg) of bound PP1γ (*upper panel*), bovine serum albumin (*middle panel*) or potato acid phosphatase (*lower panel*). PP1γ, albumin and potato acid phosphatase were all pre-treated with 750 pmol microcystin-LR while incubating overnight and adsorbing onto the well surface. **(C)** Recombinant lipin-1B wildtype and **(D)** HARA mutant were detected using rabbit antibodies against the C-terminus of lipin-1. The fluorescent-labelled goat anti-rabbit secondary antibodies were detected and quantified at 800 nm using the LI-COR Odyssey® Imaging System. The plasmid encoding recombinant lipin-1 wildtype was kindly provided by Dr. Thurl Harris (University of Virginia). Site-directed mutagenesis of the plasmid encoding lipin-1 wildtype to lipin-1 HARA mutant was performed by Tamara Arnold from the laboratory of Dr. Charles Holmes (University of Alberta). All other experiments were performed by Bernard Kok.

The effects of increasing concentrations of microcystin-LR on lipin-1B wildtype interaction with PP1γ were also examined since we had tested the binding of lipin-1B to PP1γ in separate experiments with and without 750 pmol microcystin-LR. We found that microcystin-LR up to 150 pmol did not overtly affect the interaction of lipin-1B to PP1γ (Figure 3.10). Moreover, the addition of 750 pmol microcystin-LR only reduced binding by approximately 20% (Figure 3.10).
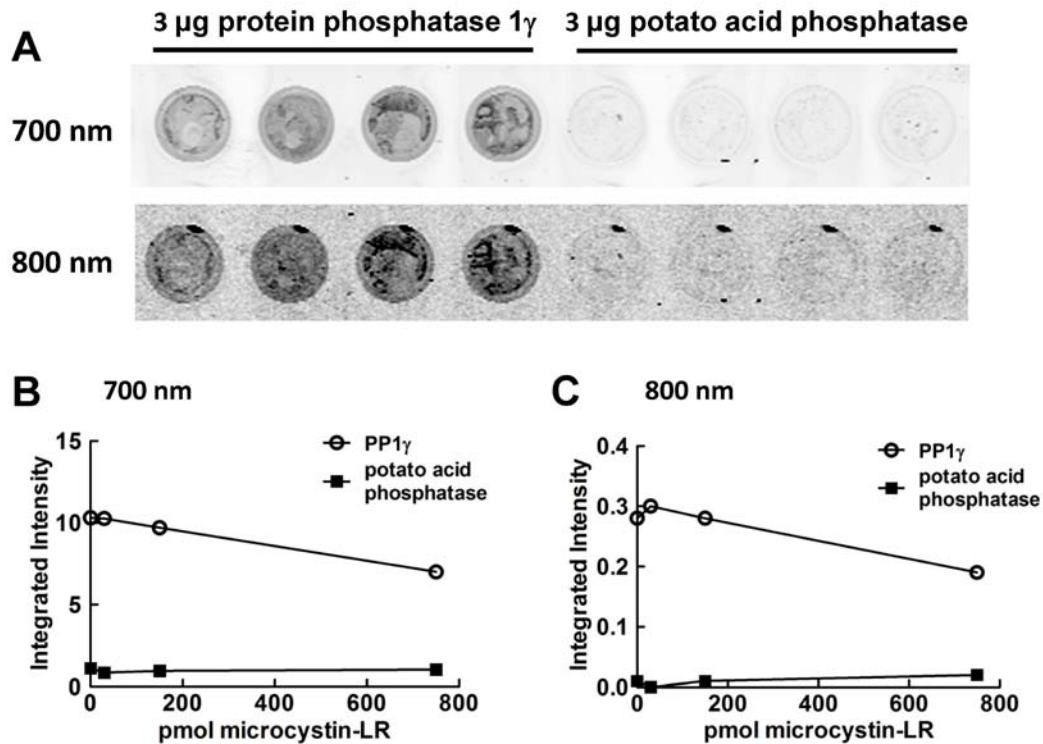
Figure 3.10 The effect of microcystin-LR on the interaction of protein phosphatase 1γ with recombinant lipin-1B wildtype. (A) Purified protein phosphatase 1γ (3 µg PP1γ) or 3 µg potato acid phosphatase were incubated with increasing concentrations of microcystin-LR (0 – 750 pmol) overnight at 4°C while gently agitating. A constant amount of human embryonic kidney 293 (HEK 293) cell lysates overexpressing N-terminal FLAG-tagged recombinant lipin-1B (2 µg) was incubated overnight at 4°C in each well. Mouse immunoglobulin (IgG) against FLAG tag (*upper panel*) or rabbit IgG against the C-terminus of lipin-1 (*lower panel*) were used to detect the lipin-1B that interacted with PP1γ or potato acid phosphatase on the wells. The fluorescent-labelled secondary antibodies were detected and quantified at **(B)** 700 nm (goat anti-mouse secondary antibody) and **(C)** 800 nm (goat anti-rabbit secondary antibody) using the LI-COR Odyssey® Imaging System. The plasmid encoding recombinant lipin-1 wildtype was kindly provided by Dr. Thurl Harris (University of Virginia). All experiments were performed by Bernard Kok.

3.4 Discussion

It is generally thought that the involvement of lipins in glycerolipid biosynthesis is regulated by their subcellular localization. Our group had previously demonstrated the ability of Mg^{2+}-dependent PAP activity (now attributed to the lipins) to translocate from the cytosol onto the membranes of the endoplasmic reticulum when stimulated with unsaturated FAs (295, 296, 303). Since 2007, several groups have shown the differential subcellular distribution of both lipin-1 and -2 (231, 241, 292). (229, 232). Importantly, Harris et al. showed that oleate can stimulate lipin-1 association to microsomal membranes (241).

We have likewise shown the translocation of both PAP activity and lipin-1 in rat hepatocytes and in cell-free rat liver homogenates (Figure 3.1). The phosphorylation state of lipin-1 appears to be important in regulating membrane association since insulin-stimulated phosphorylation sequesters lipin-1 in the cytosol due to the interaction of 14-3-3 proteins to lipin-1 phosphorylated at a serine-rich region downstream of the polybasic motif (232, 241). We have also demonstrated that the faster migrating bands in the lipin-1 Western blots are the predominant species associating with the membranes (Figure 3.1D). Previous studies have shown that these faster migrating bands represent less-phosphorylated forms of lipin-1 (241). The association of lipins with membranes is hypothesized to occur through electrostatic interactions, e.g. the polybasic motif on lipin-1 can bind to PA (Figure 1.5) (231). Furthermore, fatty acids and acyl-CoA esters can also stimulate translocation in a cell-free system, presumably by increasing the net negative charge on the membrane surface (Figure 3.1).

Thus, hyper-phosphorylated lipins would be less able to bind to negatively charged membrane surfaces in addition to the sequestration by 14-3-3. Studies in our group have shown that the amphiphilic cationic drug, chlorpromazine, donates a positive charge to membranes and it can bind to PA (265). This action is thought to be responsible for the dissociation of PAP activity from microsomal membranes (295). Furthermore, oleate-stimulated association of PAP activity to membranes can be reversed by incubation with BSA, which extracts the oleate from the membranes (295). We confirmed these studies and showed that PAP activity dissociated from membranes when treated with increasing concentrations of chlorpromazine and albumin. These studies add to the evidence that there is an electrostatic component governing the binding of lipins to membranes. This conclusion is also supported by work in which the poly-basic motif of the lipins is required for membrane association of lipin-1 (231).

Oleate can also stimulate the translocation of lipin-2 onto microsomal membranes and that the translocation was not significantly affected by the serine mutation, which occurs in some patients with the Majeed syndrome (Figure 3.2). Instead, the complete loss of PAP activity when that serine residue was mutated to leucine or aspartate suggested that the presence of a hydroxyl group at this position is critical for the conformation of the active site or catalytic mechanism. This requirement is fulfilled by the presence of threonine at this position in most single-celled eukaryotes. Indeed, secondary structure analysis and alignment to other HAD family members pinpointed the likely role of that serine residue in coordinating the phosphate group to be hydrolyzed. Therefore, mutation of this Majeed serine residue detrimentally affects the catalytic action of the lipins and not the ability to associate with membranes or interact with the PA substrate.

We also demonstrated that lipin-1B can interact with PP1γ and this interaction is possibly mediated through a HVRF motif on lipin-1B, which closely resembles the canonical RVXF motif present on all PP1γ regulatory proteins. However, the mutation of the HVRF motif to HARA also abolishes the catalytic PAP activity. Based on secondary structure prediction, the conserved N-terminus of the lipins contains an amphipathic α-helix shown to be important in facilitating membrane binding (372). Furthermore, there is a series of five predicted β-strands following the α-helix including the HVRF motif.

Harris et al. have already demonstrated that the conserved N-terminus is essential for providing catalytic activity since mutation of glycine 84 to arginine in mouse lipin-1B reduces PAP activity by 75% and removing the first 106 amino acids of lipin-1B nearly abrogates the PAP activity (241). Thus, further work needs to be carried out to determine whether the N-terminus contains residues that contribute to the catalytic mechanism or if the maintenance of tertiary structure is essential in facilitate membrane binding and substrate interaction. We postulate that the interaction with PP1 could facilitate lipin-1 dephosphorylation. Alternatively, lipin-1 could act as a regulatory subunit of PP1 and either modulates its subcellular localization or activity (371).

Overall, this study highlights the regulation of lipin subcellular localization and the effects of different mutations on the catalytic function of lipins as well as the ability of lipin-1B to interact with PP1γ.

CHAPTER 4

REGULATION OF LIPIN EXPRESSION IN NEONATAL RAT VENTRICULAR

MYOCYTES AND THE EFFECTS ON GLYCEROLIPID BIOSYNTHESIS

4.1 Introduction

The regulation of the expression of the lipins is a crucial factor in dictating the size of the cytosolic reservoir for the different lipins. Upregulated lipin expression would provide a means to compensate for a large influx of FAs into the cell and ensure that the lipins are not rate-limiting factors in FA utilization. Additionally, the increased expression of lipins could enhance the potential for their roles in transcriptional regulation. Previous studies in our group already established that lipin-1 and PAP activity are positively regulated in hepatocytes by the combination of glucocorticoid and cAMP signalling, whereas insulin antagonizes this upregulation (226, 307). Furthermore, the hepatic gene expressions of PPARα and PGC-1α are increased by glucocorticoid and cAMP signalling, although insulin did not have any antagonistic effect (307). Importantly, Manmontri, et al. demonstrated that lipin-1 expression was driven by transcriptional upregulation (307). These changes elicited by hormonal signalling are indicative of the effects on hepatic lipin-1 expression in the fed and fasted states and we wanted to determine how the lipins are regulated in cardiomyocytes.

4.2 Hormonal regulation of cardiac gene expression

4.2.1 Hormonal regulation of PAP activity and lipin expression in neonatal ventricular myocytes (NRVMs)

PAP activities were increased in NRVMs treated for 8 h with different concentrations of dexamethasone, which is a synthetic glucocorticoid analogue of cortisol (Figure 4.1A). Dexamethasone at a concentration of 10 nM was able to increase PAP activity by 50%; concentrations above 10 nM did not significantly

augment this induction (Figure 4.1A). This increase in PAP activity induced by 10

nM dexamethasone was constant whether NRVMs were treated for 8, 12 or 16 h

(Figure 4.1B).
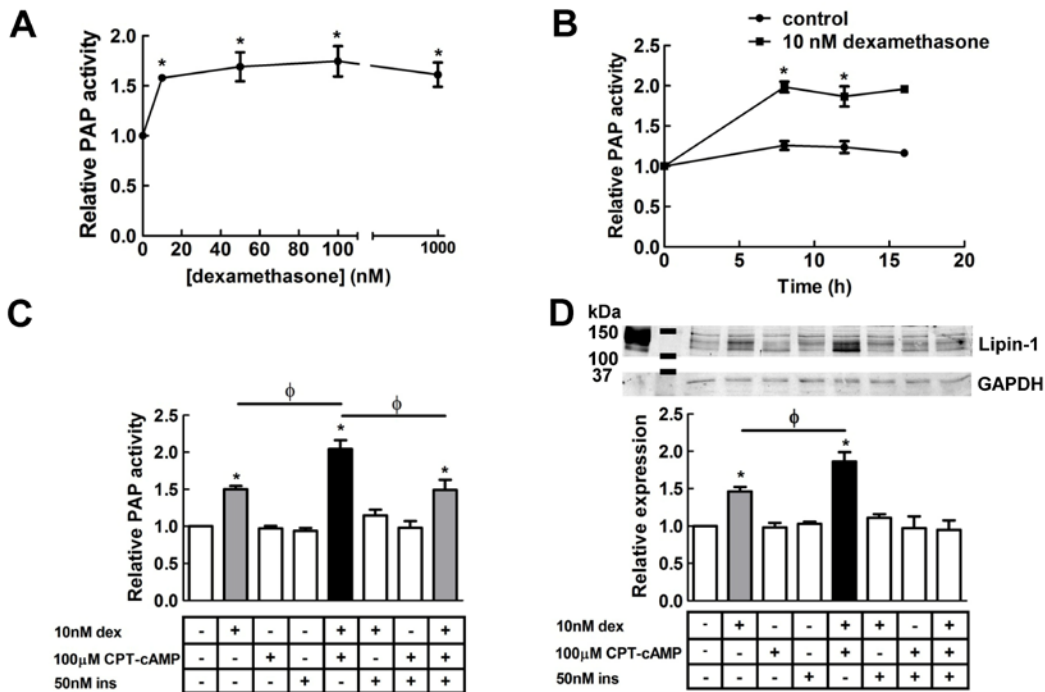
Figure 4.1 Treatment of neonatal rat ventricular myocytes (NRVMs) with different compounds and their effects on PAP activity and lipin-1 expression. (A) NRVMs were treated with different concentrations of dexamethasone in DME/F12 medium for 8 h (n = 3) and the PAP activities of the cell lysates were measured and expressed relative to the vehicle-treated control. **(B)** NRVMs were treated with 10 nM dexamethasone in DME/F12 medium for different lengths of time (n = 3) and PAP activities were measured and expressed relative to the control at time zero. **(C)** NRVMs were treated with various combinations of 10 nM dexamethasone (dex), 100 µM 8-(4-chlorophenylthio)-2′-O-methyladenosine 3′,5′-cyclic monophosphate (CPT-cAMP) and 50 nM insulin (ins) for 8 h (n = 5-12) and PAP activities were measured and expressed relative to control. **(D)** Representative Western blot (*upper panel*) and quantification (*lower panel*) of the effects of various combinations of compounds on lipin-1 expression (n = 3-8). Lipin-1 overexpressed in human embryonic kidney 293 cells from a recombinant adenoviral vector serves as a positive control. * $p < 0.05$

135

compared to respective controls and baseline groups (Figure 4.1C, D); $^{\phi}$ p < 0.05 when comparing the indicated treatments. Half of the NRVMs used in these experiments were prepared by Suzanne Kovacic and Carrie-Lynn Soltys from the laboratory of Dr. Jason Dyck (University of Alberta). The other half were prepared by Bernard Kok. All experiment were performed by Bernard Kok.

The dexamethasone-induced increase in PAP activity was significantly synergized by the addition of CPT-cAMP (cAMP analogue that is cell-permeable and resistant to phosphodiesterase activity) (Figure 4.1C). Conversely, insulin inhibited the dexamethasone effect on PAP activity (Figure 4.1C). Insulin also antagonized the dexamethasone- and CPT-cAMP-dependent increase in PAP activity, although activity was still significantly higher than baseline (Figure 4.1C). Importantly, the changes in PAP activity elicited by dexamethasone, CPT-cAMP and insulin coincided with changes in lipin-1 expression (Figure 4.1D). There was one exception, which was the effect of insulin in reducing the dexamethasone- and CPT-cAMP-dependent increase in lipin-1 expression to baseline levels.

When we determined the gene expression profile of *Lpin1* in NRVMs treated with the different combinations of compounds, we reached the same conclusions that dexamethasone increased the expression of *Lpin1* with CPT-cAMP and insulin acting as a synergist and antagonist, respectively (Figure 4.2A). Furthermore, maximal induction of *Lpin1* expression with either dexamethasone alone or the combination of dexamethasone and CPT-cAMP occurred between 4 – 7 h after treatment with a decline in expression past 7 h (Figure 4.2C).

136
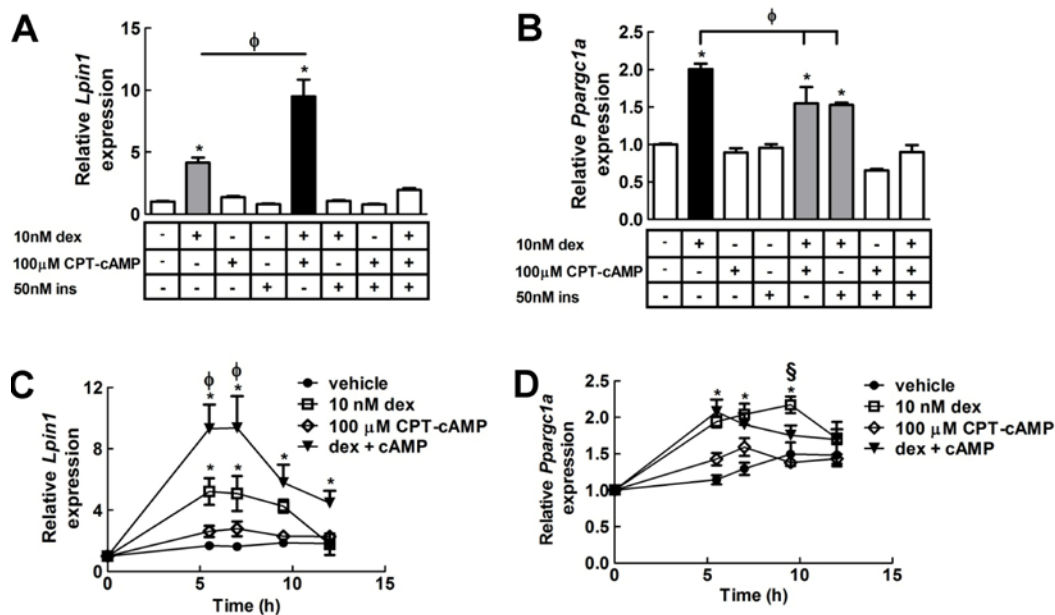
Figure 4.2 The effect of various combinations of hormones and CPT-cAMP on the expression of *Lpin1* and *Ppargc1a* in neonatal rat ventricular myocytes (NRVMs). The gene expressions of **(A)** *Lpin1* and **(B)** *Ppargc1a* in NRVMs were measured after treatment with various combinations of 10 nM dexamethasone (dex), 100 μM 8-(4-chlorophenylthio)-2′-O-methyladenosine 3′,5′-cyclic monophosphate (CPT-cAMP) and 50 nM insulin (ins) for 4 h (n = 4-6). Time course of **(C)** *Lpin1* and **(D)** *Ppargc1a* expressions in NRVMs treated with 10 nM dex and/or 100 μM CPT-cAMP (n = 3); results were expressed to the controls at time zero. * $p < 0.05$ compared to respective controls and baseline groups; ϕ $p < 0.05$ when compared to 10 nM dex treatment; $\S$ $p < 0.05$ when compared to treatment with 10 nM dex and 100 μM CPT-cAMP. NRVMs were prepared and all experiments were performed by Bernard Kok.

4.2.2 The effect of dexamethasone, CPT-cAMP and insulin on *Ppargc1a* and *Ppara* expression in NRVMs

Lipin-1 acts as a transcriptional co-activator in combination with PPARα and PGC-1α in the liver (100). Furthermore, Manmontri et al. demonstrated the coordinated regulation of *Lpin1*, *Ppargc1a*, and *Ppara* expression in hepatocytes (307). We found that *Ppargc1a* expression was increased by treatment with 10 nM dexamethasone after 4 h (Figure 4.2B). Importantly, *Ppargc1a* expression coincided with *Lpin1* expression when stimulated with dexamethasone (Figure 4.2D). Insulin partially antagonized dexamethasone-induced *Ppargc1a* expression, similar to the results obtained with *Lpin1* expression (Figure 4.2B). However, CPT-cAMP did not act synergistically; instead, CPT-cAMP treatment appears to blunt the increase in *Lpin1* expression by dexamethasone (Figure 4.2B, D). When all three compounds were used in combination, *Ppargc1a* expression remained at baseline.

On the other hand, *Ppara* expression was not regulated by any of the compounds after 4 h treatment (Figure 4.3A). Additionally, dexamethasone and/or CPT-cAMP treatment did not affect *Ppara* expression up to 12 h of treatment compared to cardiomyocytes incubated with vehicle (Figure 4.3C). However, dexamethasone and CPT-cAMP did appear to regulate the gene expression of *Cpt1b*, which is a target of PPARα transcriptional regulation (Figure 4.3B, D). *Cpt1b* expression was induced after 7 h of treatment with dexamethasone and insulin antagonized the increase when cells were treated with dexamethasone and CPT-cAMP (Figure 4.3B). Dexamethasone alone or dexamethasone and CPT-cAMP increased *Cpt1b* expression up to 12 h treatment time (Figure 4.3D).
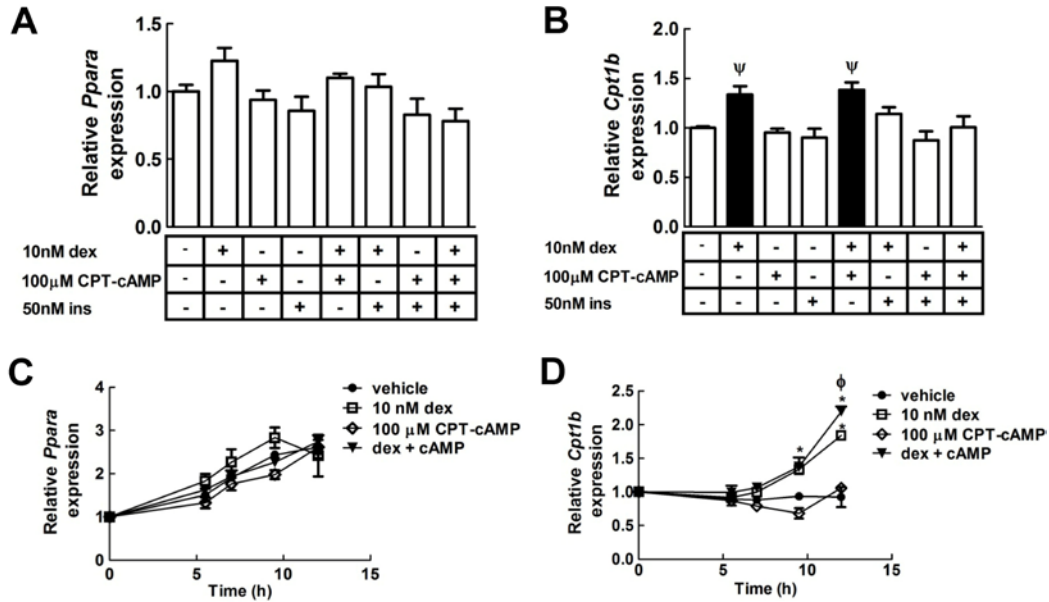
Figure 4.3 The effect of various compounds on the expression of *Ppara* and *Cpt1b* in neonatal rat ventricular myocytes (NRVMs). The gene expressions of **(A)** *Ppara* (n = 3) and **(B)** *Cpt1b* (n = 4-8) in NRVMs were measured after treatment with various combinations of 10 nM dexamethasone (dex), 100 μM 8-(4-chlorophenylthio)-2′-O-methyladenosine ′3′,5′-cyclic monophosphate (CPT-cAMP) and 50 nM insulin (ins) for 4 and 7 h, respectively (n = 3). Time course of **(C)** *Ppara* and **(D)** *Cpt1b* expression in NRVMs treated with 10 nM dex and/or 100 μM CPT-cAMP (n = 3); results were expressed to the controls at time zero. * $p < 0.05$ compared to respective controls and baseline groups; $^{\phi} p < 0.05$ when compared to 10 nM dex treatment; $^{\psi} p < 0.05$ compared to all baseline groups except for cells treated with 10 nM dex + 50 nM insulin. NRVMs were prepared and all experiments were performed by Bernard Kok.

4.2.3 Regulation of *Lpin2* and *Lpin3* expression in NRVMs

In contrast to hepatocytes (307), the expression of *Lpin2* can also be increased by treatment with CPT-cAMP after 4 h treatment (Figure 4.4A) and dexamethasone did not have a synergistic effect at this time point. However, CPT-cAMP and dexamethasone acted synergistically between 7 and 12 h treatment (Figure 4.4C). Insulin acted antagonistically on *Lpin2* expression as with the regulation of the *Lpin1* gene (Figure 4.4A). *Lpin3* expression was regulated similarly to *Lpin1* expression in that dexamethasone induced expression and cAMP acted synergistically (Figure 4.4B, D). However, these actions occurred only after 5.5 h treatment with the maximal effect of dexamethasone treatment at 9 h (Figure 4.4D). Addition of CPT-cAMP to dexamethasone prolonged the increase in *Lpin3* expression up to 12 h (Figure 4.4D). Insulin did not antagonize the upregulation of *Lpin3* expression by dexamethasone alone or dexamethasone in combination with CPT-cAMP after 7 h of treatment (Figure 4.4B).
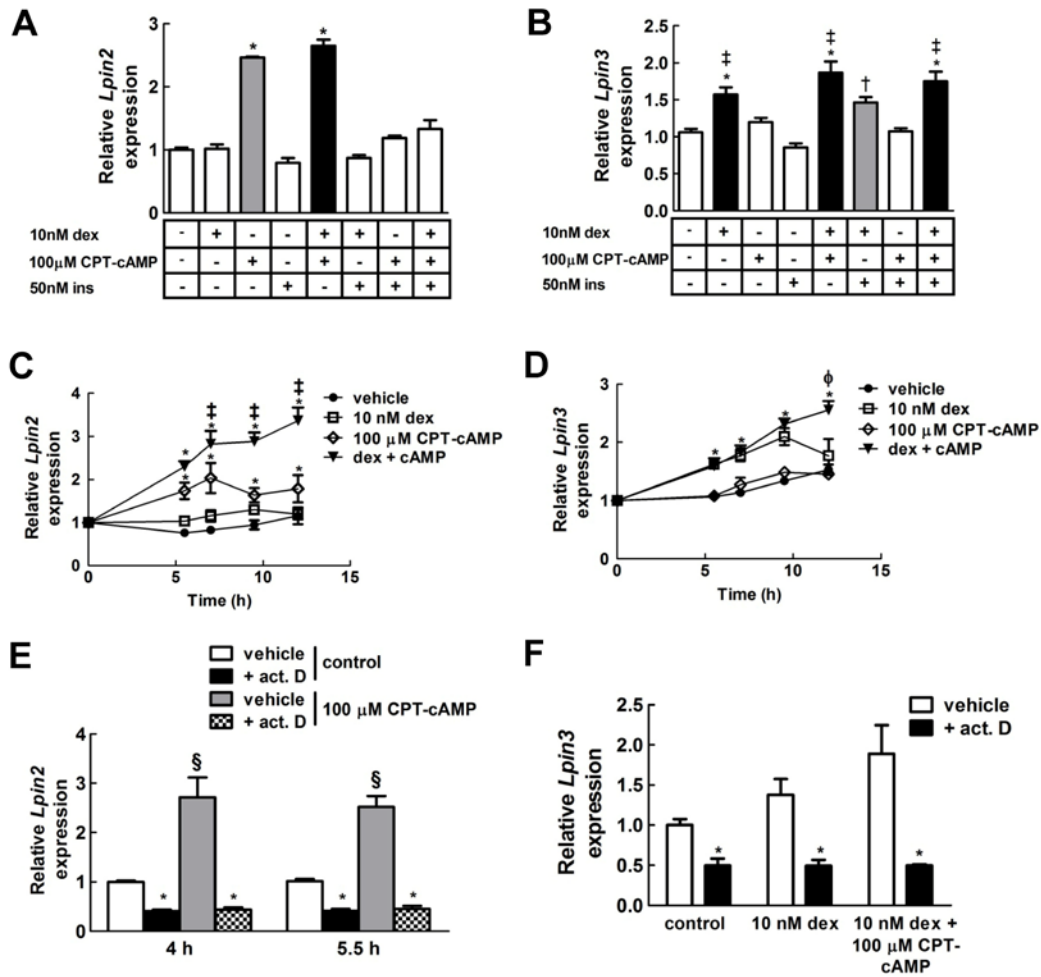
Figure 4.4 The effect of various combinations of hormones and CPT-cAMP on the gene expression of the lipins in neonatal rat ventricular myocytes (NRVMs). (A) The expression of *Lpin2* was measured after treatment of NRVMs with various combinations of 10 nM dexamethasone (dex), 100 µM 8-(4-chlorophenylthio)-2′-O-methyladenosine 3′,5′-cyclic monophosphate monosodium hydrate (CPT-cAMP) and 50 nM insulin (ins) for 4 h (n = 3). **(B)** The effect of various combinations of hormones and CPT-cAMP on *Lpin3* expression after 7 h in NRVMs (n = 4-8). The expression of **(C)** *Lpin2* and **(D)** *Lpin3* was measured after treating NRVMs with 10 nM dexamethasone, 100 µM CPT-cAMP or the combination of both for various time points up to 12 h. **(E)** NRVMs were pre-incubated for 30 min with 10 µg/ml actinomycin D or vehicle before treatment with 100 µM CPT-cAMP for 4 and 5.5 h before mRNA levels of *Lpin2* were measured (n = 3). **(F)** *Lpin3* transcript levels were also determined after 30 min pre-incubation with actinomycin D and treatment for 7 h with 10 nM dex and 100 µM CPT-cAMP (n = 3). * p < 0.05 compared to respective controls and baseline groups; [‡] p < 0.05 when compared to 100 µM CPT-cAMP treatment; [φ] p < 0.05 when compared to 10 nM dex treatment; [§] p < 0.05 compared to vehicle-treated control; [†] p < 0.05 compared to 50 nM insulin treatment. NRVMs were prepared and all experiments were performed by Bernard Kok.

141

Treatment with actinomycin D, which prevents elongation by RNA polymerase (373), significantly reduced transcript levels of *Lpin2* and *Lpin3* in NRVMs treated with dexamethasone and/or CPT-cAMP (Figure 4.4E, F). This result suggests that the effect of dexamethasone and/or CPT-cAMP on *Lpin2* and *Lpin3* expression is dependent on increased mRNA synthesis during transcription.

4.3 The effect of fasting on gene expression and PAP activity in *fld* and control hearts

Since we found effects of dexamethasone and CPT-cAMP on gene expression in cultured NRVMs, we wanted to determine if we saw similar changes in fasted mice, which are physiological models where glucocorticoid and cAMP actions are increased, and insulin signalling is minimized. First, we fasted 14- to 18-week old female *fld* and control mice for 12 h from 2200 h to 1000 h the next day. The light cycle started from 0600 h and lasted till 1800 h. We determined the heart weight to tibia length ratios in these mice since heart weight to tibia length ratios are decreased in 19- to 23-week old male *fld* mice (374). The heart weight to tibia length ratios in the female *fld* mice compared to the controls were not significantly different, indicating that there was no detrimental loss of heart mass (Figure 4.5A).
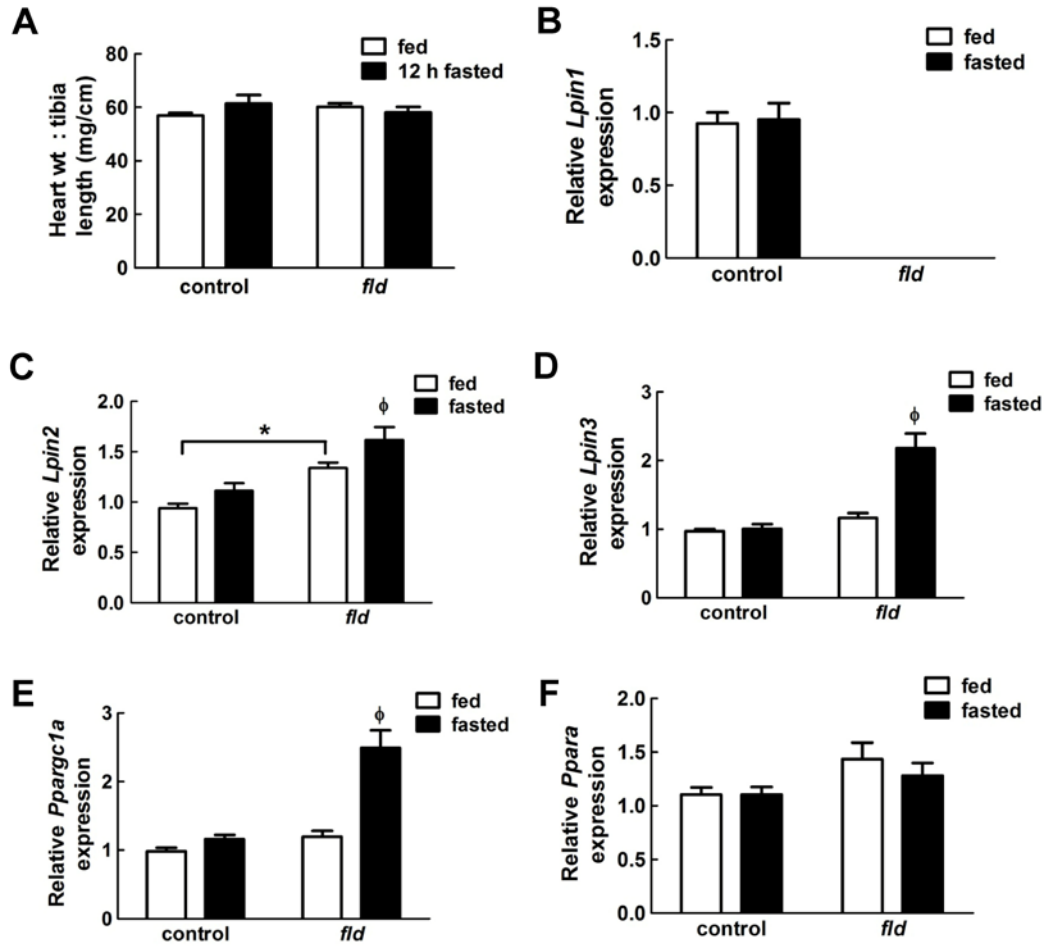
Figure 4.5 Effect of fasting for 12 h on gene expression in lipin-1 deficient *fld* (fatty liver dystrophy) and control mice. (A) The heart weight to tibia length ratios of 14-18 week old *fld* and control mice were measured. The expression of **(B)** *Lpin1*, **(C)** *Lpin2*, **(D)** *Lpin3*, **(E)** *Ppargc1a*, and **(F)** *Ppara* were measured in 14-18 week-old *fld* and control mice *ad libitum* fed or fasted for 12 h from 2200 h to 1000 h. * $p < 0.05$ when comparing the indicated groups; ϕ $p < 0.05$ compared to all other groups. All experiments were performed by Bernard Kok.

As expected, *Lpin1* expression was only observed in the control hearts and there were no changes in the 12 h fasted control animals compared to the fed controls (Figure 4.5B). Similarly, cardiac *Lpin2* expression was not significantly induced after the 12 h fasting period in control mice. However, *Lpin2* expression was increased in *fld* mice in both the fed and 12 h fasted states compared to controls (Figure 4.5C). Furthermore, *Lpin2* expression was significantly increased in fasted *fld* mice compared to fed *fld* mice. *Lpin3* expression was also increased in 12 h fasted *fld* hearts compared to fed *fld* hearts, whereas there was no difference in expression between fed and fasted control mice (Figure 4.5D). The regulation of *Ppargc1a* expression in fed versus 12 h fasted *fld* hearts was similar to the changes in cardiac *Lpin3* transcript levels in *fld* mice (Figure 4.5E). Finally, *Ppara* expression was unchanged in all groups (Figure 4.5F).

To determine whether the absence of changes in gene expression after 12 h fast in the control mice could be attributed to the length of the fast, we also examined gene expression after 24 h of fasting in control mice (1000 h to 1000 h the next day). We did not fast *fld* mice for 24 h since they do not tolerate prolonged fasting because of the lack of adipose tissue. We again measured the heart weight to tibia lengths of the fed and fasted control mice and there was no significant difference, as expected (Figure 4.6A). Surprisingly, *Lpin1*, *Ppara* and *Ppargc1a* gene expressions were all significantly decreased in the 24 h fasted control animals and there were no significant changes in *Lpin2* and *Lpin3* transcript levels (Figure 4.6B, C).

144
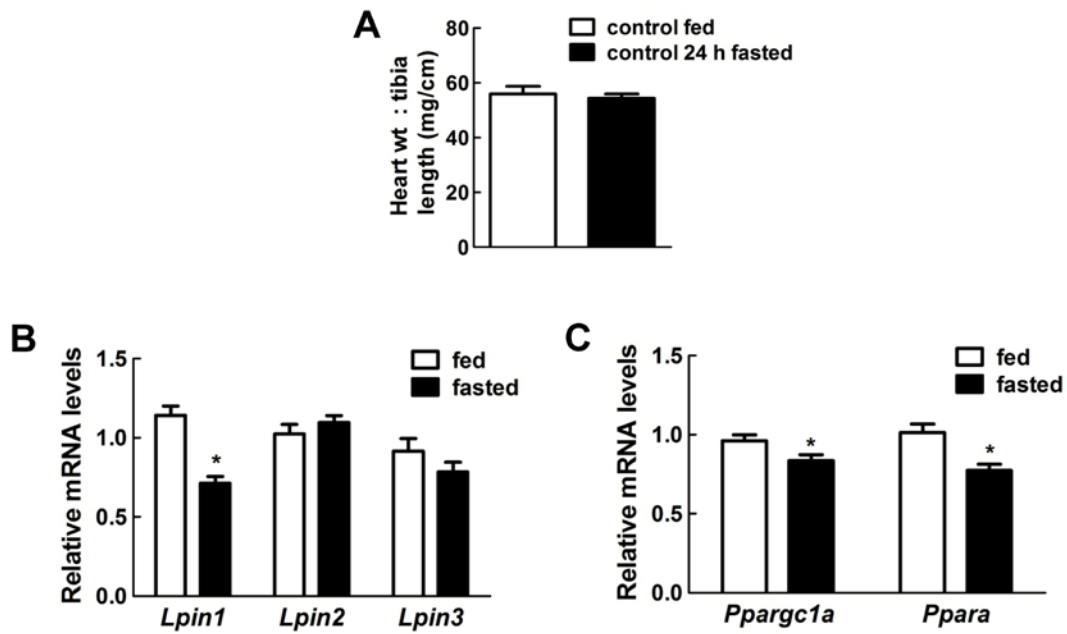
Figure 4.6 Effect of fasting for 24 h on gene expression in control mice. (A) The heart weight to tibia length ratios of 14-18 week old *fld* and control mice were measured. The expression of **(B)** *Lpin1, Lpin2, Lpin3*, **(C)** *Ppargc1a*, and *Ppara* were measured in 14-18 week-old *fld* and control mice *ad libitum* fed or fasted for 24 h from 1000 h to 1000 h the next day. * p < 0.05 compared to fed controls. All experiments were performed by Bernard Kok.

We then measured PAP activities in the hearts of the 12 h and 24 h fasted mice to determine if the changes in lipin gene expression were indicative of changes in enzymatic activity. There was no change in PAP activity in the hearts of 12 h fasted compared to fed control mice (Figure 4.7A). This corresponds to the lack of changes in cardiac gene expression of the lipins after 12 h of fasting. Surprisingly, there was no change in PAP activities in the hearts of 12 h fasted *fld* mice compared to fed *fld* mice even though there was an increase in *Lpin2* and *Lpin3* expression. In 24 h fasted control hearts, PAP activity was significantly decreased, which corresponds to the decrease in cardiac *Lpin1* gene expression after 24 h of fasting. However, we did not find significant changes in the protein levels of lipin-1 and -2 in the 24 h fasted hearts compared to the fed controls (Figure 4.7E, F).
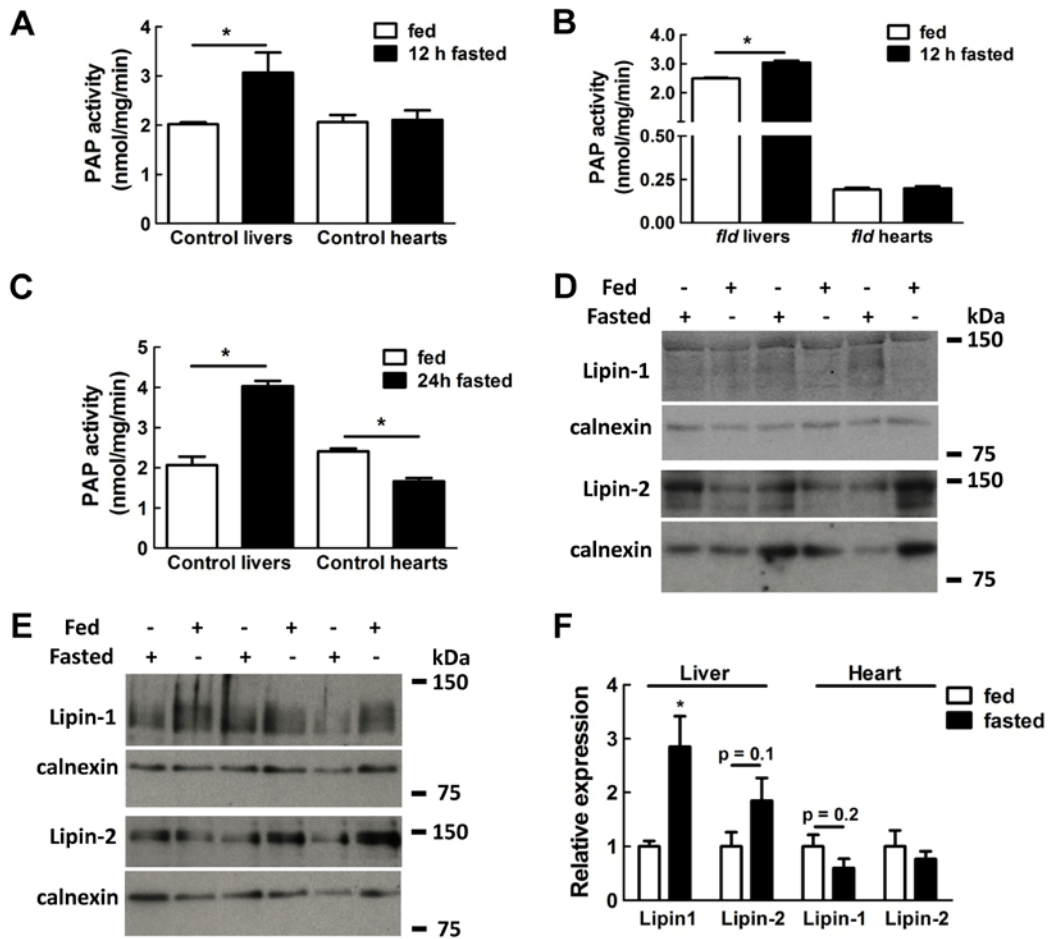
Figure 4.7 Effect of fasting on PAP activity and lipin expression in *fld* and control livers and hearts. The PAP activities in the livers and hearts of 12 h fasted and *ad libitum* fed **(A)** control and **(B)** *fld* mice (2200 h to 1000 h the next day) were measured. **(C)** Hepatic and cardiac PAP activities in 24 h fasted mice were also measured (1000 h to 1000 h the next day). **(D)** Representative Western blots showing the expression of lipin-1 and -2 in 24 h fasted and fed control livers. The LI-COR Odyssey Imaging system was used to detect lipin-1 and lipin-2 levels were identified by enzymatic chemiluminescence and autoradiography. Calnexin was used as a loading control. **(E)** Representative Western blots showing the expression of lipin-1 and -2 in 24 h fasted and fed hearts. Both lipin-1 and -2 were detected using enzymatic chemiluminescence and autoradiography. **(F)** Lipin-1, lipin-2 and calnexin levels in 24 h fasted (n = 4) or fed (n = 4-5) control livers and hearts were quantified using the LI-COR Odyssey Imaging software 1.2 or ImageJ. * p < 0.05 compared to respective *ad libitum* fed mice. All experiments were performed by Bernard Kok.

In comparison, the PAP activities in the livers of 12 h and 24 h fasted and fed mice were also measured since a previous study showed an increase in hepatic PAP activity after fasting (307). As expected, the PAP activities in the 12 h fasted control livers were increased compared to the livers of fed control mice. Similarly, 12 h fasted *fld* livers had small increases in PAP activities compared to fed *fld* mice (Figure 4.7B), demonstrating the compensatory increases in lipin-2 expression (and possibly, lipin-3) in the lipin-1 deficient liver (243, 307). Similar to 12 h fasted mice, hepatic PAP activity was increased in control mice fasted for 24 h (Figure 4.7C). Furthermore, lipin-1 protein levels in the 24 h fasted control livers were significantly increased compared to fed controls with no significant changes in lipin-2 expression (Figure 4.7D, F). In summary, there appears to be a physiological difference between the regulation of hepatic and cardiac PAP activities *in vivo* even though there are significant similarities in the regulation of lipin expression in cultured hepatocytes (307) and NRVMs.

4.4 The effect of changing lipin levels on glycerolipid synthesis in neonatal rat ventricular myocytes

4.4.1 Introduction

Since there was no increase in lipin expression and PAP activity in mouse hearts compared to the changes observed in cultured NRVMs, we wanted to determine the functional consequences of changes in lipin expression in NRVMs. We investigated whether decreasing lipin-1 expression or increasing lipin-1 and -2 expression in NRVMs using adenoviral vectors has a major effect on the rate of glycerolipid synthesis.

4.4.2 Glycerolipid synthesis in NRVMs with decreased lipin-1 expression

NRVMs were either untreated or incubated with adenovirus encoding for shRNA against *Lpin1* or *lacZ* for 38 h (AdshRNA Lpin1 and AdshRNA LacZ). PAP activity in NRVMs treated with AdshRNA Lpin1 was decreased by 50% compared to non-treated and vector controls (Figure 4.8A). After 3 h treatment with 1 mM [^{14}C]oleate and 1 mM [1,3-^{3}H]glycerol, there was no significant difference between groups in the rate of glycerol or oleate incorporation into the glycerolipids examined except for TG (Figure 4.8B, C). Oleate and glycerol incorporation into TG in AdshRNA LacZ-treated cells were significantly increased compared to non-treated controls (Figure 4.8B, C). Oleate incorporation into TG in AdshRNA Lpin1-treated cells was also significantly increased compared to non-treated controls (Figure 4.8C). However, this increase was significantly lower compared to NRVMs inoculated with AdshRNA LacZ (Figure 4.8C).
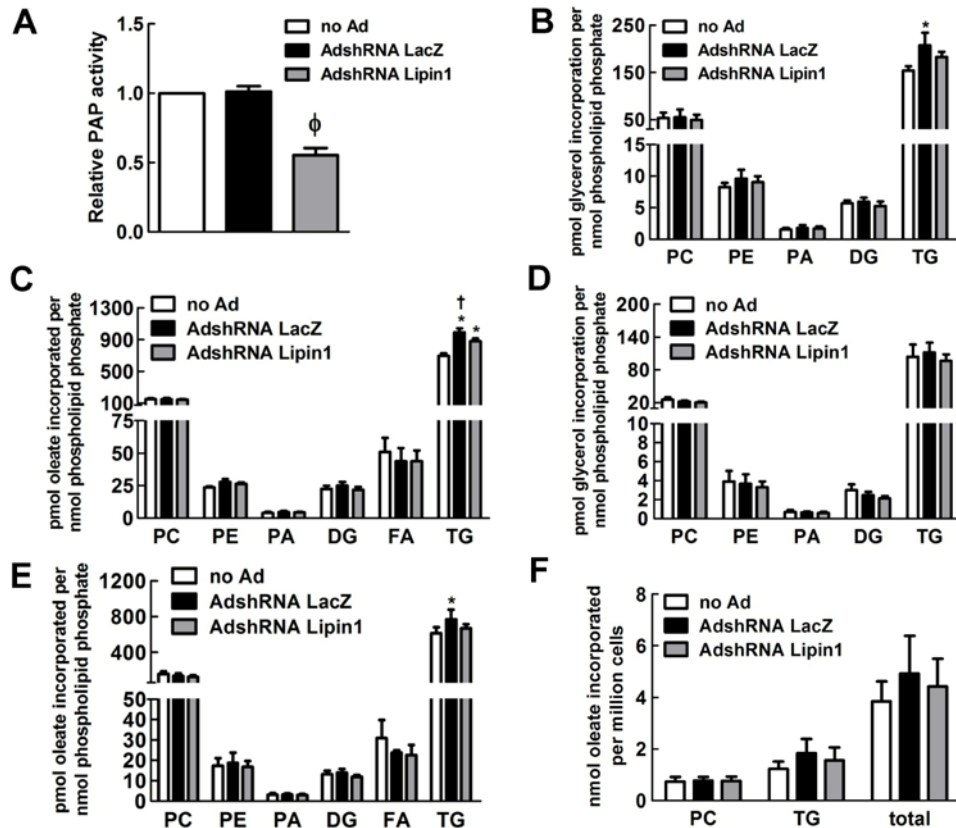
Figure 4.8 The effect of knocking down lipin-1 on the rate of glycerolipid synthesis in neonatal rat ventricular myocytes (NRVMS). (A) NRVMs were inoculated for 38 h with recombinant adenoviral (Ad) constructs expressing shRNA against *lacZ* or *Lpin1* at a multiplicity of infection (MOI) of 20 respectively, and the PAP activities in the cell lysates were measured and expressed relative to the no Ad control. NRVMs were treated with **(B)** 1 mM [^{3}H]glycerol and **(C)** 1 mM [^{14}C]oleate in DME/F12 medium containing 0.3 mM BSA for 3 h after inoculation with recombinant adenovirus for 38 h (n = 3), and the rate of glycerol and oleate incorporation into glycerolipids was measured. Similar analysis was performed for NRVMs were treated with **(D)** 0.3 mM [^{3}H]glycerol and **(E)** 0.5 mM [^{14}C]oleate in DME/F12 medium containing 0.1 mM BSA for 3 h after inoculation with recombinant adenovirus for 38 h (n = 3). **(F)** The rate of oleate incorporation into glycerolipids in NRVMs treated with 1 mM glycerol and 1 mM [^{14}C]oleate in DME/F12 medium containing 0.3 mM BSA for 45 min after adenoviral inoculation was also measured (n = 3). * $p < 0.05$ compared to no Ad control; † $p < 0.05$ compared to NRVMs inoculated with AdshRNA Lipin1. AdshRNA LacZ and AdshRNA Lipin1 were gifts from Dr. Thurl Harris (University of Virginia) and adenoviral propagation was carried out by Amy Barr (Cardiovascular Research Centre, University of Alberta). NRVMs were prepared and all experiments were performed by Bernard Kok.

A previous study had shown that there was a difference in the rate of TG synthesis in NRVMs inoculated with recombinant adenovirus expressing shRNA against lipin-1 (266). Mitra et al. treated their cells with [2-^{3}H]glycerol (10 μCi/ml) and 0.5 mM oleate and we decided to test whether we could obtain similar results. Moreover, treatment with 1 mM glycerol and 1 mM oleate in the previous experiments would provide maximum induction of lipin association with the membranes. Therefore, the effect of decreased lipin-1 expression might be more easily detected using more physiological concentrations of oleate and glycerol. When NRVMs were treated with 0.5 mM [^{14}C]oleate and 0.3 mM [1,3-^{3}H]glycerol for 3 h were used instead, there were no significant differences in the rate of glycerolipid synthesis in the AdshRNA Lpin1-treated cells compared to non-inoculated or vector controls (Figure 4.8D, E). However, oleate incorporation into TG was increased in AdshRNA LacZ-treated cells compared to non-inoculated controls (Figure 4.8E). This observation was similar to the result from the previous experiment performed with 1 mM [^{14}C]oleate and 1 mM [1,3-^{3}H]glycerol. Lastly, NRVMs were treated with 1 mM [^{14}C]oleate and 1 mM glycerol for 45 min to determine if decreased lipin-1 levels would have an effect on a shorter time scale. However, oleate incorporation into PC or TG after 45 min was not significantly different between treatments (Figure 4.8F).

4.4.3 The effect of increased lipin-1 and -2 expression on glycerolipid synthesis in NRVMs

We also wanted to determine the effect of increasing lipin expression on glycerolipid synthesis. After 38 h inoculation with recombinant adenoviral vectors expressing *Mus musculus* lipin-1B and -2 (AdLipin1b and AdLipin2), PAP activities in NRVMs were increased 14- and 5-fold, respectively (Figure 4.9A).

Inoculation with control adenovirus expressing GFP (AdGFP) did not affect PAP

activity (Figure 4.9A). Increasing PAP activity in NRVMs with either AdLipin1b or

AdLipin2 did not significantly affect glycerol or oleate incorporation into

phospholipids and diacylglycerol when treated with 1 mM [^{14}C]oleate and 1 mM

[1,3-^{3}H]glycerol for 3 h (Figure 4.9B, C).
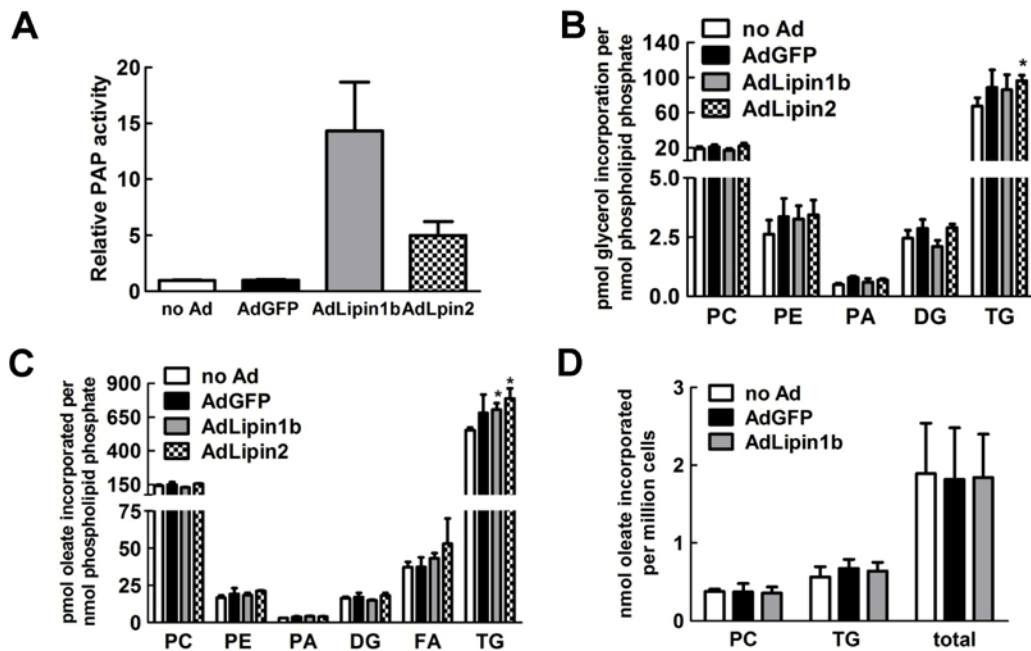
Figure 4.9 The rate of glycerolipid synthesis from glycerol and oleate in neonatal rat ventricular myocytes (NRVMs) expressing recombinant lipin-1 and -2. (A) NRVMs were inoculated for 38 h with recombinant adenoviral (Ad) constructs expressing green fluorescent protein (GFP), lipin-1b or -2 at a multiplicity of infection (MOI) of 7, and the PAP activities in the cell lysates were measured and expressed relative to the no Ad control. NRVMs were treated with **(B)** 1 mM [^{3}H]glycerol and **(C)** 1 mM [^{14}C]oleate in DME/F12 medium containing 0.3 mM BSA for 3 h after inoculation with recombinant adenovirus for 38 h (n = 3), and the rates of glycerol and oleate incorporation into glycerolipids were measured. **(D)** The rate of oleate incorporation into glycerolipids in NRVMs treated with 1 mM glycerol and 1 mM [^{14}C]oleate in DME/F12 medium containing 0.3 mM BSA for 30 min after adenoviral inoculation was also measured (n = 2). * p < 0.05 compared to no Ad control. AdGFP, AdLipin1b and AdLipin2 were gifts from Dr. Thurl Harris (University of Virginia) and adenoviral propagation was carried out by Amy Barr (Cardiovascular Research Centre, University of Alberta). NRVMs were prepared and all experiments were performed by Bernard Kok.

Instead, there was a significant increase in oleate and glycerol incorporation into TG in NRVMs inoculated with AdLipin2 compared to non-inoculated cells (Figure 4.9B, C). Moreover, a similar result was observed for oleate incorporation into TG in cells treated with AdLipin1b (Figure 4.9C). However, it is important to note that there were no significant differences in oleate and glycerol incorporation when comparing NRVMs expressing recombinant lipin-1B and -2 to control cells inoculated with AdGFP (Figure 4.9B, C). We also determined whether increased lipin-1 levels might have an effect on a shorter time scale. However, there appeared to be no changes in oleate incorporation into PC and TG when non-inoculated NRVMs and cells expressing recombinant GFP or lipin-1B were treated with 1 mM [^{14}C]oleate and 1 mM glycerol for 30 min (Figure 4.9D).

4.4.4 Translocation of PAP activity onto membranes in NRVMs

We next wanted to determine the extent to which PAP activity associates with membranes when treated with FAs since this is the metabolically active form of lipin-1 for glycerolipid synthesis. After 1 h treatment of NRVMs with 1.2 mM oleate and separation of cytosolic and cell ghost fractions by hypotonic lysis, there was no significant increase in PAP activity on cell ghost membranes (Figure 4.10A). However, there was a significant two-fold increase in membrane-associated PAP activity after 4 h treatment with either 0.3 or 1.2 mM oleate (Figure 4.10A). Since there was no significant change in total PAP activity (Figure 4.10B), this indicates that the increase in PAP activity on the membranes is due to translocation of cytosolic PAP activity. Treatment with 1.2 mM palmitate did not

significantly increase membrane-associated PAP activity after 4 h (Figure 4.10C)

and total PAP activity was not affected by palmitate treatment (Figure 4.10D).
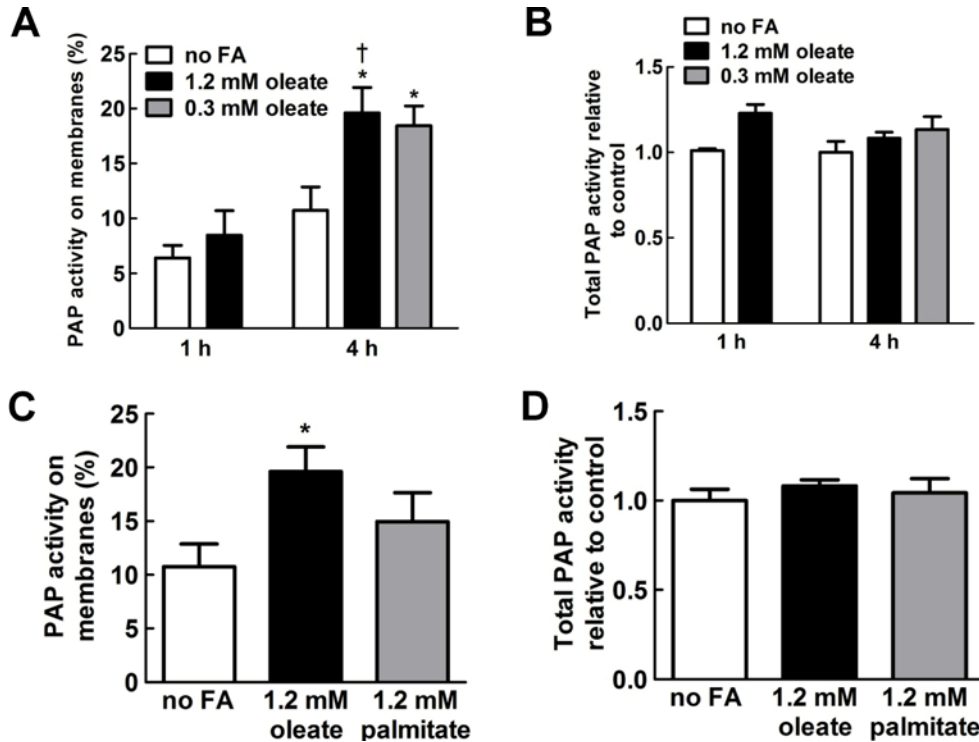
Figure 4.10 Translocation of PAP activity in neonatal rat ventricular myocytes (NRVMs) stimulated by oleate. (A) NRVMs were treated with 0.3 or 1.2 mM oleate in DME/F12 medium containing 0.3 mM BSA for 1 h (n = 3) and 4 h (n = 6). NRVMs were then incubated for 4 min with a hypotonic solution containing 0.1 mg/ml digitonin on ice. The cytosolic fractions and cell ghosts were collected separately, and the PAP activity in each fraction was measured. Results were then expressed as percentage of total PAP activity on cell ghost membranes. **(B)** Total PAP activities in NRVMs treated as previously described (Figure 4.10A) were calculated as the sum of the cytosolic and membrane-associated PAP activities. **(C)** Neonatal rat ventricular myocytes (NRVMs) were treated with 1.2 mM oleate or 1.2 mM palmitate in DME/F12 medium containing 0.3 mM BSA for 4 h before collecting the cytosolic and cell ghost fractions (n = 6). PAP activity in each fraction was measured and results were expressed as percentage of total PAP activity on cell ghost membranes. **(D)** Total PAP activities in the NRVMs treated as previously described (Figure 4.10C). * $p < 0.05$ compared to 4 h vehicle-treated control (no FA); † $p < 0.05$ compared to corresponding 1 h treatments. NRVMs were prepared and all experiments were performed by Bernard Kok.

154

4.5 Discussion

Numerous studies have shown that the gene expressions of the lipins are affected during various physiological and pathological conditions (375-377) (266, 310, 378-380). Hepatic and adipose gene expressions of the lipins are increased by fasting (100, 243, 307, 308) and the influence of lipin levels on disease phenotypes is highlighted by studies in the adipose tissue demonstrating that changes in lipin-1 and -2 levels can modulate inflammatory signalling (272, 273, 381). Hepatic lipin-2 induced by endoplasmic reticulum stress has also been shown to negatively affect insulin signalling (280). Furthermore, the regulation of lipin expression by glucocorticoids, cAMP and insulin signalling has been carefully delineated in hepatocytes and, to some extent, adipocytes. Thus, we wanted to determine whether lipin expression in cardiomyocytes is regulated by hormonal changes.

Similar to studies in hepatocytes and adipocytes, we found that lipin-1 expression in NRVMs was increased by treatment with dexamethasone with CPT-cAMP and insulin acting as synergistic and antagonistic agents, respectively (Figure 4.1) (307, 308). The mechanisms underlying the transcriptional upregulation of lipin-1 will be discussed later. CPT-cAMP alone did not increase *Lpin1* expression. This result was somewhat surprising since studies have shown that β_2-adrenergic receptor agonists could stimulate lipin-1 expression in C2C12 myotubes as well as mouse skeletal muscle and heart through PGC-1α, estrogen-related receptor α/γ and nuclear orphan receptor-1 (266, 309). The absence of a CPT-cAMP effect in NRVMs implies that β_2-adrenergic stimulation of lipin-1 expression is also reliant upon cAMP-independent signalling

downstream of the receptor. This will be explored in greater detail following the discussion on the regulation of *Ppargc1a* expression.

The changes in *Ppargc1a* expression elicited by dexamethasone, CPT-cAMP and insulin were significantly different in NRVMs compared to hepatocytes. Gene expression was increased by dexamethasone, and CPT-cAMP blunted this induction in NRVMs whereas CPT-cAMP increased *Ppargc1a* expression in both rat and mouse hepatocytes, and dexamethasone acted synergistically (307, 382). The upregulation of *Ppargc1a* transcript levels by dexamethasone is unlikely to occur through direct interaction of the activated glucocorticoid receptor since a glucocorticoid response element has yet to be found on the *Ppargc1a* promoter. Furthermore, dexamethasone alone did not induce *Ppargc1a* in hepatocytes (307). Studies have shown that PGC-1α expression is regulated by β_2-adrenergic receptor and/or cAMP signalling in skeletal muscle and liver through cAMP response element binding protein interacting at a cAMP response element on the promoter of *Ppargc1a* (382-385). Moreover, β_2-adrenergic activation by agonists such as clenbuterol also increases *Ppargc1a* expression in hearts (266). The regulation of lipin-1 gene expression by β_2-adrenergic signalling is strikingly similar (266, 309), which is not surprising given that PGC-1α upregulation tends to coincide with lipin-1 expression.

β_2-adrenergic signalling in the heart classically activates G_s, leading to the formation of cAMP by adenylyl cyclase and the activation of cAMP-dependent protein kinase A (386-388). However, β_2-adrenergic receptors are also coupled to G_i in cardiomyocytes and skeletal muscle, which can lead to downstream signals

independent of cAMP formation and protein kinase A activation (386-389). Since CPT-cAMP by itself does not affect *Ppargc1a* and *Lpin1* gene expression, it is likely that both *Ppargc1a* and *Lpin1* upregulation by β_2-adrenergic receptor signalling in the heart are mediated through G_i. Protein kinase B (Akt) and extracellular signal regulated kinase (ERK) act downstream of G_i signalling from β_2-adrenergic receptor in the heart (387, 388, 390, 391). However, neither effector has been linked to the regulation of *Ppargc1a* expression. Although the liver *Ppargc1a* promoter clearly has a cAMP response element (383), our results indicate that β_2-adrenergic signalling in the heart regulates *Ppargc1a* expression through G_i, although the direct effector is still unknown. It is likely that cAMP-dependent protein kinase A activation is still essential for regulation since Daaka et al. demonstrated the requirement for protein kinase A phosphorylation of the β_2-adrenergic receptor to desensitize G_s signalling and activate G_i (392).

Ppara expression was not affected by any combination of compounds in NRVMs whereas *Ppara* transcription was induced in hepatocytes by dexamethasone, and CPT-cAMP acted synergistically (307). In Hep G2 human hepatoma cells, lipin-1, in combination with PGC-1α, activates transcription of a luciferase reporter construct with a *Ppara* promoter (100). Furthermore, lipin-1 can interact with hepatocyte nuclear factor-4 or PPARα itself, to synergistically increase the expression of this luciferase construct (100). It is clear that PPARα is transcriptionally regulated in the liver since fasting increases hepatic *Ppara* transcript levels (393-395). Moreover, fasting-induced upregulation of *Ppara* and its target genes in the liver depends on lipin-1 expression (100). Thus, the transcriptional upregulation of PPARα gene expression appears to be an important factor in determining PPARα action in the liver.

157

PPARα has also been shown to play an important role in regulating FA oxidation in the heart using transgenic and knockout mouse models (23, 89, 102, 114). However, studies have shown that there is no upregulation of *Ppara* expression in the heart after fasting (394, 395). The importance of PPARα in cardiac metabolism is clear; however, it appears that the activation of PPARα by endogenous ligands like FAs or synthetic ligands like WY-14.643, rather than transcriptional upregulation of *Ppara*, is more essential in determining PPARα action on FA metabolism in the heart (86, 396, 397). Indeed, we found no changes in *Ppara* transcript levels in the hearts of 12 h fasted mice (Figure 4.5F), and in fact, there was a decrease in *Ppara* expression after 24 h of fasting (Figure 4.6C). In summary, the differential regulation of PPARα in the liver and heart during fasting could explain why there is a difference in the response of *Ppara* expression in the NRVMs compared to the hepatocytes. Interestingly, *Cpt1b* expression was increased by dexamethasone and CPT-cAMP treatments in NRVMs. Since the gene encoding CPT-1b is a target of PPARα (398-400), it is possible that *Cpt1b* upregulation by dexamethasone and CPT-cAMP was through PPARα activation. Alternatively, *Cpt1b* expression is also regulated by other transcription factors such as myocyte enhancer factor-2C (401) or GATA transcription factor 4 (402).

We also found that the gene expressions of lipin-2 and -3 in NRVMs were increased by the combination of dexamethasone and CPT-cAMP through increased transcription (Figure 4.4). This result was significant since Manmontri et al. did not find an increase in *Lpin2* and *Lpin3* expression after treatment with these compounds in rat hepatocytes (307). However, this study did show that treatment with dexamethasone alone stimulates *Lpin3* expression and CPT-

cAMP alone prevents the decline in *Lpin2* transcript levels in mouse hepatocytes (307). The regulation of lipin gene expression by dexamethasone and CPT-cAMP in NRVMs differs quite significantly over time. The increase in *Lpin1* expression by dexamethasone and CPT-cAMP was maximal at 4 – 7 h and slowly decreased thereafter (Figure 4.2C). In contrast, the increase in *Lpin2* and *Lpin3* expression by dexamethasone and CPT-cAMP was still not reduced after 12 h of treatment with these compounds (Figure 4.4C, D).

The maximal induction of *Lpin2* and *Lpin3* expression occurred much later compared to the regulation of *Lpin1* expression by dexamethasone and CPT-cAMP (Figure 4.2 and 4.4), suggesting a primary response of lipin-1 induction in the early stages of increased glucocorticoid and cAMP signalling with later changes in *Lpin2* and *Lpin3* expression. The effect of dexamethasone on lipin-1 is known to be mediated through the glucocorticoid response element upstream of the *Lpin1* promoter (308). Similarly, cAMP response elements have also been identified in the region surrounding the promoter (310). *Lpin2* and *Lpin3* could also be regulated in similar regions surrounding their respective promoters, although studies have yet to positively identify these sites.

The regulation of lipin gene expression is similar to the regulation of genes involved in hepatic gluconeogenesis. TORC2 (transducer of regulated CREB activity 2), PGC-1α, CREB (cAMP response element binding protein), CBP (CREB binding protein) and FOXO1 (forkhead box protein O1) act in combination to induce the expression of gluconeogenic genes (311, 383, 403, 404). Moreover, all four proteins except for FOXO1 have been previously demonstrated to be involved in the regulation of lipin-1 gene expression (100,

159

266, 310). Furthermore, the *C. elegans* FOXO homologue enhances glucocorticoid-induced expression of insulin-like growth factor binding protein-1, which can bind to and inhibit signalling from insulin-like growth factor I and II (405). This result demonstrates the possible role of FOXO1 in regulating dexamethasone-induced lipin expression. Insulin suppresses the induction of gluconeogenic genes by stimulating the phosphorylation and nuclear exclusion of TORC2 (312), FOXO1 (403, 406), and CBP (404, 407). The suppression of lipin gene induction by insulin could be regulated similarly. Alternatively, another member of the forkhead DNA-binding protein family, FOXA2 (forkhead box protein A2), could also play a role in the upregulation of lipin gene expression (408-410). FOXA2 increases the expression of genes involved in FAO and PGC-1β acts as a co-activator (409, 411). FOXA2 is also phosphorylated and inhibited by Akt downstream of insulin signalling (408).

To determine whether the changes elicited by the combinatorial treatments in NRVMs are indicative of physiological changes during fasting, *fld* and control mice were fed *ad libitum* or fasted for 12 h. We found no significant changes in transcript levels for any of the lipins, PPARα or PGC-1α between fed and 12 h fasted control hearts (Figure 4.5). However, there were increased expressions of *Lpin2*, *Lpin3* and *Ppargc1a* in the 12 h fasted versus fed *fld* mice. The differences in gene expression profiles between *fld* and control mice suggest a compensatory response in the absence of lipin-1. We also measured PAP activities in these hearts and found no change in PAP activities in the 12 h fasted compared to the fed state, even in the *fld* mice (Figure 4.7A, B). However, PAP activity in the livers of both 12 h fasted control and *fld* mice were significantly increased compared to fed mice (Figure 4.7A, B). To determine whether these

differences in cardiac and hepatic regulation of PAP activity was a matter of a slower cardiac response to fasting, we also measured PAP activity in 24 h fasted and *ad libitum* fed control mice. Similarly, hepatic PAP activity and lipin-1 expression was significantly increased by fasting. In contrast, cardiac PAP activity was significantly decreased and this decrease was accompanied by decreased *Lpin1* and *Ppargc1a* expression.

The lack of changes in the fasted control hearts compared to the dynamic increases in hepatic and adipose lipin gene expression during fasting indicates a differential requirement for lipin response in different organs (100, 243, 307, 308). It is clear that lipin gene expression can be dynamically regulated by glucocorticoid and cAMP-dependent signalling in cardiomyocytes. The absence of an increase in cardiac lipin-1 expression during fasting in contrast to the upregulation of lipin-1 expression in the livers of fasted mice is probably related to the differential expression of PGC-1α in both tissues. PGC-1α, in combination with estrogen-related receptor α (ERRα) or ERRγ, regulates lipin-1 expression in hepatocytes and cardiomyocytes (100, 243, 266, 412). As an example, overexpressing PGC-1α by itself using recombinant adenoviral vectors in hepatocytes and NRVMs increases lipin-1 expression (243, 266). Furthermore, PGC-1α deficiency prevents lipin-1 upregulation in the liver during fasting (100). Hepatic PGC-1α is strongly induced by 8-16 h of fasting and is important for the regulation of gluconeogenesis and VLDL secretion (382, 383, 385, 403, 413). We also demonstrate that PAP activity and lipin-1 expression in the liver were induced by fasting (Figure 4.7) and other studies have also shown this (100, 243, 307). Significantly, *Lpin1* gene expression and PAP activity in the heart coincided with the cardiac gene expression of PGC-1α (Figures 4.6 and 4.7).

161

Therefore, it is possible that the levels of PGC-1α regulate the expression of lipin-1. However, our group has shown that the upregulation of *Ppargc1a* and *Lpin1* expression occur with the same time course in hepatocytes (307) and NRVMs (Figure 4.2). Since the increase in *Ppargc1a* levels does not precede the increase in *Lpin1* expression, it is unlikely that the degree of PGC-1α expression regulates *Lpin1* transcript levels even though PGC-1α is clearly an important regulator of lipin-1 expression. Instead, the concurrent expression of both genes must be regulated by common transcription factors such as FOXO1, TORC2, CREB and ERRγ in the liver (310, 311, 383, 403, 412), and ERRα or ERRγ in the heart (266).

The lipins play crucial roles as PAP enzymes in glycerolipid synthesis (134, 137, 242, 243) and they can act as transcriptional co-activators in conjunction with PGC-1α and PPARα (100, 138). Therefore, the regulation of lipin levels could act as a mechanism for metabolic adaptation. Moreover, perturbations of lipin levels in the heart could potentially lead to the development of disease conditions (378, 380). Alternatively, changes in cardiac lipin levels could be symptomatic, and not causative, of metabolic adaptation or dysregulation. Studies in the lipin-1 deficient (*fld*) mice suggests that loss of lipin-1 leads to PA accumulation and aberrant cellular signalling with no detrimental changes in PC or TG synthesis after 30 min in the *ex vivo* working perfused heart system (266, 374). Further discussion of this work will be forthcoming in Chapter 5.

Primary cultured NRVMs were used as the cell model for measuring the rates of glycerolipid synthesis up to 3 h when lipin levels were increased or decreased using adenoviral vectors. We found no change in glycerol or oleate incorporation over 30 min or 3 h when recombinant adenoviral vectors expressing shRNA against lipin-1 were used to decrease PAP activity by 50% (Figure 4.8A). We did not target lipin-2 and -3 since lipin-1 is the major PAP enzyme in hearts (241, 374). Thus, results with the cultured NRVMs confirm the lack of detrimental effects on the synthesis of major phospholipids and TG in the perfused *fld* hearts as will be discussed in Chapter 5. However, we did not observe any aberrant accumulation of [^{14}C]oleate or [1,3-^{3}H]glycerol in PA and PI, unlike in the *fld* perfused hearts. This observation is accompanied by the caveat that lipin-1 expression was only decreased and it was not completely absent in the recombinant adenoviral-treated NRVMs. Glycerol is commonly used to measure glycerolipid synthesis in the liver because of the high levels of hepatic glycerol kinase (414, 415), whereas glycerol kinase was thought to be absent in adipose tissue and muscle (416) or to be present at very low levels (127). Therefore, glycerol might not be the best substrate to measure glycerolipid synthesis in myocytes. However, glycerol kinase deficiency leads to a decrease in TG and total phospholipid mass (specifically PI, PS and ethanolamine glycerophospholipids) in the heart (128). To support our work with [^{3}H]glycerol, we also used [^{14}C]oleate and included a general lipase inhibitor to block the turnover of the newly synthesized lipids (417). The conclusions obtained from the use of these two substrates of glycerolipid synthesis were essentially the same.

A recent study also used radiolabelled glycerol to determine the effect of decreasing lipin-1 levels on TG synthesis in NRVMs. Mitra et al. found that

knocking down lipin-1 by 60% in NRVMs decreased the incorporation of [2-^{3}H]glycerol (10 µCi/ml) into TG after 3 h treatment in the presence of 0.5 mM oleate (266). However, it is very difficult to compare glycerolipid synthesis under different conditions using [2-^{3}H]glycerol unless the specific radioactivity in the glycerol 3-phosphate precursor pool is also measured (418). This specific activity depends on glycerol kinase and the rate of substrate cycling between glycerol 3-phosphate and dihydroxyacetone phosphate. This cycling involves glycerol 3-phosphate dehydrogenase, which exhibits a significant isotope effect in its use of ^{3}H, i.e. glycerol 3-phosphate dehydrogenase cannot oxidize [2-^{3}H]glycerol 3-phosphate effectively compared to either unlabelled or [1,3-^{3}H]glycerol 3-phosphate (418, 419). This leads to progressive increases in the specific activity of the [2-^{3}H]glycerol 3-phosphate precursor pool compared to that obtained using [1,3-^{3}H]- or [^{14}C]glycerol (418).

We also determined the effect of increasing lipin-1 and -2 expression on glycerolipid synthesis in NRVMs. Increased expression of either lipin-1 or -2 did not dramatically affect the rate of oleate and glycerol and palmitate accumulation in phospholipids or TG (Figure 4.9). Although the rate of TG synthesis in NRVMs inoculated with AdLipin1b or AdLipin2 was significantly greater than in non-inoculated cells, we had also found that the adenoviral treatment by itself appeared to increase the incorporation of radiolabel into TG compared to non-treated cells (Figure 4.8 and 4.9). We had hypothesized that the initial rates of glycerolipid synthesis over 10-30 min could be driven by the increased availability of lipins, however, there were no striking differences in the rate of oleate incorporation into TG (Figure 4.9D).

Lipins can only participate in glycerolipid synthesis when they bind to endoplasmic reticulum membranes where PA is produced. We had assumed that there would be significant association of PAP activity with membranes in NRVMs comparable to that found in rat hepatocytes based on our own results (Figure 3.1A) as well as previous studies from our group (296). We found that there was no significant increase in oleate-stimulated PAP membrane association after 1 h in NRVMs (Figure 4.10A), which was different compared to our results in rat hepatocytes. This could be due to differences in cellular FA uptake since differing ratios of oleate to BSA were used in the experiments with NRVMs (4:1) compared to rat hepatocytes (12:1). BSA has at least three FA binding sites with strong affinity for oleate and two other sites with lower binding affinities (420-422). However, we did find that there was a two-fold increase in the membrane-associated PAP activity after 4 h treatment with either 0.3 or 1.2 mM oleate (Figure 4.4A). We also found that only 5-10% of the total PAP activity in NRVM in the absence of FA was associated with the membranes compared to 25-30% in rat hepatocytes (Figure 3.6A). This is most probably due to the relative abundance of lipin-2, which is more tightly associated with membranes (292), in the liver compared to the heart (241, 243).

Since membrane-associated PAP activity after oleate stimulation in NRVMs only comprised 20% of total PAP activity after 4 h, it explains why there were no major changes in the rate of glycerolipid synthesis when lipin levels were modified. A reduction in PAP activity by 50% still leaves a significant reservoir of PAP activity to translocate onto membranes. These results further reinforce the hypothesis that cytosolic lipins act as a reservoir of PAP activity, and that the translocation onto ER membranes is regulated such that only a small proportion

of PAP activity is required to fulfill its physiological activity. Although TG synthesis and hydrolysis in the heart is essential for normal FA metabolism (86, 149), it is apparent that low levels of PAP activity are sufficient to support cardiac glycerolipid synthesis (374). However, it remains to be seen if a relatively high abundance of lipins would be required during prolonged periods of high FA flux, e.g. starvation longer than 2-3 days. The *fld* model would not be amenable to testing this premise since the mice are devoid of mature adipose tissue and they do not tolerate prolonged periods of starvation. Alternative models include *fld* mice crossed with aP2-lipin transgenic mice, which overexpress lipin-1 through an adipocyte-specific promoter (aP2-lipin Tg) (278), or a cardiac-specific lipin-1 knockout model.

In conclusion, we have shown that expressions of lipin-1, -2 and -3 are dynamically regulated by the interplay between glucocorticoid-, cAMP- and insulin-dependent signalling in NRVMs. However, physiological changes in cardiac gene expression were not observed after fasting except where there was a compensatory response to lipin-1 deficiency, as seen in *fld* mice. Furthermore, PAP activities were unchanged in 12 h fasted mouse hearts. In fact, the gene expressions of *Lpin1* and *Ppargc1a* as well as the PAP activities were decreased in 24 h fasted hearts. In contrast, hepatic PAP activity was increased in 12 h and 24 h fasted animals, leading to the possibility that cardiac lipin-1 and PGC-1α expressions are differentially regulated compared to the liver. This is possibly due to differences in the expression of putative transcription factors responsible for upregulating these two genes concurrently in the liver versus the heart. Finally, we also demonstrated that glycerolipid synthesis in the heart can be sustained by

the reservoir of PAP activity provided by lipin-2 and -3, even when lipin-1 is depleted or absent as shown in Chapter 5.

CHAPTER 5

THE CONSEQUENCES OF WHOLE BODY LIPIN-1 DEFICIENCY ON

CARDIAC FUNCTION AND METABOLISM

5.1 Introduction

The lipins are bifunctional enzymes involved in glycerolipid synthesis as PAP enzymes and transcriptional co-activators of FAO in combination with PGC-1α and PPARα in the liver (133, 423). Instead of being considered as mutually antagonistic processes, FAO and TG synthesis are now widely viewed as being companion pathways since augmenting TG synthesis increases FAO (148, 149). Also, the rate of FA release from lipolysis can dictate the rate of FAO (86, 87, 89, 187). While many proteins have been identified to contribute to cardiac FA uptake and metabolism (124, 177), relatively little information is available about the role of lipins in the heart. Lipin-1 appears to be the major lipin in the heart because of the apparent absence of PAP activity in the hearts of lipin-1 deficient mice (241). Lipin-1 consists of full-length lipin-1B, the lipin-1A splice variant as well as another splice variant, lipin-1γ, which is expressed mainly in brain (137, 228). Lipin-1B is the predominant isoform in the heart (228).

Since lipins have been shown to play crucial roles in FA and lipid metabolism (100, 229, 238, 243, 268), we hypothesized that lipin-1 deficiency in the heart would severely inhibit TG synthesis and FAO and thereby cardiac function. As mentioned previously, the lipin-1 deficient fatty liver dystrophy (*fld*) mice develop transient fatty livers and hypertriglyceridemia, which resolve upon weaning (235-237). *Fld* mice are devoid of mature adipose tissue, which is attributed to the role of lipin-1 in inducing PPARγ expression during adipocyte differentiation (268). The *fld* mouse is also insulin resistant and is prone to developing atherosclerosis when fed a high cholesterol/cholate diet (237, 238). In addition, phosphatidate (PA) accumulation in Schwann cells of *fld* mice leads to

demyelination through aberrant ERK1/2 activation, which subsequently causes the development of peripheral neuropathy (239, 240).

Consequently, we determined the expression of various regulators of cardiac metabolism as well as cardiac function *in vivo* and *ex vivo* using transthoracic echocardiography and the perfused working heart system, respectively. Furthermore, the rates of FAO and glycerolipid synthesis were measured in the perfused working hearts.

5.2 Characterization of lipins and PAP and LPP activities in *fld* hearts

Fld mice were identified by their physical appearance resulting from their lipodystrophy, and their lower body weights (Table 5.1) compared to controls. We found no significant differences in serum glucose between 11-week old, 4 h fasted *fld* and control mice (9.8±0.5 mM in controls compared to 9.7±0.3 mM in *fld* mice). We also did not find any significant change in non-esterified fatty acid levels in 19- to 23-week old *fld* and control mice that were deprived of food for 1 h; however, serum TG levels were significantly lower in the *fld* mice compared to controls (Table 5.1).

Table 5.1 Serum profile and blood pressure measurements in 19- to 23-week-old *fld* (n = 4-8) and control (n = 5-9) mice after food was withheld for 1 h. Blood pressure measurements were performed by Brandi Sidlick (Cardiovascular Research Centre, University of Alberta) and serum measurements were carried out by Bernard Kok. This work was published in the Journal of Lipid Research (374).

Measurement	control	*fld*	p-value
Serum non-esterified FA (mM)	0.4±0.1	0.6±0.1	0.3
Serum TG (mM)	1.3±0.1	0.9±0.1	0.01
Systolic blood pressure (mmHg)	141±5	135±5	0.4
Body weight (g)	33.2±1.0	22.2±0.4	3×10^{-9}

As expected, we found no significant mRNA expression of lipin-1A or -1B in *fld* hearts (Figure 5.1A). However, mRNA expressions of lipin-2 and -3 were increased by 40-50% in *fld* hearts (p < 0.03 and 0.004, respectively) (Figure 5.1A) while protein levels of lipin-2 were similar between genotypes (Figure 5.1B, C). Although we could not obtain a successful Western blot for lipin-3, a recent study showed that lipin-3 levels in *fld* hearts are similar to those in wild-type hearts (266).

We then measured PAP activity in *fld* and control mice under optimum conditions using either PA/PC mixed liposomes or PA/Triton X-100 micelles at pH 7.4 or 6.5 (Figure 5.1D). The optimum assay conditions and the lack of stimulation by other divalent cations in *fld* hearts are described in Appendix I. Earlier work (241) showed no significant PAP activity in *fld* hearts using Triton X-100-PA micelles as the substrate and we essentially confirmed this observation

at pH 6.5 or 7.4 (Figure 5.1D). However, a Mg^{2+}-dependent, NEM-sensitive PAP

activity was detected using mixed PA/PC liposomes at both pH 6.5 and 7.4 in the

fld hearts at levels approximately 15-20% of that found in the control hearts

(Figure 5.1D).
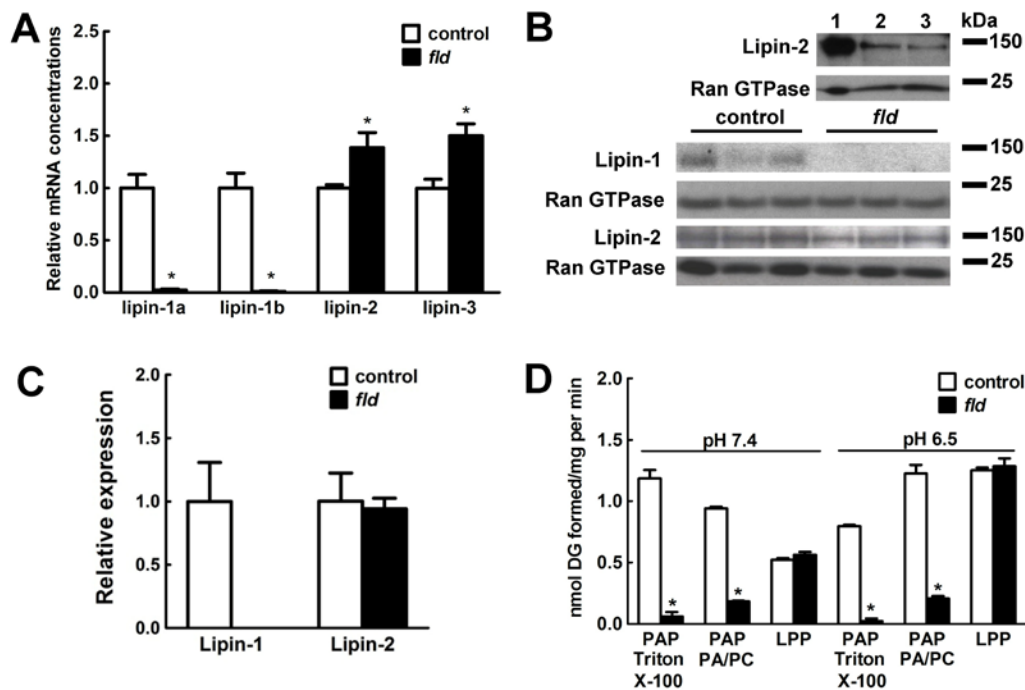
Figure 5.1 Expression and activity of lipins in control and *fld* hearts. (A) mRNA expression of lipins in 11-week-old control (n = 7) and *fld* (n = 8) hearts. **(B)** The lipin-2 antibody was verified by comparing lipin-2 in control (Lane 2) and *fld* (Lane 3) hearts to recombinant lipin-2 protein (Lane 1) (*upper panel*). Ran GTPase serves as the loading control. Representative Western blots showing protein levels of lipin-1 and -2 in control and *fld* hearts with Ran GTPase as the loading control (*lower panel*). **(C)** Densitometric analysis of single Western blots for lipin-1 and -2 in samples from 11-week old *fld* (n=7) and control (n=7) hearts. **(D)** Measurements of PAP activities using 5 mM Mg^{2+} at pH 6.5 and 1.5 mM Mg^{2+} at pH 7.4 with PA/PC liposomes or PA/Triton X-100 micelles together with Mg^{2+}-independent, NEM-insensitive LPP activities in control (n = 3-5) and *fld* (n = 3-5) hearts. The Ran GTPase antibody was kindly provided by Dr. Petra Kienesberger from the laboratory of Dr. Jason Dyck (University of Alberta). All experiments were performed by Bernard Kok and this work was published in the Journal of Lipid Research (374).

This value is similar to the work of Mitra et al. (266) who used ^{32}P-labeled PA presented in Triton X-100 and measured the formation of water-soluble ^{32}P$_i$. However, this method over-estimates PAP activity unless precautions are taken to block phospholipase A type activities, which produce labelled lysophosphatidate and glycerophosphate. These compounds can then be converted to ^{32}P$_i$ by acid or alkaline phosphatases. All of these compounds are extracted into methanol/water rather than chloroform phase and are included in the measurement of "water-soluble" products. We avoided this complication by measuring the formation of [^{3}H]DG from [^{3}H]PA and blocking the degradation of DG with tetrahydrolipstatin. This latter technique provides a valid PAP assay that can be used with tissue homogenates (212).

We conclude that the absence of lipin-1 severely decreases myocardial PAP activity and lipin-2 and -3 contribute only about 15-20% of normal cardiac PAP activity under the most optimum assay conditions we could find. LPP activities, which are thought not to participate in TG synthesis (424), were similar in *fld* and control hearts (Figure 5.1D).

5.3 Decreased cardiac function in *fld* mice *in vivo*

Having demonstrated that there was a significant decrease in PAP activity in *fld* hearts, we next determined if cardiac function was affected *in vivo*. Non-invasive transthoracic echocardiography was used to evaluate cardiac function in 19- to 23-week-old *fld* and control mice. The *fld* mice had significantly decreased systolic function as indicated by reduced ejection fraction and fractional shortening (Table 5.2). This corresponded with decreased end-diastolic left

ventricular internal diameter measurements (Table 5.2). Stroke volume and cardiac output, and measurements of pulmonary peak venous flows were also drastically decreased in *fld* hearts (Table 5.2). We also determined cardiac function in 10-week-old *fld* and control mice and found similar results (Table 5.2).

Heart sizes and tibia lengths of *fld* mice at 10 weeks of age were not significantly different compared to age-matched control mice (Table 5.2). However, these parameters were significantly lower in 19- to 23-week old *fld* mice compared to corresponding control mice (Table 5.2). This suggests that the cardiac dysfunction did not lead to compensatory hypertrophy and instead, it resulted in a loss of heart mass. Systolic blood pressure was similar between *fld* and control mice (Table 5.1) even though we might expect differences in vascular capacity and demand since *fld* mice are lipodystrophic and smaller in size.

Table 5.2 Measurements of cardiac dimensions and *in vivo* cardiac function analyzed from transthoracic echocardiographies of 19- to 23-week-old *fld* (n = 7) and control (n = 8) mice as well as 10-week-old *fld* (n = 8) and control (n = 7) mice. These studies were performed by Donna Beker and Sandra Kelly (Cardiovascular Research Centre, University of Alberta) and this work was published in the Journal of Lipid Research (374).

Measurement	19- to 23-week-old		10-week-old	
	control	*fld*	control	*fld*
Ejection fraction (%)	45±1	39±3*	52±4	41±3[†]
Fractional shortening (%)	22±1	19±2*	26±2	20±2[†]
Left ventricular internal diameter - diastole (mm)	4.26±0.07	3.83±0.09*	3.99±0.07	3.76±0.04[†]
Left ventricular internal diameter - systole (mm)	3.31±0.07	3.12±0.10	2.93±0.11	3.01±0.07
Heart rate (beats per minute)	410±10	403±15	416±11	437±11
Stroke volume (µl)	45±4	28±2*	36±2	24±2[†]
Cardiac output (ml/min)	19±1	12±1*	14.3±0.9	9.9±0.8[†]
Interventricular septum – diastole (mm)	0.90±0.04	0.85±0.03	0.76±0.01	0.81±0.02
Interventricular septum – systole (mm)	1.17±0.06	1.05±0.04	1.07±0.04	1.03±0.03
Left ventricular posterior wall – diastole (mm)	0.89±0.04	0.88±0.04	0.76±0.03	0.81±0.03
Left ventricular posterior wall – systole (mm)	1.14±0.04	1.08±0.03	1.07±0.06	1.03±0.04
Pulmonary vein s/d ratio	0.5±0.1	0.5±0.1	0.53±0.05	0.84±0.06[†]

Table 5.2 continued

Measurement	19- to 23-week-old		10-week-old	
	control	*fld*	control	*fld*
Pulmonary vein s wave (mm/s)	243±39	138±23*	266±25	276±22
Pulmonary vein d wave (mm/s)	445±35	305±28*	507±40	342±37[†]
Pulmonary vein a wave (mm/s)	157±33	132±16	173±18	219±30
Pulmonary vein a wave duration (ms)	24±2	28±2	15±2	25±3[†]
Tei index [(IVRT+IVCT)/ET]	0.81±0.04	0.86±0.04	0.79±0.05	1.01±0.13
Isovolumic relaxation time (IVRT) (ms)	22±1	26±2*	21±1	25±2
Isovolumic contraction time (IVCT) (ms)	18±2	18±1	18±2	21±3
Ejection time (ET) (ms)	50±2	52±2	50±2	46±2
Heart weight : tibia length ratio (mg/cm)	74±2	63±1[§]	72±2	71±3
Heart weight (mg)	141±4	109±3[§]	134±5	127±3
Tibia length (cm)	1.91±0.01	1.73±0.03*	1.86±0.02	1.80±0.04
Body weight (g)	33.2±1.0	22.2±0.4*	28±1	23±1[†]

*$p < 0.05$ when compared to 19- to 23-week-old control mice, [†]$p < 0.05$ when compared to 10-week-old controls and [§]$p < 0.05$ when compared to age-matched controls as well as both 10-week-old *fld* and control mice.

5.4 Metabolic gene and protein expression profiles in *fld* hearts

To determine if cardiac dysfunction in *fld* mice *in vivo* was linked to changes in FA or glucose metabolism, we analyzed the expression of genes for key metabolic regulators in control and *fld* hearts. We chose to analyze samples from 11-week-old mice to determine if there were any changes in cardiac metabolism in the absence of differences in relative heart size. mRNA levels for PGC-1α and PPARα were increased in *fld* hearts (Figure 5.2A). We further examined expression of PPARα target genes downstream of lipin-1 regulation (100). Indeed, acyl-CoA oxidase-1 (ACOX-1) and CPT-1B gene expression were upregulated. However, gene expressions of CD36 and medium-chain acyl dehydrogenase (MCAD) were similar between *fld* and control hearts (Figure 5.2A). mRNA expression for enzymes in the TG synthesis and lipolysis pathways were also similar between genotypes except for small increases in mRNA expression of GPAT1 and DGAT1 (Figure 5.2B) in *fld* hearts. There were no differences in mRNA expression of CD36, glucose transporter 4 (GLUT4), lipoprotein lipase, acetyl-CoA carboxylase (ACC), pyruvate dehydrogenase kinase 4 and malonyl-CoA decarboxylase, which are known regulators of FA and glucose metabolism (Figure 5.2A and C).
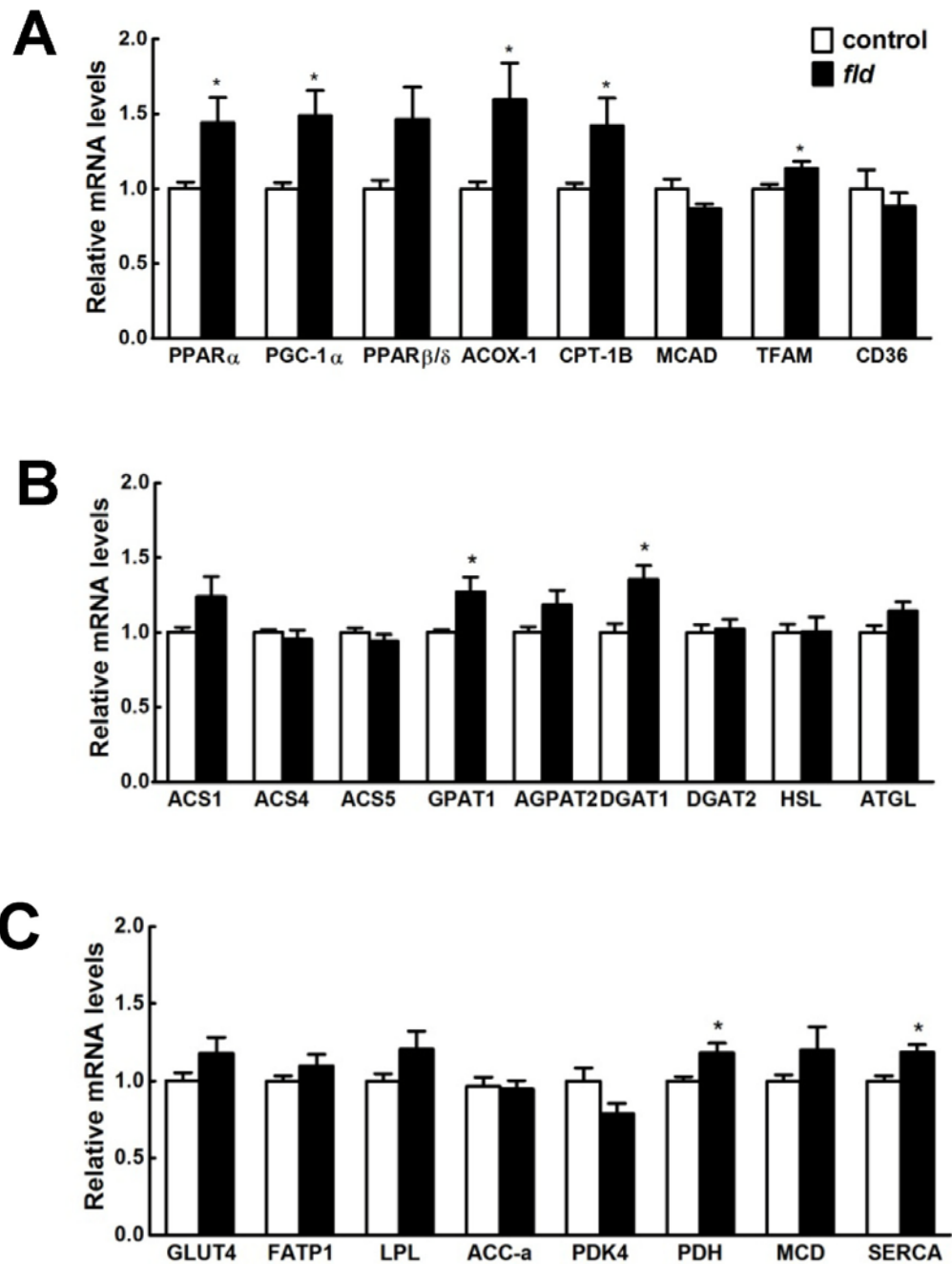
Figure 5.2 mRNA expression for various proteins involved in cardiac metabolism and function. (A) mRNA expression of genes encoding peroxisome proliferator-activated receptor α (PPARα), PPARγ co-activator-1α (PGC-1α), PPARβ/δ, acyl-CoA oxidase 1 (ACOX-1), carnitine palmitoyl transferase-1b (CPT-1B), medium-chain acyl-CoA dehydrogenase (MCAD), mitochondrial transcription factor A (TFAM) and CD36 in 11-week-old *fld* (n = 8-11) and control (n = 7-10) hearts was expressed relative to the housekeeping gene, *Tbp* (TATA-binding protein). Results for *fld* mice were then expressed relative to the control

mice. **(B)** mRNA levels of long chain cyl-CoA synthetase 1 (ACS1), ACS4, ACS5, glycerol 3-phosphate acyltransferase 1 (GPAT1), 1-acylglycerol 3-phosphate O-acyltransferase 2 (AGPAT2), diacylglycerol acyltransferase 1 (DGAT1), DGAT2, hormone-sensitive lipase (HSL) and adipose triacylglycerol lipase (ATGL) were similarly determined. **(C)** The mRNA expression of genes encoding glucose transporter 4 (GLUT4), fatty acid transport protein-1 (FATP1), lipoprotein lipase (LPL), acetyl-CoA carboxylase-a (ACC-a), pyruvate dehydrogenase kinase 4 (PDK4), pyruvate dehydrogenase (PDH), malonyl-CoA decarboxylase (MCD) and sarcoplasmic reticulum Ca^{2+}-ATPase (SERCA) were also measured.
$*p < 0.05$ when compared to controls. All experiments were performed by Bernard Kok.

In addition to profiling gene expression, we determined the protein levels

and phosphorylation states of several important regulators of cardiac metabolism

and function. Expression and phosphorylation of Akt, ACC and AMP-activated

protein kinase (AMPK) were unchanged (Figure 5.3). There were also no

significant changes in FATP1 (fatty acid transport protein 1), GLUT4, ERK1/2 or

SERCA (sarcoplasmic reticulum Ca^{2+}-ATPase) (Figure 5.3), although mRNA

levels of SERCA were slightly increased (Figure 5.2C).
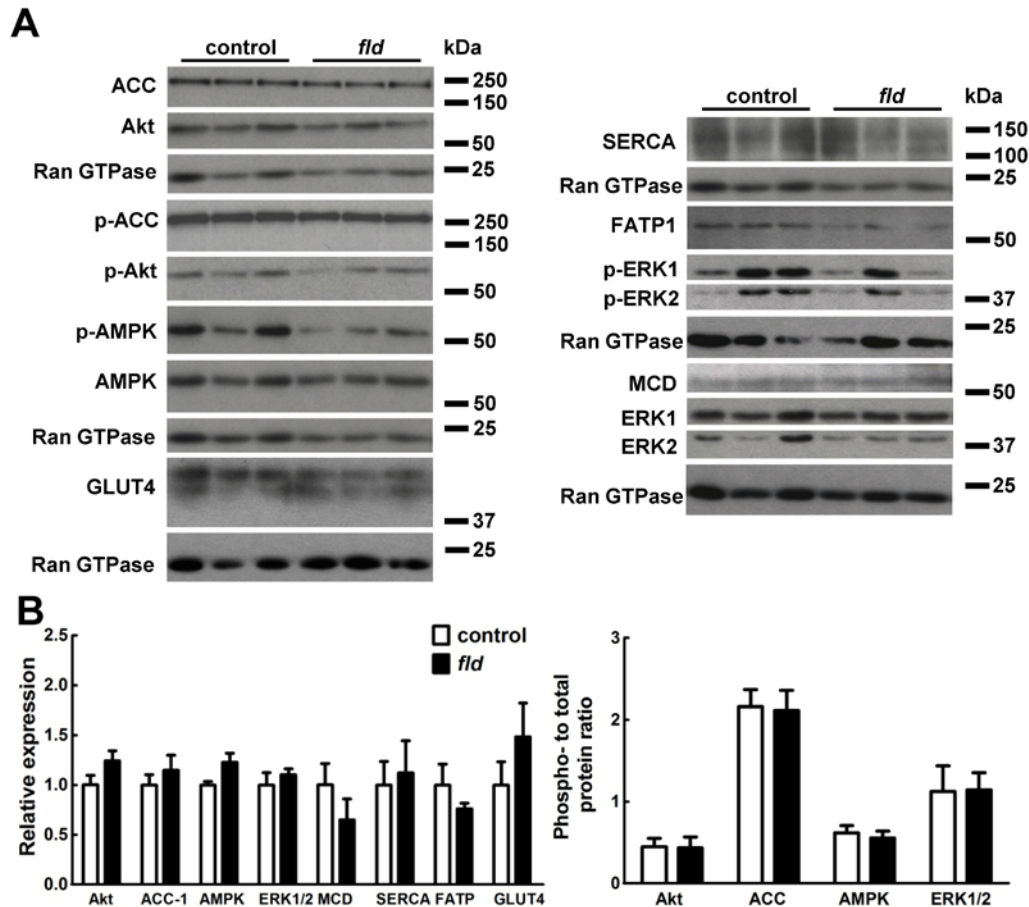
Figure 5.3 Phospho- and endogenous protein levels in *fld* and control hearts. (A) Representative Western blots and **(B)** densitometric analysis of proteins in 11-week old *fld* (n = 6-7) and control (n = 6-7) mouse hearts. Total protein was normalized to Ran GTPase and then expressed relative to control values. Phospho-ERK1/2, phospho-Akt, phospho-ACC and phospho-AMPK were normalized to Ran GTPase and expressed relative to total ERK1/2, Akt, ACC and AMPK, which were also normalized to Ran GTPase. Phospho-ERK1 (long exposure) and ERK2 (short exposure) were from the same blot but shown at two different exposures. Total ERK1 (short exposure) and ERK2 (long exposure) were similarly treated. Abbreviations: ACC, acetyl-CoA carboxylase; Akt, protein kinase B; AMPK, AMP-activated protein kinase; SERCA, sarco/endoplasmic reticulum calcium ATPase; FATP1, fatty acid transport protein 1; ERK1/2, extracellular signal-regulated kinase 1/2. Antibodies were kindly provided by Dr. Petra Kienesberger from the laboratory of Dr. Jason Dyck (University of Alberta). All experiments were performed by Bernard Kok and this work was published in the Journal of Lipid Research (374).

180

Interestingly, both adipose triacylglycerol lipase (ATGL) expression and hormone-sensitive lipase (HSL) phosphorylation at serine 660 were decreased (Figure 5.4A, B), which indicates reduced TG hydrolysis in *fld* hearts. We also observed a decrease in long-chain acyl-CoA synthetase 1 (ACSL1) expression and in the phosphorylation of pyruvate dehydrogenase (PDH) (Figure 5.4A, C). ACSL1 deficiency has been shown to affect the acyl-CoA available for FAO (85) and reduced phosphorylation of PDH leads to its increased activity (425).
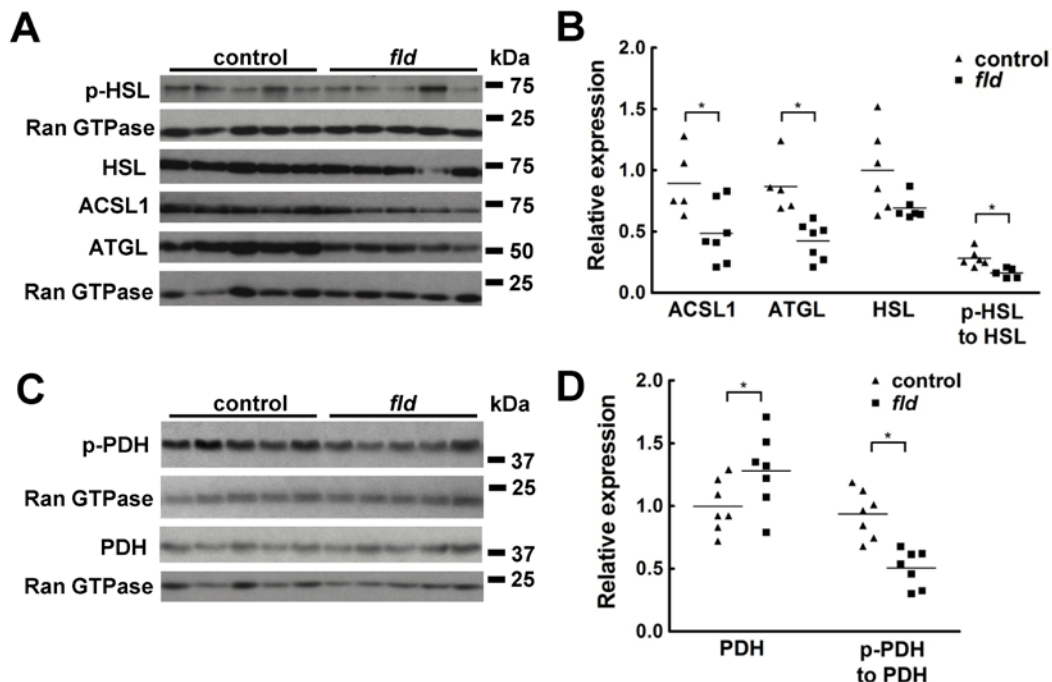
Figure 5.4 Protein expression of enzymes involved in FA metabolism. (A) Representative Western blots of HSL (hormone-sensitive lipase), ACSL1 (acyl-CoA synthetase long chain family member 1) and ATGL (adipose triacylglycerol lipase) as well as **(C)** PDH (pyruvate dehydrogenase) in 11-week old *fld* and control hearts. **(B)** Densitometric analysis of single Western blots for HSL, ACSL1 and ATGL in addition to **(D)** PDH in 11-week old *fld* (n=6-7) and control (n=6-7) hearts. Total ACSL1, ATGL, PDH and HSL were normalized to Ran GTPase and then expressed relative to control values. Phospho-HSL and phospho-PDH were normalized to Ran GTPase and expressed relative to total HSL and PDH, which were also normalized to Ran GTPase. *$p < 0.05$ when compared to controls. Antibodies were kindly provided by Dr. Petra Kienesberger from the laboratory of Dr. Jason Dyck (University of Alberta). All experiments were performed by Bernard Kok and this work was published in the Journal of Lipid Research (374).

5.5 Cardiac function and metabolism in *ex vivo* perfused working hearts of *fld* mice

We next determined the effects of the changes in gene and protein expression profiles on fatty acid and glucose metabolism in perfused working hearts. We used 19- to 23-week old *fld* mice to determine if the smaller heart sizes would further compromise cardiac function and metabolism. We hypothesized that the absence of lipin-1 would decrease TG synthesis and FAO in *fld* hearts, leading to cardiac dysfunction. To address this, we perfused control and *fld* hearts *ex vivo* in the working mode. By using this system, the nutrient supply to the perfused hearts of *fld* and control mice was equalized and differences that result from the changes in hormonal balance in the lipodystrophic *fld* mice *in vivo* were excluded.

Hearts isolated from 19- to 23-week old control and *fld* mice were perfused for 30 min to deplete TG stores as much as possible (88). This was followed by a 30 min perfusion with [^{3}H]oleate and [^{14}C]glucose to determine oleate accumulation in glycerolipids as well as oleate and glucose oxidation. Oleate was used instead of palmitate because numerous studies have shown that palmitate supplementation alone can cause lipotoxicity, which is not observed with oleate (426, 427). Additionally, oleate incorporation into TG is greater than or equal to that for palmitate (426, 428). When we analyzed functional parameters in the *fld* and control hearts, we found that there were no significant differences in contractility and function *ex vivo* (Table 5.3) even though hearts from *fld* mice were significantly smaller than the controls (Table 5.1). This was surprising since we had found cardiac dysfunction *in vivo* (Table 5.2).

Table 5.3 Cardiac function of *ex vivo* perfused hearts from 19- to 23-week-old *fld* (n = 5) and control (n = 5) mice over the 30 min perfusion period with radiolabelled glucose and FA. These studies were performed by Grant Masson from the laboratory of Dr. Jason Dyck (University of Alberta) and the work was published in the Journal of Lipid Research (374).

Measurement	control	*fld*	p-value
Heart rate (beats per min)	342±21	307±31	0.4
Peak systolic pressure (mmHg)	57.9±0.4	60.7±1.8	0.2
Developed pressure (mmHg)	12.9±0.8	13.9±2.7	0.7
Heart rate x peak systolic pressure (x 10^{-3})	20±1	19±2	0.7
Heart rate x developed pressure (x 10^{-3})	4.4±0.4	4.4±1.1	1.0
Cardiac output (ml/min)	10±1	8±1	0.2
Aortic outflow (ml/min)	7±1	5±1	0.2
Cardiac power (mW)	1.03±0.08	0.87±0.16	0.4

We also found no significant differences between control and *fld* hearts in the rates of glucose (Figure 5.5A, *left and middle panels*) and oleate oxidation (Figure 5.6A) when expressed relative to heart dry weight or cardiac power. Glucose incorporation into glycogen was also similar between genotypes (Figure 5.5A, *right panel*). Cardiac glycogen accumulated when both *fld* and control hearts were perfused with FA-free and glucose-containing buffer for 30 min, as expected (Fig 5.5B). The perfusate was switched to oleate- and glucose-containing buffer for another 30 min and we found that cardiac glycogen content was depleted significantly following this period of perfusion, in the control, but not the *fld,* hearts (Figure 5.5C).
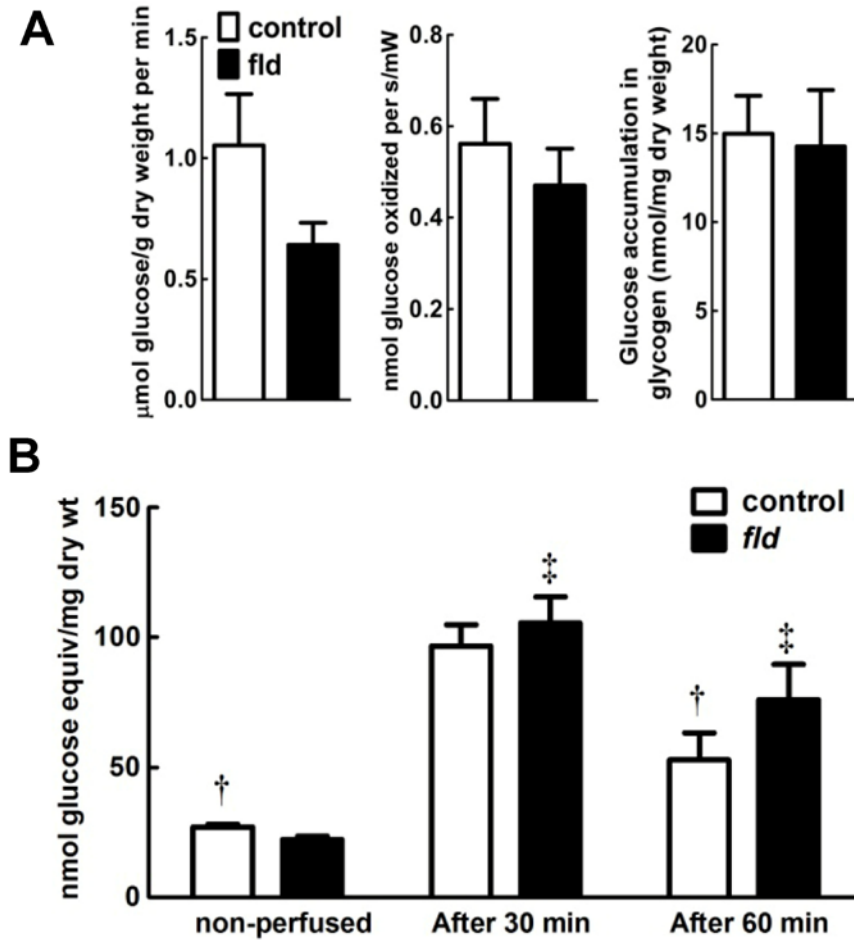
Figure 5.5 Glucose oxidation and incorporation into glycogen in *ex vivo* working perfused *fld* and control hearts. (A) Glucose oxidation expressed per mg of dry heart weight per min (*left panel*) or normalized per second per milliwatt (*middle panel)* in perfused 19- to 23-week old *fld* (n = 5) and control (n = 5) hearts; [14C]glucose incorporation into glycogen was measured in *fld* (n = 5) and control (n = 5) mouse hearts (*right panel*). **(B)** Glycogen content in non-perfused *fld* (n = 5) and control (n = 5) hearts or hearts after 30 min perfusion with glucose-containing and FA-free buffer. Glycogen content after 30 min perfusion with glucose-containing and FA-free buffer followed by another 30 min with glucose- and oleate-containing buffer is also shown. †p < 0.05 when compared to the control hearts perfused for 30 min, and ‡p < 0.05 when compared to the non-perfused *fld* hearts. The perfusions and analysis of glucose oxidation were performed by Grant Masson from the laboratory of Dr. Jason Dyck (University of Alberta). Glycogen measurements and [14C]glucose incorporation into glycogen were carried out by Bernard Kok. This work was published in the Journal of Lipid Research (374).

We also determined cardiac TG content after each perfusion period (Figure 5.6B). TG levels were depleted in control hearts after perfusion with FA-free and glucose-containing buffer after 30 min as expected (Figure 5.6B). However, there was no significant depletion of TG in *fld* hearts. When the perfused hearts were switched to oleate- and glucose-containing buffer for another 30 min, there was no significant change in TG levels at the end of the perfusion for both *fld* and control hearts. This demonstrated that TG turnover was at steady state during this 30 min period (Figure 5.6B). There were no significant differences in the accumulation of [^{3}H]oleate into total glycerolipids or TG in the *fld* hearts compared to controls (Figure 5.6C).
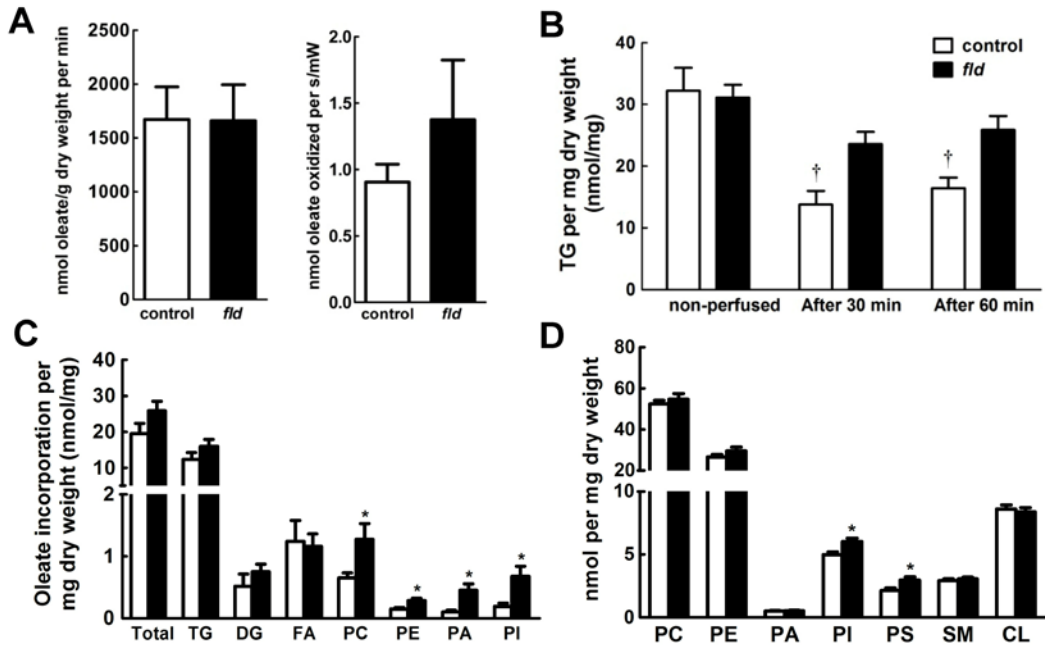
Figure 5.6 Oleate oxidation and accumulation in glycerolipids in *fld* and control hearts. (A) Oleate oxidation is expressed per mg dry heart weight per min (*left panel*) or normalized per second per milliwatt (*right panel*) in 19- to 23-week old *fld* (n = 5) and control (n = 5) hearts after 60 min of perfusion. **(B)** TG content in non-perfused *fld* (n = 7) and control (n = 7) hearts or *fld* (n=5) and control (n=5) hearts after 30 min perfusion with glucose-containing and FA-free buffer, as well as after 30 min perfusion with glucose-containing and FA-free buffer followed by another 30 min with glucose- and oleate-containing buffer. **(C)** [³H]oleate accumulation in glycerolipids extracted from *fld* (n = 5) and control (n = 5) hearts after 60 min of perfusion. **(D)** Phospholipid content in non-perfused *fld* (n = 10) and control (n = 9) hearts. †$p < 0.05$ when compared to the non-perfused control group, and *$p < 0.05$ when compared to controls. The perfusions and analysis of oleate oxidation were performed by Grant Masson from the laboratory of Dr. Jason Dyck (University of Alberta). All other experiments were carried out by Bernard Kok and this work was published in the Journal of Lipid Research (374).

However, oleate accumulation in PC, PE and PI was increased by 1.95-, 1.9- and 3.49-fold, respectively (Figure 5.6C). Consistent with reduced cardiac PAP activity, we found a 4.36-fold increase in the accumulation of oleate in PA in *fld* hearts compared to controls (Figure 5.6C). Moreover, the mass of PI and PS were increased 1.21- and 1.35-fold, respectively, in *fld* hearts compare to controls (Figure 5.6D). The mass of the other major phospholipids, including PA, were not significantly different between groups. The relative composition of different phospholipids in our study was similar to that reported previously (429). As mentioned previously, DG can act as a signaling lipid to decrease insulin signaling through activation of protein kinase C (176). Furthermore, ceramides are another group of lipids known to induce insulin resistance (176). There was no significant difference in the levels of DG and ceramide in *fld* hearts compared to controls (Figure 5.7)
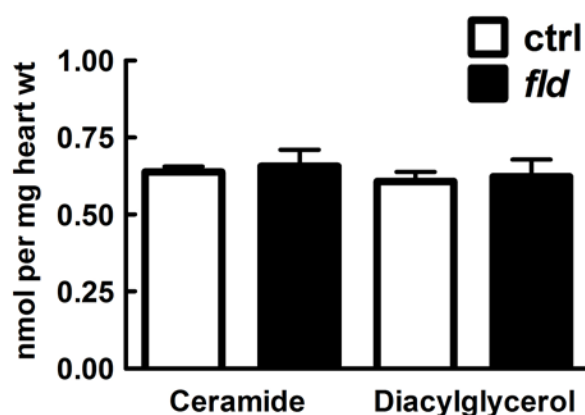
Figure 5.7 Diacylglycerol and ceramide levels in *fld* and control hearts.
Diacylglycerol and ceramide levels were measured in the hearts of 11-week old *fld* (n = 4) and control (n = 4) mice. This work was performed by Jay Dewald in our laboratory.

5.6 Examination of the downstream signalling effects of aberrant phosphatide accumulation

PA accumulation can activate the mTORC1-p70S6 kinase-S6 ribosomal protein signalling cascade (430, 431). As such, we determined whether mTORC1 signalling was increased in the *fld* mice due to aberrant PA metabolism as seen in the perfused *fld* hearts. There was a very marked 14-fold increase in the phosphorylation of S6 ribosomal protein in the *fld* hearts (Figure 5.8C, E, *right panel*). Activation of S6 ribosomal protein occurs downstream of mTOR complex-1 (mTORC1) and p70S6 kinase. Correspondingly, p70S6 kinase phosphorylation in *fld* mice was significantly increased (Figure 5.8B, E, *left panel*), although mTOR phosphorylation was not (Figure 5.8A, E, *left panel*).
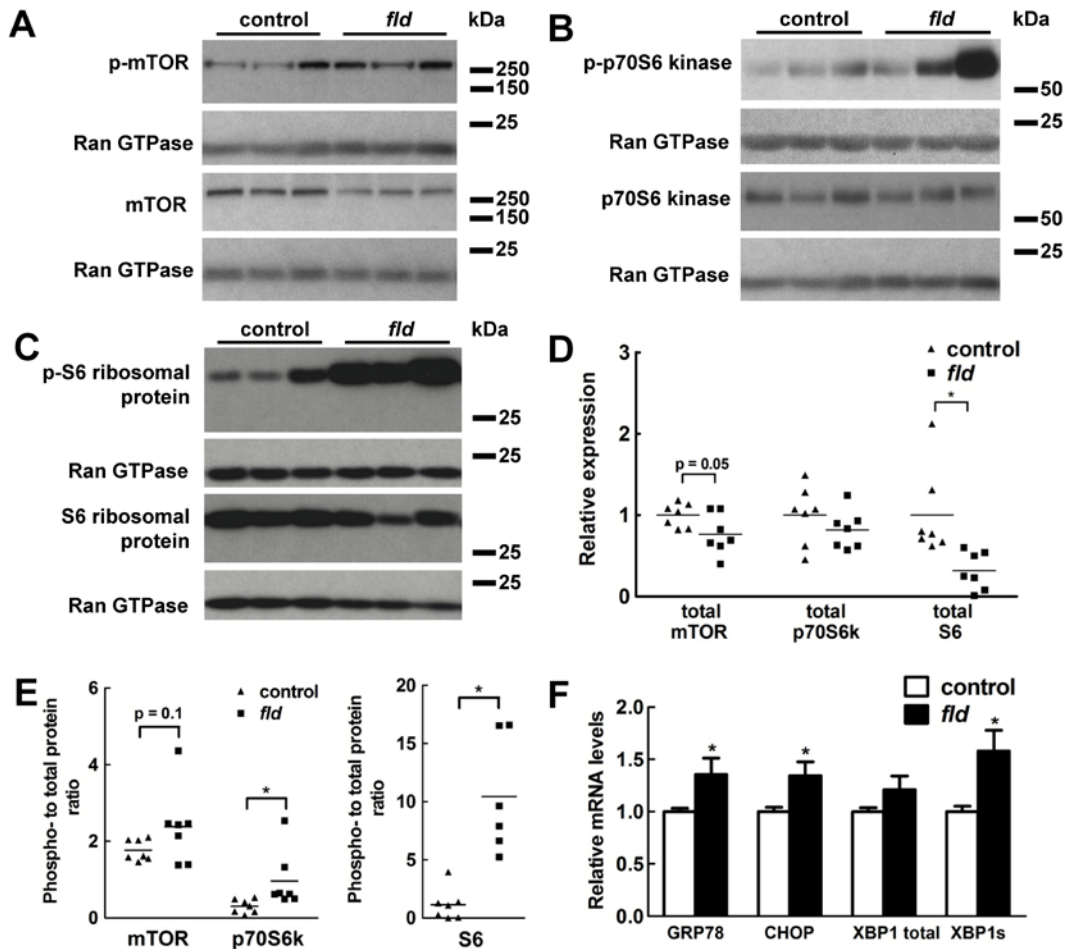
Figure 5.8 mTOR-p70S6 kinase signalling in *fld* and control hearts.
Representative Western blots of **(A)** mTOR, **(B)** p70S6 kinase and **(C)** S6
ribosomal protein in 11-week old *fld* and control hearts. Densitometric analysis of
single Western blots for **(D)** total and **(E)** phosphorylated mTOR, p70S6 kinase
and S6 ribosomal protein in 11-week old *fld* (n=6-7) and control (n=6-7) hearts.
Total mTOR, p70S6 kinase and S6 ribosomal protein was normalized to Ran
GTPase and then expressed relative to control values. Phospho-S6, phospho-
p70S6 kinase and phospho-mTOR were normalized to Ran GTPase and
expressed relative to total S6, p70S6 kinase and mTOR, which were also
normalized to Ran GTPase. *$p < 0.05$ when compared to controls. **(F)** mRNA
expression of proteins involved in endoplasmic reticulum stress response. mRNA
expression in 11-week-old *fld* (n = 8-11) and control (n = 7-10) hearts was
expressed relative to *Tbp* (TATA-binding protein). Results for *fld* mice were then
expressed relative to the control mice. *$p < 0.05$ when compared to controls.
Abbreviations: GRP78, 78 kDa glucose-regulated protein; CHOP,
CCAAT/Enhancer-Binding Protein Homologous Protein; XBP-1, X-box binding
protein 1. Antibodies were kindly provided by Dr. Petra Kienesberger from the
laboratory of Dr. Jason Dyck (University of Alberta). All experiments were
performed by Bernard Kok and this work was published in the Journal of Lipid
Research (374).

Several studies show that activation of the mTORC1 pathway often results in increased protein synthesis, cell enlargement, and eventually, cardiac hypertrophy (432, 433). However, the hearts of 19- to 23-week-old *fld* mice were significantly smaller compared to controls (Table 5.1). mTORC1 activation has also been recently implicated in the upregulation of endoplasmic reticulum (ER) stress (434, 435). Therefore, we determined the gene expression of GRP78 (78 kDa glucose-regulated protein), which is an ER chaperone induced by ER stress, and CHOP (CCAAT/enhancer-binding protein homologous protein), which is a transcription factor mediating ER stress response, and found that they were increased (Figure 5.8F). Moreover, there was an increase in the gene expression of spliced XBP1 (X-box binding protein 1), which is highly indicative of ER stress (Figure 5.8F) (436). Increased ER stress signalling associated with aberrant mTORC1 activation through phosphatidate signalling could explain why the *fld* hearts became smaller at 19- to 23-weeks of age.

5.7 Discussion

Lipin-1 is a unique protein with dual functions in promoting FA esterification and FAO (133). During starvation and diabetes, the combined effects of glucocorticoids and cAMP increase *Lpin1* gene transcription and thus PAP activity in liver (133, 307). This increase, in addition to the translocation of lipin-1 to membranes stimulated by unsaturated FAs, is thought to provide a reservoir that maintains or increases the capacity for FA utilization and storage (133, 241, 294). Furthermore, PAP activity is decreased in the hearts of insulin-resistant JCR:LA corpulent rats (380) and lipin-1 expression is decreased in the ventricles of Zucker diabetic fatty rats and in Type 2 diabetic patients (378). A recent study showed that the regulation of lipin-1 expression in the heart was

dependent on PGC-1α as well as ERRα and ERRγ (266). However, the role of lipin-1 in cardiac metabolism and function had not been systematically determined.

We hypothesized that the dynamic regulation of lipin-1 expression in the heart would be essential for regulating cardiac FA metabolism and function in different physiological and pathological conditions. We expected that complete lipin-1 deficiency would have dramatic effects on myocardial FA esterification and oxidation, resulting in cardiac dysfunction. Indeed, *fld* mice exhibited systolic dysfunction *in vivo*, as determined by non-invasive echocardiography. To determine the effects of lipin-1 deficiency on cardiac metabolism, we first assessed PAP activity in *fld* hearts. We concluded from our assays that *fld* hearts have 15-20% residual PAP activity, which is explained by the expression of lipin-2 and lipin-3 in *fld* hearts.

We chose to use the isolated perfused working heart model to study the metabolic effects of the absence of lipin-1 in the heart alone. This allowed us to determine the consequences for cardiac metabolism and function under a work load using defined conditions in the absence of systemic factors or extraneous signals from the circulatory system. The use of perfused working hearts is also preferable to cultured cardiomyocytes for assessing the role of lipin-1 on FA and glucose metabolism since metabolism is stimulated in a physiologically appropriate manner by the need to perform mechanical work. Surprisingly, cardiac function in the perfused *fld* hearts was not significantly different from the control hearts even though the *fld* hearts were smaller. This suggests that the cardiac dysfunction we observed in *fld* mice *in vivo* may be related to the

systemic changes stemming from global lipin-1 deficiency, which can be described as a combination of the absence of adipose tissue, the corresponding decrease in adipokine secretion, whole-body insulin resistance, aberrant changes in the circadian rhythm of whole-body metabolism (237, 277, 278) and higher workload *in vivo* compared to *ex vivo*. We also found decreased circulating TG levels in *fld* mice (Table 5.1), which could affect the availability of substrate for cardiac work. We only measured serum FA levels after 2 h of food deprivation in the light period and thus, we might not have detected abnormalities in the fluctuation of plasma FA levels occurring during the diurnal cycle of the lipodystrophic *fld* mice, which could also negatively affect cardiac function.

We expected that *fld* hearts would have decreased rates of glucose oxidation because *fld* mice are insulin-resistant (237, 238). The *fld* mice had similar circulating levels of glucose compared to controls, which was also shown in a previous study (237). This latter work also found that *fld* mice are hyperinsulinemic. Interestingly, there was no significant decrease in glucose oxidation and no significant difference in glucose incorporation into glycogen under defined conditions *ex vivo*, suggesting that insulin signaling in the heart is not impaired. However, glycogen depletion in the control hearts was significantly greater than in *fld* hearts when the perfusate was switched to glucose- and oleate-containing buffer. It is likely that upon the reintroduction of FA in the perfusate, glucose uptake and hence glycogen accumulation is decreased more in the controls than *fld* hearts. Glucose utilization from glycogen stores might also be greater in control hearts as compared to *fld* hearts. Furthermore, the levels of DG and ceramide between *fld* and control hearts were not significantly different (Figure 5.7), which again suggests that insulin signaling in the heart is not

impaired since increased levels of DG and ceramide have been shown to induce insulin resistance (176). Thus, insulin resistance in the *fld* mice is not reflective of the ability of the *fld* hearts to respond to insulin and most likely is a result of the impaired glucose uptake in other tissues such as skeletal muscle and the liver. Most importantly, FAO was not different in isolated perfused *fld* hearts when compared to the controls, suggesting that cardiac lipin-1 expression is not essential for maintaining myocardial FAO. Consistent with unchanged glucose and fatty acid utilization, gene and protein expression of several key proteins involved in regulating glucose and FA metabolism were similar between *fld* and control hearts.

Since fasting-induced expression of PPARα and its target genes in liver is ablated by knocking down lipin-1 expression (100), we determined the effect of lipin-1 deficiency on the transcriptional regulation of PPARα in the heart. We found transcriptional upregulation of PPARα in the *fld* hearts in addition to increased gene expression of the PPARα downstream targets, ACOX-1 and CPT-1, while mRNA expression of other PPARα target genes was unchanged. We had also determined the effect of a 12 h fast on *Ppara* gene expression in *fld* and control hearts and found that *Ppara* transcript levels were unchanged compared to fed *fld* and control hearts (Figure 4.5). Significantly, the gene expression of PPARα in the heart had been previously shown to remain unchanged in the starved state (394, 395).

The importance of PPARα in regulating FA metabolism is clear from all the studies using cardiac-specific overexpression or knockout mice (23, 89, 102,

195

114). However, it is likely that the extent of ligand-activated PPARα is more important in the regulation of genes involved in FA uptake and oxidation rather than the transcriptional upregulation of the gene encoding PPARα itself. Thus, the increase in *Ppargc1a, Ppara, Acox1*, and *Cpt1b* expression in the *fld* mice could be attributed to a compensatory response in the absence of lipin-1. Furthermore, there was increased activation of PDH in the 4 h fasted *fld* mice compared to controls as shown by the decrease in phosphorylated PDH, which suggests that glucose utilization is higher in the *fld* mice at this stage. This result reflects the inability of the *fld* mice to utilize FAs to the same extent as control mice in the fasted state (437). Overall, our results demonstrate that the absence of lipin-1 in the heart does not overtly affect cardiac FAO and glucose metabolism when assessed *ex vivo*. It is likely that the changes in cardiac function and metabolic profiling *in vivo* are attributable to the effects of global lipin-1 deficiency, as previously mentioned.

The initial concentrations of TG in perfused hearts of *fld* and control mice were similar. Considerable lipolysis took place in the control hearts during the 30 min incubation in glucose-containing buffer in the absence of oleate as was seen from the decrease of about 50% in TG content. However, lipolysis was decreased in hearts of *fld* mice since there was minimal TG depletion when *fld* hearts were perfused with oleate-free buffer. This conclusion is consistent with the decreased levels of both ATGL expression and HSL phosphorylation in the 11-week old *fld* hearts. When the perfused hearts were switched onto oleate- and glucose-containing buffer, we demonstrated that TG levels were constant at the start of this perfusion period compared to the end. This indicates that TG turnover was at steady state during the perfusion with both oleate and glucose (89), unlike

the initial perfusion period with glucose alone. There was no deficiency in the ability of the *fld* hearts to accumulate [³H]oleate in TG. This was surprising since we had hypothesized that TG synthesis would be compromised due to the 80% decrease in PAP activity. This lack of effect of lipin-1 depletion is supported by our experiments with NRVMs in Section 4 showing that knocking down PAP activity by 50% does not change the rate of glycerol or oleate incorporation into glycerolipids. Ultimately, our results with *fld* mice show that complete depletion of lipin-1 does not significantly decrease the capacity of the heart to synthesize TG.

This is probably explained by the residual PAP activity, attributed to lipin-2 and/or lipin-3, in *fld* hearts. Although *fld* hearts express relatively high phosphatidate phosphatase activity from their LPPs, these enzymes probably do not participate in glycerolipid synthesis since their active sites are facing the extracellular space or the lumenal sides of internal membranes (217, 424). By contrast, glycerolipid synthesis occurs on the cytosolic surface of internal organelles. It has been hypothesized that cytosolic PAP activity provides a reservoir of activity that can be recruited to the endoplasmic reticulum in response to the FA load (295, 296). Presumably, the reservoir of lipin-2 and lipin-3 activity in *fld* hearts is sufficient to provide the capacity for relatively normal rates of TG accumulation. Also, the accumulation of oleate in the major phospholipids, PC and PE, was not compromised in *fld* hearts; in fact, there was increased labeling of PC and PE with [³H]oleate in *fld* hearts. This observation might be due to decreased fatty acid remodelling of phospholipids, which occurs rapidly in the heart (428, 438).

We also detected increased [³H]oleate accumulation in PA in the *fld* hearts without observing an increase in total PA mass. The latter analysis of PA mass was performed after completely separating PA from PS and PI by sequential chromatography on silica gel using a basic solvent system followed by an acidic system (351). Presumably, the labeling experiment in perfused hearts identified the pool of PA that is formed de novo by lipin activity, whereas the total PA pool reflects the balance of a variety of enzymes including phospholipase D and diacylglycerol kinase that contribute to PA turnover. Another group has shown that there are increased PA levels in *fld* hearts as analyzed by liquid chromatography/mass spectrometry (266). However, no details of the molecular species of the PA are given and it is unclear whether the authors achieved efficient separation of PA from the other phospholipids, as shown in previous studies (439, 440). This would be essential since we have demonstrated an increase in PS and PI mass in the *fld* hearts.

Our group demonstrated that decreasing PAP activity diverts PA metabolism to CDP-diacylglycerol and acidic phospholipid production (299). This could contribute to the increased labeling of PI and the increase in PI mass that we observed in *fld* hearts. The accumulation of PA, PS and PI in the *fld* hearts could lead to aberrant cell signalling. For example, PA accumulation in peripheral nerves of *fld* mice increases ERK1/2 activation, leading to demyelination (240). We did not observe significant increases in ERK1/2 phosphorylation in the *fld* hearts. However, PA can also activate mTORC1 leading to the downstream activation of p70S6 kinase (430, 431), which phosphorylates and activates S6 ribosomal protein to promote cell growth (430, 431). In fact, activation of mTORC1-p70S6 kinase leads to cardiac hypertrophy (441). We now show that

there is an increase in signalling downstream of mTOR, i.e. increased p70S6 kinase phosphorylation in combination with a 14-fold increase in S6 ribosomal protein activation. However, there was no evidence of cardiac hypertrophy in 11-week-old mice, which is the age at which we first observed cardiac dysfunction. Instead, the 19- to 23-week-old *fld* mice have significantly smaller hearts in the absence of defective FAO.

Although the mTORC1 signalling pathway is classically linked to cell growth, recent studies have shown that mTORC1 activation can also result in the unfolded protein response and endoplasmic reticulum stress (434, 442). There was increased GRP78 and CHOP gene expression as well as *Xbp1* splicing in the *fld* mice, which could be due to mTORC1 activation (435). The increased endoplasmic reticulum stress response in *fld* mice could explain why the hearts became smaller at 19- to 23-weeks of age. Alternatively, mTORC1 has also been implicated in regulating metabolism. Aberrant activation of mTORC1 increases glycolysis and the oxidative arm of the pentose phosphate pathway (443). Although we did not see differences in glucose oxidation, we did find increased PDH activation. Other studies on *fld* mice show changes in energy partitioning *in vivo*, which could aberrantly affect cardiac function (277, 278).

The present work provides a comprehensive assessment of the effects of lipin-1 deficiency in *fld* mice on the work output of the heart *in vivo* and *ex vivo* relative to the use of fatty acids and glucose as fuels. Lipin-1 deficiency lead to cardiac dysfunction in *fld* mice as measured *in vivo*, probably as a consequence of systemic factors stemming from global lipin-1 deficiency such as lipodystrophy, modified hormonal regulation and fuel availability. When these factors were

equalized in the perfused working heart system, there were no significant differences in work output or the use of oleate and glucose for oxidative metabolism. We conclude that TG accumulation in *fld* hearts is similar to controls because of residual PAP activity resulting from lipin-2/3 and reduced TG hydrolysis. Despite this, *fld* hearts displayed increased oleate accumulation in PA, which could be linked to the mTORC1-p70S6 kinase signalling axis. This does not compensate for the development of significantly smaller hearts in the *fld* mice. Instead, aberrant mTORC1 activation could be associated with the development of endoplasmic reticulum stress. The present work provides novel information contributing to the understanding of lipin-1 in the regulation of glycerolipid synthesis, energy partitioning and signalling in the heart.

CHAPTER 6

GENERAL DISCUSSION AND FUTURE DIRECTIONS

The lipins are critical PAP enzymes that catalyze the penultimate step in TG synthesis, which is the conversion of PA to DG (133, 423). As such, lipins can dictate the levels of PA and DG, which are also essential precursors for phospholipid synthesis. PA is converted to CDP-DG by CDP-DG synthase and CDP-DG serves as a substrate for the formation of phosphatidylinositol, phosphatidylglycerol and cardiolipin (206, 207). In contrast, DG is required for the synthesis of phosphatidylcholine and phosphatidylethanolamine (133, 206). Lipin-1 has a second important function since it is involved in the activation of PPARγ and PPARα in the adipose tissue and liver, respectively (100, 228). Furthermore, lipin-1 regulates SREBP signalling in fibroblasts (229) and can activate PPARγ for adipocyte differentiation (230, 268). Lipin-1 and -2 can also modulate inflammatory signaling in adipocytes and macrophages (272-274).

Importantly, the expressions of lipin-1 and -2 in the liver are dynamically regulated with increased transcription and protein expression in the fasted state (100, 243, 307). The increased expression of lipin-1 in hepatocytes is dependent on glucocorticoid- and cAMP-dependent signaling and this upregulation can be blunted by insulin (307). Increased hepatic lipin expression in fasting is believed to act as a compensatory mechanism to accommodate the large influx of FAs into the liver by sequestering FAs into TG and facilitating TG secretion in VLDLs. Furthermore, the use of FAs as a fuel in the liver during fasting is augmented by the upregulation of genes involved in FAO by PPARα in complex with PGC-1α and lipin-1 (100). Thus, increasing evidence suggests that FAO and TG synthesis can occur in concert instead of acting as mutually antagonistic pathways (86, 89, 148, 192). We also demonstrated that lipin-1, lipin-2 and lipin-3 gene expression

in neonatal rat ventricular myocytes are positively regulated by dexamethasone (a synthetic glucocorticoid) and CPT-cAMP (membrane-permeable analogue of cAMP resistant to phosphodiesterases), and this upregulation can be antagonized by insulin signaling (Section 4.2).

Much of the work done to characterize the roles and regulation of lipins was performed in the liver, adipose tissue and macrophages (133, 261, 423) and little was known about the lipins in the heart. We hypothesized that the cardiac lipins would be dynamically regulated in the fed and fasted state, similar to the regulation in the liver. Surprisingly, the regulation of PAP activity during fasting in liver and heart was different with increased PAP activity in the liver and decreased cardiac PAP activity in 24 h fasted mice (Section 4.3). We hypothesize that these differences are due to the differential regulation of PGC-1α gene expression in liver compared to skeletal and cardiac muscle. Miura et al. showed that there are 3 splice variants of the PGC-1α gene, which they labelled PGC-1α-a, PGC-1α-b and PGC-1α-c (385). PGC-1α-b and PGC-1α-c are shorter by four and thirteen amino acids, respectively, at the N-terminus compared to PGC-1α-a (385). Furthermore, PGC-1α-b and PGC-1α-c are functionally similar to full-length PGC-1α-a as measured by a luciferase gene reporter assay (385). Significantly, the authors found that exercise-induced expression of PGC-1α was due to upregulation of mRNA levels encoding PGC-1α-b and PGC-1α-c with no changes in PGC-1α-a (385). This induction is probably mediated through β_2-adrenergic signaling since the β_2-adrenergic receptor agonist, clenbuterol, can induce overall PGC-1α mRNA levels (266, 384, 444), and more specifically, this upregulation is also entirely due to changes in PGC-1α-b and PGC-1α-c gene expression (385).

Conversely, PGC-1α-a is the main isoform in the liver and is the only one out of the three splice variants to be induced by fasting (385). In contrast to the heart, hepatic PGC-1α expression is important in the regulation of gluconeogenesis (382, 383, 403) and VLDL secretion (413). These additional roles of hepatic PGC-1α might explain why the regulation of PGC-1α expression in the liver is different compared to skeletal and cardiac muscle. Importantly, PGC-1α in hepatocytes is strongly induced by the combination of dexamethasone and cAMP analogues or forskolin (307, 382, 403) with CREB playing an important role in the regulation of PGC-1α expression (383). In contrast, treatment with dexamethasone only causes a modest increase in PGC-1α expression in NRVMs while CPT-cAMP has no effect (Section 4.2). Unsurprisingly, hepatic PGC-1α mRNA levels are increased rapidly after an 8 h fast (383) and remain high at 16 h of fasting (307) in mice. On the other hand, we did not find an increase in PGC-1α gene expression in the heart after a 12 h fast and *Ppargc1a* expression as well as *Lpin1* expression was significantly decreased after 24 h of fasting (1000 h to 1000 h the next day) (Section 4.3).

Lipin-1 expression correlates with PGC-1α expression to a high degree in hepatocytes (307) and NRVMs (Section 4.2) as well as the liver (100, 307) and heart (Section 4.3) (266). This is unsurprising because upregulation of lipin-1 expression is dependent on PGC-1α and decreased PGC-1α levels leads to decreased lipin-1 expression (100, 266). Alternatively, tissue-specific transcription factors that concurrently regulate *Lpin1* and *Ppargc1a* gene expression could be responsible for the differences see the heart compared to the liver, as discussed in Chapter 4. Interestingly, Lehman et al. found an

increase in PGC-1α expression in the hearts of 24 h fasted mice (fasting began at 1700 h) (116). It is likely that the timing of the fast during the light/dark cycle could explain the divergence in results because of differences in the physical activity and food intake prior to fasting as well as diurnal variations in PGC-1α expression. Therefore, it is likely that we would see an increase in cardiac lipin-1 expression in fasted mice if we used a more prolonged fasting period or if the mice were placed on the 24 h fast immediately at the end of light cycle.

In summary, the regulation of lipin-1 and PGC-1α gene expression is quite similar between rat hepatocytes and neonatal rat cardiomyocytes whereas PPARα expression is not regulated by dexamethasone, CPT-cAMP or insulin in cardiomyocytes. Unlike rat hepatocytes, lipin-2 and lipin-3 gene expression in rat cardiomyocytes is increased by dexamethasone and CPT-cAMP. However, the cardiac expression of lipins, PGC-1α and PPARα are not induced by fasting whereas hepatic expression of lipin-1, lipin-2, PGC-1α and PPARα are known to be robustly induced by fasting (243, 307, 383, 393). These differences *in vivo* are probably reflective of the relative importance of the master transcriptional regulators dictating the expression of lipin-1, PPARα and PGC-1α in the liver such as TORC2, CREB and FOXO1 (100, 310, 311, 383, 445), compared to the transcriptional regulators in the heart, e.g. NOR-1 and ERRα/γ (266, 309). Importantly, we demonstrated that PPARα expression in cardiomyocytes is not increased after the induction of lipin-1 and PGC-1α expression, unlike in hepatocytes. This result adds to the evidence that PPARα activation, rather than the level of expression, is more important in the heart compared to the liver (86, 102, 396, 397). Further studies will be required to determine whether lipin-2 and -

3 are regulated *in vivo* since the expression of these two lipin isoforms can be induced by dexamethasone and CPT-cAMP in neonatal rat cardiomyocytes.

The regulation of the subcellular localization of the lipins is also an important determinant of function by dictating the extent of association to the endoplasmic reticulum and nucleus (133). Unsaturated FAs and phosphatidate can stimulate the membrane association of lipins (138, 231, 241). Phosphorylation of lipin-1 induced by insulin signaling can increase its cytosolic localization by association with 14-3-3 proteins (229, 232). During fasting, the influx of FA and decreased insulin signaling would promote lipin localization at the endoplasmic reticulum and nucleus, which provides another means of increasing the involvement of lipins in glycerolipid synthesis and FAO. We have also confirmed the regulation of lipin-1 and lipin-2 translocation onto membranes by unsaturated FAs (Section 3.2). In particular, the predominant lipin species associated with membranes were shown to be the faster migrating lipins in Western blots, again suggesting that the less phosphorylated lipins preferentially localize to the membranes.

The translocation of lipins in the *in vitro* system using rat liver microsomal membranes also verifies the hypothesis that membrane surface charge is an important factor in the association of lipins onto membranes. The majority of the negative charges on the membrane surface are probably donated by the exogenously added FAs since acyl-CoA synthetases cannot produce acyl-CoA esters for incorporation into glycerolipids because ATP was not added to the assay. Furthermore, it is likely that the polybasic motif also known as the nuclear localization sequence (NLS) on lipin-1 mediates this interaction (231).

Translocation assays using rat liver microsomal membranes would determine whether unsaturated FAs could stimulate the membrane association of a recombinant lipin-1 mutant lacking the NLS. Overall, the combination of electrostatic interactions between the lipins and the membrane surface and the phosphorylation state of the lipins appear to regulate the extent of lipin interaction with the endoplasmic reticulum membrane.

The presence of the polybasic NLS (nuclear localization sequence) and the phosphorylation state of lipins also control translocation to the nucleus (229, 231). It is unclear whether lipin-2 and -3 can also localize to the nucleus. Although both lipin-2 and -3 possess the NLS motif, they have not been shown to be SUMOylated (276). On the other hand, lipin-2 and -3 also have the transcriptional co-activator motif (LXXIL, where L represents leucine and I represents isoleucine). Moreover, the transcriptional co-activator activity of lipin-2 has been demonstrated using the luciferase gene reporter assay containing PPARα response elements at the promoter region (138). Studies examining the subcellular localization of lipin-2 and -3 could address this hypothesis.

Our preliminary evidence in Section 3.3.2 also suggests that the protein phosphatase-1 catalytic subunit γ isoform (PP1γ) can bind to lipin-1B at the "histidine-valine-arginine-phenylalanine" (HVRF) motif on lipin-1B (Section 3.4). Importantly, mutating this motif from HVRF to HARA (where A is alanine) prevents the binding of the recombinant lipin-1B mutant to PP1γ (Section 3.4). However, this mutation also leads to a loss of PAP catalytic activity. We will determine whether the mutation causes protein misfolding by measuring the

ultraviolet circular dichroism spectrum of the purified wildtype protein compared to the HARA mutant with the help of Matthew Benesch and the laboratory of Dr. Ronald McElhaney. Furthermore, experiments using competing peptides containing the canonical PP1c interacting motif (RVXF, where X represents any amino acid but proline) as well as control peptides in which the interacting motif is mutated to RAXA will determine whether binding of wildtype lipin-1B to PP1γ can be competitively displace by the active, but not the control peptide.

The HVRF motif is conserved in lipin-2 and -3 and would likely bind to PP1 as well. It is unclear whether the interaction between lipin-1B and PP1γ serves as a means of dephosphorylating lipin-1B and enabling translocation to the endoplasmic reticulum and nucleus or to regulate PP1γ function (371). Harris et al. did demonstrate that lipin-1 could be dephosphorylated by purified, recombinant PP1α, suggesting that the interaction of lipin-1 with PP1 would act to facilitate lipin-1 dephosphorylation (241). Translocation experiments using rat liver microsomal membranes would determine whether lipin-1B and PP1γ can co-translocate. We can also assess whether lipin-1B translocation can be augmented by dephosphorylation of lipin-1B by catalytically active PP1γ. PP1 activity assays in the presence of absence of different lipin isoforms will also clarify whether interaction with lipins has any effect on its activity. Conversely, it is unlikely that PP1γ would have any effect on the PAP activity of the lipins since dephosphorylation of lipins does not affect their PAP activities (241), except on unidentified sites phosphorylated by cyclin-dependent kinase 1 (292).

The phosphorylation of lipin-1B by insulin-dependent signaling promotes 14-3-3 interaction (232). We would also ascertain whether interaction of lipin-1B with PP1γ would be abrogated if recombinant 14-3-3 proteins were bound. Plasmids encoding the 14-3-3 isoforms -β and -θ, which are the two 14-3-3 isoforms shown to interact with lipin-1 (232), have been provided as a gift by Dr. Greg Moorhead from the University of Calgary. The oligomerization state of the lipins in the presence of PP1γ and 14-3-3 proteins can also be tested using gel filtration chromatography techniques in collaboration with Tamara Arnold from the laboratory of Dr. Charles Holmes.

The dephosphorylation of lipin-1 or its yeast orthologue is also partly mediated by Dullard phosphatase and its regulatory subunit nuclear envelope phosphatase 1-regulatory subunit 1 (NEP1-R1) (246, 304, 305). Dullard phosphatase and its regulatory subunit are nuclear-localized (304, 305), whereas PP1 subcellular localization is more ubiquitous (446, 447). Therefore, it might be possible that dephosphorylation of lipin-1 to enable entry into the nucleus is mediated by Dullard phosphatase whereas lipin-1 association with the endoplasmic reticulum is dictated by PP1. However, PP1 isoforms are also present in the nucleus (446, 447). One experiment that could determine whether nuclear entry of lipin-1 is predicated on PP1 activity is to test if the lipin-1B HARA mutant can translocate into the nucleus using confocal microscopy when inhibiting mTORC1 activity like the studies performed by Peterson et al. (229). These experiments can only be performed if the lipin-1B HARA mutant is correctly folded, which we will measure by ultraviolet circular dichroism.

Since a major mechanism of lipin action is the regulation of its subcellular localization, these functional studies examining the interaction between lipin-1B and PP1γ could prove to be important in trying to understand how the lipins reach their sites of action. The consequences of the lack of lipin action can be seen in the phenotypes of lipin deficient models and patients, e.g. in the *fld* mice, and patients suffering from rhabdomyolysis or Majeed syndrome with defects in PAP activity because of mutations in lipin-1 and 2, respectively. Surprisingly, the deleterious phenotypes appear to stem from an aberrant accumulation of phosphatidate (PA) and the signaling events downstream of this bioactive lipid, e.g. mTORC1 and ERK1/2 activation (Section 5.5) (230, 240, 266, 271). In contrast, glycerolipid biosynthesis appears to be sustainable even with very low levels of the other lipin isoforms (Section 5.4). Besides mTORC1 and ERK1/2, PA accumulation can also activate other targets such as protein kinase C-ζ, Sos, Raf, phospholipase C-γ, sphingosine kinase-1, and nicotinamide adenine dinucleotide phosphate (NADPH) oxidase (173, 175, 448). Therefore, aberrant PA accumulation and sustained signaling downstream of PA could affect cell proliferation, growth, vesicular trafficking, cytoskeletal rearrangements and stress response. Microarray analysis of cells deficient in lipin isoforms, e.g. adult cardiomyocytes from *fld* mice, could present indications as to which PA-responsive proteins are aberrantly activated in the absence of particular lipin isoforms. This approach could also identify novel proteins regulated by PA. However, there is a possibility of differential regulation of PA-dependent signaling in different cell types as shown by the lack of ERK1/2 activation in *fld* hearts (Section 5.3) compared to the increased activation of ERK1/2 in adipocytes and Schwann cells (230, 240).

Overall, knowledge regarding the roles and regulation of lipins has advanced significantly in the past few years. The importance of lipins in glycerolipid synthesis, adipocyte differentiation, inflammatory signaling and hepatic fatty acid oxidation has been clearly demonstrated (133, 261, 423). The majority of the work in this thesis concentrated on lipins in the heart, in particular lipin-1, since little work had been done to characterize the functions and regulation of the cardiac lipins. We have demonstrated the regulation of lipin expression in cardiomyocytes by glucocorticoids, insulin and cAMP. Furthermore, we provide evidence that the regulation of lipin-1 expression in the fed and fasted state coincides with the gene expression of PGC-1α. We also show that the membrane association of lipin-1 and -2 can be promoted by unsaturated FAs and that dephosphorylation of the lipins could be mediated by direct interaction with PP1. Finally, glycerolipid synthesis in cardiomyocytes and *ex vivo* perfused working hearts can be sustained by the low levels of lipin-2 and -3 when lipin-1 expression is diminished or completely absent, respectively. Instead, there is an abnormal accumulation of phosphatidate as well as an increase in the activation of mTORC1 signaling and the cellular stress response in the lipin-1 deficient *fld* hearts. Future studies examining the interaction of lipin-1B with PP1γ will provide novel results with regards to the regulation of subcellular localization of the lipins, and subsequently, their physiological actions. The complexity of this regulation is highlighted by the potential interplay between insulin-dependent mTORC1 phosphorylation, 14-3-3 binding and sequestration as well as the interaction of PP1 and Dullard phosphatase when stimulatory signals, such as the influx of unsaturated FAs, promote membrane association.

Bibliography

1.   Lopaschuk, G. D., J. R. Ussher, C. D. Folmes, J. S. Jaswal, and W. C. Stanley. 2010. Myocardial fatty acid metabolism in health and disease. *Physiol. Rev.* **90**: 207-258.

2.   Neely, J. R., and H. E. Morgan. 1974. Relationship between carbohydrate and lipid metabolism and the energy balance of heart muscle. *Annu. Rev. Physiol.* **36**: 413-459.

3.   Randle, P. J., P. B. Garland, E. A. Newsholme, and C. N. Hales. 1965. The glucose fatty acid cycle in obesity and maturity onset diabetes mellitus. *Ann. N. Y. Acad. Sci.* **131**: 324-333.

4.   Randle, P. J., P. B. Garland, C. N. Hales, and E. A. Newsholme. 1963. The glucose fatty-acid cycle. Its role in insulin sensitivity and the metabolic disturbances of diabetes mellitus. *Lancet* **1**: 785-789.

5.   McGarry, J. D., G. P. Mannaerts, and D. W. Foster. 1977. A possible role for malonyl-CoA in the regulation of hepatic fatty acid oxidation and ketogenesis. *J. Clin. Invest.* **60**: 265-270.

6.   McGarry, J. D., G. F. Leatherman, and D. W. Foster. 1978. Carnitine palmitoyltransferase I. The site of inhibition of hepatic fatty acid oxidation by malonyl-CoA. *J. Biol. Chem.* **253**: 4128-4136.

7.   Dyck, J. R., J. F. Cheng, W. C. Stanley, R. Barr, M. P. Chandler, S. Brown, D. Wallace, T. Arrhenius, C. Harmon, G. Yang, A. M. Nadzan, and G. D. Lopaschuk. 2004. Malonyl coenzyme a decarboxylase inhibition protects the ischemic heart by inhibiting fatty acid oxidation and stimulating glucose oxidation. *Circ. Res.* **94**: e78-84.

8.   Saddik, M., J. Gamble, L. A. Witters, and G. D. Lopaschuk. 1993. Acetyl-CoA carboxylase regulation of fatty acid oxidation in the heart. *J. Biol. Chem.* **268**: 25836-25845.

9.   Awan, M. M., and E. D. Saggerson. 1993. Malonyl-CoA metabolism in cardiac myocytes and its relevance to the control of fatty acid oxidation. *Biochem. J.* **295 (Pt 1)**: 61-66.

10.   Lopaschuk, G. D., M. A. Spafford, N. J. Davies, and S. R. Wall. 1990. Glucose and palmitate oxidation in isolated working rat hearts reperfused after a period of transient global ischemia. *Circ. Res.* **66**: 546-553.

11.   Liu, Q., J. C. Docherty, J. C. Rendell, A. S. Clanachan, and G. D. Lopaschuk. 2002. High levels of fatty acids delay the recovery of intracellular pH and cardiac efficiency in post-ischemic hearts by inhibiting glucose oxidation. *J. Am. Coll. Cardiol.* **39**: 718-725.

12.   Newsholme, E. A., P. J. Randle, and K. L. Manchester. 1962. Inhibition of the phosphofructokinase reaction in perfused rat heart by respiration of ketone bodies, fatty acids and pyruvate. *Nature* **193**: 270-271.

13.   Garland, P. B., P. J. Randle, and E. A. Newsholme. 1963. Citrate as an Intermediary in the Inhibition of Phosphofructokinase in Rat Heart Muscle by Fatty Acids, Ketone Bodies, Pyruvate, Diabetes, and Starvation. *Nature* **200**: 169-170.

14.   Kerbey, A. L., P. J. Randle, R. H. Cooper, S. Whitehouse, H. T. Pask, and R. M. Denton. 1976. Regulation of pyruvate dehydrogenase in rat heart. Mechanism of regulation of proportions of dephosphorylated and phosphorylated enzyme by oxidation of fatty acids and ketone bodies and of effects of diabetes: role of coenzyme A, acetyl-coenzyme A and reduced and oxidized nicotinamide-adenine dinucleotide. *Biochem. J.* **154**: 327-348.

15.   Denton, R. M., P. J. Randle, B. J. Bridges, R. H. Cooper, A. L. Kerbey, H. T. Pask, D. L. Severson, D. Stansbie, and S. Whitehouse. 1975. Regulation of mammalian pyruvate dehydrogenase. *Mol. Cell. Biochem.* **9**: 27-53.

16.   Lysiak, W., P. P. Toth, C. H. Suelter, and L. L. Bieber. 1986. Quantitation of the efflux of acylcarnitines from rat heart, brain, and liver mitochondria. *J. Biol. Chem.* **261**: 13698-13703.

17.   Paulson, D. J., K. M. Ward, and A. L. Shug. 1984. Malonyl CoA inhibition of carnitine palmityltransferase in rat heart mitochondria. *FEBS Lett.* **176**: 381-384.

18.   Broderick, T. L., G. Panagakis, D. DiDomenico, J. Gamble, G. D. Lopaschuk, A. L. Shug, and D. J. Paulson. 1995. L-carnitine improvement of cardiac function is associated with a stimulation in glucose but not fatty acid metabolism in carnitine-deficient hearts. *Cardiovasc. Res.* **30**: 815-820.

19.   Dyck, J. R., T. A. Hopkins, S. Bonnet, E. D. Michelakis, M. E. Young, M. Watanabe, Y. Kawase, K. Jishage, and G. D. Lopaschuk. 2006. Absence of malonyl coenzyme A decarboxylase in mice increases cardiac glucose oxidation and protects the heart from ischemic injury. *Circulation* **114**: 1721-1728.

20.   Sakamoto, J., R. L. Barr, K. M. Kavanagh, and G. D. Lopaschuk. 2000. Contribution of malonyl-CoA decarboxylase to the high fatty acid oxidation rates seen in the diabetic heart. *Am J Physiol Heart Circ Physiol* **278**: H1196-1204.

21.   Young, M. E., G. W. Goodwin, J. Ying, P. Guthrie, C. R. Wilson, F. A. Laws, and H. Taegtmeyer. 2001. Regulation of cardiac and skeletal muscle malonyl-CoA decarboxylase by fatty acids. *Am J Physiol Endocrinol Metab* **280**: E471-479.

22.   Lee, G. Y., N. H. Kim, Z. S. Zhao, B. S. Cha, and Y. S. Kim. 2004. Peroxisomal-proliferator-activated receptor alpha activates transcription of the rat hepatic malonyl-CoA decarboxylase gene: a key regulation of malonyl-CoA level. *Biochem. J.* **378**: 983-990.

23.   Campbell, F. M., R. Kozak, A. Wagner, J. Y. Altarejos, J. R. Dyck, D. D. Belke, D. L. Severson, D. P. Kelly, and G. D. Lopaschuk. 2002. A role for peroxisome proliferator-activated receptor alpha (PPARalpha) in the control of cardiac malonyl-CoA levels: reduced fatty acid oxidation rates and increased glucose oxidation rates in the hearts of mice lacking PPARalpha are associated with higher concentrations of malonyl-CoA and reduced expression of malonyl-CoA decarboxylase. *J. Biol. Chem.* **277**: 4098-4103.

24.   Kudo, N., J. G. Gillespie, L. Kung, L. A. Witters, R. Schulz, A. S. Clanachan, and G. D. Lopaschuk. 1996. Characterization of 5'AMP-activated protein kinase activity in the heart and its role in inhibiting acetyl-CoA carboxylase during reperfusion following ischemia. *Biochim. Biophys. Acta* **1301**: 67-75.

25.   Dyck, J. R., N. Kudo, A. J. Barr, S. P. Davies, D. G. Hardie, and G. D. Lopaschuk. 1999. Phosphorylation control of cardiac acetyl-CoA carboxylase by cAMP-dependent protein kinase and 5'-AMP activated protein kinase. *Eur. J. Biochem.* **262**: 184-190.

26.   Cornier, M.-A., D. Dabelea, T. L. Hernandez, R. C. Lindstrom, A. J. Steig, N. R. Stob, R. E. Van Pelt, H. Wang, and R. H. Eckel. 2008. The Metabolic Syndrome. *Endocr. Rev.* **29**: 777-822.

27.   Moller, D. E., and K. D. Kaufman. 2005. Metabolic syndrome: a clinical and molecular perspective. *Annu. Rev. Med.* **56**: 45-62.

28.   Ford, E. S., U. A. Ajani, J. B. Croft, J. A. Critchley, D. R. Labarthe, T. E. Kottke, W. H. Giles, and S. Capewell. 2007. Explaining the decrease in U.S. deaths from coronary disease, 1980-2000. *N. Engl. J. Med.* **356**: 2388-2398.

29.   Brophy, J. M. 1997. The epidemiology of acute myocardial infarction and ischemic heart disease in Canada: data from 1976 to 1991. *Can. J. Cardiol.* **13**: 474-478.

30.   Shaw, J. E., R. A. Sicree, and P. Z. Zimmet. 2010. Global estimates of the prevalence of diabetes for 2010 and 2030. *Diabetes Res. Clin. Pract.* **87**: 4-14.

31.   Danaei, G., M. M. Finucane, Y. Lu, G. M. Singh, M. J. Cowan, C. J. Paciorek, J. K. Lin, F. Farzadfar, Y. H. Khang, G. A. Stevens, M. Rao, M. K. Ali, L. M. Riley, C. A. Robinson, and M. Ezzati. 2011. National, regional, and global trends in fasting plasma glucose and diabetes prevalence since 1980: systematic analysis of health examination surveys and epidemiological studies with 370 country-years and 2.7 million participants. *Lancet* **378**: 31-40.

32.   Pieske, B., and R. Wachter. 2008. Impact of diabetes and hypertension on the heart. *Curr. Opin. Cardiol.* **23**: 340-349.

33.   Aneja, A., W. H. Tang, S. Bansilal, M. J. Garcia, and M. E. Farkouh. 2008. Diabetic cardiomyopathy: insights into pathogenesis, diagnostic challenges, and therapeutic options. *Am. J. Med.* **121**: 748-757.

34.   An, D., and B. Rodrigues. 2006. Role of changes in cardiac metabolism in development of diabetic cardiomyopathy. *Am J Physiol Heart Circ Physiol* **291**: H1489-1506.

35.   Fox, C. S., S. Coady, P. D. Sorlie, R. B. D'Agostino, Sr., M. J. Pencina, R. S. Vasan, J. B. Meigs, D. Levy, and P. J. Savage. 2007. Increasing cardiovascular disease burden due to diabetes mellitus: the Framingham Heart Study. *Circulation* **115**: 1544-1550.

36.   Carley, A. N., and D. L. Severson. 2005. Fatty acid metabolism is enhanced in type 2 diabetic hearts. *Biochim. Biophys. Acta* **1734**: 112-126.

37.   Longnus, S. L., R. B. Wambolt, R. L. Barr, G. D. Lopaschuk, and M. F. Allard. 2001. Regulation of myocardial fatty acid oxidation by substrate supply. *Am J Physiol Heart Circ Physiol* **281**: H1561-1567.

38.   Bharadwaj, K. G., Y. Hiyama, Y. Hu, L. A. Huggins, R. Ramakrishnan, N. A. Abumrad, G. I. Shulman, W. S. Blaner, and I. J. Goldberg. 2010. Chylomicron- and VLDL-derived lipids enter the heart through different pathways: in vivo evidence for receptor- and non-receptor-mediated fatty acid uptake. *J. Biol. Chem.* **285**: 37976-37986.

39. Hussain, M. M., R. K. Kancha, Z. Zhou, J. Luchoomun, H. Zu, and A. Bakillah. 1996. Chylomicron assembly and catabolism: role of apolipoproteins and receptors. *Biochim. Biophys. Acta* **1300**: 151-170.

40. Nakajima, K., T. Nakano, Y. Tokita, T. Nagamine, A. Inazu, J. Kobayashi, H. Mabuchi, K. L. Stanhope, P. J. Havel, M. Okazaki, M. Ai, and A. Tanaka. 2011. Postprandial lipoprotein metabolism: VLDL vs chylomicrons. *Clin. Chim. Acta* **412**: 1306-1318.

41. Havel, R. J. 1958. Transport and metabolism of chylomicra. *Am. J. Clin. Nutr.* **6**: 662-668.

42. Skipski, V. P., M. Barclay, R. K. Barclay, V. A. Fetzer, J. J. Good, and F. M. Archibald. 1967. Lipid composition of human serum lipoproteins. *Biochem. J.* **104**: 340-352.

43. Heath, R. B., F. Karpe, R. W. Milne, G. C. Burdge, S. A. Wootton, and K. N. Frayn. 2003. Selective partitioning of dietary fatty acids into the VLDL TG pool in the early postprandial period. *J. Lipid Res.* **44**: 2065-2072.

44. Augustus, A., H. Yagyu, G. Haemmerle, A. Bensadoun, R. K. Vikramadithyan, S. Y. Park, J. K. Kim, R. Zechner, and I. J. Goldberg. 2004. Cardiac-specific knock-out of lipoprotein lipase alters plasma lipoprotein triglyceride metabolism and cardiac gene expression. *J. Biol. Chem.* **279**: 25050-25057.

45. Pillutla, P., Y. C. Hwang, A. Augustus, M. Yokoyama, H. Yagyu, T. P. Johnston, M. Kaneko, R. Ramasamy, and I. J. Goldberg. 2005. Perfusion of hearts with triglyceride-rich particles reproduces the metabolic abnormalities in lipotoxic cardiomyopathy. *Am J Physiol Endocrinol Metab* **288**: E1229-1235.

46. Preiss-Landl, K., R. Zimmermann, G. Hammerle, and R. Zechner. 2002. Lipoprotein lipase: the regulation of tissue specific expression and its role in lipid and energy metabolism. *Curr. Opin. Lipidol.* **13**: 471-481.

47. Davies, B. S., A. P. Beigneux, R. H. Barnes, 2nd, Y. Tu, P. Gin, M. M. Weinstein, C. Nobumori, R. Nyren, I. Goldberg, G. Olivecrona, A. Bensadoun, S. G. Young, and L. G. Fong. 2010. GPIHBP1 is responsible for the entry of lipoprotein lipase into capillaries. *Cell Metab.* **12**: 42-52.

48. Beigneux, A. P., B. S. Davies, S. Tat, J. Chen, P. Gin, C. V. Voss, M. M. Weinstein, A. Bensadoun, C. R. Pullinger, L. G. Fong, and S. G. Young. 2011. Assessing the role of the glycosylphosphatidylinositol-anchored high density lipoprotein-binding protein 1 (GPIHBP1) three-finger domain in binding lipoprotein lipase. *J. Biol. Chem.* **286**: 19735-19743.

49. Franssen, R., S. G. Young, F. Peelman, J. Hertecant, J. A. Sierts, A. W. Schimmel, A. Bensadoun, J. J. Kastelein, L. G. Fong, G. M. Dallinga-Thie, and A. P. Beigneux. 2010. Chylomicronemia with low postheparin lipoprotein lipase levels in the setting of GPIHBP1 defects. *Circ Cardiovasc Genet* **3**: 169-178.

50. Yagyu, H., G. Chen, M. Yokoyama, K. Hirata, A. Augustus, Y. Kako, T. Seo, Y. Hu, E. P. Lutz, M. Merkel, A. Bensadoun, S. Homma, and I. J. Goldberg. 2003. Lipoprotein lipase (LpL) on the surface of cardiomyocytes increases lipid uptake and produces a cardiomyopathy. *J. Clin. Invest.* **111**: 419-426.

51.   Yagyu, H., E. P. Lutz, Y. Kako, S. Marks, Y. Hu, S. Y. Choi, A. Bensadoun, and I. J. Goldberg. 2002. Very low density lipoprotein (VLDL) receptor-deficient mice have reduced lipoprotein lipase activity. Possible causes of hypertriglyceridemia and reduced body mass with VLDL receptor deficiency. *J. Biol. Chem.* **277**: 10037-10043.

52.   Obunike, J. C., E. P. Lutz, Z. Li, L. Paka, T. Katopodis, D. K. Strickland, K. F. Kozarsky, S. Pillarisetti, and I. J. Goldberg. 2001. Transcytosis of lipoprotein lipase across cultured endothelial cells requires both heparan sulfate proteoglycans and the very low density lipoprotein receptor. *J. Biol. Chem.* **276**: 8934-8941.

53.   Goudriaan, J. R., S. M. Espirito Santo, P. J. Voshol, B. Teusink, K. W. van Dijk, B. J. van Vlijmen, J. A. Romijn, L. M. Havekes, and P. C. Rensen. 2004. The VLDL receptor plays a major role in chylomicron metabolism by enhancing LPL-mediated triglyceride hydrolysis. *J. Lipid Res.* **45**: 1475-1481.

54.   Ibrahimi, A., and N. A. Abumrad. 2002. Role of CD36 in membrane transport of long-chain fatty acids. *Curr Opin Clin Nutr Metab Care* **5**: 139-145.

55.   Brinkmann, J. F., N. A. Abumrad, A. Ibrahimi, G. J. van der Vusse, and J. F. Glatz. 2002. New insights into long-chain fatty acid uptake by heart muscle: a crucial role for fatty acid translocase/CD36. *Biochem. J.* **367**: 561-570.

56.   Luiken, J. J., A. Bonen, and J. F. Glatz. 2002. Cellular fatty acid uptake is acutely regulated by membrane-associated fatty acid-binding proteins. *Prostaglandins Leukot. Essent. Fatty Acids* **67**: 73-78.

57.   Gimeno, R. E., A. M. Ortegon, S. Patel, S. Punreddy, P. Ge, Y. Sun, H. F. Lodish, and A. Stahl. 2003. Characterization of a heart-specific fatty acid transport protein. *J. Biol. Chem.* **278**: 16039-16044.

58.   Glatz, J. F., J. J. Luiken, and A. Bonen. 2001. Involvement of membrane-associated proteins in the acute regulation of cellular fatty acid uptake. *J. Mol. Neurosci.* **16**: 123-132; discussion 151-127.

59.   Luiken, J. J., D. P. Koonen, J. Willems, A. Zorzano, C. Becker, Y. Fischer, N. N. Tandon, G. J. Van Der Vusse, A. Bonen, and J. F. Glatz. 2002. Insulin stimulates long-chain fatty acid utilization by rat cardiac myocytes through cellular redistribution of FAT/CD36. *Diabetes* **51**: 3113-3119.

60.   Chiu, H. C., A. Kovacs, R. M. Blanton, X. Han, M. Courtois, C. J. Weinheimer, K. A. Yamada, S. Brunet, H. Xu, J. M. Nerbonne, M. J. Welch, N. M. Fettig, T. L. Sharp, N. Sambandam, K. M. Olson, D. S. Ory, and J. E. Schaffer. 2005. Transgenic expression of fatty acid transport protein 1 in the heart causes lipotoxic cardiomyopathy. *Circ. Res.* **96**: 225-233.

61.   Mashek, D. G., and R. A. Coleman. 2006. Cellular fatty acid uptake: the contribution of metabolism. *Curr. Opin. Lipidol.* **17**: 274-278.

62.   Chess, D. J., and W. C. Stanley. 2008. Role of diet and fuel overabundance in the development and progression of heart failure. *Cardiovasc. Res.* **79**: 269-278.

63.   Buchanan, J., P. K. Mazumder, P. Hu, G. Chakrabarti, M. W. Roberts, U. J. Yun, R. C. Cooksey, S. E. Litwin, and E. D. Abel. 2005. Reduced cardiac efficiency and altered substrate metabolism precedes the onset of hyperglycemia

and contractile dysfunction in two mouse models of insulin resistance and obesity. *Endocrinology* **146**: 5341-5349.

64. Boudina, S., S. Sena, H. Theobald, X. Sheng, J. J. Wright, X. X. Hu, S. Aziz, J. I. Johnson, H. Bugger, V. G. Zaha, and E. D. Abel. 2007. Mitochondrial energetics in the heart in obesity-related diabetes: direct evidence for increased uncoupled respiration and activation of uncoupling proteins. *Diabetes* **56**: 2457-2466.

65. Huss, J. M., and D. P. Kelly. 2004. Nuclear receptor signaling and cardiac energetics. *Circ. Res.* **95**: 568-578.

66. Brindley, D. N. 1992. Neuroendocrine regulation and obesity. *Int. J. Obes. Relat. Metab. Disord.* **16 Suppl 3**: S73-79.

67. McArthur, M. D., S. E. Graham, J. C. Russell, and D. N. Brindley. 1998. Exaggerated stress-induced release of nonesterified fatty acids in JCR:LA-corpulent rats. *Metabolism.* **47**: 1383-1390.

68. Ginsberg, H. N. 2000. Insulin resistance and cardiovascular disease. *J. Clin. Invest.* **106**: 453-458.

69. Bays, H., L. Mandarino, and R. A. DeFronzo. 2004. Role of the adipocyte, free fatty acids, and ectopic fat in pathogenesis of type 2 diabetes mellitus: peroxisomal proliferator-activated receptor agonists provide a rational therapeutic approach. *J. Clin. Endocrinol. Metab.* **89**: 463-478.

70. Lewis, G. F., A. Carpentier, K. Adeli, and A. Giacca. 2002. Disordered fat storage and mobilization in the pathogenesis of insulin resistance and type 2 diabetes. *Endocr. Rev.* **23**: 201-229.

71. Aguilera, C. M., M. Gil-Campos, R. Canete, and A. Gil. 2008. Alterations in plasma and tissue lipids associated with obesity and metabolic syndrome. *Clin Sci (Lond)* **114**: 183-193.

72. Boden, G. 1997. Role of fatty acids in the pathogenesis of insulin resistance and NIDDM. *Diabetes* **46**: 3-10.

73. Martin-Sanz, P., J. E. Vance, and D. N. Brindley. 1990. Stimulation of apolipoprotein secretion in very-low-density and high-density lipoproteins from cultured rat hepatocytes by dexamethasone. *Biochem. J.* **271**: 575-583.

74. Wang, C. N., R. S. McLeod, Z. Yao, and D. N. Brindley. 1995. Effects of dexamethasone on the synthesis, degradation, and secretion of apolipoprotein B in cultured rat hepatocytes. *Arterioscler. Thromb. Vac. Biol.* **15**: 1481-1491.

75. Park, T. S., H. Yamashita, W. S. Blaner, and I. J. Goldberg. 2007. Lipids in the heart: a source of fuel and a source of toxins. *Curr. Opin. Lipidol.* **18**: 277-282.

76. Pulinilkunnil, T., and B. Rodrigues. 2006. Cardiac lipoprotein lipase: metabolic basis for diabetic heart disease. *Cardiovasc. Res.* **69**: 329-340.

77. Ouwens, D. M., M. Diamant, M. Fodor, D. D. Habets, M. M. Pelsers, M. El Hasnaoui, Z. C. Dang, C. E. van den Brom, R. Vlasblom, A. Rietdijk, C. Boer, S. L. Coort, J. F. Glatz, and J. J. Luiken. 2007. Cardiac contractile dysfunction in insulin-resistant rats fed a high-fat diet is associated with elevated CD36-mediated fatty acid uptake and esterification. *Diabetologia* **50**: 1938-1948.

78. Coort, S. L., D. M. Hasselbaink, D. P. Koonen, J. Willems, W. A. Coumans, A. Chabowski, G. J. van der Vusse, A. Bonen, J. F. Glatz, and J. J. Luiken. 2004. Enhanced sarcolemmal FAT/CD36 content and triacylglycerol storage in cardiac myocytes from obese zucker rats. *Diabetes* **53**: 1655-1663.

79. Coort, S. L., J. J. Luiken, G. J. van der Vusse, A. Bonen, and J. F. Glatz. 2004. Increased FAT (fatty acid translocase)/CD36-mediated long-chain fatty acid uptake in cardiac myocytes from obese Zucker rats. *Biochem. Soc. Trans.* **32**: 83-85.

80. Koonen, D. P., M. Febbraio, S. Bonnet, J. Nagendran, M. E. Young, E. D. Michelakis, and J. R. Dyck. 2007. CD36 expression contributes to age-induced cardiomyopathy in mice. *Circulation* **116**: 2139-2147.

81. Steinbusch, L. K., R. W. Schwenk, D. M. Ouwens, M. Diamant, J. F. Glatz, and J. J. Luiken. 2011. Subcellular trafficking of the substrate transporters GLUT4 and CD36 in cardiomyocytes. *Cell. Mol. Life Sci.* **68**: 2525-2538.

82. Wisneski, J. A., E. W. Gertz, R. A. Neese, and M. Mayr. 1987. Myocardial metabolism of free fatty acids. Studies with ^{14}C-labeled substrates in humans. *J. Clin. Invest.* **79**: 359-366.

83. Li, L. O., E. L. Klett, and R. A. Coleman. 2010. Acyl-CoA synthesis, lipid metabolism and lipotoxicity. *Biochim. Biophys. Acta* **1801**: 246-251.

84. de Jong, H., A. C. Neal, R. A. Coleman, and T. M. Lewin. 2007. Ontogeny of mRNA expression and activity of long-chain acyl-CoA synthetase (ACSL) isoforms in Mus musculus heart. *Biochim. Biophys. Acta* **1771**: 75-82.

85. Ellis, J. M., S. M. Mentock, M. A. Depetrillo, T. R. Koves, S. Sen, S. M. Watkins, D. M. Muoio, G. W. Cline, H. Taegtmeyer, G. I. Shulman, M. S. Willis, and R. A. Coleman. 2011. Mouse cardiac acyl coenzyme a synthetase 1 deficiency impairs Fatty Acid oxidation and induces cardiac hypertrophy. *Mol. Cell. Biol.* **31**: 1252-1262.

86. Haemmerle, G., T. Moustafa, G. Woelkart, S. Buttner, A. Schmidt, T. van de Weijer, M. Hesselink, D. Jaeger, P. C. Kienesberger, K. Zierler, R. Schreiber, T. Eichmann, D. Kolb, P. Kotzbeck, M. Schweiger, M. Kumari, S. Eder, G. Schoiswohl, N. Wongsiriroj, N. M. Pollak, F. P. Radner, K. Preiss-Landl, T. Kolbe, T. Rulicke, B. Pieske, M. Trauner, A. Lass, R. Zimmermann, G. Hoefler, S. Cinti, E. E. Kershaw, P. Schrauwen, F. Madeo, B. Mayer, and R. Zechner. 2011. ATGL-mediated fat catabolism regulates cardiac mitochondrial function via PPAR-alpha and PGC-1. *Nat. Med.* **17**: 1076-1085.

87. Haemmerle, G., A. Lass, R. Zimmermann, G. Gorkiewicz, C. Meyer, J. Rozman, G. Heldmaier, R. Maier, C. Theussl, S. Eder, D. Kratky, E. F. Wagner, M. Klingenspor, G. Hoefler, and R. Zechner. 2006. Defective lipolysis and altered energy metabolism in mice lacking adipose triglyceride lipase. *Science* **312**: 734-737.

88. Saddik, M., and G. D. Lopaschuk. 1991. Myocardial triglyceride turnover and contribution to energy substrate utilization in isolated working rat hearts. *J. Biol. Chem.* **266**: 8162-8170.

89. Banke, N. H., A. R. Wende, T. C. Leone, J. M. O'Donnell, E. D. Abel, D. P. Kelly, and E. D. Lewandowski. 2010. Preferential oxidation of triacylglyceride-

derived fatty acids in heart is augmented by the nuclear receptor PPARalpha. *Circ. Res.* **107**: 233-241.

90. Swanton, E. M., and E. D. Saggerson. 1997. Effects of adrenaline on triacylglycerol synthesis and turnover in ventricular myocytes from adult rats. *Biochem. J.* **328 (Pt 3)**: 913-922.

91. McGarry, J. D., and N. F. Brown. 1997. The mitochondrial carnitine palmitoyltransferase system. From concept to molecular analysis. *Eur. J. Biochem.* **244**: 1-14.

92. Cuthbert, K. D., and J. R. Dyck. 2005. Malonyl-CoA decarboxylase is a major regulator of myocardial fatty acid oxidation. *Curr Hypertens Rep* **7**: 407-411.

93. Schulz, H. 2002. Chapter 5 Oxidation of fatty acids in eukaryotes. *In* New Comprehensive Biochemistry. J. E. V. Dennis E. Vance, editor. Elsevier. 127-150.

94. Finck, B. N., and D. P. Kelly. 2006. PGC-1 coactivators: inducible regulators of energy metabolism in health and disease. *J. Clin. Invest.* **116**: 615-622.

95. Madrazo, J. A., and D. P. Kelly. 2008. The PPAR trio: Regulators of myocardial energy metabolism in health and disease. *J. Mol. Cell. Cardiol.* **44**: 968-975.

96. Lin, J., C. Handschin, and B. M. Spiegelman. 2005. Metabolic control through the PGC-1 family of transcription coactivators. *Cell Metab.* **1**: 361-370.

97. Barger, P. M., and D. P. Kelly. 2000. PPAR signaling in the control of cardiac energy metabolism. *Trends Cardiovasc. Med.* **10**: 238-245.

98. Yang, Q., and Y. Li. 2007. Roles of PPARs on regulating myocardial energy and lipid homeostasis. *J Mol Med (Berl)* **85**: 697-706.

99. Jiang, Y. J., B. Lu, F. Y. Xu, J. Gartshore, W. A. Taylor, A. J. Halayko, F. J. Gonzalez, J. Takasaki, P. C. Choy, and G. M. Hatch. 2004. Stimulation of cardiac cardiolipin biosynthesis by PPARalpha activation. *J. Lipid Res.* **45**: 244-252.

100. Finck, B. N., M. C. Gropler, Z. Chen, T. C. Leone, M. A. Croce, T. E. Harris, J. C. Lawrence, Jr., and D. P. Kelly. 2006. Lipin 1 is an inducible amplifier of the hepatic PGC-1alpha/PPARalpha regulatory pathway. *Cell Metab.* **4**: 199-210.

101. Watanabe, K., H. Fujii, T. Takahashi, M. Kodama, Y. Aizawa, Y. Ohta, T. Ono, G. Hasegawa, M. Naito, T. Nakajima, Y. Kamijo, F. J. Gonzalez, and T. Aoyama. 2000. Constitutive regulation of cardiac fatty acid metabolism through peroxisome proliferator-activated receptor alpha associated with age-dependent cardiac toxicity. *J. Biol. Chem.* **275**: 22293-22299.

102. Leone, T. C., C. J. Weinheimer, and D. P. Kelly. 1999. A critical role for the peroxisome proliferator-activated receptor alpha (PPARalpha) in the cellular fasting response: the PPARalpha-null mouse as a model of fatty acid oxidation disorders. *Proc. Natl. Acad. Sci. U. S. A.* **96**: 7473-7478.

103.   Leone, T. C., J. J. Lehman, B. N. Finck, P. J. Schaeffer, A. R. Wende, S. Boudina, M. Courtois, D. F. Wozniak, N. Sambandam, C. Bernal-Mizrachi, Z. Chen, J. O. Holloszy, D. M. Medeiros, R. E. Schmidt, J. E. Saffitz, E. D. Abel, C. F. Semenkovich, and D. P. Kelly. 2005. PGC-1alpha deficiency causes multi-system energy metabolic derangements: muscle dysfunction, abnormal weight control and hepatic steatosis. *PLoS Biol* **3**: e101.

104.   Lehman, J. J., S. Boudina, N. H. Banke, N. Sambandam, X. Han, D. M. Young, T. C. Leone, R. W. Gross, E. D. Lewandowski, E. D. Abel, and D. P. Kelly. 2008. The transcriptional coactivator PGC-1alpha is essential for maximal and efficient cardiac mitochondrial fatty acid oxidation and lipid homeostasis. *Am J Physiol Heart Circ Physiol* **295**: H185-196.

105.   Arany, Z., H. He, J. Lin, K. Hoyer, C. Handschin, O. Toka, F. Ahmad, T. Matsui, S. Chin, P. H. Wu, Rybkin, II, J. M. Shelton, M. Manieri, S. Cinti, F. J. Schoen, R. Bassel-Duby, A. Rosenzweig, J. S. Ingwall, and B. M. Spiegelman. 2005. Transcriptional coactivator PGC-1 alpha controls the energy state and contractile function of cardiac muscle. *Cell Metab.* **1**: 259-271.

106.   Herrero, P., L. R. Peterson, J. B. McGill, S. Matthew, D. Lesniak, C. Dence, and R. J. Gropler. 2006. Increased myocardial fatty acid metabolism in patients with type 1 diabetes mellitus. *J. Am. Coll. Cardiol.* **47**: 598-604.

107.   Boudina, S., S. Sena, B. T. O'Neill, P. Tathireddy, M. E. Young, and E. D. Abel. 2005. Reduced mitochondrial oxidative capacity and increased mitochondrial uncoupling impair myocardial energetics in obesity. *Circulation* **112**: 2686-2695.

108.   Boudina, S., H. Bugger, S. Sena, B. T. O'Neill, V. G. Zaha, O. Ilkun, J. J. Wright, P. K. Mazumder, E. Palfreyman, T. J. Tidwell, H. Theobald, O. Khalimonchuk, B. Wayment, X. Sheng, K. J. Rodnick, R. Centini, D. Chen, S. E. Litwin, B. E. Weimer, and E. D. Abel. 2009. Contribution of impaired myocardial insulin signaling to mitochondrial dysfunction and oxidative stress in the heart. *Circulation* **119**: 1272-1283.

109.   Shen, X., S. Zheng, N. S. Metreveli, and P. N. Epstein. 2006. Protection of cardiac mitochondria by overexpression of MnSOD reduces diabetic cardiomyopathy. *Diabetes* **55**: 798-805.

110.   Echtay, K. S., D. Roussel, J. St-Pierre, M. B. Jekabsons, S. Cadenas, J. A. Stuart, J. A. Harper, S. J. Roebuck, A. Morrison, S. Pickering, J. C. Clapham, and M. D. Brand. 2002. Superoxide activates mitochondrial uncoupling proteins. *Nature* **415**: 96-99.

111.   Ye, G., N. S. Metreveli, J. Ren, and P. N. Epstein. 2003. Metallothionein prevents diabetes-induced deficits in cardiomyocytes by inhibiting reactive oxygen species production. *Diabetes* **52**: 777-783.

112.   Lopaschuk, G. D., R. Barr, P. D. Thomas, and J. R. Dyck. 2003. Beneficial effects of trimetazidine in ex vivo working ischemic hearts are due to a stimulation of glucose oxidation secondary to inhibition of long-chain 3-ketoacyl coenzyme a thiolase. *Circ. Res.* **93**: e33-37.

113.   Burgmaier, M., S. Sen, F. Philip, C. R. Wilson, C. C. Miller, 3rd, M. E. Young, and H. Taegtmeyer. 2010. Metabolic adaptation follows contractile

dysfunction in the heart of obese Zucker rats fed a high-fat "Western" diet. *Obesity (Silver Spring)* **18**: 1895-1901.

114.   Finck, B. N., J. J. Lehman, T. C. Leone, M. J. Welch, M. J. Bennett, A. Kovacs, X. Han, R. W. Gross, R. Kozak, G. D. Lopaschuk, and D. P. Kelly. 2002. The cardiac phenotype induced by PPARalpha overexpression mimics that caused by diabetes mellitus. *J. Clin. Invest.* **109**: 121-130.

115.   Hopkins, T. A., M. C. Sugden, M. J. Holness, R. Kozak, J. R. Dyck, and G. D. Lopaschuk. 2003. Control of cardiac pyruvate dehydrogenase activity in peroxisome proliferator-activated receptor-alpha transgenic mice. *Am J Physiol Heart Circ Physiol* **285**: H270-276.

116.   Lehman, J. J., P. M. Barger, A. Kovacs, J. E. Saffitz, D. M. Medeiros, and D. P. Kelly. 2000. Peroxisome proliferator-activated receptor gamma coactivator-1 promotes cardiac mitochondrial biogenesis. *The Journal of clinical investigation* **106**: 847-856.

117.   Lopaschuk, G. D., S. R. Wall, P. M. Olley, and N. J. Davies. 1988. Etomoxir, a carnitine palmitoyltransferase I inhibitor, protects hearts from fatty acid-induced ischemic injury independent of changes in long chain acylcarnitine. *Circ. Res.* **63**: 1036-1043.

118.   Chandler, M. P., P. N. Chavez, T. A. McElfresh, H. Huang, C. S. Harmon, and W. C. Stanley. 2003. Partial inhibition of fatty acid oxidation increases regional contractile power and efficiency during demand-induced ischemia. *Cardiovasc. Res.* **59**: 143-151.

119.   Yang, J., N. Sambandam, X. Han, R. W. Gross, M. Courtois, A. Kovacs, M. Febbraio, B. N. Finck, and D. P. Kelly. 2007. CD36 deficiency rescues lipotoxic cardiomyopathy. *Circ. Res.* **100**: 1208-1217.

120.   Foley, J. E. 1992. Rationale and application of fatty acid oxidation inhibitors in treatment of diabetes mellitus. *Diabetes Care* **15**: 773-784.

121.   Larsen, T. S., and E. Aasum. 2008. Metabolic (in)flexibility of the diabetic heart. *Cardiovasc. Drugs Ther.* **22**: 91-95.

122.   Kennedy, E. P. 1956. The biological synthesis of phospholipids. *Can J Biochem Physiol* **34**: 334-348.

123.   Weiss, S. B., E. P. Kennedy, and J. Y. Kiyasu. 1960. The enzymatic synthesis of triglycerides. *J. Biol. Chem.* **235**: 40-44.

124.   Brindley, D. N., B. P. Kok, P. C. Kienesberger, R. Lehner, and J. R. Dyck. 2010. Shedding light on the enigma of myocardial lipotoxicity: the involvement of known and putative regulators of fatty acid storage and mobilization. *Am J Physiol Endocrinol Metab* **298**: E897-908.

125.   Coleman, R. A., and D. P. Lee. 2004. Enzymes of triacylglycerol synthesis and their regulation. *Prog. Lipid Res.* **43**: 134-176.

126.   Kim, J. Y., H. S. Park, S. I. Kang, E. J. Choi, and I. Y. Kim. 2002. Redox regulation of cytosolic glycerol-3-phosphate dehydrogenase: Cys(102) is the target of the redox control and essential for the catalytic activity. *Biochim. Biophys. Acta* **1569**: 67-74.

127.   Robinson, J., and E. A. Newsholme. 1967. Glycerol kinase activities in rat heart and adipose tissue. *Biochem. J.* **104**: 2C-4C.

128.   Golovko, M. Y., J. T. Hovda, Z. J. Cai, W. J. Craigen, and E. J. Murphy. 2005. Tissue-dependent alterations in lipid mass in mice lacking glycerol kinase. *Lipids* **40**: 287-293.

129.   Takeuchi, K., and K. Reue. 2009. Biochemistry, physiology, and genetics of GPAT, AGPAT, and lipin enzymes in triglyceride synthesis. *Am J Physiol Endocrinol Metab* **296**: E1195-1209.

130.   Wendel, A. A., T. M. Lewin, and R. A. Coleman. 2009. Glycerol-3-phosphate acyltransferases: rate limiting enzymes of triacylglycerol biosynthesis. *Biochim. Biophys. Acta* **1791**: 501-506.

131.   Lewin, T. M., H. de Jong, N. J. Schwerbrock, L. E. Hammond, S. M. Watkins, T. P. Combs, and R. A. Coleman. 2008. Mice deficient in mitochondrial glycerol-3-phosphate acyltransferase-1 have diminished myocardial triacylglycerol accumulation during lipogenic diet and altered phospholipid fatty acid composition. *Biochim. Biophys. Acta* **1781**: 352-358.

132.   Lu, B., Y. J. Jiang, Y. Zhou, F. Y. Xu, G. M. Hatch, and P. C. Choy. 2005. Cloning and characterization of murine 1-acyl-sn-glycerol 3-phosphate acyltransferases and their regulation by PPARalpha in murine heart. *Biochem. J.* **385**: 469-477.

133.   Reue, K., and D. N. Brindley. 2008. Thematic Review Series: Glycerolipids. Multiple roles for lipins/phosphatidate phosphatase enzymes in lipid metabolism. *J. Lipid Res.* **49**: 2493-2503.

134.   Donkor, J., M. Sariahmetoglu, J. Dewald, D. N. Brindley, and K. Reue. 2007. Three mammalian lipins act as phosphatidate phosphatases with distinct tissue expression patterns. *J. Biol. Chem.* **282**: 3450-3457.

135.   Han, G. S., W. I. Wu, and G. M. Carman. 2006. The Saccharomyces cerevisiae Lipin homolog is a Mg^{2+}-dependent phosphatidate phosphatase enzyme. *J. Biol. Chem.* **281**: 9210-9218.

136.   Liu, G. H., J. Qu, A. E. Carmack, H. B. Kim, C. Chen, H. Ren, A. J. Morris, B. N. Finck, and T. E. Harris. 2010. Lipin proteins form homo- and hetero-oligomers. *Biochem. J.* **432**: 65-76.

137.   Han, G. S., and G. M. Carman. 2010. Characterization of the human LPIN1-encoded phosphatidate phosphatase isoforms. *J. Biol. Chem.* **285**: 14628-14638.

138.   Donkor, J., P. Zhang, S. Wong, L. O'Loughlin, J. Dewald, B. P. Kok, D. N. Brindley, and K. Reue. 2009. A conserved serine residue is required for the phosphatidate phosphatase activity but not the transcriptional coactivator functions of lipin-1 and lipin-2. *J. Biol. Chem.* **284**: 29968-29978.

139.   Zammit, V. A., L. K. Buckett, A. V. Turnbull, H. Wure, and A. Proven. 2008. Diacylglycerol acyltransferases: Potential roles as pharmacological targets. *Pharmacol. Ther.* **118**: 295-302.

140.   Yen, C. L., S. J. Stone, S. Koliwad, C. Harris, and R. V. Farese, Jr. 2008. Thematic review series: glycerolipids. DGAT enzymes and triacylglycerol biosynthesis. *J. Lipid Res.* **49**: 2283-2301.

141.   Stone, S. J., M. C. Levin, and R. V. Farese, Jr. 2006. Membrane topology and identification of key functional amino acid residues of murine acyl-CoA:diacylglycerol acyltransferase-2. *J. Biol. Chem.* **281**: 40273-40282.

142.   Stone, S. J., M. C. Levin, P. Zhou, J. Han, T. C. Walther, and R. V. Farese, Jr. 2009. The endoplasmic reticulum enzyme DGAT2 is found in mitochondria-associated membranes and has a mitochondrial targeting signal that promotes its association with mitochondria. *J. Biol. Chem.* **284**: 5352-5361.

143.   McFie, P. J., S. L. Banman, S. Kary, and S. J. Stone. 2011. Murine diacylglycerol acyltransferase-2 (DGAT2) can catalyze triacylglycerol synthesis and promote lipid droplet formation independent of its localization to the endoplasmic reticulum. *J. Biol. Chem.* **286**: 28235-28246.

144.   Harris, C. A., J. T. Haas, R. S. Streeper, S. J. Stone, M. Kumari, K. Yang, X. Han, N. Brownell, R. W. Gross, R. Zechner, and R. V. Farese, Jr. 2011. DGAT enzymes are required for triacylglycerol synthesis and lipid droplets in adipocytes. *J. Lipid Res.* **52**: 657-667.

145.   Yen, C. L., M. Monetti, B. J. Burri, and R. V. Farese, Jr. 2005. The triacylglycerol synthesis enzyme DGAT1 also catalyzes the synthesis of diacylglycerols, waxes, and retinyl esters. *J. Lipid Res.* **46**: 1502-1511.

146.   Shih, M. Y., M. A. Kane, P. Zhou, C. L. Yen, R. S. Streeper, J. L. Napoli, and R. V. Farese, Jr. 2009. Retinol Esterification by DGAT1 Is Essential for Retinoid Homeostasis in Murine Skin. *J. Biol. Chem.* **284**: 4292-4299.

147.   Stone, S. J., H. M. Myers, S. M. Watkins, B. E. Brown, K. R. Feingold, P. M. Elias, and R. V. Farese, Jr. 2004. Lipopenia and skin barrier abnormalities in DGAT2-deficient mice. *J. Biol. Chem.* **279**: 11767-11776.

148.   Liu, L., X. Shi, C. S. Choi, G. I. Shulman, K. Klaus, K. S. Nair, G. J. Schwartz, Y. Zhang, I. J. Goldberg, and Y. H. Yu. 2009. Paradoxical coupling of triglyceride synthesis and fatty acid oxidation in skeletal muscle overexpressing DGAT1. *Diabetes* **58**: 2516-2524.

149.   Liu, L., X. Shi, K. G. Bharadwaj, S. Ikeda, H. Yamashita, H. Yagyu, J. E. Schaffer, Y. H. Yu, and I. J. Goldberg. 2009. DGAT1 expression increases heart triglyceride content but ameliorates lipotoxicity. *J. Biol. Chem.* **284**: 36312-36323.

150.   Levin, M. C., M. Monetti, M. J. Watt, M. P. Sajan, R. D. Stevens, J. R. Bain, C. B. Newgard, R. V. Farese, Sr., and R. V. Farese, Jr. 2007. Increased lipid accumulation and insulin resistance in transgenic mice expressing DGAT2 in glycolytic (type II) muscle. *Am J Physiol Endocrinol Metab* **293**: E1772-1781.

151.   Monetti, M., M. C. Levin, M. J. Watt, M. P. Sajan, S. Marmor, B. K. Hubbard, R. D. Stevens, J. R. Bain, C. B. Newgard, R. V. Farese, Sr., A. L. Hevener, and R. V. Farese, Jr. 2007. Dissociation of hepatic steatosis and insulin resistance in mice overexpressing DGAT in the liver. *Cell Metab.* **6**: 69-78.

152.   Liu, L., Y. Zhang, N. Chen, X. Shi, B. Tsang, and Y. H. Yu. 2007. Upregulation of myocellular DGAT1 augments triglyceride synthesis in skeletal muscle and protects against fat-induced insulin resistance. *J. Clin. Invest.* **117**: 1679-1689.

153.   Glenn, D. J., F. Wang, M. Nishimoto, M. C. Cruz, Y. Uchida, W. M. Holleran, Y. Zhang, Y. Yeghiazarians, and D. G. Gardner. 2011. A murine model of isolated cardiac steatosis leads to cardiomyopathy. *Hypertension* **57**: 216-222.

154.   Boudina, S., and E. D. Abel. 2006. Mitochondrial uncoupling: a key contributor to reduced cardiac efficiency in diabetes. *Physiology (Bethesda)* **21**: 250-258.

155.   Aasum, E., M. Cooper, D. L. Severson, and T. S. Larsen. 2005. Effect of BM 17.0744, a PPARalpha ligand, on the metabolism of perfused hearts from control and diabetic mice. *Can. J. Physiol. Pharmacol.* **83**: 183-190.

156.   Szczepaniak, L. S., R. G. Victor, L. Orci, and R. H. Unger. 2007. Forgotten but not gone: the rediscovery of fatty heart, the most common unrecognized disease in America. *Circ. Res.* **101**: 759-767.

157.   Brookheart, R. T., C. I. Michel, and J. E. Schaffer. 2009. As a matter of fat. *Cell Metab.* **10**: 9-12.

158.   Harmancey, R., C. R. Wilson, and H. Taegtmeyer. 2008. Adaptation and maladaptation of the heart in obesity. *Hypertension* **52**: 181-187.

159.   Luiken, J. J. 2009. Sarcolemmal fatty acid uptake vs. mitochondrial beta-oxidation as target to regress cardiac insulin resistance. *Appl Physiol Nutr Metab* **34**: 473-480.

160.   Chiu, H. C., A. Kovacs, D. A. Ford, F. F. Hsu, R. Garcia, P. Herrero, J. E. Saffitz, and J. E. Schaffer. 2001. A novel mouse model of lipotoxic cardiomyopathy. *J. Clin. Invest.* **107**: 813-822.

161.   Schaffer, J. E. 2003. Lipotoxicity: when tissues overeat. *Curr. Opin. Lipidol.* **14**: 281-287.

162.   Kusminski, C. M., S. Shetty, L. Orci, R. H. Unger, and P. E. Scherer. 2009. Diabetes and apoptosis: lipotoxicity. *Apoptosis* **14**: 1484-1495.

163.   Wende, A. R., and E. D. Abel. 2009. Lipotoxicity in the heart. *Biochim. Biophys. Acta*.

164.   Sparagna, G. C., D. L. Hickson-Bick, L. M. Buja, and J. B. McMillin. 2000. A metabolic role for mitochondria in palmitate-induced cardiac myocyte apoptosis. *Am J Physiol Heart Circ Physiol* **279**: H2124-2132.

165.   Coll, T., E. Eyre, R. Rodriguez-Calvo, X. Palomer, R. M. Sanchez, M. Merlos, J. C. Laguna, and M. Vazquez-Carrera. 2008. Oleate reverses palmitate-induced insulin resistance and inflammation in skeletal muscle cells. *J. Biol. Chem.* **283**: 11107-11116.

166.   Chavez, J. A., and S. A. Summers. 2003. Characterizing the effects of saturated fatty acids on insulin signaling and ceramide and diacylglycerol accumulation in 3T3-L1 adipocytes and C2C12 myotubes. *Arch. Biochem. Biophys.* **419**: 101-109.

167.   Powell, D. J., S. Turban, A. Gray, E. Hajduch, and H. S. Hundal. 2004. Intracellular ceramide synthesis and protein kinase Czeta activation play an essential role in palmitate-induced insulin resistance in rat L6 skeletal muscle cells. *Biochem. J.* **382**: 619-629.

168.   Russell, L. K., B. N. Finck, and D. P. Kelly. 2005. Mouse models of mitochondrial dysfunction and heart failure. *J. Mol. Cell. Cardiol.* **38**: 81-91.

169.   Basu, R., G. Y. Oudit, X. Wang, L. Zhang, J. R. Ussher, G. D. Lopaschuk, and Z. Kassiri. 2009. Type 1 diabetic cardiomyopathy in the Akita (Ins2WT/C96Y) mouse model is characterized by lipotoxicity and diastolic dysfunction with preserved systolic function. *Am J Physiol Heart Circ Physiol* **297**: H2096-2108.

170.   Zhang, L., J. R. Ussher, T. Oka, V. J. Cadete, C. Wagg, and G. D. Lopaschuk. 2011. Cardiac diacylglycerol accumulation in high fat-fed mice is associated with impaired insulin-stimulated glucose oxidation. *Cardiovasc. Res.* **89**: 148-156.

171.   Park, T. S., Y. Hu, H. L. Noh, K. Drosatos, K. Okajima, J. Buchanan, J. Tuinei, S. Homma, X. C. Jiang, E. D. Abel, and I. J. Goldberg. 2008. Ceramide is a cardiotoxin in lipotoxic cardiomyopathy. *J. Lipid Res.* **49**: 2101-2112.

172.   Drosatos, K., K. G. Bharadwaj, A. Lymperopoulos, S. Ikeda, R. Khan, Y. Hu, R. Agarwal, S. Yu, H. Jiang, S. F. Steinberg, W. S. Blaner, W. J. Koch, and I. J. Goldberg. 2011. Cardiomyocyte lipids impair beta-adrenergic receptor function via PKC activation. *Am J Physiol Endocrinol Metab* **300**: E489-499.

173.   Brindley, D. N., C. Pilquil, M. Sariahmetoglu, and K. Reue. 2009. Phosphatidate degradation: phosphatidate phosphatases (lipins) and lipid phosphate phosphatases. *Biochim. Biophys. Acta* **1791**: 956-961.

174.   Zhang, Y., and G. Du. 2009. Phosphatidic acid signaling regulation of Ras superfamily of small guanosine triphosphatases. *Biochim. Biophys. Acta* **1791**: 850-855.

175.   Wang, X., S. P. Devaiah, W. Zhang, and R. Welti. 2006. Signaling functions of phosphatidic acid. *Prog. Lipid Res.* **45**: 250-278.

176.   Samuel, V. T., and G. I. Shulman. 2012. Mechanisms for insulin resistance: common threads and missing links. *Cell* **148**: 852-871.

177.   Stanley, W. C., F. A. Recchia, and G. D. Lopaschuk. 2005. Myocardial substrate metabolism in the normal and failing heart. *Physiol. Rev.* **85**: 1093-1129.

178.   Zechner, R., R. Zimmermann, T. O. Eichmann, S. D. Kohlwein, G. Haemmerle, A. Lass, and F. Madeo. 2012. FAT SIGNALS - Lipases and Lipolysis in Lipid Metabolism and Signaling. *Cell Metab.* **15**: 279-291.

179.   Holm, C., T. G. Kirchgessner, K. L. Svenson, G. Fredrikson, S. Nilsson, C. G. Miller, J. E. Shively, C. Heinzmann, R. S. Sparkes, T. Mohandas, and et al. 1988. Hormone-sensitive lipase: sequence, expression, and chromosomal localization to 19 cent-q13.3. *Science* **241**: 1503-1506.

180.   Dolinsky, V. W., S. Sipione, R. Lehner, and D. E. Vance. 2001. The cloning and expression of a murine triacylglycerol hydrolase cDNA and the structure of its corresponding gene. *Biochim. Biophys. Acta* **1532**: 162-172.

181.   Karlsson, M., J. A. Contreras, U. Hellman, H. Tornqvist, and C. Holm. 1997. cDNA cloning, tissue distribution, and identification of the catalytic triad of monoglyceride lipase. Evolutionary relationship to esterases, lysophospholipases, and haloperoxidases. *J. Biol. Chem.* **272**: 27218-27223.

182. Lass, A., R. Zimmermann, G. Haemmerle, M. Riederer, G. Schoiswohl, M. Schweiger, P. Kienesberger, J. G. Strauss, G. Gorkiewicz, and R. Zechner. 2006. Adipose triglyceride lipase-mediated lipolysis of cellular fat stores is activated by CGI-58 and defective in Chanarin-Dorfman Syndrome. *Cell Metab.* **3**: 309-319.

183. Ghosh, A. K., G. Ramakrishnan, C. Chandramohan, and R. Rajasekharan. 2008. CGI-58, the causative gene for Chanarin-Dorfman syndrome, mediates acylation of lysophosphatidic acid. *J. Biol. Chem.* **283**: 24525-24533.

184. Montero-Moran, G., J. M. Caviglia, D. McMahon, A. Rothenberg, V. Subramanian, Z. Xu, S. Lara-Gonzalez, J. Storch, G. M. Carman, and D. L. Brasaemle. 2010. CGI-58/ABHD5 is a coenzyme A-dependent lysophosphatidic acid acyltransferase. *J. Lipid Res.* **51**: 709-719.

185. Lord, C. C., J. L. Betters, P. T. Ivanova, S. B. Milne, D. S. Myers, J. Madenspacher, G. Thomas, S. Chung, M. Liu, M. A. Davis, R. G. Lee, R. M. Crooke, M. J. Graham, J. S. Parks, D. L. Brasaemle, M. B. Fessler, H. A. Brown, and J. M. Brown. 2012. CGI-58/ABHD5-derived signaling lipids regulate systemic inflammation and insulin action. *Diabetes* **61**: 355-363.

186. Schoiswohl, G., M. Schweiger, R. Schreiber, G. Gorkiewicz, K. Preiss-Landl, U. Taschler, K. A. Zierler, F. P. Radner, T. O. Eichmann, P. C. Kienesberger, S. Eder, A. Lass, G. Haemmerle, T. J. Alsted, B. Kiens, G. Hoefler, R. Zechner, and R. Zimmermann. 2010. Adipose triglyceride lipase plays a key role in the supply of the working muscle with fatty acids. *J. Lipid Res.* **51**: 490-499.

187. Duncan, J. G., K. G. Bharadwaj, J. L. Fong, R. Mitra, N. Sambandam, M. R. Courtois, K. J. Lavine, I. J. Goldberg, and D. P. Kelly. 2010. Rescue of cardiomyopathy in peroxisome proliferator-activated receptor-alpha transgenic mice by deletion of lipoprotein lipase identifies sources of cardiac lipids and peroxisome proliferator-activated receptor-alpha activators. *Circulation* **121**: 426-435.

188. Schweiger, M., A. Lass, R. Zimmermann, T. O. Eichmann, and R. Zechner. 2009. Neutral lipid storage disease: genetic disorders caused by mutations in adipose triglyceride lipase/PNPLA2 or CGI-58/ABHD5. *Am J Physiol Endocrinol Metab* **297**: E289-296.

189. Hirano, K., Y. Ikeda, N. Zaima, Y. Sakata, and G. Matsumiya. 2008. Triglyceride deposit cardiomyovasculopathy. *N. Engl. J. Med.* **359**: 2396-2398.

190. Haemmerle, G., R. Zimmermann, M. Hayn, C. Theussl, G. Waeg, E. Wagner, W. Sattler, T. M. Magin, E. F. Wagner, and R. Zechner. 2002. Hormone-sensitive lipase deficiency in mice causes diglyceride accumulation in adipose tissue, muscle, and testis. *J. Biol. Chem.* **277**: 4806-4815.

191. Park, S. Y., H. J. Kim, S. Wang, T. Higashimori, J. Dong, Y. J. Kim, G. Cline, H. Li, M. Prentki, G. I. Shulman, G. A. Mitchell, and J. K. Kim. 2005. Hormone-sensitive lipase knockout mice have increased hepatic insulin sensitivity and are protected from short-term diet-induced insulin resistance in skeletal muscle and heart. *Am J Physiol Endocrinol Metab* **289**: E30-39.

192.	Zimmermann, R., G. Haemmerle, E. M. Wagner, J. G. Strauss, D. Kratky, and R. Zechner. 2003. Decreased fatty acid esterification compensates for the reduced lipolytic activity in hormone-sensitive lipase-deficient white adipose tissue. *J. Lipid Res.* **44**: 2089-2099.

193.	Suzuki, J., W. J. Shen, B. D. Nelson, S. Patel, J. H. Veerkamp, S. P. Selwood, G. M. Murphy, Jr., E. Reaven, and F. B. Kraemer. 2001. Absence of cardiac lipid accumulation in transgenic mice with heart-specific HSL overexpression. *Am J Physiol Endocrinol Metab* **281**: E857-866.

194.	Ueno, M., J. Suzuki, Y. Zenimaru, S. Takahashi, T. Koizumi, S. Noriki, O. Yamaguchi, K. Otsu, W. J. Shen, F. B. Kraemer, and I. Miyamori. 2008. Cardiac overexpression of hormone-sensitive lipase inhibits myocardial steatosis and fibrosis in streptozotocin diabetic mice. *Am J Physiol Endocrinol Metab* **294**: E1109-1118.

195.	Kienesberger, P. C., T. Pulinilkunnil, M. M. Sung, J. Nagendran, G. Haemmerle, E. E. Kershaw, M. E. Young, P. E. Light, G. Y. Oudit, R. Zechner, and J. R. Dyck. 2012. Myocardial ATGL overexpression decreases the reliance on fatty acid oxidation and protects against pressure overload-induced cardiac dysfunction. *Mol. Cell. Biol.* **32**: 740-750.

196.	Taschler, U., F. P. Radner, C. Heier, R. Schreiber, M. Schweiger, G. Schoiswohl, K. Preiss-Landl, D. Jaeger, B. Reiter, H. C. Koefeler, J. Wojciechowski, C. Theussl, J. M. Penninger, A. Lass, G. Haemmerle, R. Zechner, and R. Zimmermann. 2011. Monoglyceride lipase deficiency in mice impairs lipolysis and attenuates diet-induced insulin resistance. *J. Biol. Chem.* **286**: 17467-17477.

197.	Yen, C. L., and R. V. Farese, Jr. 2003. MGAT2, a monoacylglycerol acyltransferase expressed in the small intestine. *J. Biol. Chem.* **278**: 18532-18537.

198.	Yen, C. L., S. J. Stone, S. Cases, P. Zhou, and R. V. Farese, Jr. 2002. Identification of a gene encoding MGAT1, a monoacylglycerol acyltransferase. *Proc. Natl. Acad. Sci. U. S. A.* **99**: 8512-8517.

199.	Gilham, D., S. Ho, M. Rasouli, P. Martres, D. E. Vance, and R. Lehner. 2003. Inhibitors of hepatic microsomal triacylglycerol hydrolase decrease very low density lipoprotein secretion. *FASEB J.* **17**: 1685-1687.

200.	Wei, E., M. Alam, F. Sun, L. B. Agellon, D. E. Vance, and R. Lehner. 2007. Apolipoprotein B and triacylglycerol secretion in human triacylglycerol hydrolase transgenic mice. *J. Lipid Res.* **48**: 2597-2606.

201.	Bartels, E. D., J. M. Nielsen, L. I. Hellgren, T. Ploug, and L. B. Nielsen. 2009. Cardiac expression of microsomal triglyceride transfer protein is increased in obesity and serves to attenuate cardiac triglyceride accumulation. *PLoS One* **4**: e5300.

202.	Boren, J., M. M. Veniant, and S. G. Young. 1998. Apo B100-containing lipoproteins are secreted by the heart. *J. Clin. Invest.* **101**: 1197-1202.

203.	Smith, M. E., B. Sedgwick, D. N. Brindley, and G. Hübscher. 1967. The role of phosphatidate phosphohydrolase in glyceride biosynthesis. *Eur. J. Biochem.* **3**: 70-77.

204.   Kennedy, E. P. 1958. The biosynthesis of phospholipids. *Am. J. Clin. Nutr.* **6**: 216-220.

205.   Smith, S. W., S. B. Weiss, and E. P. Kennedy. 1957. The enzymatic dephosphorylation of phosphatidic acids. *J. Biol. Chem.* **228**: 915-922.

206.   Choy, P. C., K. Tran, G. M. Hatch, and E. A. Kroeger. 1997. Phospholipid metabolism in the mammalian heart. *Prog. Lipid Res.* **36**: 85-101.

207.   Hatch, G. M. 2004. Cell biology of cardiac mitochondrial phospholipids. *Biochem. Cell Biol.* **82**: 99-112.

208.   Johnston, J. M., G. A. Rao, P. A. Lowe, and B. E. Schawrz. 1967. The nature of the stimulatory role of the supernatant fraction on triglyceride synthesis by the alpha-Glycerophosphate pathway. *Lipids* **2**: 14-20.

209.   Hübscher, G., D. N. Brindley, M. E. Smith, and B. Sedgwick. 1967. Stimulation of biosynthesis of glyceride. *Nature* **216**: 449-453.

210.   Stein, Y., and B. Shapiro. 1957. The synthesis of neutral glycerides by fractions of rat liver homogenates. *Biochim. Biophys. Acta* **24**: 197-198.

211.   Brindley, D. N., M. E. Smith, B. Sedgwick, and G. Hubscher. 1967. The effect of unsaturated fatty acids and the particle-free supernatant on the incorporation of palmitate into glycerides. *Biochim. Biophys. Acta* **144**: 285-295.

212.   Martin, A., P. Hales, and D. N. Brindley. 1987. A rapid assay for measuring the activity and the Mg^{2+} and Ca^{2+} requirements of phosphatidate phosphohydrolase in cytosolic and microsomal fractions of rat liver. *Biochem. J.* **245**: 347-355.

213.   Jamal, Z., A. Martin, A. Gómez-Muñoz, and D. N. Brindley. 1991. Plasma membrane fractions from rat liver contain a phosphatidate phosphohydrolase distinct from that in the endoplasmic reticulum and cytosol. *J. Biol. Chem.* **266**: 2988-2996.

214.   Brindley, D. N., and D. W. Waggoner. 1998. Mammalian lipid phosphate phosphohydrolases. *J. Biol. Chem.* **273**: 24281-24284.

215.   Waggoner, D. W., A. Gómez-Muñoz, J. Dewald, and D. N. Brindley. 1996. Phosphatidate phosphohydrolase catalyzes the hydrolysis of ceramide 1-phosphate, lysophosphatidate, and sphingosine 1-phosphate. *J. Biol. Chem.* **271**: 16506-16509.

216.   Jasinska, R., Q. X. Zhang, C. Pilquil, I. Singh, J. Xu, J. Dewald, D. A. Dillon, L. G. Berthiaume, G. M. Carman, D. W. Waggoner, and D. N. Brindley. 1999. Lipid phosphate phosphohydrolase-1 degrades exogenous glycerolipid and sphingolipid phosphate esters. *Biochem. J.* **340**: 677-686.

217.   Zhang, Q. X., C. S. Pilquil, J. Dewald, L. G. Berthiaume, and D. N. Brindley. 2000. Identification of structurally important domains of lipid phosphate phosphatase-1: implications for its sites of action. *Biochem. J.* **345 Pt 2**: 181-184.

218.   Mitchell, M. P., D. N. Brindley, and G. Hubscher. 1971. Properties of phosphatidate phosphohydrolase. *Eur. J. Biochem.* **18**: 214-220.

219.   Pritchard, P. H., M. Bowley, S. L. Burditt, J. Cooling, H. P. Glenny, N. Lawson, R. G. Sturton, and D. N. Brindley. 1977. The effects of acute ethanol feeding and of chronic benfluorex administration on the activities of some

enzymes of glycerolipid synthesis in rat liver and adipose tissue. *Biochem. J.* **166**: 639-642.

220.   Whiting, P. H., M. Bowley, R. G. Sturton, P. H. Pritchard, D. N. Brindley, and J. N. Hawthorne. 1977. The effect of chronic diabetes, induced by streptozotocin, on the activities of some enzymes of glycerolipid synthesis in rat liver. *Biochem. J.* **168**: 147-153.

221.   Glenny, H. P., and D. N. Brindley. 1978. The effects of cortisol, corticotropin and thyroxine on the synthesis of glycerolipids and on the phosphatidate phosphohydrolase activity in rat liver. *Biochem. J.* **176**: 777-784.

222.   Brindley, D. N., J. Cooling, S. L. Burditt, P. H. Pritchard, S. Pawson, and R. G. Sturton. 1979. The involvement of glucocorticoids in regulating the activity of phosphatidate phosphohydrolase and the synthesis of triacylglycerols in the liver. Effects of feeding rats with glucose, sorbitol, fructose, glycerol and ethanol. *Biochem. J.* **180**: 195-199.

223.   Kinnula, V. L., M. J. Savolainen, and I. Hassinen. 1978. Hepatic triacylglycerol and fatty-acid biosynthesis during hypoxia in vivo. *Acta Physiol. Scand.* **104**: 148-155.

224.   Brindley, D. N. 1988. Phosphatidate phosphohyrolase: its role in glycerolipid synthesis. 1st ed. CRC Press, Boca Raton.

225.   Pittner, R. A., R. Fears, and D. N. Brindley. 1985. Interactions of insulin, glucagon and dexamethasone in controlling the activity of glycerol phosphate acyltransferase and the activity and subcellular distribution of phosphatidate phosphohydrolase in cultured rat hepatocytes. *Biochem. J.* **230**: 525-534.

226.   Pittner, R. A., R. Fears, and D. N. Brindley. 1985. Effects of cyclic AMP, glucocorticoids and insulin on the activities of phosphatidate phosphohydrolase, tyrosine aminotransferase and glycerol kinase in isolated rat hepatocytes in relation to the control of triacylglycerol synthesis and gluconeogenesis. *Biochem. J.* **225**: 455-462.

227.   Simpson, K. J., S. Venkatesan, A. Martin, D. N. Brindley, and T. J. Peters. 1995. Activity and subcellular distribution of phosphatidate phosphohydrolase (EC 3.1.3.4) in alcoholic liver disease. *Alcohol Alcohol* **30**: 31-36.

228.   Peterfy, M., J. Phan, and K. Reue. 2005. Alternatively spliced lipin isoforms exhibit distinct expression pattern, subcellular localization, and role in adipogenesis. *J. Biol. Chem.* **280**: 32883-32889.

229.   Peterson, T. R., S. S. Sengupta, T. E. Harris, A. E. Carmack, S. A. Kang, E. Balderas, D. A. Guertin, K. L. Madden, A. E. Carpenter, B. N. Finck, and D. M. Sabatini. 2011. mTOR complex 1 regulates lipin 1 localization to control the SREBP pathway. *Cell* **146**: 408-420.

230.   Zhang, P., K. Takeuchi, L. S. Csaki, and K. Reue. 2012. Lipin-1 Phosphatidic Phosphatase Activity Modulates Phosphatidate Levels to Promote Peroxisome Proliferator-activated Receptor gamma (PPARgamma) Gene Expression during Adipogenesis. *J. Biol. Chem.* **287**: 3485-3494.

231.   Ren, H., L. Federico, H. Huang, M. Sunkara, T. Drennan, M. A. Frohman, S. S. Smyth, and A. J. Morris. 2010. A phosphatidic acid binding/nuclear

localization motif determines lipin-1 function in lipid metabolism and adipogenesis. *Mol. Biol. Cell* **21**: 3171-3181.

232.   Peterfy, M., T. E. Harris, N. Fujita, and K. Reue. 2010. Insulin-stimulated interaction with 14-3-3 promotes cytoplasmic localization of lipin-1 in adipocytes. *J. Biol. Chem.* **285**: 3857-3864.

233.   Wang, H., J. Zhang, W. Qiu, G. S. Han, G. M. Carman, and K. Adeli. 2011. Lipin-1gamma isoform is a novel lipid droplet-associated protein highly expressed in the brain. *FEBS Lett.* **585**: 1979-1984.

234.   Pihlajamäki, J., C. Lerin, P. Itkonen, T. Boes, T. Floss, J. Schroeder, F. Dearie, S. Crunkhorn, F. Burak, J. C. Jimenez-Chillaron, T. Kuulasmaa, P. Miettinen, P. J. Park, I. Nasser, Z. Zhao, Z. Zhang, Y. Xu, W. Wurst, H. Ren, A. J. Morris, S. Stamm, A. B. Goldfine, M. Laakso, and M. E. Patti. 2011. Expression of the splicing factor gene SFRS10 is reduced in human obesity and contributes to enhanced lipogenesis. *Cell Metab.* **14**: 208-218.

235.   Peterfy, M., J. Phan, P. Xu, and K. Reue. 2001. Lipodystrophy in the fld mouse results from mutation of a new gene encoding a nuclear protein, lipin. *Nat. Genet.* **27**: 121-124.

236.   Langner, C. A., E. H. Birkenmeier, O. Ben-Zeev, M. C. Schotz, H. O. Sweet, M. T. Davisson, and J. I. Gordon. 1989. The fatty liver dystrophy (*fld*) mutation. A new mutant mouse with a developmental abnormality in triglyceride metabolism and associated tissue-specific defects in lipoprotein lipase and hepatic lipase activities. *J. Biol. Chem.* **264**: 7994-8003.

237.   Reue, K., P. Xu, X. P. Wang, and B. G. Slavin. 2000. Adipose tissue deficiency, glucose intolerance, and increased atherosclerosis result from mutation in the mouse fatty liver dystrophy (*fld*) gene. *J. Lipid Res.* **41**: 1067-1076.

238.   Gazit, V., A. Weymann, E. Hartman, B. N. Finck, P. W. Hruz, A. Tzekov, and D. A. Rudnick. 2010. Liver regeneration is impaired in lipodystrophic fatty liver dystrophy mice. *Hepatology* **52**: 2109-2117.

239.   Langner, C. A., E. H. Birkenmeier, K. A. Roth, R. T. Bronson, and J. I. Gordon. 1991. Characterization of the peripheral neuropathy in neonatal and adult mice that are homozygous for the fatty liver dystrophy (*fld*) mutation. *J. Biol. Chem.* **266**: 11955-11964.

240.   Nadra, K., A. S. de Preux Charles, J. J. Medard, W. T. Hendriks, G. S. Han, S. Gres, G. M. Carman, J. S. Saulnier-Blache, M. H. Verheijen, and R. Chrast. 2008. Phosphatidic acid mediates demyelination in Lpin1 mutant mice. *Genes Dev.* **22**: 1647-1661.

241.   Harris, T. E., T. A. Huffman, A. Chi, J. Shabanowitz, D. F. Hunt, A. Kumar, and J. C. Lawrence, Jr. 2007. Insulin controls subcellular localization and multisite phosphorylation of the phosphatidic acid phosphatase, lipin 1. *J. Biol. Chem.* **282**: 277-286.

242.   Bou Khalil, M., M. Sundaram, H. Y. Zhang, P. H. Links, J. F. Raven, B. Manmontri, M. Sariahmetoglu, K. Tran, K. Reue, D. N. Brindley, and Z. Yao. 2009. The level and compartmentalization of phosphatidate phosphatase-1 (lipin-1) control the assembly and secretion of hepatic VLDL. *J. Lipid Res.* **50**: 47-58.

243.   Gropler, M. C., T. E. Harris, A. M. Hall, N. E. Wolins, R. W. Gross, X. Han, Z. Chen, and B. N. Finck. 2009. Lipin 2 is a liver-enriched phosphatidate phosphohydrolase enzyme that is dynamically regulated by fasting and obesity in mice. *J. Biol. Chem.* **284**: 6763-6772.

244.   Hu, M., F. Wang, X. Li, C. Q. Rogers, X. Liang, B. N. Finck, M. S. Mitra, R. Zhang, D. A. Mitchell, and M. You. 2012. Regulation of hepatic lipin-1 by ethanol: Role of AMP-activated protein kinase/sterol regulatory element-binding protein 1 signaling in mice. *Hepatology* **55**: 437-446.

245.   Fakas, S., Y. Qiu, J. L. Dixon, G. S. Han, K. V. Ruggles, J. Garbarino, S. L. Sturley, and G. M. Carman. 2011. Phosphatidate phosphatase activity plays key role in protection against fatty acid-induced toxicity in yeast. *J. Biol. Chem.* **286**: 29074-29085.

246.   Santos-Rosa, H., J. Leung, N. Grimsey, S. Peak-Chew, and S. Siniossoglou. 2005. The yeast lipin Smp2 couples phospholipid biosynthesis to nuclear membrane growth. *EMBO J.* **24**: 1931-1941.

247.   Adeyo, O., P. J. Horn, S. Lee, D. D. Binns, A. Chandrahas, K. D. Chapman, and J. M. Goodman. 2011. The yeast lipin orthologue Pah1p is important for biogenesis of lipid droplets. *J. Cell Biol.* **192**: 1043-1055.

248.   Han, G. S., S. Siniossoglou, and G. M. Carman. 2007. The cellular functions of the yeast lipin homolog PAH1p are dependent on its phosphatidate phosphatase activity. *J. Biol. Chem.* **282**: 37026-37035.

249.   O'Hara, L., G. S. Han, S. Peak-Chew, N. Grimsey, G. M. Carman, and S. Siniossoglou. 2006. Control of phospholipid synthesis by phosphorylation of the yeast lipin Pah1p/Smp2p Mg2+-dependent phosphatidate phosphatase. *J. Biol. Chem.* **281**: 34537-34548.

250.   Loewen, C. J., M. L. Gaspar, S. A. Jesch, C. Delon, N. T. Ktistakis, S. A. Henry, and T. P. Levine. 2004. Phospholipid metabolism regulated by a transcription factor sensing phosphatidic acid. *Science* **304**: 1644-1647.

251.   Golden, A., J. Liu, and O. Cohen-Fix. 2009. Inactivation of the C. elegans lipin homolog leads to ER disorganization and to defects in the breakdown and reassembly of the nuclear envelope. *J. Cell Sci.* **122**: 1970-1978.

252.   Gorjánácz, M., and I. W. Mattaj. 2009. Lipin is required for efficient breakdown of the nuclear envelope in Caenorhabditis elegans. *J. Cell Sci.* **122**: 1963-1969.

253.   Nakamura, Y., R. Koizumi, G. Shui, M. Shimojima, M. R. Wenk, T. Ito, and H. Ohta. 2009. Arabidopsis lipins mediate eukaryotic pathway of lipid metabolism and cope critically with phosphate starvation. *Proc. Natl. Acad. Sci. U. S. A.* **106**: 20978-20983.

254.   Carman, G. M., and G. S. Han. 2006. Roles of phosphatidate phosphatase enzymes in lipid metabolism. *Trends Biochem. Sci.* **31**: 694-699.

255.   Burroughs, A. M., K. N. Allen, D. Dunaway-Mariano, and L. Aravind. 2006. Evolutionary genomics of the HAD superfamily: understanding the structural adaptations and catalytic diversity in a superfamily of phosphoesterases and allied enzymes. *J. Mol. Biol.* **361**: 1003-1034.

256.   Reue, K., and P. Zhang. 2008. The lipin protein family: dual roles in lipid biosynthesis and gene expression. *FEBS Lett.* **582**: 90-96.

257.   Mul, J. D., K. Nadra, N. B. Jagalur, I. J. Nijman, P. W. Toonen, J. J. Medard, S. Gres, A. de Bruin, G. S. Han, J. F. Brouwers, G. M. Carman, J. S. Saulnier-Blache, D. Meijer, R. Chrast, and E. Cuppen. 2011. A hypomorphic mutation in Lpin1 induces progressively improving neuropathy and lipodystrophy in the rat. *J. Biol. Chem.* **286**: 26781-26793.

258.   Douglas, D. S., J. L. Moran, J. R. Bermingham, Jr., X. J. Chen, D. N. Brindley, B. Soliven, D. R. Beier, and B. Popko. 2009. Concurrent Lpin1 and Nrcam mouse mutations result in severe peripheral neuropathy with transitory hindlimb paralysis. *J. Neurosci.* **29**: 12089-12100.

259.   Majeed, H. A., H. El-Shanti, H. Al-Rimawi, and N. Al-Masri. 2000. On mice and men: An autosomal recessive syndrome of chronic recurrent multifocal osteomyelitis and congenital dyserythropoietic anemia. *J. Pediatr.* **137**: 441-442.

260.   Mietkiewska, E., R. M. Siloto, J. Dewald, S. Shah, D. N. Brindley, and R. J. Weselake. 2011. Lipins from plants are phosphatidate phosphatases that restore lipid synthesis in a pah1Delta mutant strain of Saccharomyces cerevisiae. *FEBS J* **278**: 764-775.

261.   Csaki, L. S., and K. Reue. 2010. Lipins: multifunctional lipid metabolism proteins. *Annu. Rev. Nutr.* **30**: 257-272.

262.   Carman, G. M., R. A. Deems, and E. A. Dennis. 1995. Lipid signaling enzymes and surface dilution kinetics. *J. Biol. Chem.* **270**: 18711-18714.

263.   Wu, W. I., Y. P. Lin, E. Wang, A. H. Merrill, Jr., and G. M. Carman. 1993. Regulation of phosphatidate phosphatase activity from the yeast Saccharomyces cerevisiae by sphingoid bases. *J. Biol. Chem.* **268**: 13830-13837.

264.   Wu, W. I., and G. M. Carman. 1996. Regulation of phosphatidate phosphatase activity from the yeast Saccharomyces cerevisiae by phospholipids. *Biochemistry (Mosc).* **35**: 3790-3796.

265.   Bowley, M., J. Cooling, S. L. Burditt, and D. N. Brindley. 1977. The effects of amphiphilic cationic drugs and inorganic cations on the activity of phosphatidate phosphohydrolase. *Biochem. J.* **165**: 447-454.

266.   Mitra, M. S., J. D. Schilling, X. Wang, P. Y. Jay, J. M. Huss, X. Su, and B. N. Finck. 2011. Cardiac lipin 1 expression is regulated by the peroxisome proliferator activated receptor gamma coactivator 1alpha/estrogen related receptor axis. *J. Mol. Cell. Cardiol.* **51**: 120-128.

267.   Bou Khalil, M., A. Blais, D. Figeys, and Z. Yao. 2010. Lipin - The bridge between hepatic glycerolipid biosynthesis and lipoprotein metabolism. *Biochim. Biophys. Acta* **1801**: 1249-1259.

268.   Phan, J., M. Peterfy, and K. Reue. 2004. Lipin expression preceding peroxisome proliferator-activated receptor-gamma is critical for adipogenesis in vivo and in vitro. *J. Biol. Chem.* **279**: 29558-29564.

269.   Koh, Y. K., M. Y. Lee, J. W. Kim, M. Kim, J. S. Moon, Y. J. Lee, Y. H. Ahn, and K. S. Kim. 2008. Lipin1 is a key factor for the maturation and maintenance of adipocytes in the regulatory network with CCAAT/enhancer-

binding protein alpha and peroxisome proliferator-activated receptor gamma 2. *J. Biol. Chem.* **283**: 34896-34906.

270.   Festuccia, W. T., P. G. Blanchard, V. Turcotte, M. Laplante, M. Sariahmetoglu, D. N. Brindley, and Y. Deshaies. 2009. Depot-specific effects of the PPARgamma agonist rosiglitazone on adipose tissue glucose uptake and metabolism. *J. Lipid Res.* **50**: 1185-1194.

271.   Zeharia, A., A. Shaag, R. H. Houtkooper, T. Hindi, P. de Lonlay, G. Erez, L. Hubert, A. Saada, Y. de Keyzer, G. Eshel, F. M. Vaz, O. Pines, and O. Elpeleg. 2008. Mutations in *LPIN1* cause recurrent acute myoglobinuria in childhood. *Am J Hum Genet* **83**: 489-494.

272.   Kim, H. B., A. Kumar, L. Wang, G. H. Liu, S. R. Keller, J. C. Lawrence, Jr., B. N. Finck, and T. E. Harris. 2010. Lipin 1 represses NFATc4 transcriptional activity in adipocytes to inhibit secretion of inflammatory factors. *Mol. Cell. Biol.* **30**: 3126-3139.

273.   Valdearcos, M., E. Esquinas, C. Meana, L. Pena, L. Gil-de-Gomez, J. Balsinde, and M. A. Balboa. 2012. Lipin-2 reduces proinflammatory signaling induced by saturated fatty acids in macrophages. *J. Biol. Chem.*

274.   Takahashi, N., T. Yoshizaki, N. Hiranaka, T. Suzuki, T. Yui, M. Akanuma, K. Oka, K. Kanazawa, M. Yoshida, S. Naito, M. Fujiya, Y. Kohgo, and M. Ieko. 2011. Suppression of lipin-1 expression increases monocyte chemoattractant protein-1 expression in 3T3-L1 adipocytes. *Biochem. Biophys. Res. Commun.* **415**: 200-205.

275.   Tsuchiya, Y., N. Takahashi, T. Yoshizaki, S. Tanno, M. Ohhira, W. Motomura, K. Takakusaki, Y. Kohgo, and T. Okumura. 2009. A Jak2 inhibitor, AG490, reverses lipin-1 suppression by TNF-alpha in 3T3-L1 adipocytes. *Biochem. Biophys. Res. Commun.* **382**: 348-352.

276.   Liu, G. H., and L. Gerace. 2009. Sumoylation regulates nuclear localization of lipin-1alpha in neuronal cells. *PLoS One* **4**: e7031.

277.   Xu, J., W. N. Lee, J. Phan, M. F. Saad, K. Reue, and I. J. Kurland. 2006. Lipin deficiency impairs diurnal metabolic fuel switching. *Diabetes* **55**: 3429-3438.

278.   Phan, J., and K. Reue. 2005. Lipin, a lipodystrophy and obesity gene. *Cell Metab.* **1**: 73-83.

279.   Mangiapane, E. H., K. A. Lloyd-Davies, and D. N. Brindley. 1973. A study of some enzymes of glycerolipid biosynthesis in rat liver after subtotal hepatectomy. *Biochem. J.* **134**: 103-112.

280.   Ryu, D., W. Y. Seo, Y. S. Yoon, Y. N. Kim, S. S. Kim, H. J. Kim, T. S. Park, C. S. Choi, and S. H. Koo. 2011. Endoplasmic reticulum stress promotes LIPIN2-dependent hepatic insulin resistance. *Diabetes* **60**: 1072-1081.

281.   Valdearcos, M., E. Esquinas, C. Meana, L. Gil-de-Gomez, C. Guijas, J. Balsinde, and M. A. Balboa. 2011. Subcellular localization and role of lipin-1 in human macrophages. *J. Immunol.* **186**: 6004-6013.

282.   Chen, Z., M. C. Gropler, J. Norris, J. C. Lawrence, Jr., T. E. Harris, and B. N. Finck. 2008. Alterations in hepatic metabolism in fld mice reveal a role for lipin 1 in regulating VLDL-triacylglyceride secretion. *Arterioscler. Thromb. Vac. Biol.* **28**: 1738-1744.

283.   Al-Mosawi, Z. S., K. K. Al-Saad, R. Ijadi-Maghsoodi, H. I. El-Shanti, and P. J. Ferguson. 2007. A splice site mutation confirms the role of LPIN2 in Majeed syndrome. *Arthritis Rheum.* **56**: 960-964.

284.   Ferguson, P. J., S. Chen, M. K. Tayeh, L. Ochoa, S. M. Leal, A. Pelet, A. Munnich, S. Lyonnet, H. A. Majeed, and H. El-Shanti. 2005. Homozygous mutations in LPIN2 are responsible for the syndrome of chronic recurrent multifocal osteomyelitis and congenital dyserythropoietic anaemia (Majeed syndrome). *J. Med. Genet.* **42**: 551-557.

285.   Nanjundan, M., and F. Possmayer. 2003. Pulmonary phosphatidic acid phosphatase and lipid phosphate phosphohydrolase. *Am J Physiol Lung Cell Mol Physiol* **284**: L1-23.

286.   Jiang, Y., Z. Lu, Q. Zang, and D. A. Foster. 1996. Regulation of phosphatidic acid phosphohydrolase by epidermal growth factor. Reduced association with the EGF receptor followed by increased association with protein kinase Cepsilon. *J. Biol. Chem.* **271**: 29529-29532.

287.   Grkovich, A., and E. A. Dennis. 2009. Phosphatidic acid phosphohydrolase in the regulation of inflammatory signaling. *Adv. Enzyme Regul.* **49**: 114-120.

288.   Grkovich, A., C. A. Johnson, M. W. Buczynski, and E. A. Dennis. 2006. Lipopolysaccharide-induced cyclooxygenase-2 expression in human U937 macrophages is phosphatidic acid phosphohydrolase-1-dependent. *J. Biol. Chem.* **281**: 32978-32987.

289.   Grkovich, A., A. Armando, O. Quehenberger, and E. A. Dennis. 2009. TLR-4 mediated group IVA phospholipase A(2) activation is phosphatidic acid phosphohydrolase 1 and protein kinase C dependent. *Biochim. Biophys. Acta* **1791**: 975-982.

290.   Fujita, K., M. Murakami, F. Yamashita, K. Amemiya, and I. Kudo. 1996. Phospholipase D is involved in cytosolic phospholipase A2-dependent selective release of arachidonic acid by fMLP-stimulated rat neutrophils. *FEBS Lett.* **395**: 293-298.

291.   Kitatani, K., S. Akiba, and T. Sato. 2000. Role of phospholipase D-derived phosphatidic acid as a substrate for phospholipase A2 in RBL-2H3 cells. *Biol. Pharm. Bull.* **23**: 1430-1433.

292.   Grimsey, N., G. S. Han, L. O'Hara, J. J. Rochford, G. M. Carman, and S. Siniossoglou. 2008. Temporal and spatial regulation of the phosphatidate phosphatases lipin 1 and 2. *J. Biol. Chem.* **283**: 29166-29174.

293.   Brindley, D. N. 1984. Intracellular translocation of phosphatidate phosphohydrolase and its possible role in the control of glycerolipid synthesis. *Prog. Lipid Res.* **23**: 115-133.

294.   Gómez-Muñoz, A., E. H. Hamza, and D. N. Brindley. 1992. Effects of sphingosine, albumin and unsaturated fatty acids on the activation and translocation of phosphatidate phosphohydrolases in rat hepatocytes. *Biochim. Biophys. Acta* **1127**: 49-56.

295.   Hopewell, R., P. Martin-Sanz, A. Martin, J. Saxton, and D. N. Brindley. 1985. Regulation of the translocation of phosphatidate phosphohydrolase

between the cytosol and the endoplasmic reticulum of rat liver. Effects of unsaturated fatty acids, spermine, nucleotides, albumin and chlorpromazine. *Biochem. J.* **232**: 485-491.

296. Cascales, C., E. H. Mangiapane, and D. N. Brindley. 1984. Oleic acid promotes the activation and translocation of phosphatidate phosphohydrolase from the cytosol to particulate fractions of isolated rat hepatocytes. *Biochem. J.* **219**: 911-916.

297. Brindley, D. N., and M. Bowley. 1975. Drugs affecting the synthesis of glycerides and phospholipids in rat liver. The effects of clofibrate, halofenate, fenfluramine, amphetamine, cinchocaine, chlorpromazine, demethylimipramine, mepyramine and some of their derivatives. *Biochem. J.* **148**: 461-469.

298. Martin, A., R. Hopewell, P. Martin-Sanz, J. E. Morgan, and D. N. Brindley. 1986. Relationship between the displacement of phosphatidate phosphohydrolase from the membrane-associated compartment by chlorpromazine and the inhibition of the synthesis of triacylglycerol and phosphatidylcholine in rat hepatocytes. *Biochim. Biophys. Acta* **876**: 581-591.

299. Brindley, D. N., D. Allan, and R. H. Michell. 1975. Letter: The redirection of glyceride and phospholipid synthesis by drugs including chlorpromazine, fenfluramine, imipramine, mepyramine and local anaesthetics. *J. Pharm. Pharmacol.* **27**: 462-464.

300. Michell, R. H., D. Allan, M. Bowley, and D. N. Brindley. 1976. A possible metabolic explanation for drug-induced phospholipidosis. *J. Pharm. Pharmacol.* **28**: 331-332.

301. Butterwith, S. C., A. Martin, and D. N. Brindley. 1984. Can phosphorylation of phosphatidate phosphohydrolase by a cyclic AMP-dependent mechanism regulate its activity and subcellular distribution and control hepatic glycerolipid synthesis? *Biochem. J.* **222**: 487-493.

302. Choi, H. S., W. M. Su, J. M. Morgan, G. S. Han, Z. Xu, E. Karanasios, S. Siniossoglou, and G. M. Carman. 2011. Phosphorylation of phosphatidate phosphatase regulates its membrane association and physiological functions in Saccharomyces cerevisiae: identification of SER(602), THR(723), AND SER(744) as the sites phosphorylated by CDC28 (CDK1)-encoded cyclin-dependent kinase. *J. Biol. Chem.* **286**: 1486-1498.

303. Martin-Sanz, P., R. Hopewell, and D. N. Brindley. 1984. Long-chain fatty acids and their acyl-CoA esters cause the translocation of phosphatidate phosphohydrolase from the cytosolic to the microsomal fraction of rat liver. *FEBS Lett.* **175**: 284-288.

304. Han, S., S. Bahmanyar, P. Zhang, N. Grishin, K. Oegema, R. Crooke, M. Graham, K. Reue, J. E. Dixon, and J. M. Goodman. 2012. Nuclear Envelope Phosphatase 1-Regulatory Subunit 1 (Formerly TMEM188) Is the Metazoan Spo7p Ortholog and Functions in the Lipin Activation Pathway. *J. Biol. Chem.* **287**: 3123-3137.

305. Kim, Y., M. S. Gentry, T. E. Harris, S. E. Wiley, J. C. Lawrence, Jr., and J. E. Dixon. 2007. A conserved phosphatase cascade that regulates nuclear membrane biogenesis. *Proc. Natl. Acad. Sci. U. S. A.* **104**: 6596-6601.

306.   Huffman, T. A., I. Mothe-Satney, and J. C. Lawrence, Jr. 2002. Insulin-stimulated phosphorylation of lipin mediated by the mammalian target of rapamycin. *Proc. Natl. Acad. Sci. U. S. A.* **99**: 1047-1052.

307.   Manmontri, B., M. Sariahmetoglu, J. Donkor, M. B. Khalil, M. Sundaram, Z. Yao, K. Reue, R. Lehner, and D. N. Brindley. 2008. Glucocorticoids and cyclic AMP selectively increase hepatic lipin-1 expression, and insulin acts antagonistically. *J. Lipid Res.* **49**: 1056-1067.

308.   Zhang, P., L. O'Loughlin, D. N. Brindley, and K. Reue. 2008. Regulation of lipin-1 gene expression by glucocorticoids during adipogenesis. *J. Lipid Res.* **49**: 1519-1528.

309.   Pearen, M. A., S. A. Myers, S. Raichur, J. G. Ryall, G. S. Lynch, and G. E. Muscat. 2008. The orphan nuclear receptor, NOR-1, a target of beta-adrenergic signaling, regulates gene expression that controls oxidative metabolism in skeletal muscle. *Endocrinology* **149**: 2853-2865.

310.   Ryu, D., K. J. Oh, H. Y. Jo, S. Hedrick, Y. N. Kim, Y. J. Hwang, T. S. Park, J. S. Han, C. S. Choi, M. Montminy, and S. H. Koo. 2009. TORC2 regulates hepatic insulin signaling via a mammalian phosphatidic acid phosphatase, LIPIN1. *Cell Metab.* **9**: 240-251.

311.   Koo, S. H., L. Flechner, L. Qi, X. Zhang, R. A. Screaton, S. Jeffries, S. Hedrick, W. Xu, F. Boussouar, P. Brindle, H. Takemori, and M. Montminy. 2005. The CREB coactivator TORC2 is a key regulator of fasting glucose metabolism. *Nature* **437**: 1109-1111.

312.   Dentin, R., Y. Liu, S. H. Koo, S. Hedrick, T. Vargas, J. Heredia, J. Yates, 3rd, and M. Montminy. 2007. Insulin modulates gluconeogenesis by inhibition of the coactivator TORC2. *Nature* **449**: 366-369.

313.   Ishimoto, K., H. Nakamura, K. Tachibana, D. Yamasaki, A. Ota, K. Hirano, T. Tanaka, T. Hamakubo, J. Sakai, T. Kodama, and T. Doi. 2009. Sterol-mediated regulation of human lipin 1 gene expression in hepatoblastoma cells. *J. Biol. Chem.* **284**: 22195-22205.

314.   Pritchard, P. H., J. Cooling, S. L. Burditt, and D. N. Brindley. 1979. Can the alterations in serum glucocorticoid concentrations explain the effects of ethanol and benfluorex on the synthesis of hepatic triacylglycerols? *J. Pharm. Pharmacol.* **31**: 406-407.

315.   Scheig, R., and K. J. Isselbacher. 1965. Pathogenesis of Ethanol-Induced Fatty Liver. 3. In Vivo and Vitro Effects of Ethanol on Hepatic Fatty Acid Metabolism in Rats. *J. Lipid Res.* **6**: 269-277.

316.   Mylonis, I., H. Sembongi, C. Befani, P. Liakos, S. Siniossoglou, and G. Simos. 2012. Hypoxia causes triglyceride accumulation via HIF-1-mediated stimulation of lipin 1 expression. *J. Cell Sci.*

317.   Assaily, W., D. A. Rubinger, K. Wheaton, Y. Lin, W. Ma, W. Xuan, L. Brown-Endres, K. Tsuchihara, T. W. Mak, and S. Benchimol. 2011. ROS-mediated p53 induction of Lpin1 regulates fatty acid oxidation in response to nutritional stress. *Mol. Cell* **44**: 491-501.

318. Hermier, D., P. Hales, and D. N. Brindley. 1991. Effects of the lipase inhibitors, Triton WR-1339 and tetrahydrolipstatin, on the synthesis and secretion of lipids by rat hepatocytes. *FEBS Lett.* **286**: 186-188.

319. Sturton, R. G., and D. N. Brindley. 1978. Problems encountered in measuring the activity of phosphatidate phosphohydrolase. *Biochem. J.* **171**: 263-266.

320. Butterwith, S. C., R. Hopewell, and D. N. Brindley. 1984. Partial purification and characterization of the soluble phosphatidate phosphohydrolase of rat liver. *Biochem. J.* **220**: 825-833.

321. Martin, A., A. Gómez-Muñoz, Z. Jamal, and D. N. Brindley. 1991. Characterization and assay of phosphatidate phosphatase. *Methods Enzymol.* **197**: 553-563.

322. Kovacic, S., C. L. Soltys, A. J. Barr, I. Shiojima, K. Walsh, and J. R. Dyck. 2003. Akt activity negatively regulates phosphorylation of AMP-activated protein kinase in the heart. *J. Biol. Chem.* **278**: 39422-39427.

323. Azuma, A., P. Huang, A. Matsuda, and W. Plunkett. 2001. 2'-C-cyano-2'-deoxy-1-beta-D-arabino-pentofuranosylcytosine: a novel anticancer nucleoside analog that causes both DNA strand breaks and G(2) arrest. *Mol. Pharmacol.* **59**: 725-731.

324. Yao, Z. M., and D. E. Vance. 1988. The active synthesis of phosphatidylcholine is required for very low density lipoprotein secretion from rat hepatocytes. *J. Biol. Chem.* **263**: 2998-3004.

325. Birnboim, H. C., and J. Doly. 1979. A rapid alkaline extraction procedure for screening recombinant plasmid DNA. *Nucleic Acids Res* **7**: 1513-1523.

326. Vogelstein, B., and D. Gillespie. 1979. Preparative and analytical purification of DNA from agarose. *Proc. Natl. Acad. Sci. U. S. A.* **76**: 615-619.

327. Houts, G. E., M. Miyagi, C. Ellis, D. Beard, and J. W. Beard. 1979. Reverse transcriptase from avian myeloblastosis virus. *J. Virol.* **29**: 517-522.

328. Blackburn, P. 1979. Ribonuclease inhibitor from human placenta: rapid purification and assay. *J. Biol. Chem.* **254**: 12484-12487.

329. Morris, K. E., L. M. Schang, and D. N. Brindley. 2006. Lipid phosphate phosphatase-2 activity regulates S-phase entry of the cell cycle in Rat2 fibroblasts. *J. Biol. Chem.* **281**: 9297-9306.

330. Wells, C. A., J. A. Salvage-Jones, X. Li, K. Hitchens, S. Butcher, R. Z. Murray, A. G. Beckhouse, Y. L. Lo, S. Manzanero, C. Cobbold, K. Schroder, B. Ma, S. Orr, L. Stewart, D. Lebus, P. Sobieszczuk, D. A. Hume, J. Stow, H. Blanchard, and R. B. Ashman. 2008. The macrophage-inducible C-type lectin, mincle, is an essential component of the innate immune response to Candida albicans. *J. Immunol.* **180**: 7404-7413.

331. Di-Poi, N., B. Desvergne, L. Michalik, and W. Wahli. 2005. Transcriptional repression of peroxisome proliferator-activated receptor beta/delta in murine keratinocytes by CCAAT/enhancer-binding proteins. *J. Biol. Chem.* **280**: 38700-38710.

332.   Yamashita, H., K. G. Bharadwaj, S. Ikeda, T. S. Park, and I. J. Goldberg. 2008. Cardiac metabolic compensation to hypertension requires lipoprotein lipase. *Am J Physiol Endocrinol Metab* **295**: E705-713.

333.   Reid, B. N., G. P. Ables, O. A. Otlivanchik, G. Schoiswohl, R. Zechner, W. S. Blaner, I. J. Goldberg, R. F. Schwabe, S. C. Chua, Jr., and L. S. Huang. 2008. Hepatic overexpression of hormone-sensitive lipase and adipose triglyceride lipase promotes fatty acid oxidation, stimulates direct release of free fatty acids, and ameliorates steatosis. *J. Biol. Chem.* **283**: 13087-13099.

334.   Tsuchiya, M., C. E. Tye, R. Sharma, C. E. Smith, and J. D. Bartlett. 2008. XBP1 may determine the size of the ameloblast endoplasmic reticulum. *J. Dent. Res.* **87**: 1058-1062.

335.   Babu, G. J., P. Bhupathy, N. N. Petrashevskaya, H. Wang, S. Raman, D. Wheeler, G. Jagatheesan, D. Wieczorek, A. Schwartz, P. M. Janssen, M. T. Ziolo, and M. Periasamy. 2006. Targeted overexpression of sarcolipin in the mouse heart decreases sarcoplasmic reticulum calcium transport and cardiac contractility. *J. Biol. Chem.* **281**: 3972-3979.

336.   Feingold, K. R., A. Moser, S. M. Patzek, J. K. Shigenaga, and C. Grunfeld. 2009. Infection decreases fatty acid oxidation and nuclear hormone receptors in the diaphragm. *J. Lipid Res.* **50**: 2055-2063.

337.   Chan, A. Y., C. L. Soltys, M. E. Young, C. G. Proud, and J. R. Dyck. 2004. Activation of AMP-activated protein kinase inhibits protein synthesis associated with hypertrophy in the cardiac myocyte. *J. Biol. Chem.* **279**: 32771-32779.

338.   Laemmli, U. K. 1970. Cleavage of structural proteins during the assembly of the head of bacteriophage T4. *Nature* **227**: 680-685.

339.   Mackall, J., M. Meredith, and M. D. Lane. 1979. A mild procedure for the rapid release of cytoplasmic enzymes from cultured animal cells. *Anal. Biochem.* **95**: 270-274.

340.   Zuurendonk, P. F., and J. M. Tager. 1974. Rapid separation of particulate components and soluble cytoplasm of isolated rat-liver cells. *Biochim. Biophys. Acta* **333**: 393-399.

341.   Schnaitman, C., and J. W. Greenawalt. 1968. Enzymatic properties of the inner and outer membranes of rat liver mitochondria. *J. Cell Biol.* **38**: 158-175.

342.   Saggerson, E. D., and A. L. Greenbaum. 1969. The effect of dietary and hormonal conditions on the activities of glycolytic enzymes in rat epididymal adipose tissue. *Biochem. J.* **115**: 405-417.

343.   Janski, A. M., and N. W. Cornell. 1980. Subcellular distribution of enzymes determined by rapid digitonin fractionation of isolated hepatocytes. *Biochem. J.* **186**: 423-429.

344.   de Domenech, E. M., C. E. Domenech, and A. Blanco. 1970. Distribution of lactate dehydrogenase isozymes in subcellular fractions of rat tissues. *Arch. Biochem. Biophys.* **141**: 147-154.

345.   Agostoni, A., C. Vergani, and L. Villa. 1966. Intracellular distribution of the different forms of lactic dehydrogenase. *Nature* **209**: 1024-1025.

346.   Kline, E. S., R. B. Brandt, J. E. Laux, S. E. Spainhour, E. S. Higgins, K. S. Rogers, S. B. Tinsley, and M. G. Waters. 1986. Localization of L-lactate dehydrogenase in mitochondria. *Arch. Biochem. Biophys.* **246**: 673-680.

347.   Graham, A., V. A. Zammit, and D. N. Brindley. 1988. Fatty acid specificity for the synthesis of triacylglycerol and phosphatidylcholine and for the secretion of very-low-density lipoproteins and lysophosphatidylcholine by cultures of rat hepatocytes. *Biochem. J.* **249**: 727-733.

348.   Graham, A., A. J. Bennett, A. A. McLean, V. A. Zammit, and D. N. Brindley. 1988. Factors regulating the secretion of lysophosphatidylcholine by rat hepatocytes compared with the synthesis and secretion of phosphatidylcholine and triacylglycerol. Effects of albumin, cycloheximide, verapamil, EGTA and chlorpromazine. *Biochem. J.* **253**: 687-692.

349.   Pilquil, C., J. Dewald, A. Cherney, I. Gorshkova, G. Tigyi, D. English, V. Natarajan, and D. N. Brindley. 2006. Lipid phosphate phosphatase-1 regulates lysophosphatidate-induced fibroblast migration by controlling phospholipase D2-dependent phosphatidate generation. *J. Biol. Chem.* **281**: 38418-38429.

350.   Mangiapane, E. H., and D. N. Brindley. 1986. Effects of dexamethasone and insulin on the synthesis of triacylglycerols and phosphatidylcholine and the secretion of very-low-density lipoproteins and lysophosphatidylcholine by monolayer cultures of rat hepatocytes. *Biochem. J.* **233**: 151-160.

351.   Martin, A., P. A. Duffy, C. Liossis, A. Gómez-Muñoz, L. O'Brien, J. C. Stone, and D. N. Brindley. 1997. Increased concentrations of phosphatidate, diacylglycerol and ceramide in ras- and tyrosine kinase (fps)-transformed fibroblasts. *Oncogene* **14**: 1571-1580.

352.   Dolinsky, V. W., J. S. Morton, T. Oka, I. Robillard-Frayne, M. Bagdan, G. D. Lopaschuk, C. Des Rosiers, K. Walsh, S. T. Davidge, and J. R. Dyck. 2010. Calorie restriction prevents hypertension and cardiac hypertrophy in the spontaneously hypertensive rat. *Hypertension* **56**: 412-421.

353.   Sung, M. M., D. P. Koonen, C. L. Soltys, R. L. Jacobs, M. Febbraio, and J. R. Dyck. 2011. Increased CD36 expression in middle-aged mice contributes to obesity-related cardiac hypertrophy in the absence of cardiac dysfunction. *J Mol Med (Berl)* **89**: 459-469.

354.   Teichholz, L. E., T. Kreulen, M. V. Herman, and R. Gorlin. 1976. Problems in echocardiographic volume determinations: echocardiographic-angiographic correlations in the presence of absence of asynergy. *Am. J. Cardiol.* **37**: 7-11.

355.   Tei, C., L. H. Ling, D. O. Hodge, K. R. Bailey, J. K. Oh, R. J. Rodeheffer, A. J. Tajik, and J. B. Seward. 1995. New index of combined systolic and diastolic myocardial performance: a simple and reproducible measure of cardiac function--a study in normals and dilated cardiomyopathy. *J. Cardiol.* **26**: 357-366.

356.   Trinder, P. 1969. Determination of blood glucose using 4-amino phenazone as oxygen acceptor. *J. Clin. Pathol.* **22**: 246.

357.   Trinder, P. 1969. Determination of blood glucose using an oxidase-peroxidase system with a non-carcinogenic chromogen. *J. Clin. Pathol.* **22**: 158-161.

358.   Megraw, R. E., D. E. Dunn, and H. G. Biggs. 1979. Manual and continuous-flow colorimetry of triacylglycerols by a fully enzymic method. *Clin. Chem.* **25**: 273-278.

359.   Bell, R. M., M. M. Mocanu, and D. M. Yellon. 2011. Retrograde heart perfusion: the Langendorff technique of isolated heart perfusion. *J. Mol. Cell. Cardiol.* **50**: 940-950.

360.   Larsen, T. S., D. D. Belke, R. Sas, W. R. Giles, D. L. Severson, G. D. Lopaschuk, and J. V. Tyberg. 1999. The isolated working mouse heart: methodological considerations. *Pflugers Arch.* **437**: 979-985.

361.   Zimmer, H. G. 1998. The Isolated Perfused Heart and Its Pioneers. *News Physiol Sci* **13**: 203-210.

362.   Skrzypiec-Spring, M., B. Grotthus, A. Szelag, and R. Schulz. 2007. Isolated heart perfusion according to Langendorff---still viable in the new millennium. *J Pharmacol Toxicol Methods* **55**: 113-126.

363.   Belke, D. D., T. S. Larsen, G. D. Lopaschuk, and D. L. Severson. 1999. Glucose and fatty acid metabolism in the isolated working mouse heart. *Am. J. Physiol.* **277**: R1210-1217.

364.   Kuang, M., M. Febbraio, C. Wagg, G. D. Lopaschuk, and J. R. Dyck. 2004. Fatty acid translocase/CD36 deficiency does not energetically or functionally compromise hearts before or after ischemia. *Circulation* **109**: 1550-1557.

365.   Jaswal, J. S., M. Gandhi, B. A. Finegan, J. R. Dyck, and A. S. Clanachan. 2007. Inhibition of p38 MAPK and AMPK restores adenosine-induced cardioprotection in hearts stressed by antecedent ischemia by altering glucose utilization. *Am J Physiol Heart Circ Physiol* **293**: H1107-1114.

366.   Kates, M. 1972. Techniques of Lipidology: isolation, analysis and identification of lipids. North-Holland Publishing Company, Amsterdam.

367.   de Leiris, J., D. P. Harding, and S. Pestre. 1984. The isolated perfused rat heart: a model for studying myocardial hypoxia or ischaemia. *Basic Res. Cardiol.* **79**: 313-321.

368.   Fraser, H., G. D. Lopaschuk, and A. S. Clanachan. 1998. Assessment of glycogen turnover in aerobic, ischemic, and reperfused working rat hearts. *Am. J. Physiol.* **275**: H1533-1541.

369.   Brindley, D. N., M. Bowley, R. G. Sturton, P. H. Pritchard, S. L. Burditt, and J. Cooling. 1977. The control of phosphatidate metabolism by amphiphilic drugs and by bivalent cations. *Biochem. Soc. Trans.* **5**: 40-43.

370.   Cole, C., J. D. Barber, and G. J. Barton. 2008. The Jpred 3 secondary structure prediction server. *Nucleic Acids Res* **36**: W197-201.

371.   Ceulemans, H., and M. Bollen. 2004. Functional diversity of protein phosphatase-1, a cellular economizer and reset button. *Physiol. Rev.* **84**: 1-39.

372.   Karanasios, E., G. S. Han, Z. Xu, G. M. Carman, and S. Siniossoglou. 2010. A phosphorylation-regulated amphipathic helix controls the membrane translocation and function of the yeast phosphatidate phosphatase. *Proc. Natl. Acad. Sci. U. S. A.* **107**: 17539-17544.

373. Sobell, H. M. 1985. Actinomycin and DNA transcription. *Proc. Natl. Acad. Sci. U. S. A.* **82**: 5328-5331.

374. Kok, B. P., P. C. Kienesberger, J. R. Dyck, and D. N. Brindley. 2012. Relationship of glucose and oleate metabolism to cardiac function in lipin-1 deficient (fld) mice. *J. Lipid Res.* **53**: 105-118.

375. Croce, M. A., J. C. Eagon, L. L. LaRiviere, K. M. Korenblat, S. Klein, and B. N. Finck. 2007. Hepatic lipin 1beta expression is diminished in insulin-resistant obese subjects and is reactivated by marked weight loss. *Diabetes* **56**: 2395-2399.

376. Donkor, J., L. M. Sparks, H. Xie, S. R. Smith, and K. Reue. 2008. Adipose tissue lipin-1 expression is correlated with peroxisome proliferator-activated receptor alpha gene expression and insulin sensitivity in healthy young men. *J. Clin. Endocrinol. Metab.* **93**: 233-239.

377. Lindegaard, B., L. F. Larsen, A. B. Hansen, J. Gerstoft, B. K. Pedersen, and K. Reue. 2007. Adipose tissue lipin expression levels distinguish HIV patients with and without lipodystrophy. *Int J Obes (Lond)* **31**: 449-456.

378. Burgdorf, C., L. Hansel, M. Heidbreder, O. Johren, F. Schutte, H. Schunkert, and T. Kurz. 2009. Suppression of cardiac phosphatidate phosphohydrolase 1 activity and lipin mRNA expression in Zucker diabetic fatty rats and humans with type 2 diabetes mellitus. *Biochem. Biophys. Res. Commun.* **390**: 165-170.

379. Chang, Y. C., L. Y. Chang, T. J. Chang, Y. D. Jiang, K. C. Lee, S. S. Kuo, W. J. Lee, and L. M. Chuang. 2010. The associations of LPIN1 gene expression in adipose tissue with metabolic phenotypes in the Chinese population. *Obesity (Silver Spring)* **18**: 7-12.

380. Jamal, Z., A. Martin, A. Gómez-Muñoz, P. Hales, E. Chang, J. C. Russell, and D. N. Brindley. 1992. Phosphatidate phosphohydrolases in liver, heart and adipose tissue of the JCR:LA corpulent rat and the lean genotypes: implications for glycerolipid synthesis and signal transduction. *Int. J. Obes. Relat. Metab. Disord.* **16**: 789-799.

381. Lu, B., Y. Lu, A. H. Moser, J. K. Shigenaga, C. Grunfeld, and K. R. Feingold. 2008. LPS and proinflammatory cytokines decrease lipin-1 in mouse adipose tissue and 3T3-L1 adipocytes. *Am J Physiol Endocrinol Metab* **295**: E1502-1509.

382. Yoon, J. C., P. Puigserver, G. Chen, J. Donovan, Z. Wu, J. Rhee, G. Adelmant, J. Stafford, C. R. Kahn, D. K. Granner, C. B. Newgard, and B. M. Spiegelman. 2001. Control of hepatic gluconeogenesis through the transcriptional coactivator PGC-1. *Nature* **413**: 131-138.

383. Herzig, S., F. Long, U. S. Jhala, S. Hedrick, R. Quinn, A. Bauer, D. Rudolph, G. Schutz, C. Yoon, P. Puigserver, B. Spiegelman, and M. Montminy. 2001. CREB regulates hepatic gluconeogenesis through the coactivator PGC-1. *Nature* **413**: 179-183.

384. Chinsomboon, J., J. Ruas, R. K. Gupta, R. Thom, J. Shoag, G. C. Rowe, N. Sawada, S. Raghuram, and Z. Arany. 2009. The transcriptional coactivator PGC-1alpha mediates exercise-induced angiogenesis in skeletal muscle. *Proc. Natl. Acad. Sci. U. S. A.* **106**: 21401-21406.

385.   Miura, S., Y. Kai, Y. Kamei, and O. Ezaki. 2008. Isoform-specific increases in murine skeletal muscle peroxisome proliferator-activated receptor-gamma coactivator-1alpha (PGC-1alpha) mRNA in response to beta2-adrenergic receptor activation and exercise. *Endocrinology* **149**: 4527-4533.

386.   Xiao, R. P., X. Ji, and E. G. Lakatta. 1995. Functional coupling of the beta 2-adrenoceptor to a pertussis toxin-sensitive G protein in cardiac myocytes. *Mol. Pharmacol.* **47**: 322-329.

387.   Xiao, R. P., W. Zhu, M. Zheng, C. Cao, Y. Zhang, E. G. Lakatta, and Q. Han. 2006. Subtype-specific alpha1- and beta-adrenoceptor signaling in the heart. *Trends Pharmacol. Sci.* **27**: 330-337.

388.   Xiao, R. P. 2001. Beta-adrenergic signaling in the heart: dual coupling of the beta2-adrenergic receptor to G(s) and G(i) proteins. *Sci STKE* **2001**: re15.

389.   Gosmanov, A. R., J. A. Wong, and D. B. Thomason. 2002. Duality of G protein-coupled mechanisms for beta-adrenergic activation of NKCC activity in skeletal muscle. *Am J Physiol Cell Physiol* **283**: C1025-1032.

390.   Zhu, W. Z., M. Zheng, W. J. Koch, R. J. Lefkowitz, B. K. Kobilka, and R. P. Xiao. 2001. Dual modulation of cell survival and cell death by beta(2)-adrenergic signaling in adult mouse cardiac myocytes. *Proc. Natl. Acad. Sci. U. S. A.* **98**: 1607-1612.

391.   Chesley, A., M. S. Lundberg, T. Asai, R. P. Xiao, S. Ohtani, E. G. Lakatta, and M. T. Crow. 2000. The beta(2)-adrenergic receptor delivers an antiapoptotic signal to cardiac myocytes through G(i)-dependent coupling to phosphatidylinositol 3'-kinase. *Circ. Res.* **87**: 1172-1179.

392.   Daaka, Y., L. M. Luttrell, and R. J. Lefkowitz. 1997. Switching of the coupling of the beta2-adrenergic receptor to different G proteins by protein kinase A. *Nature* **390**: 88-91.

393.   Kersten, S., J. Seydoux, J. M. Peters, F. J. Gonzalez, B. Desvergne, and W. Wahli. 1999. Peroxisome proliferator-activated receptor alpha mediates the adaptive response to fasting. *J. Clin. Invest.* **103**: 1489-1498.

394.   Escher, P., O. Braissant, S. Basu-Modak, L. Michalik, W. Wahli, and B. Desvergne. 2001. Rat PPARs: quantitative analysis in adult rat tissues and regulation in fasting and refeeding. *Endocrinology* **142**: 4195-4202.

395.   Van der Lee, K. A., P. H. Willemsen, S. Samec, J. Seydoux, A. G. Dulloo, M. M. Pelsers, J. F. Glatz, G. J. Van der Vusse, and M. Van Bilsen. 2001. Fasting-induced changes in the expression of genes controlling substrate metabolism in the rat heart. *J. Lipid Res.* **42**: 1752-1758.

396.   Keller, H., C. Dreyer, J. Medin, A. Mahfoudi, K. Ozato, and W. Wahli. 1993. Fatty acids and retinoids control lipid metabolism through activation of peroxisome proliferator-activated receptor-retinoid X receptor heterodimers. *Proc. Natl. Acad. Sci. U. S. A.* **90**: 2160-2164.

397.   Gilde, A. J., K. A. van der Lee, P. H. Willemsen, G. Chinetti, F. R. van der Leij, G. J. van der Vusse, B. Staels, and M. van Bilsen. 2003. Peroxisome proliferator-activated receptor (PPAR) alpha and PPARbeta/delta, but not PPARgamma, modulate the expression of genes involved in cardiac lipid metabolism. *Circ. Res.* **92**: 518-524.

398.   Barrero, M. J., N. Camarero, P. F. Marrero, and D. Haro. 2003. Control of human carnitine palmitoyltransferase II gene transcription by peroxisome proliferator-activated receptor through a partially conserved peroxisome proliferator-responsive element. *Biochem. J.* **369**: 721-729.

399.   Mascaro, C., E. Acosta, J. A. Ortiz, P. F. Marrero, F. G. Hegardt, and D. Haro. 1998. Control of human muscle-type carnitine palmitoyltransferase I gene transcription by peroxisome proliferator-activated receptor. *J. Biol. Chem.* **273**: 8560-8563.

400.   Brandt, J. M., F. Djouadi, and D. P. Kelly. 1998. Fatty acids activate transcription of the muscle carnitine palmitoyltransferase I gene in cardiac myocytes via the peroxisome proliferator-activated receptor alpha. *J. Biol. Chem.* **273**: 23786-23792.

401.   Baldan, A., J. Relat, P. F. Marrero, and D. Haro. 2004. Functional interaction between peroxisome proliferator-activated receptors-alpha and Mef-2C on human carnitine palmitoyltransferase 1beta (CPT1beta) gene activation. *Nucleic Acids Res* **32**: 4742-4749.

402.   Moore, M. L., G. L. Wang, N. S. Belaguli, R. J. Schwartz, and J. B. McMillin. 2001. GATA-4 and serum response factor regulate transcription of the muscle-specific carnitine palmitoyltransferase I beta in rat heart. *J. Biol. Chem.* **276**: 1026-1033.

403.   Puigserver, P., J. Rhee, J. Donovan, C. J. Walkey, J. C. Yoon, F. Oriente, Y. Kitamura, J. Altomonte, H. Dong, D. Accili, and B. M. Spiegelman. 2003. Insulin-regulated hepatic gluconeogenesis through FOXO1-PGC-1alpha interaction. *Nature* **423**: 550-555.

404.   He, L., A. Sabet, S. Djedjos, R. Miller, X. Sun, M. A. Hussain, S. Radovick, and F. E. Wondisford. 2009. Metformin and insulin suppress hepatic gluconeogenesis through phosphorylation of CREB binding protein. *Cell* **137**: 635-646.

405.   Nasrin, N., S. Ogg, C. M. Cahill, W. Biggs, S. Nui, J. Dore, D. Calvo, Y. Shi, G. Ruvkun, and M. C. Alexander-Bridges. 2000. DAF-16 recruits the CREB-binding protein coactivator complex to the insulin-like growth factor binding protein 1 promoter in HepG2 cells. *Proc. Natl. Acad. Sci. U. S. A.* **97**: 10412-10417.

406.   Guo, S., G. Rena, S. Cichy, X. He, P. Cohen, and T. Unterman. 1999. Phosphorylation of serine 256 by protein kinase B disrupts transactivation by FKHR and mediates effects of insulin on insulin-like growth factor-binding protein-1 promoter activity through a conserved insulin response sequence. *J. Biol. Chem.* **274**: 17184-17192.

407.   Zhou, X. Y., N. Shibusawa, K. Naik, D. Porras, K. Temple, H. Ou, K. Kaihara, M. W. Roe, M. J. Brady, and F. E. Wondisford. 2004. Insulin regulation of hepatic gluconeogenesis through phosphorylation of CREB-binding protein. *Nat. Med.* **10**: 633-637.

408.   Wolfrum, C., D. Besser, E. Luca, and M. Stoffel. 2003. Insulin regulates the activity of forkhead transcription factor Hnf-3beta/Foxa-2 by Akt-mediated phosphorylation and nuclear/cytosolic localization. *Proc. Natl. Acad. Sci. U. S. A.* **100**: 11624-11629.

409.   Wolfrum, C., E. Asilmaz, E. Luca, J. M. Friedman, and M. Stoffel. 2004. Foxa2 regulates lipid metabolism and ketogenesis in the liver during fasting and in diabetes. *Nature* **432**: 1027-1032.

410.   O'Brien, R. M., E. L. Noisin, A. Suwanichkul, T. Yamasaki, P. C. Lucas, J. C. Wang, D. R. Powell, and D. K. Granner. 1995. Hepatic nuclear factor 3- and hormone-regulated expression of the phosphoenolpyruvate carboxykinase and insulin-like growth factor-binding protein 1 genes. *Mol. Cell. Biol.* **15**: 1747-1758.

411.   Wolfrum, C., and M. Stoffel. 2006. Coactivation of Foxa2 through Pgc-1beta promotes liver fatty acid oxidation and triglyceride/VLDL secretion. *Cell Metab.* **3**: 99-110.

412.   Kim, D. K., J. R. Kim, M. Koh, Y. D. Kim, J. M. Lee, D. Chanda, S. B. Park, J. J. Min, C. H. Lee, T. S. Park, and H. S. Choi. 2011. Estrogen-related receptor gamma (ERRgamma) is a novel transcriptional regulator of phosphatidic acid phosphatase, LIPIN1, and inhibits hepatic insulin signaling. *J. Biol. Chem.* **286**: 38035-38042.

413.   Chen, Z., J. Y. Norris, and B. N. Finck. 2010. Peroxisome proliferator-activated receptor-gamma coactivator-1alpha (PGC-1alpha) stimulates VLDL assembly through activation of cell death-inducing DFFA-like effector B (CideB). *J. Biol. Chem.* **285**: 25996-26004.

414.   Grunnet, N., and F. Lundquist. 1967. Kinetics of glycerol kinases from mammalian liver and Candida mycoderma. *Eur. J. Biochem.* **3**: 78-84.

415.   Robinson, J., and E. A. Newsholme. 1969. Some properties of hepatic glycerol kinase and their relation to the control of glycerol utilization. *Biochem. J.* **112**: 455-464.

416.   Newsholme, E. A., and K. Taylor. 1969. Glycerol kinase activities in muscles from vertebrates and invertebrates. *Biochem. J.* **112**: 465-474.

417.   Ko, K. W., B. Erickson, and R. Lehner. 2009. Es-x/Ces1 prevents triacylglycerol accumulation in McArdle-RH7777 hepatocytes. *Biochim. Biophys. Acta* **1791**: 1133-1143.

418.   Manning, R., and D. N. Brindley. 1972. Tritium isotope effects in the measurement of the glycerol phosphate and dihydroxyacetone phosphate pathways of glycerolipid biosynthesis in rat liver. *Biochem. J.* **130**: 1003-1012.

419.   Carnicero, H. H., C. L. Moore, and H. D. Hoberman. 1972. Oxidation of glycerol 3-phosphate by the perfused rat liver. *J. Biol. Chem.* **247**: 418-426.

420.   Bojesen, I. N., and E. Bojesen. 1994. Binding of arachidonate and oleate to bovine serum albumin. *J. Lipid Res.* **35**: 770-778.

421.   Spector, A. A. 1975. Fatty acid binding to plasma albumin. *J. Lipid Res.* **16**: 165-179.

422.   Richieri, G. V., A. Anel, and A. M. Kleinfeld. 1993. Interactions of long-chain fatty acids and albumin: determination of free fatty acid levels using the fluorescent probe ADIFAB. *Biochemistry (Mosc).* **32**: 7574-7580.

423.   Harris, T. E., and B. N. Finck. 2011. Dual function lipin proteins and glycerolipid metabolism. *Trends Endocrinol Metab* **22**: 226-233.

424.   Brindley, D. N. 2004. Lipid phosphate phosphatases and related proteins: signaling functions in development, cell division, and cancer. *J. Cell. Biochem.* **92**: 900-912.

425.   Linn, T. C., F. H. Pettit, F. Hucho, and L. J. Reed. 1969. Alpha-keto acid dehydrogenase complexes. XI. Comparative studies of regulatory properties of the pyruvate dehydrogenase complexes from kidney, heart, and liver mitochondria. *Proc. Natl. Acad. Sci. U. S. A.* **64**: 227-234.

426.   Listenberger, L. L., X. Han, S. E. Lewis, S. Cases, R. V. Farese, Jr., D. S. Ory, and J. E. Schaffer. 2003. Triglyceride accumulation protects against fatty acid-induced lipotoxicity. *Proc. Natl. Acad. Sci. U. S. A.* **100**: 3077-3082.

427.   Ostrander, D. B., G. C. Sparagna, A. A. Amoscato, J. B. McMillin, and W. Dowhan. 2001. Decreased cardiolipin synthesis corresponds with cytochrome c release in palmitate-induced cardiomyocyte apoptosis. *J. Biol. Chem.* **276**: 38061-38067.

428.   Vasdev, S. C., and K. J. Kako. 1977. Incorporation of fatty acids into rat heart lipids. In vivo and in vitro studies. *J. Mol. Cell. Cardiol.* **9**: 617-631.

429.   Reibel, D. K., B. O'Rourke, K. A. Foster, H. Hutchinson, C. E. Uboh, and R. L. Kent. 1986. Altered phospholipid metabolism in pressure-overload hypertrophied hearts. *Am. J. Physiol.* **250**: H1-6.

430.   O'Neil, T. K., L. R. Duffy, J. W. Frey, and T. A. Hornberger. 2009. The role of phosphoinositide 3-kinase and phosphatidic acid in the regulation of mammalian target of rapamycin following eccentric contractions. *J Physiol* **587**: 3691-3701.

431.   Fang, Y., M. Vilella-Bach, R. Bachmann, A. Flanigan, and J. Chen. 2001. Phosphatidic acid-mediated mitogenic activation of mTOR signaling. *Science* **294**: 1942-1945.

432.   Sengupta, S., T. R. Peterson, and D. M. Sabatini. 2010. Regulation of the mTOR complex 1 pathway by nutrients, growth factors, and stress. *Mol. Cell* **40**: 310-322.

433.   Wullschleger, S., R. Loewith, and M. N. Hall. 2006. TOR signaling in growth and metabolism. *Cell* **124**: 471-484.

434.   Bachar, E., Y. Ariav, M. Ketzinel-Gilad, E. Cerasi, N. Kaiser, and G. Leibowitz. 2009. Glucose amplifies fatty acid-induced endoplasmic reticulum stress in pancreatic beta-cells via activation of mTORC1. *PLoS One* **4**: e4954.

435.   Ozcan, U., L. Ozcan, E. Yilmaz, K. Duvel, M. Sahin, B. D. Manning, and G. S. Hotamisligil. 2008. Loss of the tuberous sclerosis complex tumor suppressors triggers the unfolded protein response to regulate insulin signaling and apoptosis. *Mol. Cell* **29**: 541-551.

436.   Calfon, M., H. Zeng, F. Urano, J. H. Till, S. R. Hubbard, H. P. Harding, S. G. Clark, and D. Ron. 2002. IRE1 couples endoplasmic reticulum load to secretory capacity by processing the XBP-1 mRNA. *Nature* **415**: 92-96.

437.   Xu, H. E., M. H. Lambert, V. G. Montana, D. J. Parks, S. G. Blanchard, P. J. Brown, D. D. Sternbach, J. M. Lehmann, G. B. Wisely, T. M. Willson, S. A. Kliewer, and M. V. Milburn. 1999. Molecular Recognition of Fatty Acids by Peroxisome Proliferator Activated Receptors **3**: 397-403.

438.   Gloster, J., M. Achillea, and P. Harris. 1978. Subcellular distribution of [1-^{14}C]palmitate and [1-^{14}C]oleate incorporated into lipids in the perfused rat heart: a comparison under isothermal and hypothermic conditions. *J. Mol. Cell. Cardiol.* **10**: 439-448.

439.   Hvattum, E., S. Uran, A. G. Sandbaek, A. A. Karlsson, and T. Skotland. 2006. Quantification of phosphatidylserine, phosphatidic acid and free fatty acids in an ultrasound contrast agent by normal-phase high-performance liquid chromatography with evaporative light scattering detection. *J. Pharm. Biomed. Anal.* **42**: 506-512.

440.   Stith, B. J., J. Hall, P. Ayres, L. Waggoner, J. D. Moore, and W. A. Shaw. 2000. Quantification of major classes of Xenopus phospholipids by high performance liquid chromatography with evaporative light scattering detection. *J. Lipid Res.* **41**: 1448-1454.

441.   Boluyt, M. O., Z. B. Li, A. M. Loyd, A. F. Scalia, G. M. Cirrincione, and R. R. Jackson. 2004. The mTOR/p70S6K signal transduction pathway plays a role in cardiac hypertrophy and influences expression of myosin heavy chain genes in vivo. *Cardiovasc. Drugs Ther.* **18**: 257-267.

442.   Inoki, K., H. Mori, J. Wang, T. Suzuki, S. Hong, S. Yoshida, S. M. Blattner, T. Ikenoue, M. A. Ruegg, M. N. Hall, D. J. Kwiatkowski, M. P. Rastaldi, T. B. Huber, M. Kretzler, L. B. Holzman, R. C. Wiggins, and K. L. Guan. 2011. mTORC1 activation in podocytes is a critical step in the development of diabetic nephropathy in mice. *J. Clin. Invest.* **121**: 2181-2196.

443.   Duvel, K., J. L. Yecies, S. Menon, P. Raman, A. I. Lipovsky, A. L. Souza, E. Triantafellow, Q. Ma, R. Gorski, S. Cleaver, M. G. Vander Heiden, J. P. MacKeigan, P. M. Finan, C. B. Clish, L. O. Murphy, and B. D. Manning. 2010. Activation of a metabolic gene regulatory network downstream of mTOR complex 1. *Mol. Cell* **39**: 171-183.

444.   Miura, S., K. Kawanaka, Y. Kai, M. Tamura, M. Goto, T. Shiuchi, Y. Minokoshi, and O. Ezaki. 2007. An increase in murine skeletal muscle peroxisome proliferator-activated receptor-gamma coactivator-1alpha (PGC-1alpha) mRNA in response to exercise is mediated by beta-adrenergic receptor activation. *Endocrinology* **148**: 3441-3448.

445.   Zhang, W., S. Patil, B. Chauhan, S. Guo, D. R. Powell, J. Le, A. Klotsas, R. Matika, X. Xiao, R. Franks, K. A. Heidenreich, M. P. Sajan, R. V. Farese, D. B. Stolz, P. Tso, S. H. Koo, M. Montminy, and T. G. Unterman. 2006. FoxO1 regulates multiple metabolic pathways in the liver: effects on gluconeogenic, glycolytic, and lipogenic gene expression. *J. Biol. Chem.* **281**: 10105-10117.

446.   Andreassen, P. R., F. B. Lacroix, E. Villa-Moruzzi, and R. L. Margolis. 1998. Differential subcellular localization of protein phosphatase-1 alpha, gamma1, and delta isoforms during both interphase and mitosis in mammalian cells. *J. Cell Biol.* **141**: 1207-1215.

447.   Trinkle-Mulcahy, L., J. E. Sleeman, and A. I. Lamond. 2001. Dynamic targeting of protein phosphatase 1 within the nuclei of living mammalian cells. *J. Cell Sci.* **114**: 4219-4228.

448.   Jang, J. H., C. S. Lee, D. Hwang, and S. H. Ryu. 2012. Understanding of the roles of phospholipase D and phosphatidic acid through their binding partners. *Prog. Lipid Res.* **51**: 71-81.

449.   Brindley, D. N., and C. Pilquil. 2009. Lipid phosphate phosphatases and signaling. *J. Lipid Res.* **50 Suppl**: S225-230.

450.   Cogan, E. B., G. B. Birrell, and O. H. Griffith. 1999. A robotics-based automated assay for inorganic and organic phosphates. *Anal. Biochem.* **271**: 29-35.

451.   Havriluk, T., F. Lozy, S. Siniossoglou, and G. M. Carman. 2008. Colorimetric determination of pure Mg^{2+}-dependent phosphatidate phosphatase activity. *Anal. Biochem.* **373**: 392-394.

452.   Kooijman, E. E., K. M. Carter, E. G. van Laar, V. Chupin, K. N. Burger, and B. de Kruijff. 2005. What makes the bioactive lipids phosphatidic acid and lysophosphatidic acid so special? *Biochemistry (Mosc).* **44**: 17007-17015.

453.   Abramson, M. B., R. Katzman, C. E. Wilson, and H. P. Gregor. 1964. Ionic Properties of Aqueous Dispersions of Phosphatidic Acid. *J. Biol. Chem.* **239**: 4066-4072.

APPENDIX I

OPTIMIZATION OF THE PHOSPHATIDATE PHOSPHATASE ACTIVITY IN

***FLD* HEARTS AND THE DEVELOPMENT OF THE MALACHITE GREEN-**

BASED PHOSPHATIDATE PHOSPHATASE ASSAY

1 Introduction

The phosphatidate phosphatase (PAP) assay was designed by our group as a sensitive method of measuring the PAP activities in cell lysates and tissue homogenates before the identity of the PAP enzyme was discovered (212, 319-321). After the lipins were discovered to act as PAP enzymes (134, 248), Harris et al. measured little to no PAP activity in various organs of the lipin-1 deficient *fld* mice, including the heart (241). However, it was unclear how these results could be correct since PAP catalyzes an essential step in the glycerolipid biosynthesis, which would be required for the turnover of PC and PE in the heart. Furthermore, there were no developmental abnormalities in these mice. Since our assay system is different from that used by Harris et al., we determined whether we would obtain similar measurements.

2 Effects of different polyvalent cations and Tween-20 on PAP activity in *fld* hearts

Initial attempts at measuring PAP activities in lipin-1 deficient (*fld*) hearts showed similar results to those found previously (241). There was essentially no Mg^{2+}-dependent PAP activity in the *fld* hearts when assayed under standard conditions at pH 6.5 using PA/PC liposomes and 5 mM $MgCl_2$ (Figure 1A). One exception to the protocol described in Section 2.2.3 was the inclusion of Tween-20, which had previously been shown to increase PAP activity (320). We wanted to determine whether the inability to detect PAP activity in *fld* hearts was due to limitations in the assay system or a preferential requirement for other cations in measuring lipin-2 and/or -3 catalytic activity in the absence of lipin-1 activity.
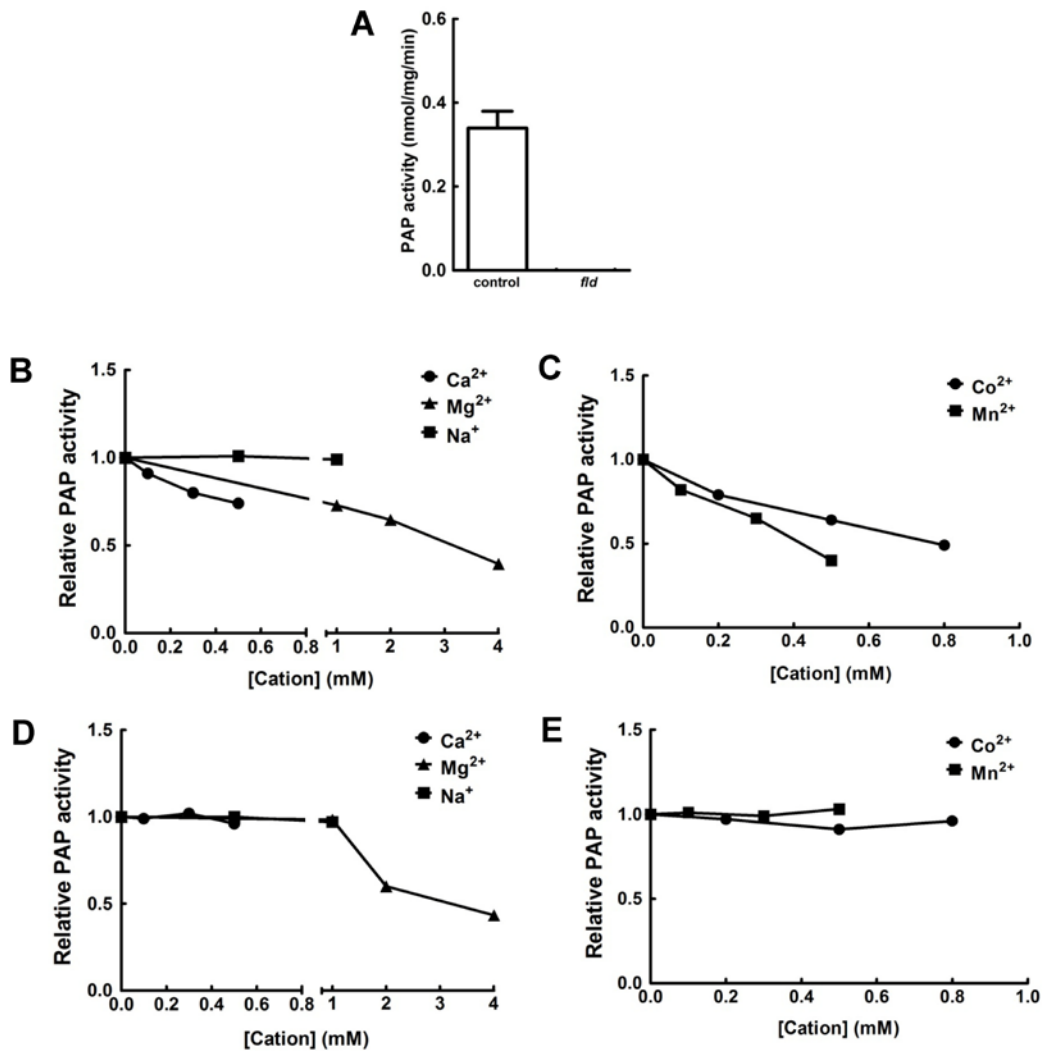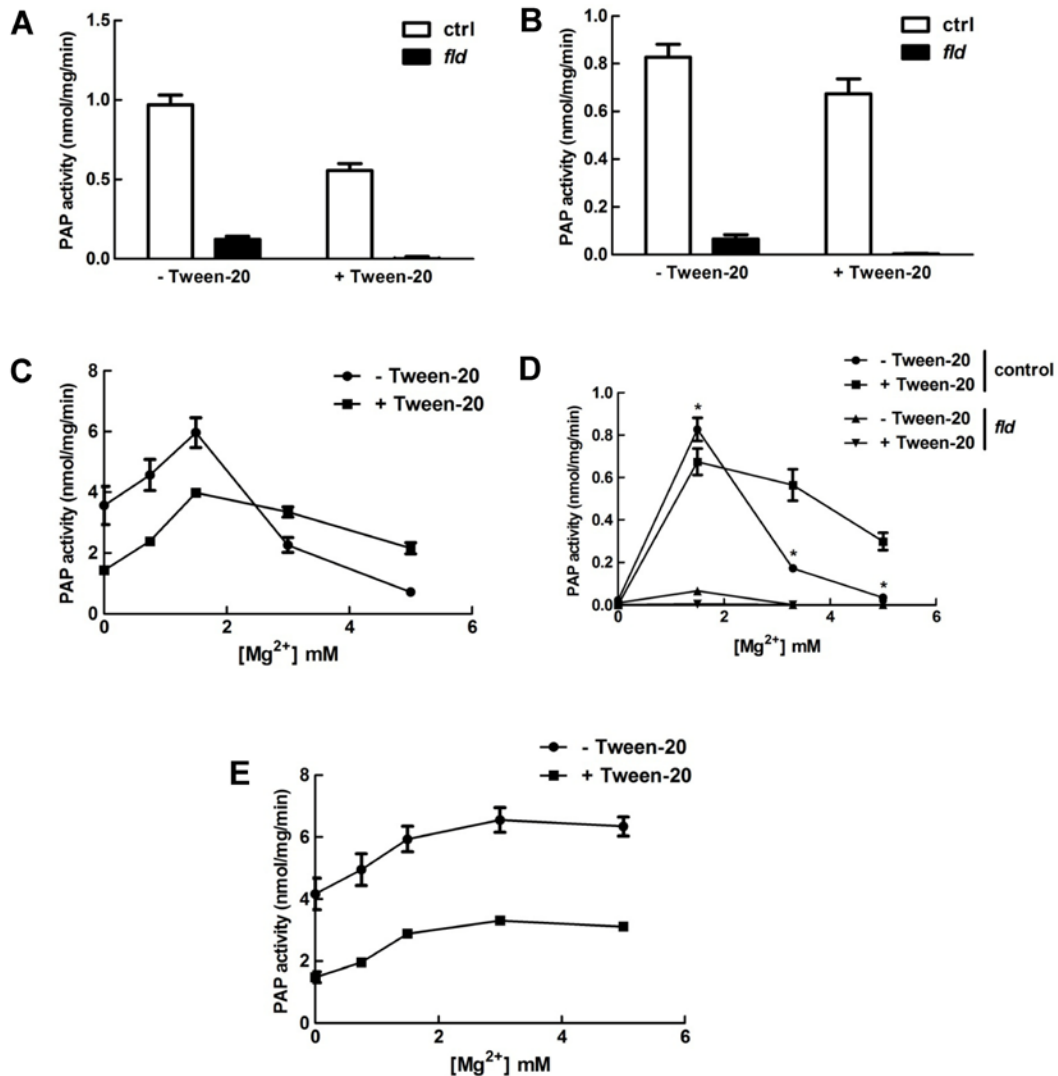
Figure 1 Effect of different cations on phosphatidate phosphatase (PAP) activities in the hearts of lipin-1 deficient (*fld*) and control mice. (A) PAP activities in the hearts of 11-week-old *fld* (n = 8) and control (n = 6) mice were measured using 0.6 mM phosphatidate and 0.4 mM phosphatidylcholine mixed liposomes in 100 mM Tris/maleate pH 6.5 with 5 mM $MgCl_2$ and 0.05% Tween-20. Different concentrations of **(B)** Ca^{2+}, Na^+, Mg^{2+}, **(C)** Co^{2+} and Mn^{2+} were used to assay for PAP activity in 60 μg of protein from an *fld* heart at pH 6.5 in the presence of 0.05% Tween-20 with 1 mM EDTA/1 mM EGTA excluded. **(D, E)** A similar assay was performed for the same cations mentioned above except that 1 mM EDTA/1 mM EGTA was included. All experiments were performed by Bernard Kok.

When testing the effects of different divalent cations on the PAP activity in an *fld* heart, 1 mM EDTA/1 mM EGTA was removed from the assay to prevent chelating the divalent cations. Different concentrations of Mg^{2+} were tested and there was no stimulation of PAP activity in *fld* hearts; in fact, Mg^{2+} appeared to have an inhibitory effect (Figure 1B). Assaying PAP activity in the presence of Co^{2+}, Mn^{2+} and Ca^{2+} cations produced similar results (Figure 1B, C). Supplementation with Na^+ cations did not positively or negatively affect PAP activity in *fld* hearts (Figure 1B). When 1 mM EDTA/1 mM EGTA was left in the assay, the divalent cations were chelated and no longer affected PAP activity, except for concentrations of Mg^{2+} above 1 mM (Figure 1D, E).

Since there did not appear to be any changes in PAP activity when different cations were tested, we looked to see if there were any other conditions in the PAP assay that could be modified. Interestingly, PAP activity was detectable in *fld* hearts at pH 6.5 and 7.4 using 5 mM and 1.5 mM $MgCl_2$ respectively when 0.05%Tween-20 was excluded from the assay with PA/PC liposomes as the substrate (Figure 2A, B). This result was surprising given that Butterwith et al. found a stimulation of PAP activity with the addition of Tween-20 (320). To address this, we assayed samples from *fld* and control hearts as well as NRVM lysates at different Mg^{2+} concentrations in the presence or absence of 0.05% Tween-20. The PAP activities in both NRVM lysates and mouse hearts were optimal at 1.5 mM $MgCl_2$ at pH 7.4 using PA/PC liposomes as the substrate in the presence or absence of Tween-20 (Figure 2C, D). However, the addition of 0.05% Tween-20 significantly suppresses PAP activity in mouse hearts assayed at 1.5 mM Mg^{2+} (Figure 2D). A similar decrease in the presence of Tween-20 was seen in the NRVM lysates (Figure 2C). Notably, Tween-20 appears to stimulate

PAP activity at the higher, non-optimal Mg^{2+} concentrations in the samples from the hearts and NRVMs when assayed at pH 7.4 (Figure 2C, D). In contrast to the PAP assay at pH 7.4, Tween-20 appears to suppress PAP activity in NRVM lysates at pH 6.5 using the PA/PC liposomes, regardless of the Mg^{2+} concentration (Figure 2E).

Figure 2 Effect of Tween-20 on phosphatidate phosphatase (PAP) activities in the hearts of lipin-1 deficient (*fld*) and control mice as well as in neonatal rat ventricular myocytes (NRVMs). PAP activities in *fld* (n = 3) and control (n = 3) hearts were assayed using 0.6 mM phosphatidate and 0.4 mM phosphatidylcholine mixed liposomes in **(A)** 100 mM Tris/maleate pH 6.5 with 5 mM MgCl$_2$ or **(B)** 100 mM Tris/HCl pH 7.4 with 1.5 mM MgCl$_2$, in the presence or absence of 0.05% Tween-20. PAP activities in **(C)** 15 µg of protein from NRVMs (n = 2) or **(D)** 60 µg of protein from *fld* (n = 3) and control (n = 3) hearts were assayed using 0.6 mM phosphatidate and 0.4 mM phosphatidylcholine mixed liposomes in 100 mM Tris/HCl pH 7.4 with different concentrations of MgCl$_2$, in the presence or absence of 0.05% Tween-20. **(E)** PAP activities in 15 µg protein from NRVMs (n = 2) were also assayed using 0.6 mM phosphatidate and 0.4 mM phosphatidylcholine mixed liposomes in 100 mM Tris/maleate pH 6.5 with different concentrations of MgCl$_2$, in the presence or absence of 0.05% Tween-20. *p < 0.05 when compared to control samples assayed in the presence of Tween-20. All experiments were performed by Bernard Kok.

253

3 Effects of Mg^{2+} concentrations, pH and substrate presentation on PAP activity in *fld* hearts

Since PAP activity was detected in *fld* mice when Tween-20 was excluded from the PAP assay, we next tested the effects of Mg^{2+} on PAP activity in *fld* and control hearts using two different assay systems. As expected, PAP activities in both *fld* and control hearts were optimal at 5 mM and 1.5 mM MgCl$_2$ at pH 6.5 and 7.4, respectively when PA/PC mixed liposomes were used as the substrate (Figure 3A, B). Moreover, the reactions at both pH 6.5 and 7.4 were linear over a wide range of protein concentrations from *fld* and control hearts (Figure 3C, D).
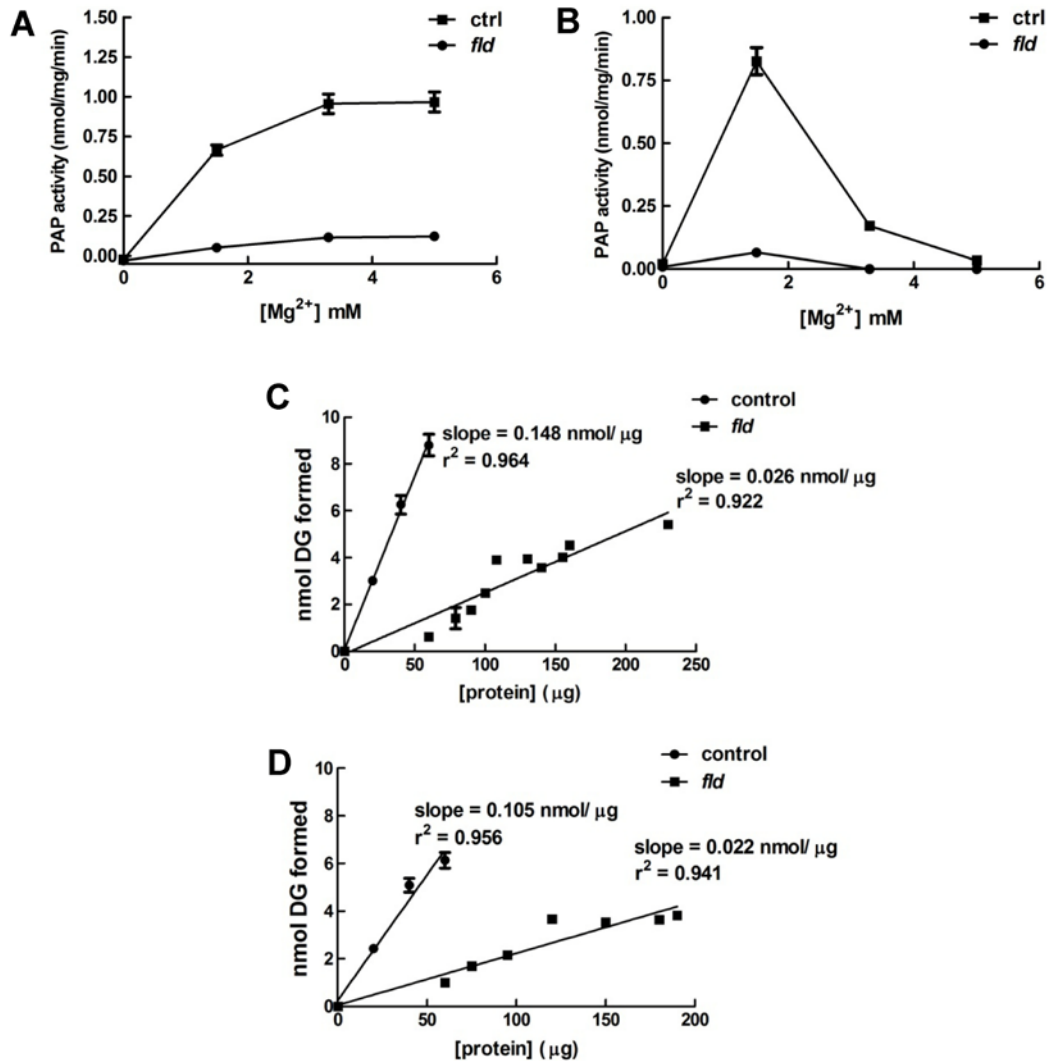
Figure 3 Effect of Mg²⁺ on PAP activities in lipin-1 deficient (*fld*) and control hearts and proportionality of the PAP assay using phosphatidate and phosphatidylcholine mixed liposomes. PAP activities in 60 µg protein from *fld* (n = 3) and control (n = 3) hearts were assayed using 0.6 mM phosphatidate and 0.4 mM phosphatidylcholine mixed liposomes in **(A)** 100 mM Tris/maleate pH 6.5 or **(B)** 100 mM Tris/HCl pH 7.4 with different concentrations of $MgCl_2$. Different amounts of protein from *fld* (n = 3) or control (n = 3) hearts were assayed using mixed liposomes containing phosphatidate and phosphatidylcholine at **(C)** pH 6.5 and **(D)** pH 7.4 in addition to 5 mM and 1.5 mM $MgCl_2$, respectively. Regression analysis was performed to determine the linearity of the PAP assays. All experiments were performed by Bernard Kok.

255

Another common method of measuring PAP activity is to present the substrate in a Triton X-100 micelle. The advantage of this method of measuring PAP activity is that Triton X-100 micelles are relatively uniform and adding low amounts of different phospholipids into these micelles does not alter micellar structure (262). As such, the surface dilution kinetic model, which accounts for three-dimensional interactions between enzyme and micelle in solution and two-dimensional interactions at the micellar surface, can be applied to this system and precise measurements of enzyme kinetics can be performed (262). The optimal Mg^{2+} concentrations at pH 6.5 and 7.4 using PA/Triton X-100 micelles as the substrate were 6 mM and 1 mM Mg^{2+}, respectively (Figure 4A, B). These concentrations are similar to the optimal concentrations obtained using PA/PC mixed liposomes. Interestingly, the PAP activities in *fld* hearts at pH 7.4 using 1 mM Mg^{2+} were much lower than the measurements using the PA/PC liposomes (Figure 3B versus Figure 4B). Furthermore, the PAP activities in *fld* hearts measured using PA/Triton X-100 micelles were not linear over the same range of protein concentrations (Figure 4C). On the other hand, the linearity of the PAP reaction against PA/Triton X-100 micelles in control hearts was similar to the measurements using PA/PC liposomes at pH 7.4. It should also be noted that PAP activities in the *fld* hearts were nearly undetectable at 6 mM Mg^{2+} using the PA/Triton X-100 micelles at pH 6.5 (Figure 4A).

256
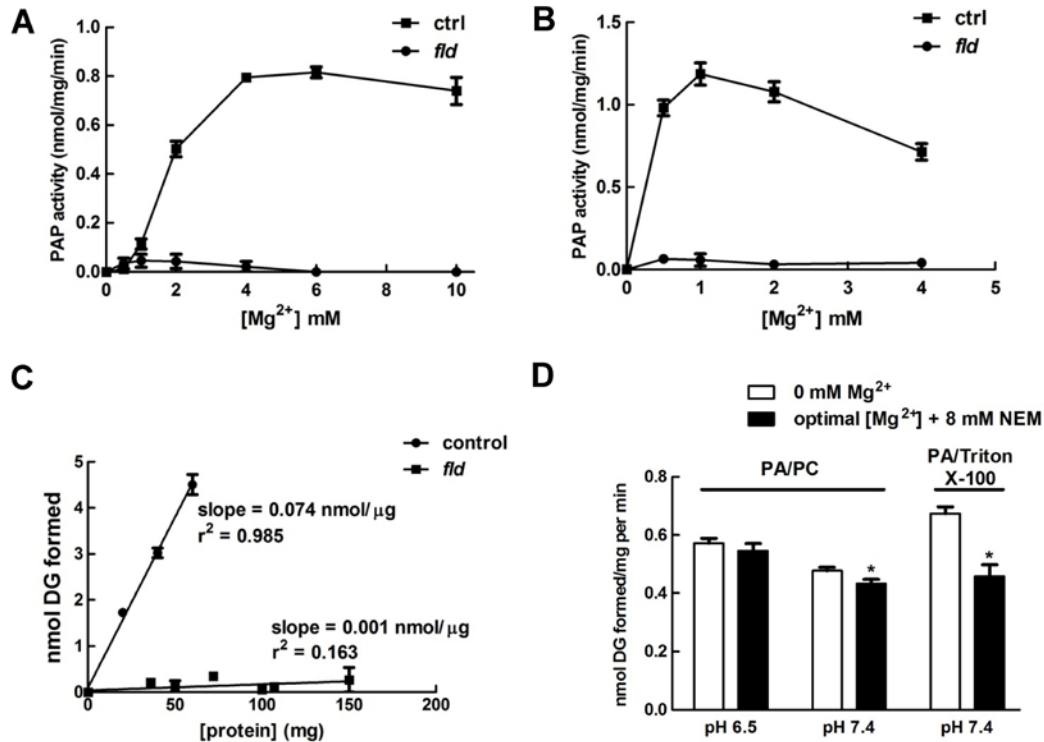
Figure 4 Effect of Mg^{2+} on PAP activities in lipin-1 deficient (*fld*) and control hearts and proportionality of the PAP assay using phosphatidate and Triton X-100 mixed micelles. PAP activities in 60 μg of protein from *fld* (n = 3) and control (n = 3) hearts were assayed using 0.1 mM phosphatidate and 0.9 mM Triton X-100 mixed micelles in **(A)** 100 mM Tris/maleate pH 6.5 or **(B)** 100 mM Tris/HCl pH 7.4 with different concentrations of MgCl$_2$. **(C)** Different amounts of protein from *fld* (n = 3) or control (n = 3) hearts were also assayed using phosphatidate/Triton X-100 micelles at pH 7.4 in the presence of 1 mM MgCl$_2$. Regression analysis was performed to determine the linearity of the PAP assay. **(D)** The contribution of lipid phosphate phosphatase activities in mouse hearts (n = 6) against phosphatidate using the mixed phosphatidate/phosphatidylcholine liposomes or PA/Triton X-100 micelles was measured at pH 6.5 and 7.4 in the absence of Mg^{2+} or in the presence of optimal Mg^{2+} concentrations and 8 mM N-ethylmaleimide. *$p < 0.05$ compared to measurements at 0 mM Mg^{2+} pH 7.4. All experiments were performed by Bernard Kok.

When measuring the PAP activities of the lipins, the hydrolysis of phosphatidate by the LPPs must also be taken into account. Parallel assays performed in the absence of Mg^{2+} or in the presence of the optimal Mg^{2+} concentrations and excess NEM are the two most common methods used to account for LPP activity since LPPs are Mg^{2+}-independent and NEM-insensitive (213, 449). Both methods of accounting for LPP activity are similar at pH 6.5 and 7.4 in the assay using PA/PC liposomes with the NEM-insensitive activity at 95% and 90% compared to the Mg^{2+}-independent activity, respectively (Figure 4D). In contrast, the NEM-insensitive LPP activity is 70% that of the Mg^{2+}-independent activity at pH 7.4 using the PA/Triton X-100 micelles as the substrate (Figure 4D).

In conclusion, both methods of presenting PA in the PAP assay systems are reliable and precise when PAP activities in the samples are easily detectable. However, samples with very low PAP activities appear to be more easily detected with PA/PC liposomes as the substrate.

4 Developing a non-radioactive method to measure PAP activity: using malachite green to detect phosphate release from phosphatidate

We wanted to test a non-radioactive method for detecting PAP activity as a secondary means of measuring lipin-1 and -2 levels in cell lysates by specifically measuring the release of inorganic phosphate from phosphatidate hydrolyzed by PAP activity. The reason why we developed this assay was to test whether the [^{3}H]PA substrate prepared for the radioactive PAP assay (Section 2.2.2) was suitable for measuring PAP activities. The method of substrate

preparation could have potentially produced [³H]dipalmitoyl-PA as the major product and dipalmitoyl-PA is a poor substrate for lipin-1 PAP activity (137).

We based our methodology on principles outlined in two previous studies (216, 450, 451). We first determined whether we could develop an assay that could discriminate between free inorganic phosphate and other compounds like glycerol 3-phosphate, glucose-6-phosphate and lysophosphatidate. A previous study had demonstrated the usefulness of molybdate in preferentially interacting with free inorganic phosphate to form a complex in a 12:1 ratio of molybdate to phosphate (450). The cationic dyes, malachite green and crystal violet, can then bind to the phosphate-molybdate complexes and the change in absorbance can be measured. In our experiments, we chose to use malachite green, which is the most sensitive of the cationic dyes (450). It should also be noted that the standard phosphate assay, where ascorbic acid is used as a reducing agent to form molybdenum blue, was found to be less sensitive than the assay using malachite green (450).

Under acidic conditions, unbound malachite green has a different absorption maximum compared to the dye bound to the complex (450). The degree of colour change can be used to establish a linear detection range such that the amount of inorganic phosphate release can be calculated. To increase specificity, we also used perchloric acid to precipitate proteins as well as bound lipids (216). Ammonium molybdate was then added to interact with free inorganic phosphate and the complex of inorganic phosphate and molybdate was extracted into isobutanol-benzene (1:1, by vol.). The phosphate-molybdate complex will

partition into the organic phase unlike the other water-soluble phosphates, e.g. glycerol 3-phosphate (216).

The specificity of the malachite green interaction with the phosphomolybdate complex was tested by assaying 30 nmol of different compounds containing phosphate groups and Na_2HPO_4 was used as the positive control. Only Na_2HPO_4 had an absorbance at 600 nm above the background value, showing that malachite green can only interact with free inorganic phosphate complexed to molybdate (Table 1). This interaction was proportional to the concentration of Na_2HPO_4 (Figure 5A). When we assayed endogenous PAP activity or overexpressed lipin-1 and -2 in HEK293 cell lysates, we measured the rate of [^{3}H]DG formation or the release of inorganic phosphate from phosphatidate in parallel assays using the same samples and found that the results were relatively similar (Figure 5B-D).

Table 1 Detection of different phosphate-containing compounds using molybdate and malachite green. Different compounds were reacted with 6 mM ammonium molybdate and 0.122 mM malachite green in 0.45 M H_2SO_4, and the absorbance was measured at 600 nm. All experiments were performed by Bernard Kok.

Compound	Absorbance (600 nm)
Blank	0.194
30 nmol Na_2HPO_4	2.477
30 nmol lysophosphatidate	0.204
30 nmol phosphatidate	0.199
30 nmol *rac*-glycerophosphate	0.193
30 nmol glycerol-2-phosphate	0.198
30 nmol *D*-glucose-6-phosphate	0.205
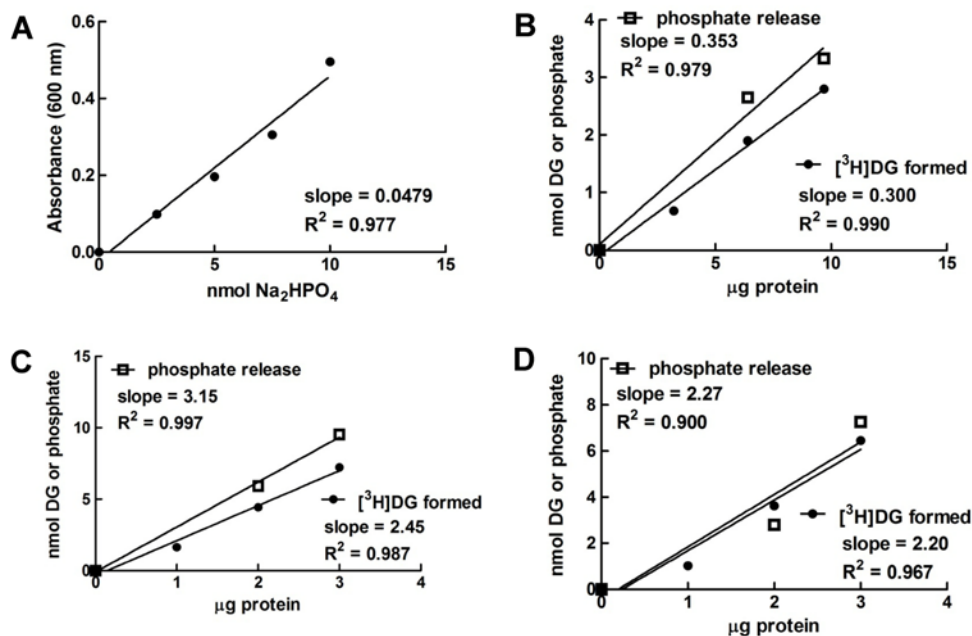
Figure 5 Measurement of phosphate release from phosphatidate using malachite green. (A) Different amounts of Na_2HPO_4 were incubated under standard PAP assay conditions at pH 6.5 using 5 mM $MgCl_2$ and the absorbance of malachite green bound to the phosphate-molybdate complex was measured at 600 nm. **(B)** Endogenous PAP activity in HEK293 cells or PAP activities in HEK293 cells inoculated with recombinant adenoviral vectors expressing **(C)** lipin-1 and **(D)** lipin-2 were assayed by determining the amount of phosphate released or by measuring the formation of [³H]diacylglycerol from [³H]phosphatidate. All experiments were performed by Bernard Kok.

However, the lower detection limit of the malachite green assay was the absorbance at 600 nm of 2.5 nmol phosphate. The traditional radioactive PAP assay can measure 0.5 – 1 nmol [³H]DG formation at the lower limit. Moreover, the upper range of the PAP assay is set at 10 – 12 nmol of PA hydrolyzed since the assay is often not proportional to protein concentration after this upper limit is reached. From these results, it is clear that using malachite green to measure phosphate release from PA is a viable assay to measure PAP activity. This

assay could enable us to measure PAP activity of recombinant lipin-2 and -3 as well as mutant constructs with different PA substrates such as dioleoyl-PA without having to prepare radioactive compounds in the future.

5 Discussion

The parameters and conditions established for the PAP assay used by our group have been established since the 1980s (212, 319-321). It was shown that PAP activity has a requirement for Mg^{2+} and that other divalent cations, e.g. Ca^{2+}, Co^{2+} and Mn^{2+} could also stimulate PAP activity (212, 218, 265). Furthermore, the Mg^{2+}-dependent PAP activity could be differentiated from Mg^{2+}-insensitive PAP activity (contributed by LPPs) by their differing sensitivities to thiol-alkylating reagents, such as NEM (213, 320). The contribution of the LPPs in hydrolyzing PA is usually taken into account by assaying the samples in parallel while excluding Mg^{2+} or supplementing with NEM. Both methods are equivalent when assaying PAP activity with PA/PC liposomes (Figure 4D). However, there is a 30% decrease in the NEM-insensitive PAP activity from LPPs compared to the measurements made without Mg^{2+} when the PA/Triton X-100 micelles were used, suggesting that measuring PAP activity in the absence of Mg^{2+} might be the more appropriate control in this instance.

Work by Butterwith et al. also demonstrated that PAP activity was stimulated by the addition of 0.05% Tween-20. From these studies, we established an optimal PAP enzymatic assay wherein PAP activities in cell or tissue extracts were measured using the PA/PC mixed liposomes and the optimal concentration of 5 mM $MgCl_2$ at pH 6.5. Furthermore, 0.05% Tween-20 was supplemented in the assay. We continued to use these conditions until we

discovered that samples from *fld* (lipin-1 deficient) hearts had no detectable PAP activity (Figure 1A). This result was not surprising given that a previous study had already established that *fld* hearts possessed little to no PAP activity (241).

We hypothesized that our PAP assay was unable to detect the PAP activity of lipin-2 and -3, possibly due to a requirement for a different concentration of Mg^{2+} or for a divalent cation other than Mg^{2+}. This seemed unlikely since our group in collaboration with Donkor et al. had detected activity from recombinant lipin-2 and lipin-3 using our standard assay conditions (134). Alternatively, *fld* hearts could truly be devoid of PAP activity and the DG required for PC and PE biosynthesis in the *fld* hearts might be obtained from a different route such as from monoacylglycerol by monoacylglycerol acyltransferase activity. However, it is unclear how much this enzymatic pathway contributes to glycerolipid synthesis in the heart. It is also thought that the LPPs are unlikely to substitute for PAP in the glycerolipid biosynthetic pathway since the catalytic sites of the LPPs face the lumen of organelles (217), whereas glycerolipid biosynthesis occurs on the cytosolic side of the endoplasmic reticulum and, to some extent, the mitochondria (125).

A previous study had shown that lipin-1 PAP activity can be stimulated by Mn^{2+} (137). We did not find stimulation of PAP activity with different cations and, in fact, the divalent cations tested appeared to suppress the hydrolysis of [^{3}H]PA. These results are reminiscent of the studies performed by Jamal et al. who used the same assay at pH 6.5 in the presence of PA/PC liposomes as described in Section 2.2.3 to measure plasma membrane PAP activities (213). The only exceptions were that 1 mM DTT was used instead of 0.6 mM DTT and

microcystin-LR and tetrahydrolipstatin were absent. Jamal et al. showed that PAP activities isolated from the plasma membrane are suppressed with increasing concentrations of Mg^{2+} and Ca^{2+} (213). Since plasma membrane-localized PAP activity can be attributable to the LPPs (215), it is most probable that we were measuring the effects of divalent cations on the PAP activity of the LPPs in *fld* hearts. Although we did not observe a stimulation of PAP activity in *fld* hearts in our experiments, this does not mean that lipin-2 or -3 cannot be stimulated by divalent cations other than Mg^{2+} since the assay was conducted in the presence of Tween-20, which suppressed PAP activity at pH 6.5 using PA/PC liposomes (Figure 2A). It is possible that we might have demonstrated the stimulation of PAP activity in *fld* hearts by Mn^{2+}, Co^{2+} or other divalent cations if Tween-20 were excluded, with the caveat that the PAP activity of lipin-2/-3 in the *fld* hearts only represented 20% of the total activity in control hearts using optimal assay conditions (Figure 2A, B). Therefore, the determination of the effects of different divalent cations on lipin-2 and -3 catalytic activities would be best investigated using overexpressed recombinant lipin proteins. It should also be noted that the Mg^{2+}-dependence of recombinant lipin-2 and -3 expressed in 293T cells were previously determined using PA/Triton X-100 mixed micelles as the substrate, and it was shown that the PAP activities of lipin-1A, -1B, -2 and -3 are optimum at the same concentration of Mg^{2+} (134).

The effect of Tween-20 on the PAP assay was surprising given the results obtained by Butterwith et al. in 1984. However, closer examination of the conditions used by Butterwith et al. revealed that the samples were assayed at pH 7.4 using 5 mM $MgCl_2$ (320). Under these conditions, Tween-20 does in fact stimulate PAP activity (Figure 3.2D, E), although the assay was not optimum.

The differential effects of Tween-20 on PAP activity could be related to the availability of PA as a substrate. Tween-20 at 0.05% is equivalent to 0.4 mM, which is four times its critical micellar concentration. Moreover, the concentrations of PA and PC in the PAP assay are 0.6 and 0.4 mM, respectively. Therefore, the decrease in PA hydrolyzed when Tween-20 is present at pH 6.5 is probably due to the dilution of the surface concentration of PA. The same principles would apply for the results seen at pH 7.4 and low Mg^{2+} concentrations. However, there was a stimulation of PAP activity in the presence of Tween-20 at higher Mg^{2+} concentrations. The ionization of the phosphate group of PA has a pK_{a1} and pK_{a2} of approximately 3.2 and 7.9 depending on the composition of the micelle/liposome as well as the presence of different cations (452, 453). Therefore, there would be approximately ten times more PA with two ionized groups at pH 7.4 compared to that at pH 6.5. Mg^{2+} would strongly chelate these PA species at pH 7.4 and cause aggregation. The addition of 0.05% Tween-20 could possibly decrease this aggregation and increase access of PAP to the PA substrate.

It is unclear why low levels of PAP activity in the *fld* hearts are detectable using PA/PC liposomes and not PA/Triton X-100 micelles, although PA/PC liposomes could be more representative of the physiological substrate. Alternatively, the surface concentration of PA could again be an important consideration. PA/PC liposomes at a molar ratio of 3:2 compared to PA/Triton X-100 at a molar ratio of 1:9 (10 mol% surface concentration) could be more accessible to the limiting amounts of PAP activity from lipin-2 and -3 in *fld* tissue especially since other proteins in the tissue homogenate might also bind to or associate with liposomes. Thus, it might be possible to detect low levels of PAP

activity using the Triton X-100 system if the concentration of PA in the assay were increased. However, Han et al. demonstrated that purified lipin-1α, -1β and -1γ had equivalent K_m's of approximately 4.5 mol%. Furthermore, our group also demonstrated that the K_m's of HEK 293 cell lysates overexpressing lipin-2 and -3 were approximately 4-5 mol% (173). The likely explanation lies in the preference of the LPPs for PA presented in mixed Triton X-100 micelles as opposed to PA/PC liposomes (213, 321). As such, it would be more difficult to detect low levels of lipin-2 and -3 PAP activity using PA/Triton X-100 micelles because of the higher detection of LPP activities.

The use of malachite green to detect phosphate release from PA in the PAP assay had been previously characterized by the laboratory of Dr. George Carman (451). We also wanted to determine if our assay could be adapted to detect phosphate release. The difference between these two studies was that we did not purify the enzymes and, instead, we measured the PAP activity of overexpressed lipins in cell lysates. Importantly, this assay enabled us to measure the hydrolysis of PA prepared from egg yolk PC. This substrate consists of multiple PA species containing various fatty acyl side chains such as palmitate, oleate and linoleate as opposed to the [3H]PA, which could be predominantly dipalmitoyl-PA. As previously mentioned, results from the malachite green assay were similar to the radioactive PAP assay, although we detected 15-20% more phosphate released from PA on average than [3H]DG formed. This result suggests that PAP activity is less efficient at hydrolyzing the [3H]PA, which could be predominantly [3H]dipalmitoyl-PA. Future preparation of the PA substrate would include the use of oleate instead of palmitate (or a mixture of oleate and palmitate) during the incorporation of [3H]palmitate into glycerol 3-phosphate

using liver microsomal protein. Alternatively, this difference could also be due to phosphodiesterase activity in the cell lysates against other compounds. Havriluk et al. had previously raised the issue of high background when measuring cell lysates using this assay (451). A parallel assay performed in the absence of PA would have controlled for this.

In summary, the malachite green assay has a narrower range of detection and also requires more methodological steps compared to the radioactive PAP assay. Moreover, the use of benzene in the extraction procedure poses a health risk. Overall, measuring phosphate release from PA with malachite green is a viable alternative to detecting the formation of [^{3}H]DG. Although PAP activity appears to be 15% less efficient at hydrolyzing the [^{3}H]PA (which is predicted to be predominantly [^{3}H]dipalmitoyl-PA), the radioactive assay is still more sensitive and less technically involved. There is also less risk of detecting non-specific products. In conclusion, we prefer using the radioactive PAP assay because it is still more sensitive in comparison and the range of detection is not as limited as the malachite green assay.